Characterising Fibrillin Microfibril Structural Diversity and Photo-induced Damage

A thesis submitted to The University of Manchester for the degree of

Doctor of Philosophy

in the Faculty of Biology, Medicine and Health

2018

Alexander Eckersley

School of Biological Sciences

Division of Cell Matrix and Regenerative Medicine

Table of Contents

Word Count: 54,811

List of Figures

List of Tables

List of Supplementary Tables

All Supplementary Tables have been uploaded to the online data repository Mendeley Data and can be accessed by copying and pasting the following link:

https://data.mendeley.com/datasets/7t8hxk7bwb/draft?a=45c5494a-55e9-49b8-9ac6-b505a148e07e

List of Abbreviations

ACN	Acetonitrile
AA	Amino acid
ADAMTS	A disintegrin and metalloproteinase with thrombospondin motifs
ADAMTSL	ADAMTS-like
AFM	Atomic force microscopy
ANOVA	Analysis of variance
BMP	Bone morphogenetic protein
$CaCl_2$	Calcium chloride
CB	Ciliary body
CO_2	Carbon dioxide
COL6A	Collagen VI alpha chain
COPD	Chronic obstructive pulmonary disease
CSV	Comma separated value file extension
DAT	Data file extension
DEJ	Dermal-epidermal junction
DMEM	Dulbecco's Modified Eagle's Medium
DMSO	Dimethyl sulfoxide
DNA	Deoxyribonucleic acid
DTT	Dithiothreitol
E:S	Enzyme to substrate ratio
ECM	Extracellular matrix
EDTA	Ethylenediaminetetraacetic acid
EGF	Epidermal growth factor-like domain
EM	Electron microscopy
EMILIN	Elastin microfibril interfacers
FA	Formic acid
FBN1	Fibrillin-1
FCS	Foetal calf serum
FDR	False discovery rate
GAG	Glycosaminoglycans
Gu-HCl	Guanidine hydrochloride
HBSS	Hanks' balanced salt solution
HCl	Hydrochloric acid
HDF	Human dermal fibroblast
IAM	Iodoacetamide
IGF	Insulin-like growth factor
IGFBP	Insulin-like growth factor-binding protein
IMS	Industrial methylated spirits
IQR	Interquartile range
LC-MS/MS	Liquid chromatography tandem MS
LOX	Lysyl oxidase
LTBP	Latent TGFβ-binding protein
MAGP	Microfibril-associated glycoprotein
MFAP	Microfibril-associated protein
MFS	Marfan syndrome
MGF	Mascot generic file
MMP	Matrix metalloproteinase

MS	Mass spectrometry
MSHB	University of Manchester Skin Health Biobank
NaCl	Sodium chloride
NEM	N-ethylmaleimide
NMR	Nuclear magnetic resonance
NPE	Non-pigmented epithelial
OCT	Optimal cutting temperature compound
PAI1	Plasminogen activator inhibitor 1
PBS	Phosphate-buffered saline
PF	Protein fragment
PFA	Paraformaldehyde
PMSF	Phenylmethylsulfonyl fluoride
PSM	Peptide spectrum match
PTM	Post-translational modification
RAW	Raw file extension
RGB	Red, green, blue image type
ROS	Reactive oxygen species
RSLC	Rapid separation liquid chromatography
S/N	Signal to noise
SAXS	Small angle X-ray scattering
SB	*Stratum basale*
SC	*Stratum corneum*
SDS	Sodium dodecyl sulphate
SG	*Stratum granulosum*
SS	*Stratum spinosum*
STEM	Scanning transmission EM
TB	LTBP-like domain
TBS	Tris-buffered saline
TGFβ	Transforming growth factor beta
TIFF	Tagged image file format extension
TIMP	Tissue inhibitor of metalloproteinase
Tris	Trisaminomethane
UV	Ultraviolet
UVA	Ultraviolet-A
UVB	Ultraviolet-B
UVC	Ultraviolet-C
UVR	Ultraviolet radiation
v/v	Volume / volume
V_0	Void volume
VAM	Vimentin-associated matrix adhesion
V_F	Final volume
v-WF-A	A-domains of von Willibrand factor
WARP	von Willebrand factor-A domain-related protein
βig-H3	TGFβ-induced glycoprotein-H3

Abstract

Fibrillin microfibrils are supramolecular, extracellular matrix assemblies which play a number of important roles in different tissues. In eye, they exist as ciliary zonules which are inherent to the process of lens accommodation. By contrast, in skin dermis, they exist both as constituents of elastic fibres, endowing tissue with elasticity, and also as stand-alone oxytalan fibres, which extend through the papillary dermis. Although these assemblies play distinct key roles within these two tissues, it remains unknown whether their ultrastructure and molecular composition is tissue-dependent as a result. Fibrillin microfibrils have also been implicated in skin photoageing, which is characterised by the degeneration of its dermal architecture. Additionally, irradiation with physiological doses of ultraviolet (UV) radiation causes quantifiable changes to its beads-on-a-string ultrastructure, *in vitro*. As a result, the UV-susceptibility of this assembly has been implicated in the photoageing process. Although its ultrastructure is susceptible to UV, the molecular foci of this damage within the fibrillin-1 monomer remain undetermined. Also, in contrast to fibrillin, collagen VI microfibrils remain remarkably unaffected both by photoageing in skin and by UV irradiation. The molecular reasons behind this differential susceptibility also remain unknown.

To address these gaps in knowledge, the first aim was to develop a novel mass spectrometry (MS)-based proteomic approach capable of characterising microfibril composition and monomeric structure of both fibrillin and collagen VI microfibril assemblies. Two digestion methods were successfully optimised: the elastase method led to a high fibrillin-1 primary coverage and revealed protein regions previously uncharacterised by proteomics. The SMART Digestion™ method also led to the identification of numerous co-purifying microfibril-associated proteins.

Using this developed proteomic approach and atomic force microscopy (AFM), the next aim was to characterise tissue-dependent ultrastructural and compositional differences between skin-, eye- and human dermal fibroblast (HDF)-derived fibrillin microfibrils. This work revealed that, not only did the ultrastructure of eye fibrillin microfibrils differ from skin, but also tissue-specific regions of the fibrillin-1 structure were differentially susceptible to proteolysis. Furthermore, this work found that skin and HDF fibrillin microfibrils also differed in ultrastructure and fibrillin-1 proteolytic susceptibility. In contrast, collagen VI microfibrils from the same samples were invariant. Finally, it was observed that fibrillin microfibrils isolated from skin and eye exhibited unique protein compositions mirroring tissue function. This study showcased the diversity of this key assembly.

Finally, this PhD aimed to discover which regions of the fibrillin-1 monomer were susceptible to UV and how this differs to the collagen VI alpha-3 (COL6A3) monomer. HDF fibrillin microfibril ultrastructure was significantly altered by both solar simulated radiation (SSR; 30 J/cm^2) and UVB irradiation (100 mJ/cm^2) whereas, comparatively, collagen VI microfibril ultrastructure was not. UV irradiation consistently enhanced the total yield of digested fibrillin-1 peptide, but not COL6A3. Mapping these peptides revealed that UV exposure increases regional susceptibility within the fibrillin-1 structure to proteolysis, allowing the identification of UV-susceptible foci on a molecular scale. Data-dependent quantification also revealed two fibrillin-1 peptides and ten COL6A3 peptides from skin isolations which matched UV-signatures also identified in HDF isolations indicating that this damage may also translate to microfibrils in native skin.

This PhD successfully characterised fibrillin microfibril structural diversity and photo-induced molecular damage. In doing so, it has made a significant contribution to the field of ECM biology and photobiology, with the prospect of future research projects arising from this endeavour.

Declaration

The author, Alexander Eckersley, declares that no portion of the work referred to in the thesis has been submitted in support of an application for another degree or qualification of this or any other university or other institute of learning.

Copyright Statement

i. The author of this thesis (including any appendices and/or schedules to this thesis) owns certain copyright or related rights in it (the “Copyright”) and s/he has given The University of Manchester certain rights to use such Copyright, including for administrative purposes.

ii. Copies of this thesis, either in full or in extracts and whether in hard or electronic copy, may be made **only** in accordance with the Copyright, Designs and Patents Act 1988 (as amended) and regulations issued under it or, where appropriate, in accordance with licensing agreements which the University has from time to time. This page must form part of any such copies made.

iii. The ownership of certain Copyright, patents, designs, trademarks and other intellectual property (the “Intellectual Property”) and any reproductions of copyright works in the thesis, for example graphs and tables (“Reproductions”), which may be described in this thesis, may not be owned by the author and may be owned by third parties. Such Intellectual Property and Reproductions cannot and must not be made available for use without the prior written permission of the owner(s) of the relevant Intellectual Property and/or Reproductions.

iv. Further information on the conditions under which disclosure, publication and commercialisation of this thesis, the Copyright and any Intellectual Property and/or Reproductions described in it may take place is available in the University IP Policy (see http://documents.manchester.ac.uk/DocuInfo.aspx?DocID=2442 0), in any relevant Thesis restriction declarations deposited in the University Library, The University Library’s regulations (see http://www.library.manchester.ac.uk/about/regulations/) and in The University’s policy on Presentation of Theses

v. Result chapters (chapters three to six) of this thesis are presented in journal format. As such, these sections contain collaborative, co-authored work. Details on the individual contributions of the co-authors, including that of the thesis author, can be found within

each of these chapters: 1) in paragraphs immediately following the chapter titles and 2) in subsections titled “Author contributions” at the end of each chapter.

Publications arising from this PhD

1. **Eckersley, Alexander**, Kieran T. Mellody, Suzanne M. Pilkington, Christopher E. M. Griffiths, Rachel E. B. Watson, Ronan O'Cualain, Clair Baldock, David Knight, and Michael J. Sherratt. 2018. "Structural and Compositional Diversity of Fibrillin Microfibrils in Human Tissues." *Journal of Biological Chemistry* jbc-RA117.

2. Thomson, Jennifer, Mukti Singh, **Alexander Eckersley**, Stuart A. Cain, Michael J. Sherratt, and Clair Baldock. 2018. "Fibrillin Microfibrils and Elastic Fibre Proteins: Functional Interactions and Extracellular Regulation of Growth Factors." *Seminars in Cell & Developmental Biology*.

Full texts of both manuscripts can be found in the Appendix section. Both are published under CC-BY licences and can be reproduced without permission.

Acknowledgments

First, I would like to thank my supervisors Dr Mike Sherratt and Professor Rachel Watson. Their wisdom and advice over the last four years has not only enabled me to become the researcher I always strived to be but has also given me the confidence needed to lead a project independently. It has been a pleasure to work with you both.

Next, I would like to thank Dr Mike Bell, Mrs Clare O'Connor and the rest of the team at Walgreens Boots Alliance for funding this PhD.

Special thanks must go to all the eye and skin donors who voluntarily donated the tissue used in this PhD project, as well as to all the clinical staff at the Manchester Eye Bank, University of Bradford and Salford Royal Hospital which were involved in the collection process.

I would also like to thank my close colleague Matiss Ozols for his help, support and all the good times. Having tackled our respective PhD projects together, simultaneously, I believe many of its challenges were made easier through your friendship and wacky statements.

Next, I would like to thank all my fellow PhD student friends over the last four years. Your companionship and comradery has truly been the foundation behind the success of my PhD. Thank you for all the support and entertainment. You guys are great! Also, thanks Nathan for all the tequila… and an extra special thanks to our De Longhi filter coffee machine.

A big thank you to my family for all the love and support they've given me throughout my life. Without you beside me, always encouraging me, I would not have been able to get through this immense challenge. Even though we're far apart, we will always remain close.

Finally I would like to thank the love of my life, Catherine Disney. Thank you for being there for me through all the hard times and pushing me to become the person I've always wanted to be, while always staying true to my weird, crazy self. I love you.

Structure and Scope of Thesis

This PhD thesis was written in journal format. This felt appropriate, as the majority of my PhD project was spent producing original research with the purpose of publishing my work in scientific journals. As an aspiring academic researcher, I always felt it important to strive towards producing outputs which impact on my field. As such, a big part of my PhD was spent writing, updating and editing manuscripts as well as dealing with reviewers' comments and the peer review process. Therefore, the four manuscripts I have written during this PhD project are presented here as four separate results chapters. Despite these manuscripts functioning as stand-alone, original research papers, the work they contain comes together to form a complete, coherent and continuous thesis. This thesis is written as follows:

Chapter 1 provides the rationale for the research conducted during this PhD with an in-depth literature review of fibrillin microfibril biology in the context of tissue function, composition, structure and its role in photoageing. It begins by reviewing skin anatomy and components of the dermal extracellular matrix (ECM), with a particular focus on elastic fibres and the fibrillin microfibrils that constitute them. The eye anatomy and the role of fibrillin microfibrils within this tissue is then reviewed where it becomes clear that the function of these assemblies is tissue-dependent. The chapter then continues with an in-depth review of fibrillin and collagen VI microfibril structure, composition, and assembly. The gaps in knowledge are then discussed, revealing that the tissue-dependent functions of fibrillin microfibrils within eye and skin may be reflected in their structure and composition, but this remains to be demonstrated. The process of skin photoageing and the proposed contributions of these assemblies to its progression are next reviewed. Although ultraviolet (UV) radiation causes demonstrable changes to fibrillin microfibril ultrastructure, its effect on the fibrillin-1 monomer remain unknown. In contrast, collagen VI microfibril architecture and ultrastructure is unaffected by photoageing and UV. However, whether one of its alpha chains (namely alpha-3; COL6A3) remains unaffected, also remains unknown. Finally this chapter concludes with a literature review of fibrillin microfibril proteomics. This is necessary for the development of a mass spectrometry (MS)-based approach capable of measuring molecular changes in microfibril isolations (fibrillin-1 and COL6A3 structure and microfibril composition).

Chapter 2 contains in depth descriptions of all the methods used to produce this work. Due to the journal format style, these methods are also described within the results chapters.

The next four results chapters are comprised of manuscripts which have been reformatted to the style of this thesis. As such, the pagination and references within, remain continuous. This begins with **chapter 3,** which presents the successful development of pre-MS digestion methods capable of enhancing fibrillin and collagen VI microfibril proteomic analysis compared to previously published efforts. The developed elastase digestion method successfully generated sufficient fibrillin-1 and COL6A3 peptides for structural analysis, from microfibrils isolated from human eye and skin tissue. Furthermore, the developed SMART™ Digestion method successfully generated peptides from co-purifying microfibril-associated proteins which enabled the characterisation of microfibril composition.

Results **chapter 4** used a combination of atomic force microscopy (AFM) to assess fibrillin and collagen VI microfibril ultrastructure, and these newly developed proteomic approaches to assess differences in fibrillin-1 and COL6A3 structure and microfibril composition. In doing so, this chapter reveals tissue- and cell culture-dependent differences in the ultrastructure, fibrillin-1 regional proteolytic susceptibility and composition of fibrillin microfibrils isolated from human ciliary body, skin and dermal fibroblast (HDF) culture. In contrast, collagen VI microfibril structure and composition was invariant in comparison. These results showcase the structural diversity of these key ECM assemblies, which may relate to their distinct roles in the tissues where they reside.

Results **chapter 5** successfully characterises UV-induced damage in fibrillin and collagen VI microfibrils on an ultrastructural and molecular scale in HDF-derived isolations. Physiological doses of both solar simulated radiation (SSR) and broadband UVB not only induced ultrastructural changes, but also led to an increase in the regional susceptibility of fibrillin-1 to proteolysis. As expected, this was in contrast to collagen VI microfibrils, which remained resistant to UV, both ultrastructurally and molecularly. Despite these differences in UV susceptibility, data-dependent quantification of fibrillin-1 and COL6A3 revealed specific peptide signatures of UV-induced damage within both microfibril assemblies. This study successfully identified regional foci of UV-induced damage to the fibrillin-1 structure, common to both sources of UV irradiation, for the first time. Additionally, it led to the detection of peptide signatures of UV damage from the comparatively UV-resistant collagen VI microfibrils, indicating that proteomic approaches may be more sensitive in characterising this damage than ultrastructural measurements with AFM. This study may have important implications for photoageing, as it reveals the possible molecular mechanism of UV-induced damage within these assemblies.

Having successfully characterised fibrillin-1 and COL6A3 UV-induced damage in HDF-derived microfibril isolations, **chapter 6** presents a study which attempts to test whether broadband UVB-susceptibility translates to native skin-derived microfibrils. Proteomic approaches failed to adequately characterise molecular-scale UV-induced damage to skin fibrillin-1 structure. Despite this, two fibrillin-1 peptide signatures of broadband UVB-induced damage were identified. These corresponded to signatures previously detected in the UV-irradiated HDF-derived microfibril study. Additionally, the overall resistance of skin-derived COL6A3 structure to UV-induced damage was confirmed. Despite this, ten COL6A3 peptide signatures of broadband UVB-induced damage, which corresponded to signatures identified in the previous HDF study, were identified. This indicates that the proteomic approach was successful in characterising molecular damage in COL6A3, in contrast to fibrillin-1.

Chapter 7 summarises the thesis and critically discusses the findings and limitations of the work. Potential future research projects arising from this PhD are also proposed. Finally, this chapter concludes the thesis by clearly summarising the key research questions addressed by this work.

Chapter 1: Introduction and literature review

Fibrillin microfibrils are megadalton-sized, macromolecular assemblies (Baldock *et al.* 2001) of the extracellular matrix (ECM) present in a variety of connective tissues such as skin (Dahlbäck *et al.* 1990), eye (Godwin *et al.* 2018; Hiraoka *et al.* 2010), lung (Neptune *et al.* 2003) and arteries (Carta *et al.* 2006). Although they play a structural, mechanical and even homeostatic role (Kaartinen and Warburton 2003) in these tissues, how this relates to their ultrastructure and composition remains poorly understood. Furthermore, the dissolution of the fibrillin microfibril architecture in skin is a hallmark of the photoageing process (Watson *et al.* 1999) and thought to be the main cause of skin wrinkling and loss of elasticity seen clinically in aged individuals (Langton *et al.* 2017). Although ultraviolet radiation (UVR) has been shown to cause measurable changes to the ultrastructure of these extracted microfibril assemblies (Hibbert *et al.* 2015; Sherratt *et al.* 2010), the molecular location of damage and its effects on microfibril composition also remains unknown. This PhD strives to bridge the gap between known tissue-specific and photodamage-specific differences in fibrillin microfibril architecture and ultrastructure and the unknown consequences for fibrillin microfibril molecular composition. To do so, however, it is necessary to first review what is known about this versatile and multi-functional assembly in the context of its different biological roles, the tissues in which it resides and the pathologies associated with its remodelling.

Fibrillin microfibrils can play very different roles depending on the tissue in which they reside. Skin fibrillin microfibrils exist predominantly as elastic fibre components (Feneck *et al.* 2018; Rock *et al.* 2004) where they play a major role in tissue compliance (Kielty, Sherratt, et al. 2002; Langton et al. 2017). In contrast, ciliary fibrillin microfibrils in eye exist as stand-alone assemblies (Godwin *et al.* 2018; Hiraoka *et al.* 2010) that play a central role in lens accommodation (Burd *et al.* 1999; Delamere 2005). Although it is clear that microfibrils from these different tissues play distinct functional roles, this PhD aims to answer whether or not this is reflected in their structure and supramolecular composition. As a result, it is first necessary to review the anatomy, function and ECM composition of both skin and eye as a whole.

1.1 Skin anatomy

The skin is composed of a complex architecture of layers **(Fig. 1.1)**. The epidermis is the outermost layer, and can be segmented into four micro-layers. The *stratum corneum* consists of a tightly bound sheet of corneocytes and acts as the primary defence against dehydration (Blank 1952), infection (Vernon *et al.* 1990) and damage (Hunter *et al.* 1974) (for a comprehensive review, see

Proksch *et al.* 2008). The *stratum granulosum* and the *stratum spinosum* consist mainly of keratinocytes, progressing through distinct stages of differentiation into corneocytes (Kömüves *et al.* 2000; Weil *et al.* 1999; Yuspa *et al.* 1988). The *stratum basale* is made of a single layer of progenitor keratinocytes which act as a source of proliferation, continuously replacing cells in the more superficial layers of the epidermis (Aberdam 2003), and as a physical barrier between the epidermis and the dermis. It lies directly above the basement membrane which marks the dermal-epidermal junction (DEJ) (Woodley *et al.* 1983).

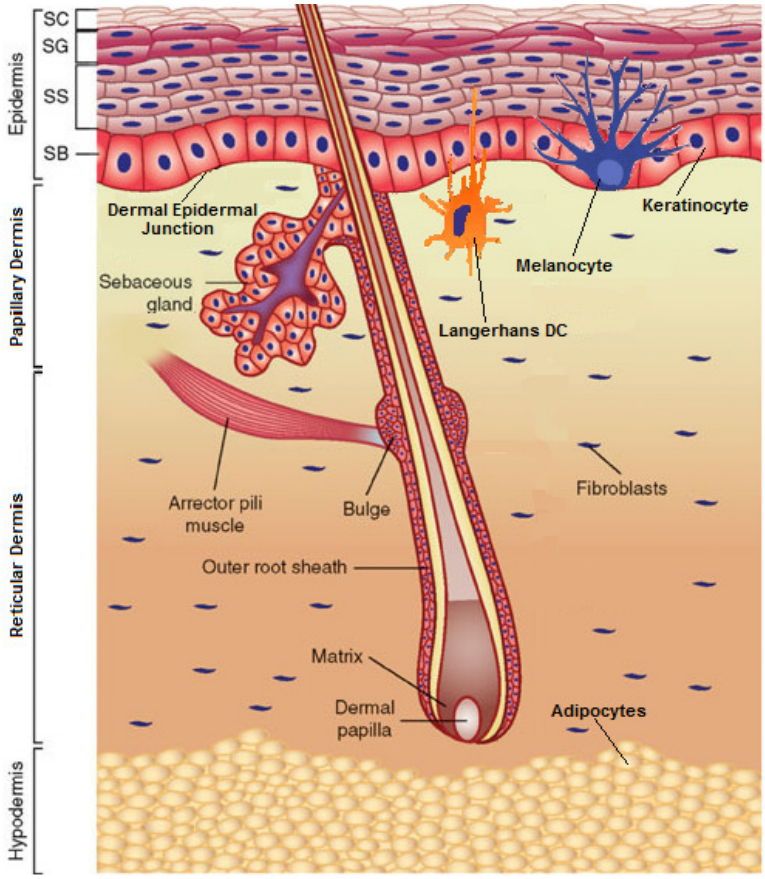

Figure 1.1: The gross histological anatomy of the skin. The epidermis constitutes of four layers: the stratum corneum *(SC),* stratum granulosum *(SG),* stratum spinosum *(SS) and the* stratum basale *(SB). The dermis constitutes of two layers: the papillary dermis and the reticular dermis. The epidermis and dermis are separated by the dermal-epidermal junction (DEJ). Adapted from Wong and Chang (2008).*

Along with the basement membrane, the DEJ also contains hemidesmosomes and anchoring fibrils which anchor the epidermis to the dermis (Burgeson and Christiano 1997; McGrath *et al.* 1995). The dermis is located directly under the DEJ and is comprised of the upper papillary dermis and a thicker reticular dermis. Since the epidermis lacks blood vessels, it is solely reliant on the papillary dermis for nutrient exchange via diffusion through the basement membrane (Imanishi *et al.* 2008).

The DEJ forms rete ridges which penetrate deep into the papillary dermis and, much like the villi of the small intestine, maximise the surface area between the two layers. This increases the efficiency of nutrient delivery from the dermis to the epidermis (Briggaman and Wheeler 1975). Mechanically, this high surface area enhances the adhesion between the dermis and the epidermis and also protects the dermis from physical trauma by diffusing external forces along the area of contact (Xiong *et al.* 2013). The reticular dermis is mostly responsible for providing the skin's elasticity and acts as a primary architectural cushion for the underlying tissues (Dempsey and Lansing 1954; Langton *et al.* 2017). Below the dermis is the hypodermis which is primarily comprised of adipocytes. These store triglycerides and cholesteryl esters as a metabolic energy source (Prattes *et al.* 2000). Aside from vascular and neural cells, the mesenchyme-derived fibroblast is the main resident cell of the dermis (McDougall *et al.* 2006). This cell is tasked with the production and deposition of a variety of ECM components (Abraham *et al.* 2010; Lamme *et al.* 1996).

1.2 Components of the dermal extracellular matrix

The most important constituent of the dermis is the ECM itself. Some components of the ECM in the dermis are highly structured **(Fig. 1.2)**. They exhibit a variety of functions other than providing structural support, such as endowing the skin with elasticity, acting as a substrate for cell adhesion and mediating cell proliferation, migration, differentiation and gene expression (Naylor *et al.* 2011; Proksch *et al.* 2008).

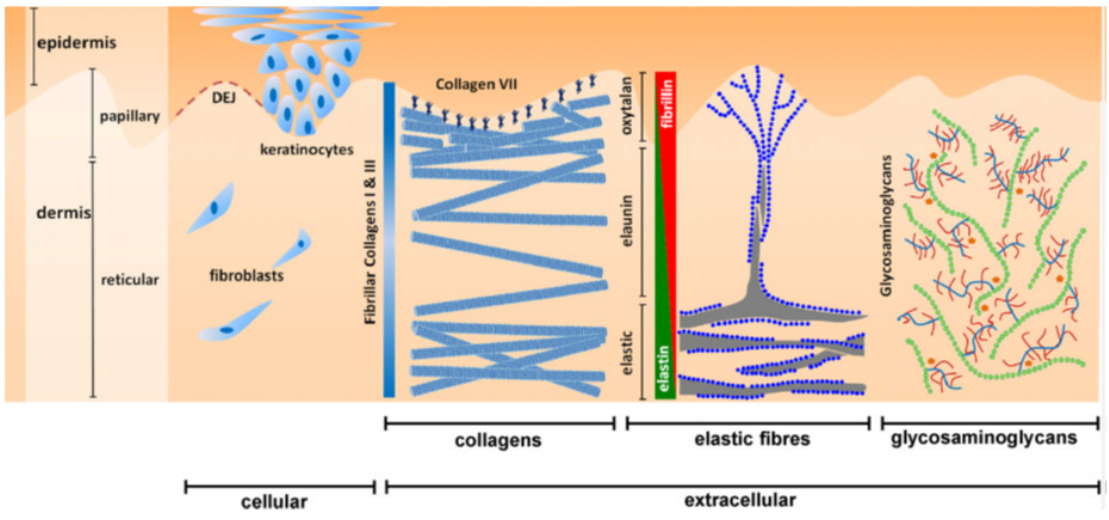

Figure 1.2: Cellular and molecular composition of the skin. The dermis is composed mainly of ECM. Collagens confer structural stability, elastic fibres endow the skin with resilience and glycosaminoglycans play an important role in skin hydration and metabolism. Reproduced from Naylor et al. *(2011).*

1.2.1 General overview of collagens, proteoglycans and major modifiers of the extracellular matrix

The collagens are a major ECM component, important in the scaffolding and maintenance of various connective tissues. The fibril forming collagens are composed of a triple helix (Gelse *et al.* 2003) with each polypeptide consisting of Gly-X-Y repeats (Brodsky and Persikov 2005). Type I is the most abundant of all the fibril forming collagens and can combine with type III in fibres of the reticular dermis (Fleischmajer *et al.* 1990; Gelse *et al.* 2003). Helical integrity of fibril forming collagens gives them a high load bearing and tensile strength (Kadler *et al.* 2007; Roeder *et al.* 2002). In contrast to fibril forming collagens, collagen IV creates an aggregating network by binding fibronectin, laminins and nidogens, forming a flattened, porous mesh in basement membranes such as in the DEJ (Fleischmajer *et al.* 1998; Gelse *et al.* 2003). As such, it plays a key role in the transduction of signalling molecules and nutrients.

Another major component of the ECM is the proteoglycans. Although these are found within the ECM of most connective tissues, they are most abundant in joints (Onnerfjord *et al.* 2012). They are defined by a glycoprotein chain with at least one, but often more, glycosaminoglycans (GAGs) interspersed along the core polypeptide (Sarrazin *et al.* 2011). Within the skin, the hydroscopic and flexible nature of hyaluronans, in particular, make them an effective space filler within the ECM which has even been described as a hydraulic shock absorber (Evanko *et al.* 2007; Scott *et al.* 1998).

The ability of these assemblies to bind and crosslink is inherent to the overall network and structure of the ECM in all tissues. This is achieved through the induction of crosslinks by enzymes such as transglutaminase and lysyl oxidase (LOX) (Heck *et al.* 2013). LOX is also involved in the crosslinking of elastin in elastic fibres (Liu *et al.* 2004). Laminins and fibronectins, integral to basement membranes, are also crosslinked via di-sulphide bonding (Keski-Oja 1976; Yurchenco 2011; Kalkhof et al. 2008). These mechanisms are not only important to the stability of the ECM, but also for rendering the network insoluble. Transglutaminase-2, for instance, is extremely important for maintaining ECM insolubility (Hynes and Naba 2012; Lorand and Graham 2003).

Equally as important, the ability of a tissue system to selectively dismantle this vast, multicomponent ECM network is vital for turnover and repair. An important subset of ECM proteases is the matrix metalloproteinase (MMP). This major group of zinc-dependent

endopeptidases is found in most tissues and have the ability to hydrolytically cleave a variety of ECM substrates (Stamenkovic 2003; Chakraborti *et al.* 2003).

1.2.2 Fibrillin microfibrils and the dermal elastic fibres

Along with other members of the ECM, the elastic fibre is an integral ECM component of all dynamic connective tissues such as, lungs, blood vessels, bladder and skin. It has a particular role in endowing these tissues with elastic properties (Kielty *et al.* 2002; Langton *et al.* 2017). The elastic fibre itself exhibits remarkable resilience and elasticity, capable of unforced, passive deformation and recoil (Baldwin *et al.* 2013; Bhushan *et al.* 2010; Kao *et al.* 2016). Both fibrillin microfibrils and elastin are the two integral constituents of elastic fibres, the structural degradation of which can have deleterious effects on the dermal elastic fibre system (Rock *et al.* 2004; Sakai *et al.* 1986; Sherratt 2009).

1.2.3 Dermal elastic fibre organisation

Elastic fibres exhibit a structured organisation in skin **(Fig. 1.2)** (Cotta-Pereira *et al.* 1976; Dahlbäck *et al.* 1990). Thick horizontal bundles of elastic fibres dominate the deep reticular dermis of the skin. These so called reticular fibres run parallel to the surface of the skin and form an elastic layer. Thinner, perpendicular elastic elaunin fibres crosslink with the reticular fibres and run to the more superficial papillary dermis, where they connect with oxytalan fibres (Montes 1996). Oxytalan fibres are composed solely of fibrillin microfibrils and extend through the papillary dermis to the basement membrane where they are thought to interact with the heparin sulphate proteoglycan: perlecan (Tiedemann *et al.* 2005). This organized network of elastic fibres endows the skin with elasticity throughout all its layers (Kielty, Sherratt, *et al.* 2002) and provides the continuous flexibility all vertebrates need during motion. Interestingly both fibrillin microfibril and elastin exhibit marked longevity (Shapiro *et al.* 1991); however, certain MMPs and serine proteases are known to cleave elastic fibres (Ashworth, Murphy, *et al.* 1999). These enzymes become deregulated with age (Brennan *et al.* 2003; Quan *et al.* 2009). In fact, a major factor of connective tissue degeneration is attributed to the progressive deterioration of the elastic fibre network and its components (Langton *et al.* 2010; Warren *et al.* 1991; Watson *et al.* 1999).

1.2.4 Elastic fibre composition

The accepted dogma is that fibrillin microfibrils are assembled followed by elastin deposition directly on the microfibril template (Feneck *et al.* 2018; Rock *et al.* 2004). As such, the elastic fibre is comprised of an amorphous elastin core, surrounded by a protective fibrillin microfibril sheath.

Elastin itself constitutes 90% of the elastic fibre, making it the most abundant constituent (Kielty, Sherratt, *et al.* 2002).

1.2.5 Elastic fibre longevity

Whereas most intracellular proteins and extracellular proteins have a biological half-life ranging from minutes and hours (Aziz *et al.* 2016; Brinster *et al.* 1979; Kuehl and Sumsion 1970) to a few days (Price *et al.* 2010), several components of the ECM are remarkably long-lived by comparison. In skin, the half-life of collagen type I was an estimated 15 years and, in cartilage, collagen type II was estimated at a staggering 117 years (Verzijl, DeGroot, Thorpe, *et al.* 2000). Elastic fibres are no exception to this longevity. Although mean turnover for elastin was extrapolated in the late seventies using dietary estimates (Stenhouse and Baxter 1977), the permanence of elastin and its microfibrillar template in resident human tissues was elegantly demonstrated by Shapiro *et al.* (1991) using two distinct methods. The first was using aspartic acid racemization whereby L-enantiomers of amino acids slowly and predictably convert to D-enantiomers over an individual's lifetime. This allowed the age of long-lived elastic fibre proteins to be determined. The second was by measuring the levels of radioactive isotope ^{14}C within purified elastin, which had been incorporated into the carbonaceous tissues of organisms in the late 1950s as a result of nuclear weapons tests and provides a useful dating tool in biogenic material. Using both these means, Shapiro *et al.* (1991) estimated the mean residence time of elastin, purified from human lung parenchyma, to be 74 years. In the same study, they went on to show that microfibrils and other non-elastin components of the elastic fibre also contributed a large proportion of total D-aspartate. This indicated that the age of fibrillin microfibrils highly correlated with that of elastin and they were, therefore, equally long-lived. It is important to consider the longevity of these ECM assemblies in this PhD project as it serves as the fundamental reason behind the damage accumulation during the photoageing process.

This section has reviewed the anatomy, function and ECM composition of skin, with a particular focus on the dermal elastic fibre and its fibrillin microfibril constituent. Since this PhD aims to demonstrate tissue-dependent differences between fibrillin microfibrils derived from skin and eye, it is next necessary to review the eye with a similar context. Intriguingly, as an organ, although the eye plays an entirely unique function in comparison to skin, both share the presence of these versatile ECM components.

1.3 Eye anatomy

The eye is a complex organ composed of many different tissues and cell types whose combined functions allow the remarkable evolutionary feat of sight **(Fig. 1.3)**. Diffuse light first passes through the cornea which, much like skin, is mainly comprised of an epithelium, a stroma and an endothelium (Jacob and Naveen 2016). It then travels through the aqueous humour-filled anterior chamber and the pupil, which functions as a varying aperture, creating and directing a column of light to the lens. Here, light is focused through to the posterior chamber and onto the macular region of the retina.

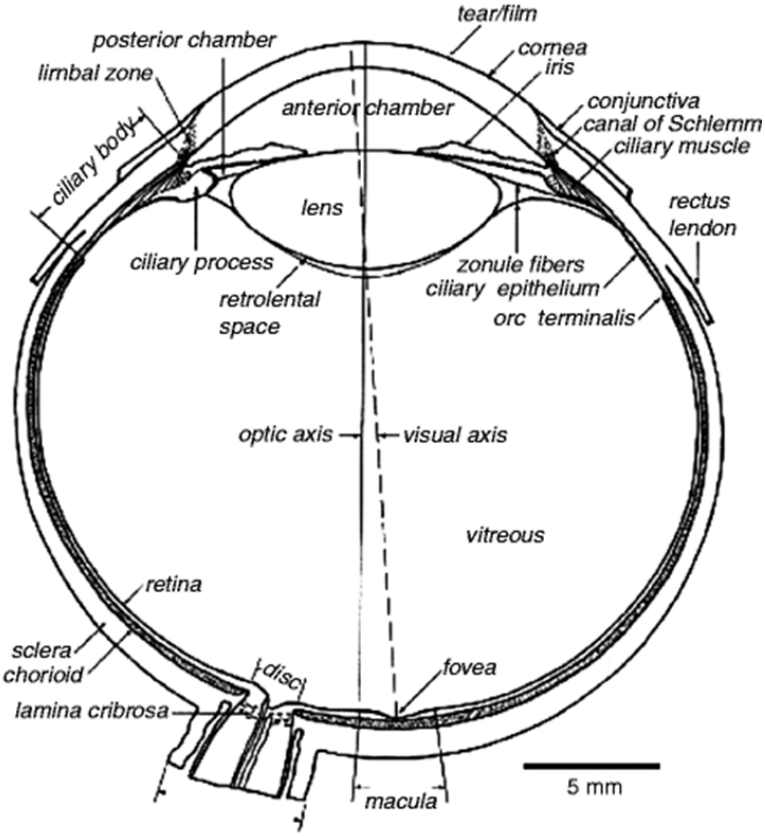

Figure 1.3: Cross-section depicting the gross anatomy of the eye. It is comprised of three main compartments: the anterior chamber between the cornea and the iris, the posterior chamber between the anterior side of the iris and the posterior side of the lens and the vitreous chamber behind the lens and ciliary zonule. Within these chambers are three layers: the outer fibrous layer consisting of the cornea and sclera, the middle vascular layer consisting of the iris, ciliary body and the choroid, and the inner nervous layer consisting of the retina. The lens sits against the iris, within the posterior chamber, suspended in place by the ciliary zonules. Reproduced from Garhart and Lakshminarayanan (2014).

1.4 Ciliary components of the eye

Focusing of light through the lens is achieved through the process of accommodation driven by the ciliary components of the eye **(Fig. 1.4)**, where the muscles within the ciliary body exert a tensile pull on the zonular fibres attached to the lens (Burd *et al.* 1999). This leads to its deformation which changes the angle of light refraction.

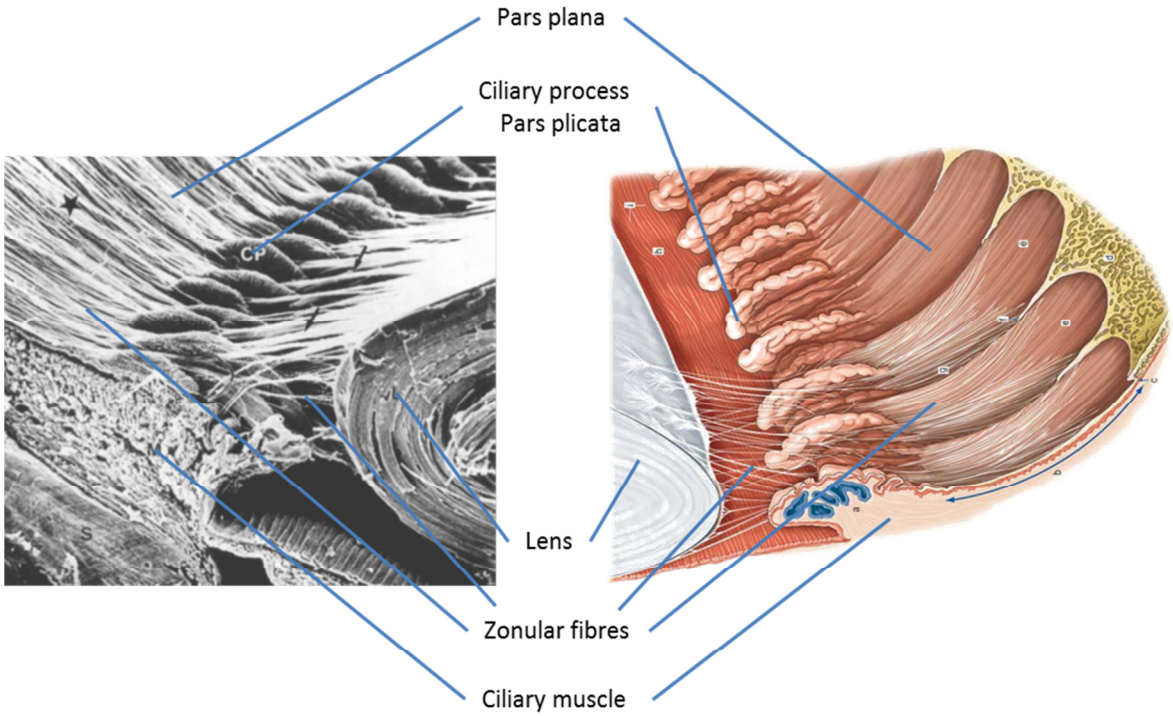

Figure 1.4: A scanning electron micrograph (EM) and schematic presenting the anatomy of the eye's ciliary tissue. The ciliary body consists of the smooth pars plana, the ridged pars plicata (with the ciliary processes at its ends) and the underlying ciliary muscle. The zonular fibres are seen in two distinct locations: along the surface of the pars plana and between the lens and the base of the pars plicata where they are referred to as the ciliary zonules. Scanning EM taken from Tamm and Lütjen-Drecoll (1996) and schematic adapted from Hogan et al. *(1971).*

1.4.1 Ciliary body

The ciliary body itself consists of three parts: the overlying anterior pars plicata and posterior pars plana and the underlying ciliary muscle (Tamm and Lütjen-Drecoll 1996). The ridges of the pars plicata are known as the ciliary processes, which protrude outward into the posterior chamber. These are densely vascularised and function mainly as producers and secretors of aqueous humour. The valleys of the pars plicata between the ciliary processes, however, function as the main anchoring site of the ciliary zonules which consist of fibres which connect to the lens. These insert directly into the basal lamina of non-pigmented epithelial (NPE) cells of the ciliary epithelium deep within these valleys. Since these cells highly express both fibrillin-1 and fibrillin-2, it is

hypothesised that they may be responsible for zonule fibre synthesis during development (Godwin *et al.* 2018; Shi *et al.* 2013). The valleys become the pars plana which are mostly covered by a dense layer of parallel zonular fibres. Contrary to the ciliary zonules, which insert within the valleys of the anterior pars plicata, these fibres run along the surface on the pars plana without insertion until they reach the posterior extremity of the ciliary body where they aggregate and insert into the basal lamina of NPE cells (Tamm and Lütjen-Drecoll 1996). The ciliary muscle lies below the pars plana and pars plicata at the base of the ciliary body, and consists mainly of smooth muscle bundles capable of contraction during the accommodation process. The contraction of the muscle is inversely proportional to the tensile pull of the ciliary zonules by shifting their anchoring points within the plans plicata distally toward the lens. This relaxes the tension on the ciliary zonules which returns the lens to its default spherical shape (Burd *et al.* 1999; Delamere 2005).

1.4.2 Ciliary zonules

The ciliary zonules refer specifically to the zonular fibres which run from the base of the pars plicata to the lens itself, where there they anchor directly into the lens epithelium. The fibres exist as macro-fascicle-like structures comprising of aligned bundles of fibrillin microfibrils held together by secondary bundles which circumferentially wrap around the main structure (Godwin *et al.* 2018; Hiraoka *et al.* 2010). As networking assemblies of the ECM, fibrillin microfibrils associate to several proteins within the ciliary zonules, such as latent transforming growth factor beta (TGFβ)-binding protein 2 (LTBP2; Inoue *et al.* 2014) and a disintegrin and metalloproteinase with thrombospondin motifs protein 10 (ADAMTS10; Kutz *et al.* 2011), which are thought to stabilise the zonule structure. As with skin basement membranes, these fibrillin microfibrils are also thought to anchor directly to the basal lamina of the lens and pars plicata epithelia by interacting with perlecan (Tiedemann *et al.* 2005) but also with ADAMTS4 (Collin *et al.* 2015).

1.5 Fibrillin microfibrils

Having reviewed both the anatomy of both skin and eye, and the major roles fibrillin microfibrils play within, it is next necessary to review these assemblies in more detail. In skin, fibrillin microfibrils exist predominantly within elastic fibres (Feneck *et al.* 2018; Rock *et al.* 2004; Sakai *et al.* 1986). However, they also exist completely separate from elastic fibres in tissues such as the ciliary zonule (Godwin *et al.* 2018; Hiraoka *et al.* 2010). Since zonular fibrillin microfibrils function very differently from those in elastic fibres, contributing heavily to the eye's ability to focus (Burd *et al.* 1999), it indicates that these assemblies play other major roles which are not elastic fibre-

mediated. Although, it is clear that fibrillin microfibrils play structurally and mechanically distinct roles in skin compared to in eye, how they do this on a molecular scale remains poorly understood. However, the answer may lie in how adaptable their structure and composition might be in relation to those different roles. In order to put this in context, it is next necessary to review the structure and composition of the fibrillin microfibril itself.

1.5.1 Fibrillin microfibril ultrastructure

The fibrillin microfibril is an exceptionally large macromolecular, polymeric glycoprotein (Cain *et al.* 2006) whose ultrastructure resembles beads on a string **(Fig. 1.5)** (Baldock *et al.* 2001; Godwin *et al.* 2018). The average periodicity (inter-bead distance) is commonly considered to be 56 nm and the length of an individual repeat is 160 nm. Atomic force microscopy (AFM) and rotary shadowing electron microscopy (EM) show these repeats as flexible molecules with both rod-like (interbead) and globular (bead) regions (Kielty *et al.* 2005).

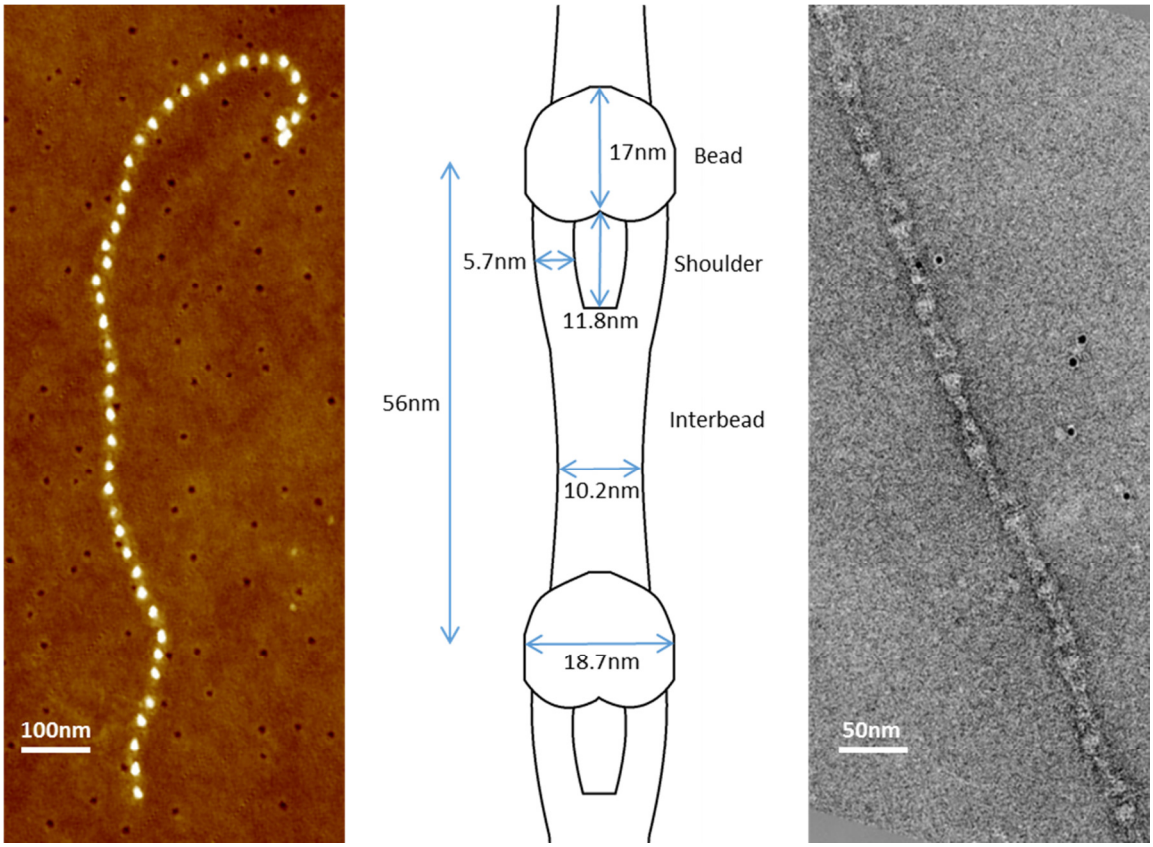

Figure 1.5: The fibrillin microfibril's characteristic beads-on-a-string ultrastructure. Having been studied extensively with AFM and EM, it consists of a polymeric assembly of individual bead and interbead repeats. The periodicity (bead to bead distance) is reportedly ~56 nm, however, this can vary depending on species, tissue location (Lu et al. *2006; Sherratt* et al. *1997), maturation (Sherratt* et al. *1997) and damage (Hibbert* et al. *2015; Sherratt* et al. *2010). The bead itself is globular and easily visualised. The shoulder region stems from the bead and consists of two arms*

which join together with a physical space in between. EM image and microfibril dimensions reproduced and adapted from Baldock et al. *(2001).*

Although all fibrillin microfibrils have the same characteristic beads-on-a-string ultrastructure, they play very distinct roles in different tissues. Within elastic fibres, they serve as a template to amorphous elastin (Rock *et al.* 2004) and endow the connective tissues with elasticity and resilience (Kielty, Sherratt, et al. 2002; Langton et al. 2017) whereas in the ciliary zonule they act as stand-alone, suspensory ligaments (Godwin *et al.* 2018; Hiraoka *et al.* 2010) whose tensile strength allows lens accommodation (Burd *et al.* 1999). It is clear that this microfibrillar assembly has evolved to fit these two distinct roles; however, it remains unclear as to how and whether their structures have changed as a result. Additionally, fibrillin microfibrils are markedly long-lived (Shapiro *et al.* 1991) and laid down early in development (Sherratt *et al.* 1997), which suggests that tissue-specific differences to ultrastructure may be developmentally-mediated. Only two studies have demonstrated that fibrillin microfibril ultrastructure is both tissue- and development-dependent. Using scanning transmission EM and rotary shadowing EM, Sherratt *et al.* (1997) showed that both the mass and periodicity (bead to bead distance) of fibrillin microfibrils isolated and purified from foetal bovine tissues differed between aorta, skin and nuchal ligament. This served as the first indication that the structures and composition of these assemblies may be directly related to the functions they play in different tissues. Additionally, Sherratt *et al.* (1997) also found that a decrease in microfibril mass and periodicity correlated directly with foetal age, indicating that these assemblies undergo a post-translational process of maturation. Lu *et al.* (2006) later went on to show specific differences in fibrillin microfibril bead morphology between ciliary zonule and aorta isolations from bovine tissue. Although these studies indicate that fibrillin microfibril ultrastructure may correlate directly with its tissue function and maturation, these observations have never been made in humans. The protein composition of the fibrillin microfibril is predominantly fibrillin; however, a host of associated proteins are also able to network with it (Thomson *et al.* 2018). To this effect, tissue- and developmental-dependent differences in fibrillin microfibril composition have not been studied to date.

1.5.2 Fibrillin-1 structure

Three fibrillin isoforms have been identified in humans. Fibrillin-1 **(Fig. 1.6)** is expressed most abundantly and represents the most common constituent of fibrillin microfibrils. Fibrillin-2 is mostly expressed during neonatal development (Zhang *et al.* 1994). Structurally, it is largely homologous to fibrillin-1 but exhibits dissimilar expression patterns. Fibrillin-3 expression has been detected

solely in the brain; however, its ability to form microfibrils remains unknown (Corson *et al.* 2004). In skin, fibrillin-1 expression, secretion and deposition is mostly attributed to fibroblasts, although keratinocytes have been shown to express fibrillin-1 (Haynes *et al.* 1997). Interestingly, fibrillin-1 and its microfibrils exhibit remarkable conservation throughout most of life's evolution. Its initial formation, (first mapped to the cnidarians) predates the formation of elastin (first mapped to the jawed vertebrates) by ~3.4 billion years (Baldwin *et al.* 2013; Piha-Gossack *et al.* 2012).

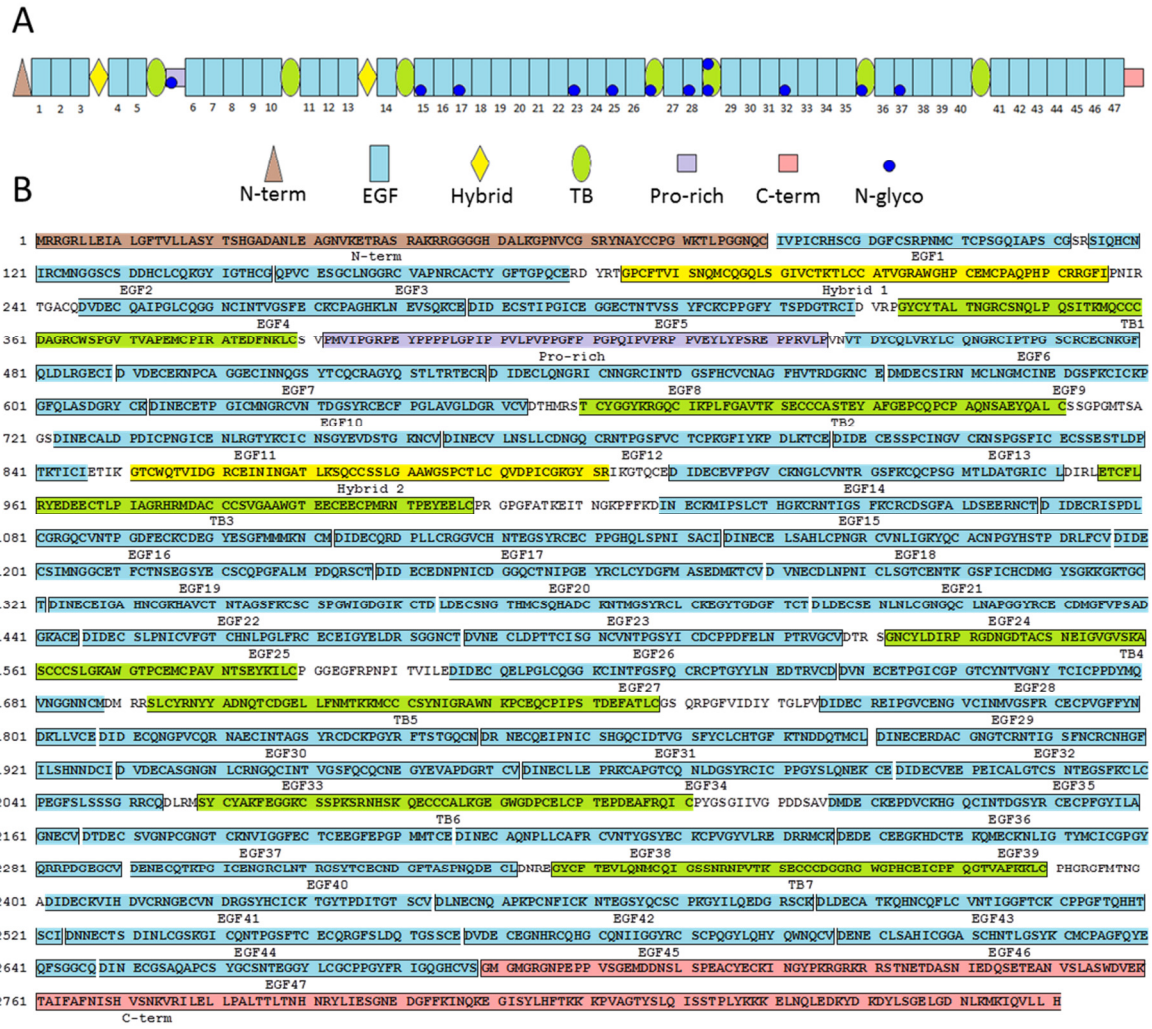

Figure 1.6: The primary and domain structures of fibrillin-1. Fibrillin-1 has a molecular weight of 312.2 kDa (Kielty et al. *2005) and is comprised of an N-terminal region, 47 epidermal growth factor-like domains (EGF), 7 cysteine-rich TB domains (latent transforming growth factor β binding protein (LTBP) – like regions) and 2 hybrid domains which bear homology to EGF domains and TB domains* ***(A)****. On the N-terminal side, there is a proline-rich domain, suggested to be a hinge region (Kielty* et al. *2005). This motif is glycine-rich in fibrillin-2 and both proline- and glycine-rich in fibrillin-3 (Corson* et al. *2004). The primary sequence of fibrillin-1 consists of 2871 amino acids* ***(B)****. Sequences corresponding to each domain are colour-coded and labelled to match the domains in the schematic* ***(A)****.*

EGF domains of fibrillin-1 are also commonly found in other large proteins such as agrin (Hoch *et al.* 1994), hemicentin (Dong *et al.* 2006) the thrombospondins (Liu *et al.* 2009), the LTBPs (Jensen *et al.* 2009) and the mucins (Dekker *et al.* 2002). They each contain three disulphide bonds between cysteine residues which convey high stability to their internal structure (Downing *et al.* 1996). The majority of the EGF domains in fibrillin-1 contain calcium binding regions (Handford *et al.* 1995). Varying the presence of calcium greatly changes the ultrastructure of fibrillin microfibrils. There is a reduction of periodicity between beads in the absence of calcium and a measurable widening of the bead (Werner *et al.* 2000). An increase in flexibility is also observed (Kielty *et al.* 2005).

The TB domains are named after their homology to LTBP and some of these regions are known to covalently bind and store TGF-β (Lack *et al.* 2003). These domains are unique to the fibrillin superfamily (including LTBPs) and occur in no other protein structure. They contain four di-sulphide bonds which stabilise the domain's internal structure (Yuan *et al.* 1997). TB domains are found seeded among the various EGF-rich regions of fibrillin-1. They are globular motifs comprising of two α-helices and six β-sheets (Kielty *et al.* 2005). The fourth TB domain between EGF26 and 27, has an RGD amino acid sequence capable of binding to integrin receptors α5β1 and αvβ3 (Bax *et al.* 2003). These indicate adherence points that may be integral for fibrillin microfibril deposition and assembly.

Fibrillin's hybrid motifs are also unique to their protein superfamily. At the N-terminal side of the domain, they adopt a TB motif-like structure and at the C-terminal side they adopt a EGF-like structure (Reinhardt, Gambee, *et al.* 2000). These hybrid domains have been hypothesised to be important in intramolecular di-sulphide crosslinking which stabilizes the internal microfibril structure (Kielty *et al.* 2005). Two furin cleavage sites have been identified in fibrillin-1 (Kielty *et al.* 2005): The N-terminus of fibrillin-1 contains the first site within the first 29 amino acid sequence and the C-terminus contains the second site located after the final EGF domain, both comprising of an RAKRR motif (Ritty *et al.* 1999). Furin processing appears be very important to fibrillin microfibril deposition and assembly (Raghunath *et al.* 1999).

1.5.3 Marfan syndrome

The protein structure and folding of fibrllin-1 is inherently linked to ultrastructure of its native microfibril. As a result, mutations in fibrillin-1 can lead to measurable changes in microfibril ultrastructure, and hence its function (Kielty, Raghunath, *et al.* 1998). Marfan syndrome (MFS) is

an autosomal dominant disorder specifically caused by mutations in fibrillin-1 (Pyeritz 2000). As such, it provides an indispensable opportunity to study the pathological effects of genetically induced abnormalities in the assembly, deposition and structure of fibrillin microfibrils. The incidence of MFS is estimated as 1 in 10,000 within the general population, with 85% being attributed to family history (Kielty *et al.* 2005). Clinically, MFS is characterised by life threatening cardiovascular disease along with severe skeletal and ocular defects (Giampietro *et al.* 2002). Skeletally, patients exhibit increased height and limb length, skeletal chest deformities, joint laxity and scoliosis (Kaissi *et al.* 2013). Ocular defects often include myopia and lens dislocation (ectopia lentis) due to the disruption of the ciliary zonules (Kainulainen *et al.* 1994). By far the most serious clinical complication for MFS patients is aortic rupture or heart valve (mitral or aortic) prolapse, both of which cause cardiac failure in over 90% of associated patient deaths (Murdoch *et al.* 1972). MFS can also manifest in neonatal stages of human development however, these individuals suffer perinatal death usually due to congestive heart failure (Kainulainen *et al.* 1994).

Over 350 mutations have been identified in fibrillin-1 with 68% of these categorised as missense mutations localised mainly within the EGF regions (Kielty *et al.* 2005). Classical MFS is normally attributed to changes either in cysteine residues or within the calcium binding epitopes of fibrillin-1. The severity of the disease, however, is dependent on the mutation's location within the protein structure and the domain's propensity to bind calcium (Kettle *et al.* 1999; Kielty *et al.* 2005). Mutations unrelated to cysteine residues or calcium affinity are rarer and usually found as alterations in N-glycosylation sites or in glycine (Robinson *et al.* 2002). The fact that fibrillin-1 mutation location correlates with MFS severity suggests different domains of fibrillin-1 play distinct roles within the native fibrillin microfibril structure and function. For instance, mutations specifically between fibrillin-1 domains TB3-EGF22 have been shown to cause neonatal MFS and severe symptoms such as aortic dissection in individuals younger than 16 years of age (Tiecke *et al.* 2001).

The fact that mutations in fibrillin-1 can cause such severe downstream effects highlights the importance of the fibrillin microfibril, not only in tissue structure and mechanics, but also in tissue homeostasis. As a networking ECM assembly, the fibrillin microfibril interacts with a number of extracellular associated proteins, the disruption of which may be the reason behind these fibrillinopathies. Furthermore, it demonstrates that changes in fibrillin microfibril ultrastructure go hand-in-hand with changes in fibrillin-1 protein structure. This is an important consideration when

investigating tissue-dependent differences and UV-induced changes to fibrillin microfibrils during this PhD.

1.5.4 Associated proteins

Although fibrillin microfibrils are primarily composed of fibrillin-1, a variety of proteins have been shown to associate with these assemblies. As such, it is perhaps more appropriate to classify the fibrillin microfibril as a multi-component structure. Identifying and studying these interactions is inherent for understanding the role of the fibrillin microfibrils in health and disease.

The N-terminal region of fibrillin-1 has proved to be the most interactive, capable of binding itself and the C-terminal region of other fibrillin-1 pro-peptides (Marson *et al.* 2005), as well as many associated proteins (Kielty *et al.* 2005; Thomson *et al.* 2018). Many of these interactions **(Fig. 1.7)** implicate fibrillin microfibrils in a host of novel roles, some integral to the ECM's architecture, and others to the control of the cellular microenvironment.

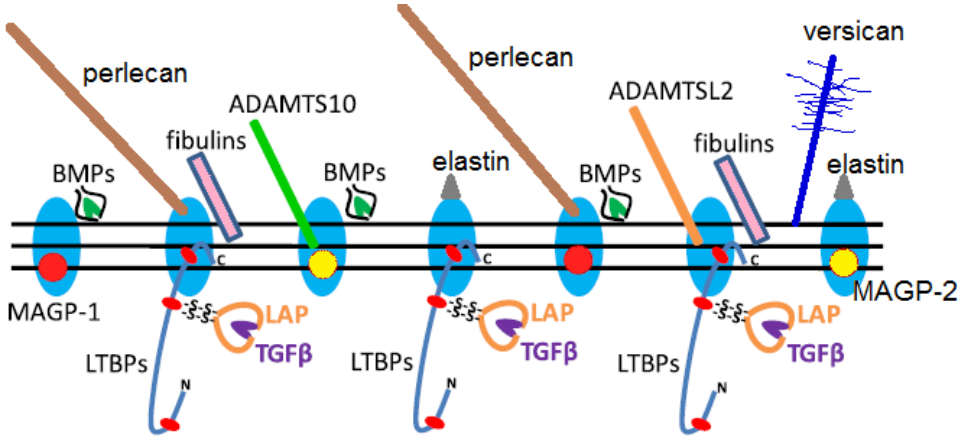

Figure 1.7: A variety of proteins are known to associate to fibrillin microfibrils. Aside from elastin (grey) in the elastic fibre, these also include signalling peptides and growth factors such as TGF-β (purple) and BMP (bone morphogenetic protein) (green), fibrillin-like LTBPs (blue), ECM fibulins (pink), zinc-dependent protease ADAMTS (light green) / ADAMTS ligand (orange) and the microfibril assembly controlling MFAP2 (red) and MFAP5 (yellow). Certain proteoglycans such as versican (dark blue) and perlecan (brown) have also been shown to associate. Adapted from Jensen et al. *(2012).*

As an integral component of the elastic fibre system, tropoelastin is a long known associated protein which co-purifies with fibrillin microfibrils at high affinities when extracted from elastic fibre tissue (Rock *et al.* 2004).

The microfibril-associated proteins (MFAPs) are a glycoprotein family heavily integrated with the ultrastructure of fibrillin microfibrils. MFAP2 (also known as microfibril-associated glycoprotein 1:

MAGP1) has one of the highest affinities to fibrillin-1 and binds specifically to the bead region of the microfibril (Henderson *et al.* 1996). It consists of a negatively charged N-terminal region, a positively charged C-terminal region (Kielty *et al.* 2005) and a matrix binding domain which enables its interaction with fibrillin-1 and other components of the ECM (Segade *et al.* 2002). Its calcium dependent interactions have been implicated not only in elastic fibre assembly (Jensen *et al.* 2001) but in ciliary zonule formation (Fujita *et al.* 2014) and ageing (Zheng *et al.* 2013) as well. MFAP4 contains a distinctive RGD region capable of binding αvβ3 integrin (Gibson *et al.* 1999) and plays a role in cell mediated microfibril assembly and elastogenesis (Pilecki *et al.* 2016). MFAP5 (MAGP2) has multiple binding sites on fibrillin-1 and its microfibril (Hanssen *et al.* 2004) and, like all other members of its family, it also plays a role in elastic fibre formation (Lemaire *et al.* 2007). Its interactions with fibrillin microfibrils have also been implicated in thoracic aortic aneurism and dissection (Barbier *et al*. 2014).

A number of proteoglycans interact with fibrillin microfibrils. Versican plays a versatile role in networking ECM assemblies and regulating their adhesion to cells (Wight 2002). It binds directly to the N-terminal region of fibrillin-1 and has been implicated in the structural integration of fibrillin microfibrils into the surrounding ECM (Isogai *et al.* 2002). Together with hyaluronan, it also forms a complex within the ciliary body (Ohno-Jinno *et al.* 2008). Additionally, the interaction between fibrillin microfibrils and basement membranes at the ciliary body and at the dermal epidermal junction is mediated by its association with the proteoglycan perlecan (Shi *et al.* 2013; Tiedemann *et al.* 2005).

The fibulins are another family of proteins with functional interactions with fibrillin microfibrils. Both fibulins-1 and -2 have been shown to bind the N-terminal region of fibrillin-1 (Reinhardt, Sasaki, *et al.* 1996; Roark *et al.* 1995), the lectin domains on versican as well as the proteoglycans aggrecan and brevican (Olin *et al.* 2001). This suggests that, like versican, fibulin-2 and fibulin-1 may play a role in the integration of fibrillin microfibrils into the surrounding ECM. Fibulin-4 has also been shown to interact with fibrillin-1 (Choudhury *et al.* 2009). Although removing the exposure to fibulin-4 does not affect microfibril assembly, it decreases elastogenesis (McLaughlin *et al.* 2006). Its association to tropoelastin (Kobayashi *et al.* 2007) and LOX (Horiguchi *et al.* 2009) as well as fibrillin-1 (Choudhury *et al.* 2009), also suggests that it may be involved in the correct crosslinking and deposition of tropoelastin onto its fibrillin microfibril template. Interactions with fibulin-5 may

also play a role in microfibril function as depletion of this protein causes a disruption to elastic fibre assembly (Yanagisawa *et al.* 2002).

The LTBPs are a unique group fibrillin microfibril-associated proteins. As members of the fibrillin superfamily, they contain a number of regions of homology to all fibrillins. Once secreted, TB regions of LTBPs 1, 3 and 4 covalently bind the latent TGFβ complex (Saharinen *et al.* 1996). This then co-localises to fibrillin microfibrils in the ECM (Ono *et al.* 2009) and enables local regulation of TGFβ bioavailability. TGF-β is a multifunctional cytokine which acts as a mediator of neurogenesis, angiogenesis, immunorecruitment, wound healing, lineage determination, differentiation, proliferation, cell adhesion, apoptosis and ECM regulation (Massagué 1998). The storage of TGF-β by fibrillin microfibrils suggests that they play a major role in controlling tissue homeostasis (Lemaire *et al.* 2006). In fact, disruption of TGFβ signalling is a characteristic pathology of MFS (Neptune *et al.* 2003) and may play a role in its associated aortopathies (Franken *et al.* 2015). Interestingly, LTBP2 is the only member of its family which does not sequester TGFβ, however, it still co-localises to the fibrillin microfibril (Vehviläinen *et al.* 2009) and interacts with fibulin-5 to negatively regulate elastic fibre formation (Hirai *et al.* 2007; Sideek *et al.* 2014). It has also been implicated in correct ciliary zonule function since mutations can cause ectopia lentis (Khan *et al.* 2011). Additional to the sequestering of TGFβ, LTBP4 and its interplay with fibulins 4 and 5 is a requirement for elastic fibre assembly (Bultmann-Mellin *et al.* 2016; Noda *et al.* 2013).

Latent BMPs are another group of cytokines which associate with fibrillin microfibrils both *in vitro* and *in vivo* (Sengle *et al.* 2008). As with TGFβ, fibrillin microfibrils act as natural storage for BMP, co-localizing the growth factor to within the tissue matrix. This minimizes diffusion and enables its controlled mobilisation (Jensen *et al.* 2012). BMP cytokines induce a variety of changes in cell differentiation and migration.

Fibronectin is an ECM protein who's interaction with the fibrillin microfibril is integral to its assembly (Sabatier *et al.* 2009) and deposition (Kinsey *et al.* 2008). This association is also thought to regulate the interaction between LTBP1 and the fibrillin microfibril, which indicates another role of fibronectin in fibrillin-mediated TGFβ signalling (Zilberberg *et al.* 2012).

ADAMTSs and ADAMTS-like proteins (ADAMTSLs) are a group of fibrillin microfibril-associated proteins which have been implicated in a number of roles including tissue integrity, development, angiogenesis and inflammation (Apte 2009). Mutations in a number of these glycoproteins causes

similar genetic pathologies to those seen in fibrillin-1 (Ahram *et al.* 2009; Dagoneau *et al.* 2004; Le Goff *et al.* 2008). Interestingly, different members of the ADAMTSs are able to regulate fibrillin microfibril deposition. ADAMTS6 inhibits deposition whereas ADAMTS10 enhances and maintains it (Cain *et al.* 2016; Kutz *et al.* 2011). ADAMTSL2 interacts with both fibrillin-1 and LTBP1 which indicates a role in TGFβ signalling (Le Goff *et al.* 2008). ADAMTSL4 associates to fibrillin microfibrils in eye tissue and enhances microfibril deposition *in vitro* (Gabriel *et al.* 2012).

Although the elastin microfibril interfacers (EMILINs) were initially identified within elastic fibres, between elastin and their fibrillin microfibril templates (Bressan *et al.* 1993), only recently have EMILINS-1 and -2 been shown to be specifically targeted to the microfibril in skin, requiring the presence of fibronectin in the process (Schiavinato *et al.* 2016). These glycoproteins are also multifunctional regulators of cell activity such as adhesion (Spessotto *et al.* 2003), proliferation (Danussi *et al.* 2011), migration (Spessotto *et al.* 2006) and apoptosis (Mongiat *et al.* 2007, 2010), with a capability of modulating TGFβ processing (Schiavinato *et al.* 2012; Zacchigna *et al.* 2006). It is likely that the sequestration of EMILINs-1 and -2 within the elastic fibre contribute to tissue homeostasis

In summary, fibrillin microfibrils associate with a variety of proteins within their resident ECM, most of which play an important role in their assembly, elastic fibre integration, or homeostatic function. As such, this assembly is often described as supramolecular with its molecular composition being inherent to the myriad of functions it plays in different tissues.

1.5.5 Processing, secretion and assembly

The synthesis and deposition of fibrillin microfibrils is mainly attributed to fibroblasts (Long and Tranquillo 2003; Milewicz *et al.* 1992; Sakai *et al.* 1986). That being said, it remains unknown whether epithelial cells contribute to fibrillin microfibril assembly in tissue. In 1997, Haynes *et al.* demonstrated that isolated primary keratinocytes have the capacity to express fibrillin-1 and synthesise fibrillin microfibrils *in vitro* (Haynes *et al.* 1997). With this, they suggested these cells may contribute to oxytalan fibre synthesis in the dermis through the DEJ. Additionally, the epithelial-mesenchymal state of these cells may influence their ability to synthesise these assemblies (Baldwin et al. 2014).

Fibrillin microfibril assembly commences with cell production and secretion of monomeric fibrillin-1 (Ashworth, Kelly, *et al.* 1999; Jensen *et al.* 2014). The intracellular aggregation of fibrillin-1 is

prevented by the molecular chaperone calreticulin and the enzyme protein disulphide isomerase, which bind to the monomer and inhibit its homotypic interaction (Ashworth *et al.* 1999). Post-secretion, the N and C termini of fibrillin-1 are cleaved by furin, after which, it is proposed that these monomers dimerise through the homotypic interaction between these N and C termini (Ashworth *et al.* 1999; Marson *et al.* 2005). These dimers form the basic intermediate building blocks of fibrillin microfibril assembly. The cellular deposition of fibrillin-1 dimers and the assembly of the microfibril is thought to be mediated by interactions between fibronectin and RGD-dependent α5β1 integrin receptors on the cell surface (Sabatier *et al.* 2009). This suggests that the cells may physically adhere to an assembling microfibril, via fibronectin, before adding a fibrillin-1 dimer to the structure.

Two major models of fibrillin-1 alignment within the microfibril have been proposed **(Fig. 1.8)**: the hinged model (Baldock *et al.* 2001, 2006) and the staggered model (Kuo *et al.* 2007; Reinhardt *et al.* 1996) (see reviews : Jensen and Handford 2016 and Kielty *et al.* 2005). Both models were constructed by: 1) relating the ultrastructural features seen via negative stain and rotary shadowing scanning EM to fibrillin-1 specific antibody binding sites and 2) by relating the predicted theoretical axial mass distributions of the microfibril's bead and interbead to that of the fibrillin-1 domains' actual mass. Both models present eight fibrillin-1 monomers per microfibril bead and interbead repeat.

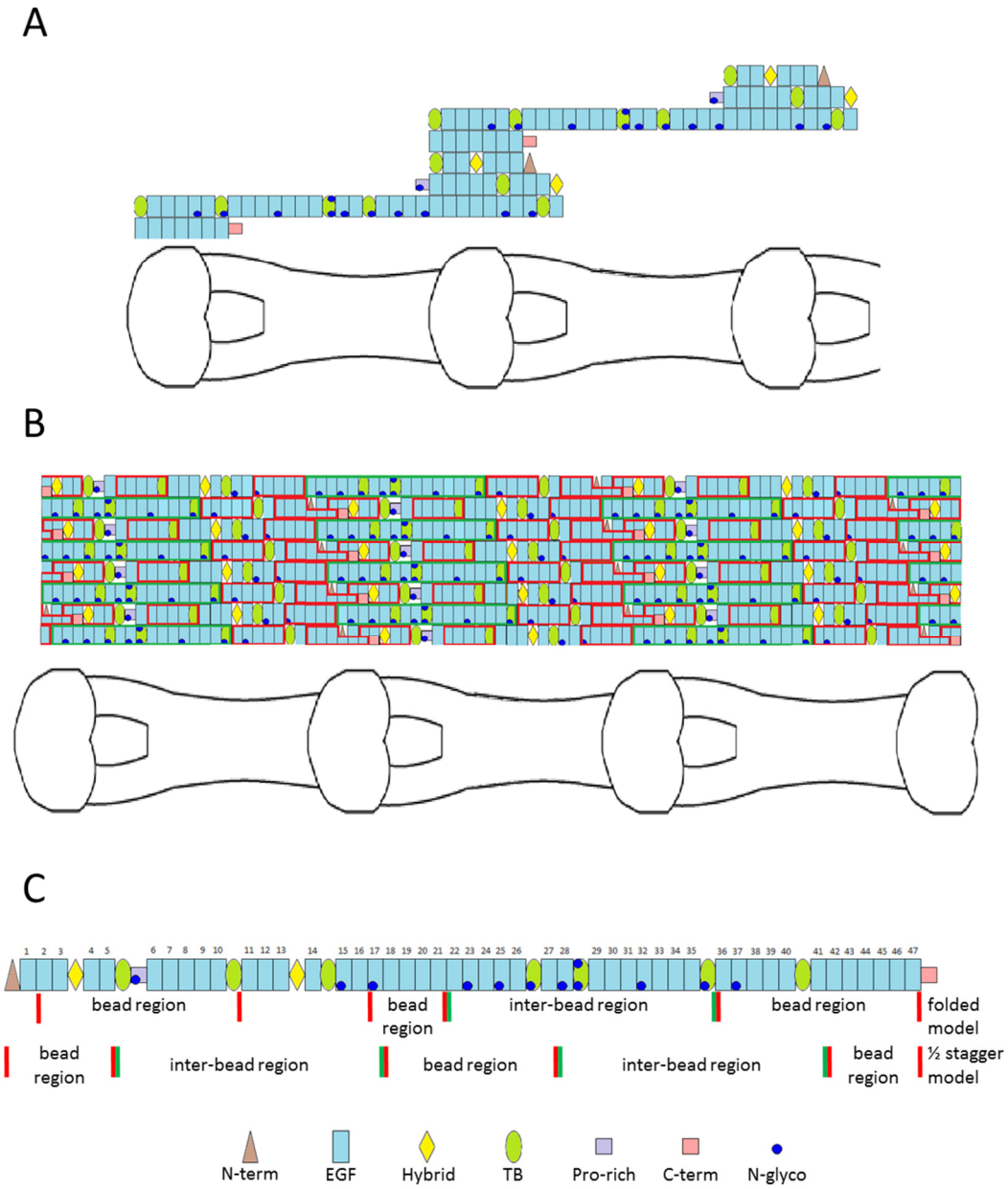

Figure 1.8: The folded model and staggered model of supramolecular organisation of fibrillin-1 within the microfibril. The folded model ***(A)*** *(Baldock* et al. *2001, 2006) proposes that the microfibril bead and shoulder region is composed of both the N-terminal half of the fibrillin-1 monomer up to EGF21 bound to the C-terminal epitope between EGF36 and 47, of another fibrillin-1 monomer. The N-terminal half is arranged as a globular epitope in three folds with a hinge predicted at the proline-rich domain and another at the second hybrid domain. The C-terminal region contains a single fold predicted to be at domain TB7. The inter-bead region is putatively composed exclusively of domains EGF22 to TB6. For simplification, two fibrillin monomers are shown in this schematic, although a total of eight are predicted per repeat. In contrast, the staggered model* ***(B)*** *(Jensen and Handford 2016; Kielty* et al. *2005) proposes that fibrillin-1 monomers (all eight are shown in this schematic) are aligned in 50% staggered array with a four domain overlap between the N- and C-termini. Due to this stagger and the consequential shift in domain alignment, the proposed bead and inter-bead overlap of fibrillin-1 domains differs heavily with that of the hinged model. Whereas the folded model proposed a single inter-bead region per fibrillin-1 monomer* ***(C)****, the half staggered proposes two: one estimated between TB1 and EGF17 and another between EGF28 and EGF41.*

1.5.6 Fundamental gaps in knowledge

Over the last half a century, we have learned much about the macromolecular nature of the fibrillin microfibril and the diverse roles it plays in the ECM. However, several fundamental gaps in knowledge persist, as its composition, supramolecular organisation and their relation to ultrastructure, remains poorly understood. Not only this, but evidence that the microfibril's ultrastructure can be dependent on tissue location (Lu *et al.* 2006; Sherratt *et al.* 1997), maturity and developmental stage (Sherratt *et al.* 1997) adds further complexity and further widens the knowledge gap. The tissue- and developmental-dependency of the fibrillin microfibril ultrastructure has only been shown in foetal and adult bovine, elastic fibre-rich tissues. Whether these variances relate to differences in composition or molecular arrangement still remains unknown. As such, part of this this PhD aims to assess these differences in humans, and between elastic fibre-rich and elastic fibre-poor tissues (such as ciliary body and skin), where fibrillin microfibrils play very different biophysical and structural roles. Doing so will reveal more about their ultrastructural diversity and its relation to composition and macromolecular organisation.

1.6 Collagen VI microfibrils

The collagen VI microfibril is another important, supramolecular ECM assembly often present in the same connective tissues as the fibrillin microfibrils. Due to similarities in size and dimension, these microfibrillar assemblies often co-purify together. During the PhD, this turned out to be advantageous, since its ultrastructure and composition could also be assessed alongside that of the fibrillin microfibril. This allowed comparisons to be made in order to ascertain whether changes seen in fibrillin microfibril structure and composition were assembly-specific or not. Because of this, it is also necessary to review the structure, composition and function of the collagen VI microfibril in comparison to fibrillin.

1.6.1 Collagen VI microfibril composition, assembly and ultrastructure

Like the fibrillin microfibril, the collagen VI microfibril is a large macromolecular, beaded ECM assembly commonly found in several connective tissues (Engvall *et al.* 1986). Unlike the fibrillin microfibril, which is predominantly composed of fibrillin-1, human skin collagen VI microfibrils can contain up to five different alpha (COL6A)-chains: COL6A1, COL6A2, COL6A3, COL6A5, COL6A6 **(Fig. 1.9)** (Cescon *et al.* 2015). The COL6A4 chain is not functional in humans due to a chromosome inversion which prevents its translation (Fitzgerald *et al.* 2008; Gara *et al.* 2008).

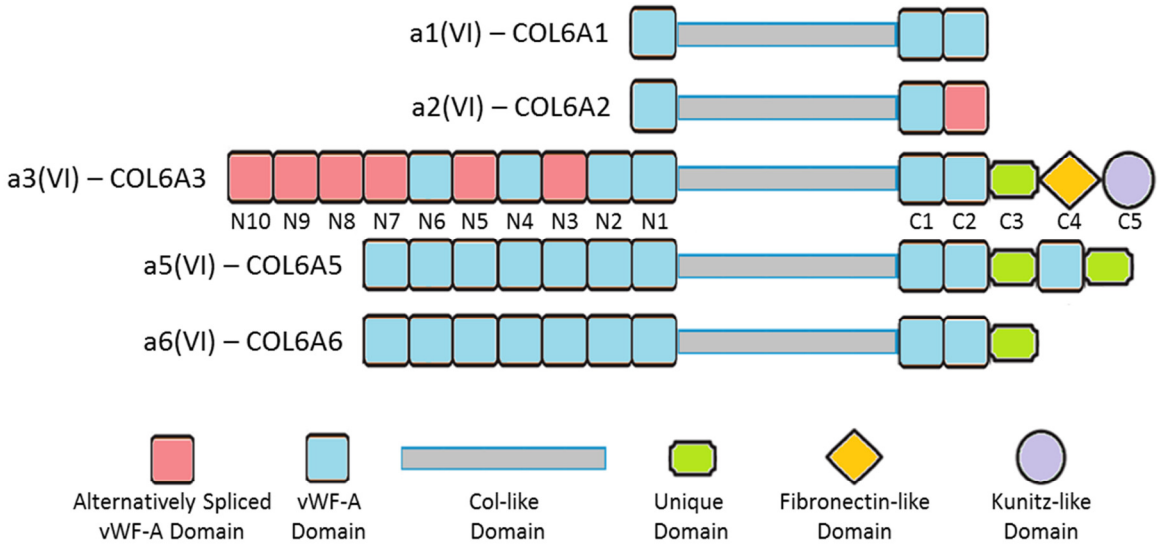

Figure 1.9: Domain structures of collagen VI alpha 1, 2, 3, 5 and 6 chains. All chains consist of a long helical col-like domain which is flanked at either side by two globular regions (Chu et al. *1989). COL6A1 and COL6A2 are the smallest chains and similar in molecular weight (~120kDa). Their helical domains are flanked by one so-called A-domain of von Willibrand factor (vWF-A) at position N1 and two vWF-A domains at positions C1 and C2 (Chu* et al. *1989). The COL6A3 chain is the largest of the five (~340 kDa), consisting of 10 vWF-A domains on the N-terminal side of the col-like helical region and two more on the C-terminal side (Chu* et al. *1990). The C3 position, at the C-terminal region of COL6A3, contains a proline-rich, unique region. The domain at the C4 position is homologous to the type III domains in fibronectin and the domain at the C5 position shares regions of identity with the Kunitz protease inhibitors. Although this domain is important for collagen VI microfibril assembly (Lamandé* et al. *2006), it is cleaved and removed shortly after (Aigner* et al. *2002). In fact, it is possible that the entire C2-C5 region is cleaved prior to microfibril maturation (Beecher* et al. *2011). COL6A5 and COL6A6 are rarer than the other three chains and structurally related to COL6A3 (Fitzgerald* et al. *2008). Both COL6A2 and COL6A3 are alternatively spliced. COL6A2 can contain three splice variants of the C2 vWF-A domain (Saitta* et al. *1990) and equally with COL6A3 which can also contain three splice variants encompassing the N3, N5 and N7-N10 vWF-A domains (Dziadek* et al. *2002).*

Collagen VI microfibril synthesis requires both COL6A1 and COL6A2 chains (Bonaldo *et al.* 1998). As such, initial collagen VI microfibril assembly begins intracellularly, where three alpha chains form a monomer consisting of a 1:1:1 stoichiometric ratio of COL6A1, COL6A2 and either COL6A3, COL6A5, or COL6A6 (which can be interchangeable) (Gara *et al.* 2011). These monomers go on to form dimers and then tetramers within the cell, which go on to assemble a collagen VI microfibril **(Fig. 1.10)** extracellularly, post-secretion (Chu *et al.* 1988; Furthmayr *et al.* 1983). Recent work by Maaß *et al.* (2016) has shown that, although all five alpha chains of collagen VI are all able form functional collagen VI microfibrils, each monomer within the tetramer is homotypic, consisting of either COL6A3, -4 or -5 chains alongside COL6A1 and -2 chains (Maaß *et al.* 2016). This means

that a single tetramer cannot contain a mixture of all these three alpha chains, but a microfibril may consist of different heterotypic tetramers containing up to all of them. Although the presence of either COL6A3, -4 and -5 within a tetramer is interchangeable, vWF-A domain N5 of the COL6A3 chain is required for collagen VI microfibril assembly (Fitzgerald *et al.* 2001). This indicates that although collagen VI microfibrils vary in their COL6A5 and COL6A6 chain composition, and may not contain these two chains at all, the COL6A3 chain is consistently present within all these microfibrils (Maaß *et al.* 2016). Like the fibrillin microfibril, collagen VI microfibrils have a beads-on-a-string ultrastructure which has also been studied extensively over the years using EM (Baldock *et al.* 2003; Godwin *et al.* 2017; Kielty *et al.* 1991) and AFM (Hibbert *et al.* 2015; Sherratt *et al.* 2004).

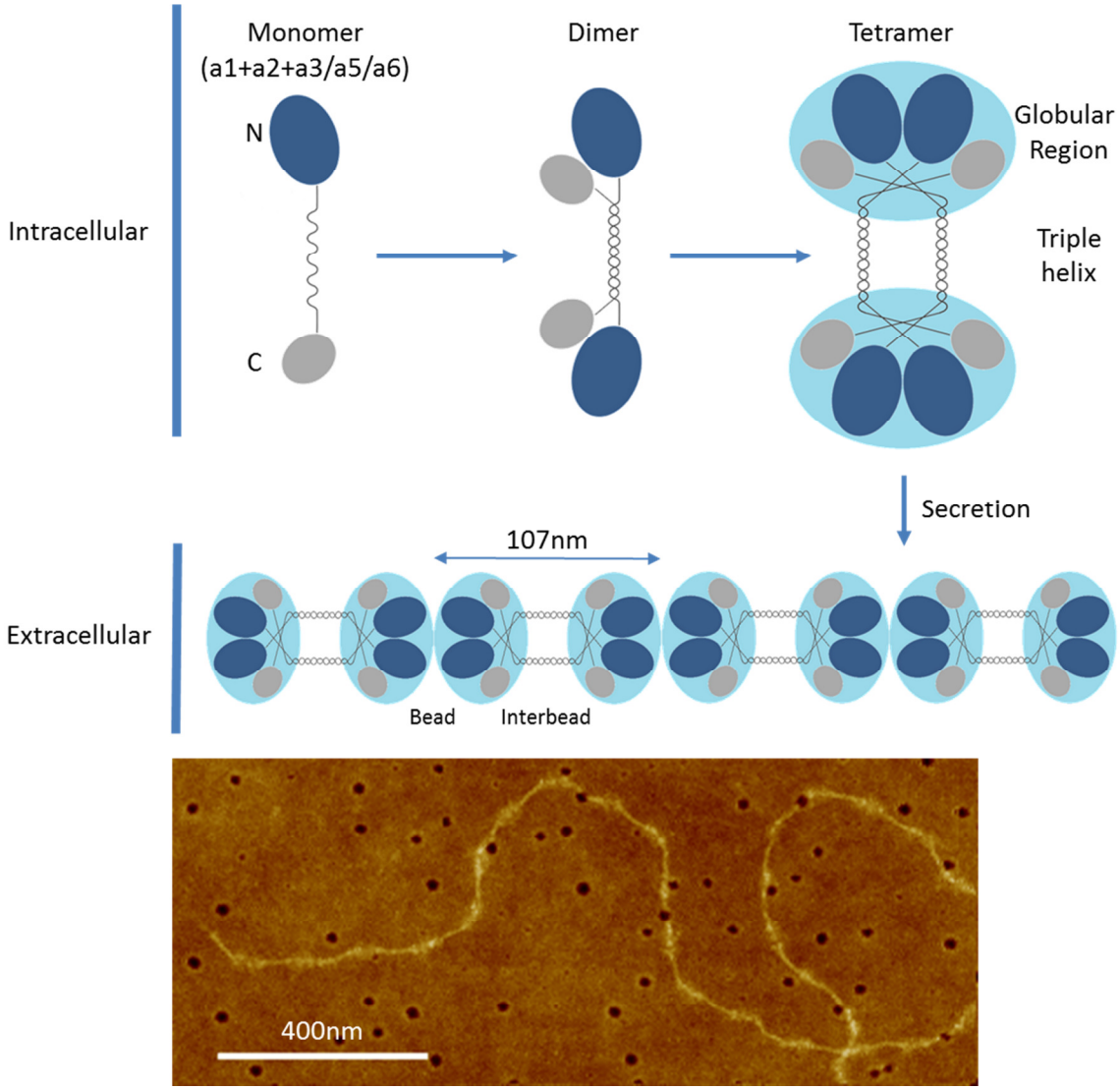

Figure 1.10: Collagen VI microfibril assembly and ultrastructure. The collagen VI microfibril monomer is a heterotrimer containing an a1 chain and an a2 chain. In humans, the third chain is interchangeable between a3, a5 and a6 (Gara et al. *2011). Disulphide bonding between these three chains are thought to stabilise them within the monomer (~500 kDa) (Chu* et al. *1988; Furthmayr* et al. *1983). The monomers progress to dimers (~1000 kDa) via an anti-parallel, disulphide bonding which then go on to form a tetramer (~2000 kDa) (Furthmayr* et al. *1983). These tetramer repeats exist as the intermediate, rudimentary building blocks of the collagen VI microfibril and are secreted from the cell where they undergo end to end association during cell-mediated microfibril assembly (Furthmayr* et al. *1983). This, in turn, leads to the characteristic beaded structure which can be observed and analysed with AFM. The bead to bead periodicity of these microfibrils has been shown to be ~107 nm (Sherratt* et al. *2005, 2007).*

1.6.2 Collagen VI microfibril-associated proteins and tissue function

As a structural ECM assembly, most of the collagen VI microfibril's interactions can be attributed to the network it forms with other matrix proteins and cells (see review (Cescon *et al.* 2015)). As such, the proposed function of these microfibrils is to anchor cells within the matrix and maintain its organisation and structural integrity. Collagen VI interacts with perlecan within basement

membranes which enables a link between cells and the basal lamina within muscle (Kuo *et al.* 1997) and perhaps even in skin, at the DEJ (Watson *et al.* 2001). These microfibrils also associate to other members of the collagen family including type I (through its COL6A3 chain) (Bonaldo *et al.* 1990) , type II (Bidanset *et al.* 1992) and type XIV (via its triple helix region) (Brown *et al.* 1993). Adaptor proteins such as the matrilins have also been shown to facilitate the interactions between collagen VI, collagen II and the proteoglycan aggrecan (Wiberg *et al.* 2003). Collagen VI microfibril secretion and assembly itself is thought to be mediated by its interaction with biglycan (Wiberg *et al.* 2002) and WARP (von Willebrand factor-A domain-related protein) (Hansen *et al.* 2012). Contrastingly, collagen VI presence is also important for fibronectin deposition (Sabatelli *et al.* 2001). Since both collagen VI and fibrillin microfibrils are often present within the same connective tissue, it stands to reason that they would share some of their associated protein interactions. Like fibrillin, collagen VI is able to bind MFAP2 (but not MFAP5) through its COL6A3 chain (Finnis and Gibson 1997) and fibulin-2 (Sasaki *et al.* 1995), however, the function behind these interactions remains elusive.

Collagen VI microfibrils are able to anchor cells and stabilise them within the ECM by binding to the core protein of chondroitin sulphate proteoglycan NG2 receptor (Stallcup *et al.* 1990) and the integrins via RGD-dependent binding (Aumailley, Mann, *et al.* 1989; Pfaff *et al.* 1993). This effectively enables the transduction of biomechanical signals between the cells and the matrix around them (Burg *et al.* 1996). Disruption of this collagen VI-mediated interaction induces autophagy (Grumati *et al.* 2010; Irwin *et al.* 2003). A role of this interaction in stem cell self-renewal has also been shown in muscle (Urciuolo *et al.* 2013).

In skin, collagen VI microfibrils form a filamentous mesh, mainly in the papillary dermis below the DEJ, but also around blood vessels (Watson *et al*. 2001). Primary dermal fibroblasts readily synthesise collagen VI microfibrils *in vitro*, which has proved useful to characterise abnormalities (Dziadek *et al.* 2002; Lamandé *et al.* 1999, 2001; Martoni *et al.* 2009; Sasaki *et al.* 2000). More recently, collagen VI microfibrils have even been shown to play a role in mediating hair growth (Chen *et al.* 2015).

The presence of this microfibrillar assembly, which co-locates and co-purifies with fibrillin microfibrils enables differential susceptibilities of their structures and compositions to be studied and compared.

1.7 Skin ageing

As well as attempting to ascertain structural and molecular variation in fibrillin microfibrils in different tissues and gain insight into function, this PhD also aims to assess this in the context of photoageing in skin. Photoageing is characterised by UVR dose-dependent deterioration of the elastic fibre network, and its constituent fibrillin microfibrils. Although UVR-induced ultrastructural damage to fibrillin microfibrils has been assessed previously, the molecular location of this damage and its effects on composition remains unknown. In order to consider these gaps in knowledge, is it necessary to first review the biology behind skin ageing and the effect of photoageing and UVR on fibrillin microfibril biology as a whole.

1.7.1 Ageing in skin

Intrinsic ageing is defined as the gradual accumulation of physiological and molecular defects over time, through random molecular damage (Kirkwood 2008). Although the molecular damage is classified as random, there are extrinsic factors such as smoking, obesity and exposure to UVR which statistically increase the likelihood of molecular damage occurring. When environmental effects or lifestyle decisions are factored in, the process is referred to as extrinsic ageing. The effects of ageing on skin have been a particular focus of research for a number of years. This is not only because of its associated morbidity and dysfunction but also due to the aesthetic and cosmetic implications which impact on an individual's psyche and quality of life.

Skin exhibits unique consequences of the ageing process which causes a variety of changes both biochemically and architecturally, impacting heavily on its appearance and function. The majority of these changes can be attributed to extrinsic factors; however, changes in architecture, macro-mechanics and gene expression are also caused by an intrinsic ageing process specifically. The effects of intrinsic ageing on skin can be studied at photoprotected sites such as the buttocks where the skin is usually kept covered. Although photoprotected skin remains smooth and unblemished, the clinical effects of intrinsic ageing manifest as fine wrinkles with deep expression lines. A gradual decrease in skin elasticity is also observed in intrinsic ageing (Farage *et al.* 2008; Langton *et al.* 2010).

The skin is exposed to a variety of environmental challenges which can accelerate its ageing process. This is particularly relevant to fibrillin microfibrils, since UVR has a severe impact on their structure and organisation over time. As background for understanding how age induces

remodelling in fibrillin microfibrils, it is imperative the process of direct UV damage and the acute and chronic consequences of its exposure to the skin anatomy be introduced.

1.7.2 Ultraviolet radiation

UVR is a band of electromagnetic radiation between the wavelengths of 10 nm and 400 nm, the common source of which is sunlight. Not all UVR emitted by the sun reaches the Earth's surface and 77% is absorbed by the atmosphere (particularly the ozone layer) (Rai and Srinivas 2007). The radiation that does penetrate the atmosphere typically consists of ≥95% UVA (wavelengths 315-400 nm) depending on the sun's angle to the surface (El Ghissassi *et al.* 2009). The remaining percentage consists of UVB (wavelengths 280-315 nm). Virtually all UVC (wavelength 100-280 nm) is absorbed by the ozone layer (World Health Organization 2002). UVB is the more damaging than UVA, with an energy of 3.94-4.43 eV per photon compared to UVA which has an energy of 3.10-3.94 eV per photon (all wavelength and energy information was taken from the ISO standard ISO-21348 (Tobiska and Nusinov 2005)). Despite the differences in damage potential, both wavebands are known to contribute to photo-induced damage accumulation during ageing (Yaar and Gilchrest 2007). UVR is not ionising, however, it has the capacity to transfer enough energy to molecules to elicit a chemical reaction, often leading to the association and disassociation of chemical bonds (Goodsell 2001; Itri *et al.* 2016; Mozziconacci *et al.* 2010).

1.7.3 Acute consequences of ultraviolet radiation

The consequences of UVR exposure to skin can be either acute or chronic. The short term effects of skin overexposure to UVR generally manifests as a sunburn (Hönigsmann 2002). This is attributed as consequences of direct DNA damage and acute inflammation of the damaged area with a marked increase in vasodilation causing the classical reddening of the skin (Young 2006). An example of the DNA damage caused is the ability of UV to elicit the formation of a thymine-thymine cyclobutane bond (Goodsell 2001; Setlow 1966; Antusch *et al.* 2017). The body generally recovers from this damage via the activation of a variety of DNA repair mechanisms. Along with the classical sunburn, acute UVR exposure can also cause skin depigmentation, immune suppression, damage to the dermal architecture and carcinogenic mutations (Cadet *et al.* 2005).

In terms of cellular consequences to photodamage, various studies have highlighted the capacity for UVR to induce programmed cell death of various skin cells. Acute exposure of UVR initiates apoptosis in human keratinocytes via the induction of proteolytic caspases which cleave and activate protein kinase C (Denning *et al.* 1998). Indeed, protein kinase C is an important family of

proteins which initiate apoptosis in response to ionising radiation in other cell types. Acute exposure to UVR also initiates Bcl-2 (B-cell lymphoma-2)-dependent apoptosis through the activation of a pro-apoptotic gene; noxa (Naik *et al.* 2007). It is hypothesised that the activation of programmed cell death by acute UVR exposure is an essential mechanism of tumour suppression. Keratinocytes and fibroblasts that receive heavy doses of UVR are more likely to have acquired cancer inducing mutations and are therefore eliminated by the preventative mechanism of induced apoptosis.

1.7.4 Chronic consequences of ultraviolet radiation

Clinically, there is a marked difference in the appearance of photoaged skin compared to photoprotected skin. Whereas photoprotected sites are dominated by smoothly textured skin and fine wrinkles with a relatively homogeneous pigmentation, photoaged sites consist of rough skin and coarse wrinkles with a mottled pigmentation (Montagna *et al.* 1989; Warren *et al.* 1991). There is also a significantly larger decrease in skin elasticity of photoaged skin compared to intrinsically aged skin (Langton *et al.* 2017, 2010). This is putatively due to the profound disassociation of the elastic fibre architecture (Langton *et al.* 2010; Lee *et al.* 2008; Watson *et al.* 1999) as a consequence of accumulated UVR damage (Naylor *et al.* 2011; Watson *et al.* 2014).

Counterintuitively, however, solar elastosis is one of the effects of photodamage on elastic fibres in skin tissue. The degree of solar exposure in skin correlates with the level of hyperplasticity exhibited by solar elastosis. As a result, a defining feature of chronic photoageing in skin manifests as an increase in elastin expression (Bernstein *et al.* 1994, 1995) which leads to an accumulation of fragmented elastotic material (namely elastin) in the reticular dermis (Mitchell 1967; Chen *et al.* 1986; Raimer *et al.* 1986). An increase in elastic material in skin coupled with a decrease in elasticity (Langton *et al.* 2017) suggests a severe disruption in the function of the elastic fibre network due to chronic UVR exposure. The reason behind this was discovered in 1986 where antibody staining showed a significant deposition of elastin in the reticular dermis of photoaged skin compared to photoprotected skin (Chen *et al.* 1986). It was later found in transgenic mice, that acute broadband UVB exposure to the human promoter region of elastin leads to a ~8.5 fold increase in activation (Bernstein *et al.* 1995). This UVR induced activation of the elastin promoter region led to a significant increase in elastin expression (Bernstein *et al.* 1994) and consequently to the enhanced deposition of elastin in the reticular dermis of photoaged skin. An increase in LOX

expression was also observed in photoaged skin, which suggests the enhanced crosslinking of the elastin accumulated in the reticular dermis.

Contrary to elastin, a loss of fibrillin microfibril deposition is also seen in photoaged papillary dermis (Watson *et al.* 1999). Fibrillin microfibrils also exhibit a change in ultrastructure due to acute UVR exposure (Hibbert *et al.* 2015; Sherratt *et al.* 2010). Microfibril-associated proteins are also affected by this loss of fibrillin microfibrils and the elastotic remodelling of the elastic fibre network during photoageing. Fibulin-5, which co-localises with the oxytalan fibres in the papillary dermis, is also lost alongside the fibrillin microfibrils (Kadoya *et al.* 2005). Fibulin-2 deposition onto elastic fibres in the deeper reticular dermis increases as a result of solar elastosis (Hunzelmann *et al.* 2001). A number of other large ECM assemblies are affected in a similar manner to the elastic fibres. The fibrillar collagens types I and III are also markedly reduced in the dermis of photoaged skin (El-Domyati *et al.* 2002; Talwar *et al.* 1995). The anchoring fibrils, collagen VII, are also lost at the DEJ (Craven *et al.* 1997). Interestingly, this chronic reduction with photoageing does not appear to be the case for all structural collagens. A study by Watson *et al.* (2001) showed no significant change in the distribution of collagen VI microfibrils or in the expression of its alpha chains in chronically photoexposed skin compared to photoprotected.

Several mechanisms of skin photoageing have been proposed over the years, all of which likely and collectively lead to the histopathologies observed for these ECM assemblies. Of the twenty amino acids, tryptophan, tyrosine and double-bonded cysteine (also known as cystine) are capable of absorbing UVA and UVB wavelength bands (Bensasson *et al.* 1993). As such, one proposed mechanism of photoageing is the direct photodamage caused to these proteins by UVR itself, where absorption by these amino acid chromophores induces a photochemical reaction at the primary sequence level (Sherratt *et al.* 2010). This reaction causes the dissolution of molecular bonds (ie. disulphide bonds) which, in turn, leads to protein photodegradation (Mozziconacci *et al.* 2010). Another proposed mechanism is thought to occur as an indirect consequence of UVR itself, whereby the photochemical reactions caused by the absorption of these protein photosensitizers leads to the creation of reactive oxygen species (ROS) in the extracellular space which, in turn, increases oxidative stress within the tissue (Wondrak *et al.* 2006). These can oxidise amino acids causing the degradation and denaturation of nearby proteins (Stadtman 1992). Another proposed mechanism is more cellular in origin whereby exposure of UVR to keratinocytes and fibroblasts can lead to an increase in the expression of ECM proteases such as the MMPs (Brennan *et al.* 2003;

Brenneisen *et al.* 1998; Fisher *et al.* 1996; Saarialho-Kere *et al.* 1999). The consequential increase in protease activity within the dermis is thought to promote the degradation of these ECM assemblies via proteolysis (Fligiel *et al.* 2003; Quan *et al.* 2009). Additionally, several studies have hypothesised a dysfunctional change in phenotype of cell populations chronically exposed to UVR, especially when studying its effects on the ECM. Talwar *et al.* noticed a significant ~ 40% reduction in type I and type III procollagen levels in chronically photoexposed forearm skin when compared to photoprotected buttock. Since they failed to measure a significant elevation in MMP levels between the two areas, they hypothesised that this reduction may be due to an impairment in collagen biosynthesis (Talwar *et al.* 1995). This indicates that's chronic UV exposure may also significantly alter a fibroblasts capability to synthesise and hence, repair matrix.

The inherent reason behind the ability of these mechanisms to cause such damage to these large ECM assemblies in skin is thought to lie with their longevity. As discussed previously, several of these components are built to last a lifetime (Ritz-Timme *et al.* 2003; Shapiro *et al.* 1991; Verzijl *et al.* 2000). As a result, their continuous exposure to UVR and UVR-related mechanisms over a lifetime, leads to an accrual of structural damage which impacts their functional roles in tissue mechanics and homeostasis (Naylor *et al.* 2011; Watson *et al.* 2014).

1.8 Effects of photoageing on fibrillin microfibrils

1.8.1 Consequences to fibrillin microfibril architecture

Photoageing in skin leads to the loss of fibrillin microfibrils (Watson *et al.* 1999) and an increase in aberrant elastin deposition (Warren *et al.* 1991). Ultimately, this dis-regulation of elastin coupled with the degradation of fibrillin microfibrils surrounding the elastin cores, leads to the complete deterioration of elastic fibre architecture. The elastic fibre system in young photoprotected dermis is organised by thick reticular elastic fibres running parallel to the DEJ and perpendicular elaunin fibres penetrating through the reticular dermis and into the papillary dermis (Cotta-Pereira *et al.* 1976). A marked loss in this ordered architecture is observed in severely photoaged skin and highly disorganised accumulations of fragmented elastic fibres can be observed throughout the dermis (Sherratt 2009; Warren *et al.* 1991; Watson *et al.* 1999). The disorganisation and structural changes in aged elastic fibres was seen as early as 1981 when scanning EM was used to image fixed sections of young and old dermis **(Fig. 1.11)** (Tsuji & Hamada 1981). The imaging showed a marked increase in the thickness of elastic fibres of aged dermis compared to young dermis with

visible areas of elastin accumulation. Whereas young dermal elastic fibres appear to run in parallel bundles, old dermal elastic fibres are highly fragmented and disorganised in comparison.

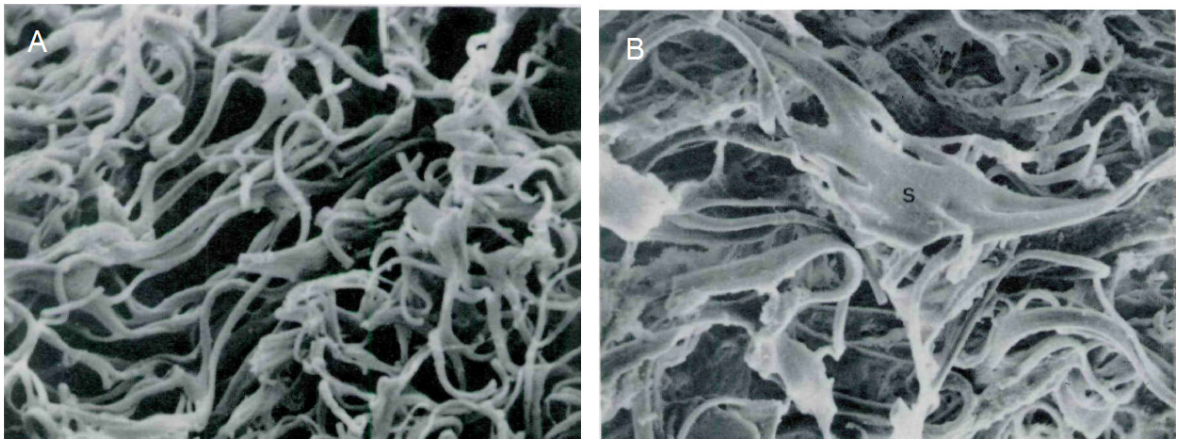

*Figure 1.11: Scanning EMs of dermal elastic fibres. Shown in 20 year old **(A)** and 62 year old human skin **(B)**, there is an observable increase in elastic fibre thickness and disorganisation in old versus young. Accumulations of material, thought to be elastin, are also observed in old dermis (black S). Reproduced from Tsuji and Hamada (1981).*

The same study noted a loss of the ordered oxytalan fibres in photoaged skin (Tsuji and Hamada 1981). These non-elastin associated fibrillin microfibrils form structured candelabra bundles which penetrate the papillary dermis and connect the base of the DEJ to the elaunin fibres of the reticular dermis (Cotta-Pereira *et al.* 1976). Watson *et al.* (1999) observed a marked loss in the organisation of these arrayed fibres in photoaged skin and, although the fibrillin microfibrils were still seen in the papillary dermis, they appeared severely truncated and disorganised in comparison to those in photoprotected skin. This study highlighted that, along with the elastic fibre network, the stand-alone fibrillin microfibril network of the dermis is also highly disorganised and reduced after chronic UVR exposure. Since these observations are seen both in mildly and severe photoaged skin, it infers that the fibrillin microfibril network is one of the first components of the ECM to degrade following UV irradiation (Watson *et al.* 1999). Interestingly, this implication has led to the hypothesis that the degradation of fibrillin microfibrils could be used an early marker of photoageing in skin (Watson *et al.* 2009).

1.8.2 Consequences to fibrillin microfibril ultrastructure

It was not until more recently that a study by Sherratt *el al.* (2010) proved that fibrillin microfibrils were ultrastructurally susceptible to degradation directly via broadband UVB irradiation **(Fig. 1.12)**. Fibrillin microfibrils derived from fibroblast-like COS-1 cells were irradiated with broadband UVB at three different doses and their ultrastructure assessed using AFM. These exhibited a marked

increase in periodicity **(Fig. 1.12 B)** and flexibility **(Fig. 1.12 C)** when compared to non-irradiated **(Fig. 1.12 A)**. Additionally, an increased presence of fragmented fibrillin microfibrils was seen **(Fig. 1.12 D)**.

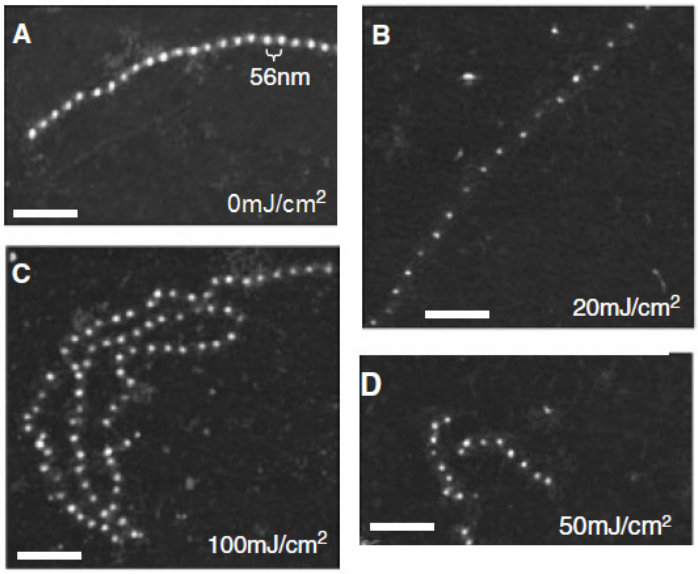

*Figure 1.12: AFM of fibrillin microfibrils, irradiated with UV at increasing doses. Non-irradiated microfibrils **(A)** retain a wild type structure compared to UV irradiated microfibrils which exhibit an increase in periodicity **(B)**, flexibility **(C)** and fragmentation **(D)**. Reproduced from Sherratt* et al. *(2010).*

In addition to these quantifiable changes in fibrillin microfibril ultrastructure in response to UVB irradiation, Sherratt *et al.* (2010) also noticed a significant reduction in the mass per repeat of irradiated microfibrils compared to non-irradiated **(Fig. 1.13)**. In fact, doses of broadband UVB irradiation (100 mJ/cm^2) induced a 28% reduction in fibrillin microfibril mass compared to non-irradiated. It was noted that the central bead region was the primary location of this mass loss. This finding suggests that UVR may directly disassociate a variety of bonds within the fibrillin microfibril structure, causing its gradual degradation. Interestingly, a significant structural reorganisation was also detected within the bead region. Additionally, a sub-proportion of fibrillin microfibril regions showed an accumulation of heterogeneous material, suggesting that perhaps UVR exposure causes the erroneous formation as well as the disassociation of bonds within the structure.

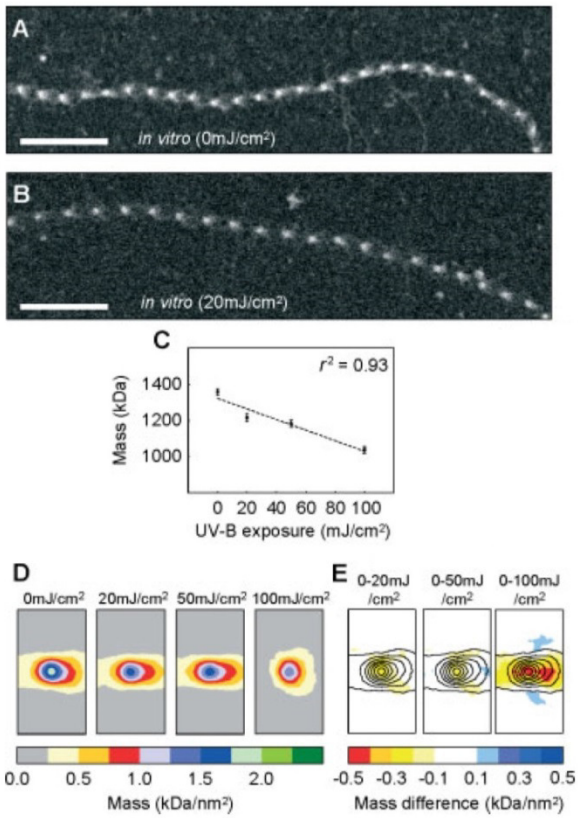

Figure 1.13: Changes in fibrillin microfibril bead mass correlate with UV dose. Sherratt et al. (2010) *observed that broadband UVB-irradiated fibrillin microfibrils **(B)** had a loss of mass compared to non-irradiated microfibrils **(A)**. They also observed that this occurred in a dose-dependent manner where the higher the exposure of UVB, the lower the microfibril bead mass **(C)**. Heat maps of bead mass **(D)** and differences in them **(E)** indicated that changes within the average microfibril bead were local and regional in nature. Reproduced from Sherratt* et al. *(2010).*

Sherratt *et al.* (2010) also went on to show that this susceptibility to UV was also shared by fibronectin but likely not by collagen I. Using gel electrophoresis, they observed that, even at their highest dose used (500 mJ/cm^2), broadband UVB had no effect on the mobility or intensity of released alpha 1 and alpha 2 chains of collagen I. These effects, however, were not tested on native collagens until more recently, where Hibbert *et al.* (2015) went on to show that physiological doses of UVA and solar simulated radiation (SSR) led to a marked changes in purified human dermal fibroblast (HDF)-derived fibrillin microfibril periodicity, but not to collagen VI microfibril periodicity. This study served as the first indication that two different supramolecular microfibril assemblies, both of which form a networking architecture within the dermis, had very different susceptibilities to physiological doses of UVR. These observations made a strong case in implicating chronic UVR exposure in the direct dissolution and loss of the dermal fibrillin microfibril and elastic fibre system, but not in the collagen VI microfibril network, both seen histologically by Watson *et al.* (1999 and 2001). These revelations recently led to a new *in vitro* assay which uses

the observed ultrastructural damage to fibrillin microfibrils to test sunscreen protection of dermal ECM assemblies (Hibbert *et al.* 2017).

Over the last two decades the role fibrillin microfibril degeneration plays in the photoageing process of skin has become increasingly clear. Chronic damage to this macromolecular assembly has so far been observed histologically with the dissolution of its architecture, and acute damage has been observed ultrastructurally, when direct UVR exposure causes quantifiably changes to its beaded assembly. However, the molecular location of the damage and its effect on the microfibril's primary constituent: fibrillin-1, has never been assessed. As such, why and how these assemblies are susceptible to UVR, remains unknown. Assessing the effect of UVR on the molecular composition of these fibrillin microfibrils, in conjunction with the ultrastructural changes, may reveal the answer.

1.9 Proteomics of fibrillin microfibrils

In order to assess molecular differences in fibrillin microfibrils from different tissues and in photoageing, it is first necessary to effectively characterise their composition. However, this has proved to be challenging. The megadalton-size of these native assemblies rules out conventional biochemical analysis such as gel electrophoresis and x-ray crystallography, without first fragmenting its components. In defiance to this, recent mass spectrometry (MS)-based proteomic approaches have been used in an attempt to analyse microfibril composition, with encouraging results.

1.9.1 Challenges facing proteomics of extracellular matrix assemblies

Before discussing recent attempts at characterising fibrillin microfibril composition using proteomics, it is important to consider the challenges behind the proteomic analysis of ECM proteins in general. The ECM consists of a vast array of networking supramolecular assemblies which contribute heavily not only to tissue structure, but also to cell adhesion, communication and homeostasis. The sheer complexity and large size of these assemblies means that their continual synthesis and turnover would put a large pressure on tissue metabolism. As a result, many of these assemblies are built to last a lifetime, removing the stress of long-term cell production. Consequently, these networking structures are tightly bonded, highly modified and covalently crosslinked (Wilson 2010). This, along with the hierarchical assembly of macromolecular ECM components (as seen in fibrillary collagens, collagen VI microfibrils and fibrillin microfibrils) renders them highly insoluble and, therefore, a real challenge for conventional methods of biochemical analysis, proteomics included (Chang *et al.* 2016).

Over the years, MS-based proteomic technologies have allowed for both large scale and detailed analyses of biological systems enabling the characterisation of 1) protein presence and quantity, 2) protein interactions and 3) protein structure (Byron *et al.* 2013). However, the insolubility and complexity of many ECM assemblies in connective tissue has put real constraints on the ability to generate peptides for MS analysis. Additionally, many ECM-rich tissues, such as skin, are composed of a few dominating assemblies, such as the fibrillar collagens. This means that even if near-complete solubility is achieved, detection and quantification of lower abundant proteins of interest may be masked by these predominating components (Wilson 2010). In fact, although a recent attempt to characterise the whole proteome of human skin successfully detected and quantified a number of matrix components such as several collagens and keratins, they failed to detect any of the fibrillins and collagen IV alpha chains despite these assemblies being highly present within this tissue (Mikesh *et al.* 2013). To overcome the challenges of masking and insolubility, proteomic analyses of ECM-heavy tissues often require an adaptation in the workflow.

To reduce the complexity of a sample and prevent masking, tissues can often be dissected and separated so that the proteomes of sub-tissues can be characterised independently (Alves *et al.* 2011; Byron *et al.* 2013; Garcia *et al.* 2006; Vincourt *et al.* 2006). Additionally, if the researcher is interested in a specific subset of assemblies, isolation of these proteins is often possible. In some cases, selective extraction of certain assemblies can be achieved enzymatically using proteases. Fibrillin and collagen VI microfibrils are resistant to bacterial collagenase, which enables the selective digestion of native collagen I around these assemblies (Hibbert *et al.* 2015; Kielty *et al.* 1991; Kielty, Hanssen, *et al.* 1998; Sherratt *et al.* 2010). Following this up with a purification method such as size exclusion chromatography (Cain *et al.* 2006; Handford *et al.* 1995; Sherratt *et al.* 2003) or caesium chloride density-gradient centrifugation (Cain *et al.* 2008; Kielty, Hanssen, *et al.* 1998) allows the separation of these larger assemblies from smaller proteins and digested collagen I products, based on size or density respectively. Fractionation using 1D or 2D gel electrophoresis is also a good option for separating proteins based on mass and isoelectric point (Pecora *et al.* 2007). Reducing the complexity of a sample mixture by either completely removing any masking contaminants or by stratifying them, often leads to a more complete characterisation of a tissue or assembly's composition.

Conversely, once complexity is reduced, increasing the peptide generation necessary for MS, from large, insoluble ECM assemblies, often involves a combination of techniques. Physical and

mechanical disruption using pulverisation, homogenisation (Wilson *et al.* 2011) and/or ultrasonication (Hansen *et al.* 2009) is often a good initial step for the disassociation of ECM still present in whole tissue form. Chemical disruption using denaturing agents like guanidine hydrochloride (Gu-HCl), sodium dodecyl sulphate (SDS) and urea (Medzihradszky 2005), reducing agents such as dithiothreitol (DTT) and alkylating agents such as iodoacetamide (IAM) can effectively disrupt di-sulphide bonds and crosslinks within these large macromolecular components, unravelling their quaternary and tertiary structures and improving the accessibility of peptide-generating enzymes to deeper regions of their ultrastructures (Naba *et al.* 2015). Finally, selecting a suitable enzyme for peptide generation based on its activity or cleavage specificity can markedly improve the detection of ECM assemblies using MS (Hustoft *et al.* 2012; Rietschel *et al.* 2009).

As a result of these challenges, several attempts have been made at using proteomics to assess different aspects of fibrillin microfibril composition from whole tissue, purified assemblies and recombinant fragments.

1.9.2 Whole tissue proteomic analysis of fibrillin microfibrils

In the last decade, a number of studies have attempted to characterise the proteome of elastic tissues using liquid chromatography tandem MS (LC-MS/MS). Using laser microdissection, Mikesh *et al.* (2013) captured three specific regions of human skin (basement membrane, papillary dermis and reticular dermis) for proteomic analysis. Since the majority of the dermis is comprised of ECM, they successfully managed to identify several of these assemblies including many collagens and proteoglycans. Surprisingly however, they failed to detect any of the fibrillins despite detecting elastin. Additionally, they failed to detect collagen IV, a prominent basement membrane assembly, despite sub-tissue microdissecting the DEJ. Histologically, it is expected that these two components should contribute to a significant proportion of these sub-proteomes analysed. Failure in detection may have been due to their insufficient extraction and processing prior to MS analysis. Another study by Didangelos *et al.* (2010) aimed proteomically characterise the human aorta by specifically focusing on the extracellular space. Having acknowledged the difficulty of disassociating and solubilising ECM assemblies, they effectively analysed these components by first decellularising and mechanically disrupting the tissue followed by extracting matrix components using strong denaturing agents such as Gu-HCl and deglycosylating enzymes. As a result, they successfully detected a vast number of assemblies, including fibrillin (albeit a poor detection of only 10 unique peptides in 3 samples).

These whole tissue studies aimed to characterise the vast proteomes of elastic tissues as opposed to fibrillin microfibril composition specifically. Recently however, De Maria *et al*. (2017) published the proteomic analysis of the human and bovine ciliary zonule. Since the ciliary zonules are comprised predominantly of fibrillin microfibrils, this was the first attempt at characterising their molecular composition using a whole tissue proteomics approach. Encouragingly, they were able to remove the ciliary zonules precisely with little contamination from surrounding tissues by cutting them free close the ciliary body and the lens using iridectomy scissors. They then used a combination of denaturing agents (ammonium bicarbonate and urea), alkylating agents (IAM), mechanical disruption (sonication) and high temperature (90^{o}C) to extract, disassociate and solubilise the tissue prior to peptide generation using trypsin and LC-MS/MS. They found that the glycoproteins made up the majority of the ciliary zonule proteome with fibrillin-1 contributing to 63% of it in human tissue. The remaining 37% of the zonular proteome consisted heavily of previously known microfibril-associated proteins such as LTBPs, MFAPs, EMILIN-1 and ADAMTSLs, further exemplifying the macro-molecular nature of the fibrillin microfibril assembly. LTBP2 was the second most abundant protein after fibrillin-1 (7%) which is interesting considering it is the only member of the LTBP which does not sequester TGFβ and whose role in tissue remains widely unknown. A number of crosslinking enzymes such as LOXL1 and several transglutaminases as well as some protease inhibitors such as tissue inhibitor of metalloproteinase-3 (TIMP3), also co-localised within the zonule, indicating that these functional modifiers may play a site-specific role in maintaining the zonular structure. Comparing between bovine and human, they also found that although over 95% of the zonular proteome was homologous, there appeared to be some species-specific compositional differences. Fibrillin-1 constituted a higher proportion of the zonular proteome in bovine (76%) than in human (63%). Interestingly, MFAP5 was identified in the top nine in the human zonule, but not in bovine zonule.

1.9.3 Proteomic analysis of isolated fibrillin microfibrils

Although De Maria *et al.* (2017) successfully defined the whole zonular proteome, their study fell short of strictly characterising the molecular composition of the fibrillin microfibril itself since a number of the proteins identified may not have bound the microfibril directly but rather indirectly, through a network of associations. Cain *et al.* (2006) however, did successfully define and characterise the fibrillin microfibril composition specifically, by extracting them from human ciliary zonules using bacterial collagenases IA, VII and Gu-HCl and isolating them using size exclusion chromatography. Fibrillin microfibril peptide fragments were then generated by denaturation with

urea, reduction with DTT, alkylation with IAM and digestion with trypsin prior to LC-MS/MS analysis.

The peptide profiles generated by Cain *et al.* (2006) from these isolated microfibrils identified fibrillin-1 as the top hit. Additionally, MFAP2 was also detected. Intriguingly, the recurrent identification of the annexins (V and II) within the human ciliary zonule extracts led to the speculation within this publication that they may also be microfibril associates. They attributed the lack any other associated component identification such as LTBP, perlecan and versican to "*loss of loosely associated components in preparation*" or simply due to lack of presence.

Additionally, Cain *et al.* (2006) were also able to obtain structural information of fibrillin-1 from their native microfibrils by mapping the number of detected peptide sequences onto the protein's domain structure **(Fig. 1.14)**. Most fibrillin-1 TB domains appeared to yield a particularly high number of peptide hits. Various EGF domains were also identified, including most of the N-terminal region. A number of regions were not identified, however, such as the proline-rich domain and much of the C-terminal region. Cain *et al.* (2006) labelled these regions as resistant to urea reduction, possibly due to covalent crosslinks of non-reducible transglutaminase bonds. Furthermore, when these mapped domains were related to the folded model of fibrillin-1 microfibril alignment (Baldock *et al.* 2006) **(Fig. 1.15)**, it was deduced that the majority of the domains that were susceptible to trypsin were located inter-bead, one such region was the exposed 'shoulder' of the fibrillin-1 monomer. Areas which were primarily resistant to reduction and trypsinisation, such as the C-terminal region were deduced to be located within the bead. They proposed, therefore, that external areas of fibrillin-1 which were protruding out of the microfibril may be more exposed and, hence, more susceptible to reduction and proteolytic degradation, whereas masked areas within the microfibril bead region were not. Cain *et al.* (2006) also suggested that microfibril-associated proteins may be masking these epitopes.

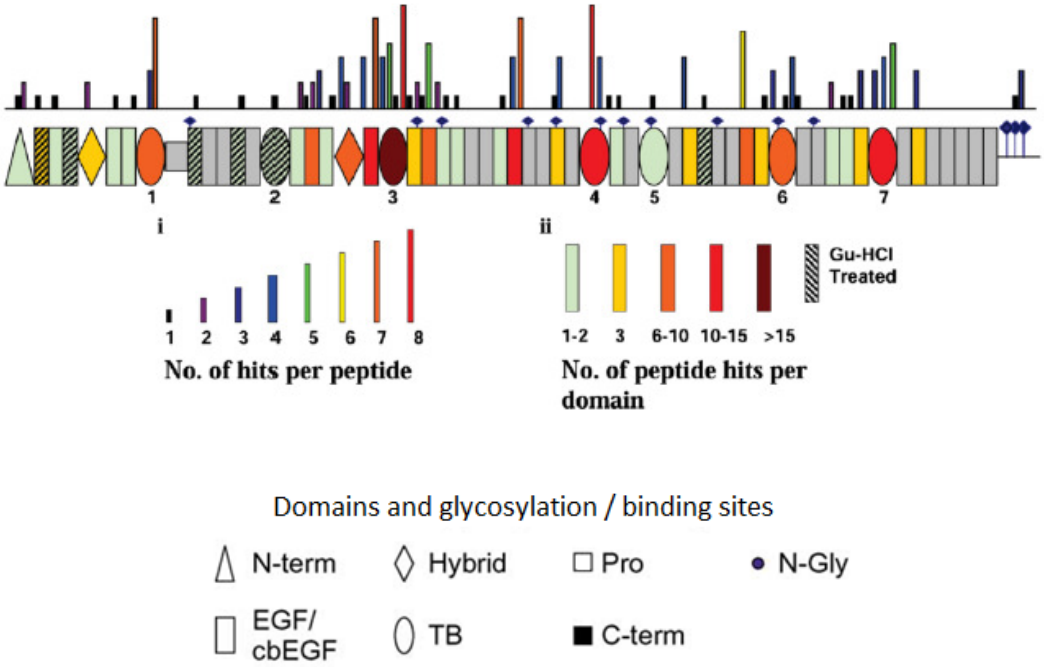

Figure 1.14: LC-MS/MS detected peptides mapped onto fibrillin-1 domains. Figure reproduced from Cain et al. *(2006) who mapped all the peptide sequences they detected, in human ciliary zonule-derived fibrillin microfibril purifications, to their corresponding fibrillin-1 domains. This shows the extent of primary sequence coverage and abundance achieved by their proteomic analysis. Several domains and the C-terminal region remained largely undetected. On the other hand, a number of peptides were detected from the TB domains and the N-terminal region. Reproduced from Cain* et al. *(2006).*

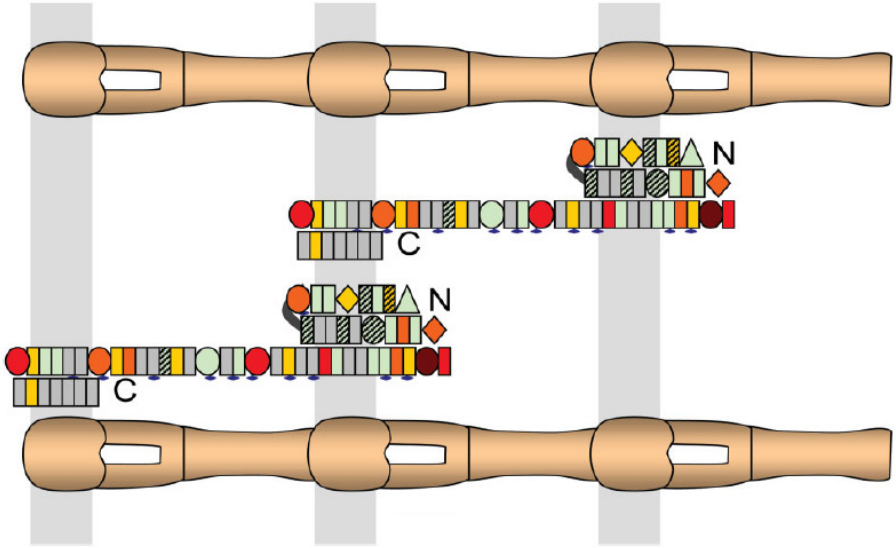

Figure 1.15: Folded model incorporating LC-MS/MS peptide-mapped fibrillin-1. After mapping fibrillin-1 peptides to their corresponding domains, Cain et al. *(2006) then applied this to the folded model of fibrillin-1 alignment (Baldock* et al. *2006) within the microfibril. By doing so, they observed that a majority of unmapped regions lay within the microfibril beads. On the other hand, the shoulder hinged, inter-bead regions contained a majority of mapped domains. Reproduced from Cain* et al. *(2006).*

Cain *et al.* 's (2006) proteomic analysis of fibrillin microfibrils provided a number of novel insights not only into the molecular composition of the fibrillin microfibril (by identifying potential new associated proteins such as the annexins) but also into its supramolecular organisation, by referring the proteolytic exposure of the fibrillin-1 domain structure to previous models of microfibril assembly.

1.9.4 Proteomic analysis of microfibril-associated proteins

Although a number of fibrillin microfibril-associated proteins have been identified, there are likely many more interactions within the vast ECM network of proteins which still remain largely uncharacterised and understudied. Also using LC-MS/MS-based proteomics, Cain *et al.* (2009) went on to identify a number of novel proteins which co-purify with recombinant fibrillin-1 fragments **(Fig. 1.16)**, *in vitro,* in a molecular fishing study. Although this was done using recombinant fragments of fibrillin-1 and a cell culture model, it is possible that at least some of the identified associated components are able to bind fibrillin microfibrils in native tissue and reveal a novel mechanistic function.

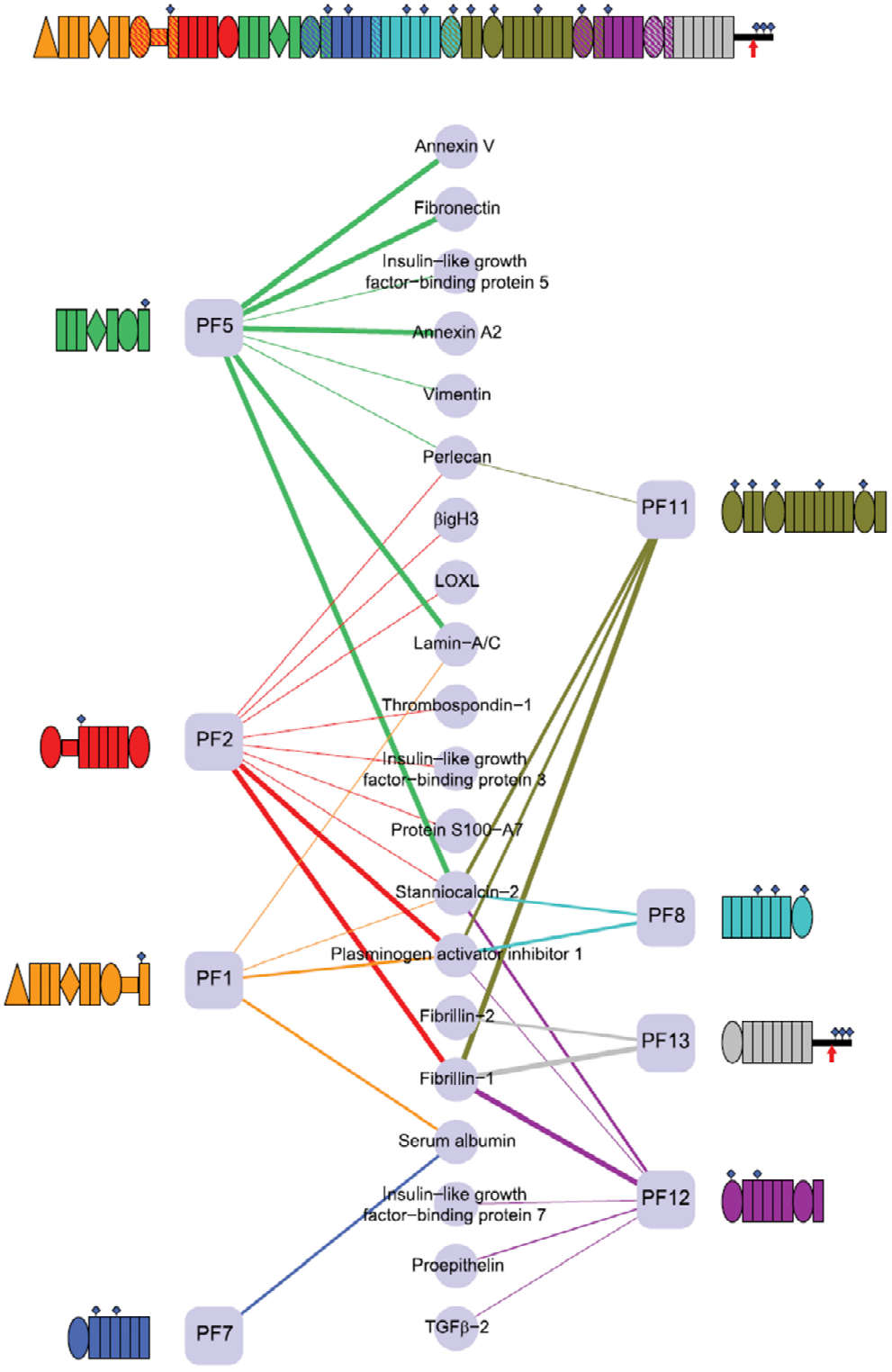

Figure 1.16: Proteins identified via molecular fishing with fibrillin-1 recombinant fragments. Cain et al. *(2009) used fibrillin-1 recombinant fragments (PF) as bait to fish interacting proteins from cultured dermal fibroblast ECM. This interaction map illustrates the number of associated proteins which were found to co-purify with each fragment, and the significance of this interaction (width of line). Many of these proteins such as fibrillin-2, fibronectin, perlecan, TGFβ-2 and LOXL were already known to associate to fibrillin microfibrils; however, this study discovered a number of potentially novel interactors such as thrombospondin-1, S100-A7, TGFβ-induced glycoprotein-H3 (βig-H3) and plasminogen activator inhibitor 1 (PAI1). The relevance and function of these identified proteins remains unknown. Reproduced from Cain* et al. *(2009).*

Reviewing the literature has revealed the potential of MS-based proteomics to effectively characterise and assess both the composition of the fibrillin microfibril and native fibrillin-1 structure. As such, it is necessary to first optimise and develop this methodology further in order to effectively assess these traits in the context of tissue diversity and photoageing. Therefore, this PhD also aims to further optimise and develop both the ultrastructural analysis methods employed by Sherratt *et al.* (2010) and Hibbert *et al.* (2015) and the proteomic analysis methods employed by Cain *et al.* (2006) to effectively assess fibrillin microfibril molecular composition and ultrastructure hand-in-hand. This can then be applied to study the role fibrillin microfibrils play in different tissues and in cutaneous photoageing.

1.10 Aims and research questions

Fibrillin microfibrils play distinct roles in elastic fibre-rich tissue, such as in the dermis, and elastic fibre poor-tissue, such as in the ciliary body and zonules of the eye. Whether the fibrillin microfibril ultrastructure and molecular composition reflect these distinct roles in different tissues remains poorly characterised, especially in humans. Although previous studies suggest that fibrillin microfibril ultrastructure is tissue-specific, this has only been observed in foetal bovine tissue, between skin and aorta (Sherratt *et al.* 1997) and in adult bovine tissue between aorta and the ciliary zonules (Lu *et al.* 2006), never in human tissue. Additionally, whether the molecular composition (fibrillin-1 structure and associated protein presence) of the fibrillin microfibrils is tissue-dependent or not has never been studied.

One of the defining characteristics of photoageing in skin is the deterioration of the fibrillin microfibril network and elastic fibre architecture. The effect of chronic photoageing on this assembly has been shown histologically *in vivo* (Watson *et al.* 1999), and direct damage by UVR on the fibrillin microfibril has been shown ultrastructurally *in vitro* (Hibbert *et al.* 2015, 2017; Sherratt *et al.* 2010). However, the molecular location of this damage, specifically to the structure of fibrillin-1 within its native microfibril, has never been shown. In contrast, collagen VI microfibril architecture and ultrastructure is resistant to photoageing and UV-damage respectively. Comparing differences between COL6A3 structure and fibrillin-1 structure may reveal the reasons behind the differential susceptibility of these two microfibrillar assemblies to UV and photoageing.

To date, only a single study has highlighted the potential of MS-based proteomics in assessing and characterising the molecular composition (fibrillin-1 structure and associated protein presence) of fibrillin microfibrils (Cain *et al.* 2006). However this study was performed more than a decade ago.

New advances in MS technology (Byron *et al.* 2013) and further optimisation and development of the methodology employed by Cain *et al.* (2006) should allow the fibrillin microfibril composition to be characterised further. This would effectively enable comparisons to be made and allow the assessment of fibrillin microfibril tissue diversity and photodamage on a never-before-seen molecular scale.

To this end, this PhD hopes to answer four key research questions:

1. Can the proteomic characterisation (fibrillin-1 coverage and associated protein detection) of isolated and purified human fibrillin microfibrils be improved further through the development of novel sample preparation methods and with advances in MS technology?
2. Do human fibrillin microfibrils exhibit tissue-specific differences in ultrastructure and molecular composition and can newly developed proteomics methods be used to address this?
3. Does UV irradiation of primary human dermal fibroblast-derived fibrillin microfibrils, *in vitro,* cause specific changes to fibrillin-1 structure within its microfibril and can this be used to detect photodamage?
4. Can these UV-induced changes to fibrillin-1 structure be validated in native human skin-derived fibrillin microfibrils?

These four questions are addressed in four separate manuscripts (written up as results chapters).

Chapter 2: Materials and methods

2.1 Human tissue and cell acquisition

2.1.1 Materials

All chemicals were sourced from Sigma-Aldrich Co. Ltd (Poole, UK) unless stated otherwise.

2.1.2 Eye acquisition

Human donor eye tissue was acquired in accordance with the Human Tissue Act (2004) via the Manchester Eye Bank, within 24 hours of corneal retrieval (for corneal transplant services). The use of this tissue for age-related studies was approved by University of Manchester Research Ethics Committee (UREC ref 11305).

2.1.3 Ciliary body dissection

Microfibril-containing ciliary bodies were dissected from the remaining tissue and then carefully separated **(Fig 2.1)**. These were placed in cryovials, snap-frozen in liquid nitrogen and stored at -80°C prior to microfibril isolation

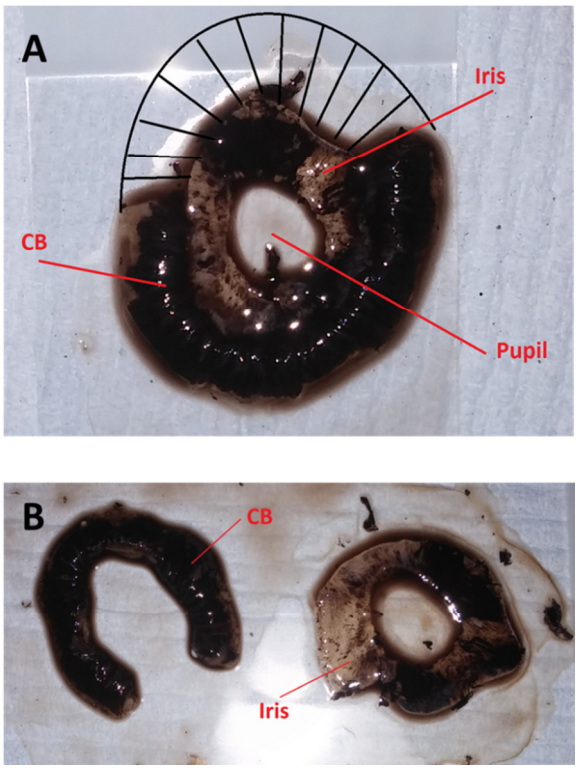

*Figure 2.1: Dissecting the human ciliary body. Tissue was acquired in the form of the ciliary body (CB) still attached to the iris **(A)**. The two sub-tissues were carefully separated on a glass microscope slide, using watchmaker's forceps and a scalpel blade **(B)**. The iris was discarded and the ciliary body retained for microfibril isolation.*

2.1.4 Skin acquisition

Abdominal skin samples were sourced from middle-aged donors (post-abdominoplasty surgery) through University of Bradford collaborators, acquired via the University of Manchester Skin Health Biobank (MSHB). The MSHB is conducted in accordance with the Declaration of Helsinki 1964 (revised Seoul 2008) and the European Medicines Agency Note for Guidance on Good Clinical Practice. North West Research Ethics Committee has approved this biobank (Research Ethics Committee reference 09/H1010/10).

Forearm skin biopsies (3mm) and buttock skin biopsies (bisected 6mm) were collected from middle-aged donors as part of a larger study titled: “Investigating the effects of intrinsic and extrinsic ageing on fibrillin-rich microfibrils”. The use of this tissue was approved by The University of Manchester Research Ethics Committee 3 (UREC ref 15464). Donors gave informed and written consent. All tissue samples were snap frozen in liquid nitrogen and stored at -80°C.

2.1.5 Human dermal fibroblast acquisition and culture

Cryopreserved primary human dermal fibroblasts (HDFs) were acquired as a kind gift from Dr Suzanne Pilkington who cultivated the cells from donor photoprotected buttock skin biopsies. Once again, all donors gave informed and written consent and the use of this tissue was also approved by the University of Manchester Ethics Committee (UREC ref 14415).

Dulbecco's Modified Eagle’s Medium (DMEM) was supplemented with 10% foetal calf serum (FCS) (Gibco; Thermo Fisher Scientific; Paisley, UK), 1% amphotericin, 1% penicillin streptomycin (Pen Strep) and 1% L-glutamine (all v/v). Cryogenically frozen HDFs were removed from liquid nitrogen and quick-thawed in a 37°C water bath. Under sterile conditions, 2 ml of pre-warmed (37°C) supplemented DMEM was slowly added to the cells within their cryovials (Corning; Flintshire, UK) at a rate of 1 drop every 10 seconds. Cells were homogenously suspended via slow pipetting, and transferred into a T75 cell culture flask (Thermo Fisher Scientific; Paisley, UK) containing a total volume of 10 ml supplemented DMEM. All incubations were performed in humid conditions at 37°C, in 5% CO_2. Cell adherence was checked after a 24 hr incubation, after which medium was aspirated and replaced with pre-warmed, supplemented DMEM to remove remaining dimethyl sulfoxide (DMSO; cryoprotectant originally present in the freezing media). Supplemented DMEM was changed twice a week until cells reached ~80% confluency.

To achieve a high yield of isolated microfibrils, HDFs were passaged. Medium was aspirated and cells were washed with pre-warmed, sterile phosphate-buffered saline (PBS) which was then also aspirated off. Cells were then incubated in 2.4 ml of 0.25% (v/v) trypsin-EDTA (Ethylenediaminetetraacetic acid) solution (Sigma) for 5 minutes. Adhered cells were dislodged with careful agitation (confirmed by light phase contrast microscopy) and total volume was split into 3 T75 culture flasks (800 µl of cell suspension in each) containing 10 ml of pre-warmed, supplemented DMEM. All cell experiments were performed with passage 2 HDFs.

Cells were grown to 100% confluency where they were then maintained with bi-weekly changes of supplemented DMEM (medium was aspirated and replaced with 10 ml fresh, pre-warned medium) for a further 5 weeks. This enabled sufficient extracellular matrix (ECM) synthesis for microfibril isolations (Kielty *et al.* 1991).

2.2 Microfibril extraction and purification

2.2.1 Tissue extraction

To extract fibrillin and collagen VI microfibrils from human ciliary body and skin, tissue was minced with a scalpel blade on a glass microscope slide and placed in a 2 ml aliquot of collagenase buffer (400 mM sodium chloride [NaCl], 1 mM calcium chloride [$CaCl_2$], 50 mM trishydroxymethylaminomethane [Tris], buffered to pH7.4 with hydrochloric acid [HCl]). To this, protease inhibitors: 0.01 mM phenylmethylsulfonyl fluoride (PMSF) and 0.03 mM N-ethylmaleimide (NEM) were added to prevent non-specific digestion. Bacterial collagenase type IA (Collagenase from *Clostridium histolyticum*) was then added (to a final concentration of 1 mg/ml) and tissue was digested on a rotary table for 4 hours at room temperature **(Fig. 2.2 A)** (Hibbert *et al.* 2015; Kielty *et al.* 1991; Sherratt *et al.* 2010).

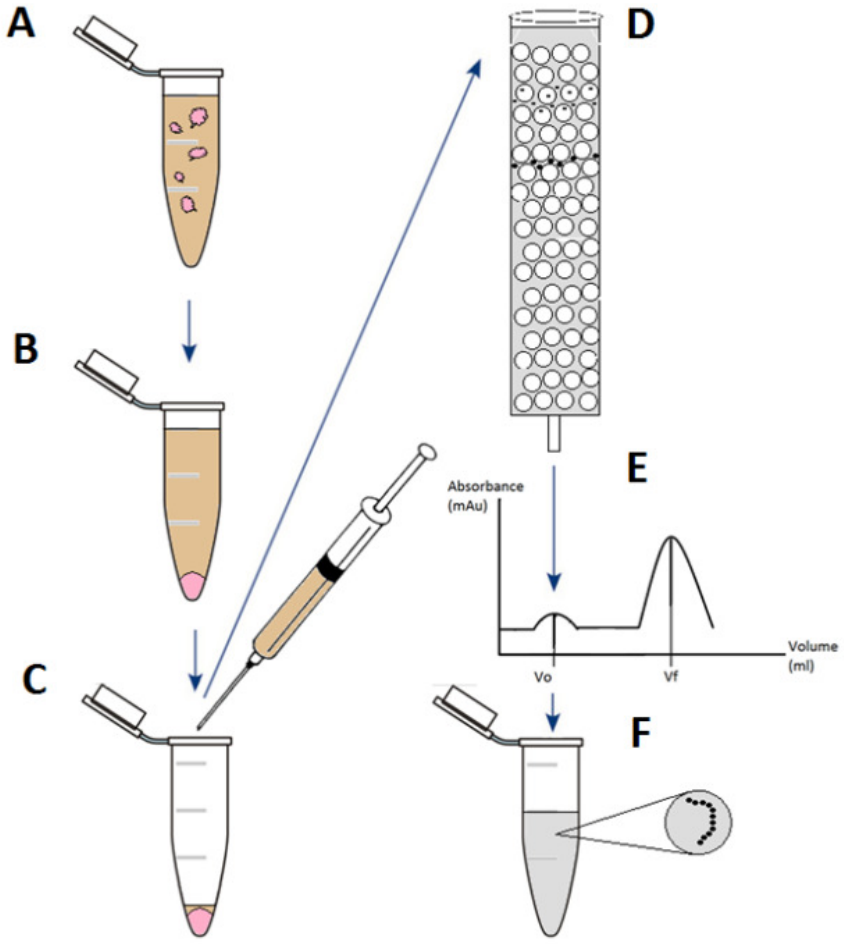

Figure 2.2: Fibrillin and collagen VI microfibril extraction. Tissues were digested with bacterial collagenase IA ***(A)*** *before being centrifuged* ***(B)****. The supernatant was then collected* ***(C)*** *and run through a size-exclusion column* ***(D)****. The fractions collected generated two spectrographic absorbance peaks* ***(E)****. Fibrillin and collagen VI microfibrils were found within the first peak (V_0)* ***(F)****.*

2.2.2 Cell culture extraction

Five week, post-confluent HDFs (passage 2) were washed three times with 10 ml PBS to remove media. Two ml of collagenase buffer containing 2 mg of bacterial collagenase IA (1 mg/ml), 0.01 mM PMSF and 0.03 mM NEM were added directly to the HDF-containing T75 culture flasks. These were digested for 2 hrs on an orbital shaker at room temperature (Hibbert *et al.* 2015; Kielty *et al.* 1991; Sherratt *et al.* 2010).

2.2.3 Purification by size-exclusion chromatography

Post-digestion, mixtures were centrifuged at 5000 g for 5 minutes **(Fig. 2.2 B)**. Supernatants were collected and pellets discarded **(Fig. 2.2 C)**. Fibrillin and collagen VI microfibrils were purified using an ÄKTA Prime Plus Liquid Chromatography System (GE Healthcare; Little Chalfont, UK). Supernatants were injected and run at a flow rate of 0.5 ml/min within a buffer composed of 400 mM NaCl and 50mM Tris-HCl (buffered to pH 7.4), through a GE HiScale 16/40 column packed

with Sepharose® Cl2B beads **(Fig. 2.2 D)**. One ml fractions were collected based on spectrophotometric absorbance at 280 nm which indicates the total protein concentration in each fraction. Two absorbance peaks are detected during microfibril purification: an initial peak equating to the void volume (V_0) which correlates to large proteins and a second, larger peak equating to the final volume (V_F) which correlates to smaller proteins **(Fig. 2.2 E)**. Fibrillin and collagen VI microfibrils typically co-purify within the V_0, which is collected at the height of the absorbance peak **(Fig. 2.2 F)** (Hibbert *et al.* 2015; Kielty *et al.* 1991; Sherratt *et al.* 2010) and yields 2 ml of isolated extracts.

2.3 Peptide generation for mass spectrometry

2.3.1 Desalting and freeze drying

Microfibril isolations were de-salted via dialysis in 0.22 µm filtered ultrapure water (see **Fig. 2.3** for workflow of entire proteomics sample preparation process). This was achieved using Slide-A-Lyzer™ MINI Dialysis Devices (Thermo Fisher Scientific; Paisley, UK) and dialysing for 4 hours at 4°C. These were subsequently frozen at -80°C and freeze-dried using a CoolSafe freeze dryer (LaboGene; Allerød, Denmark) coupled to a hybrid vacuum pump system (Vacuubrand; Rochdale, UK) at -60°C for 48 hours. Samples were stored at -80°C until mass spectrometry (MS) analysis.

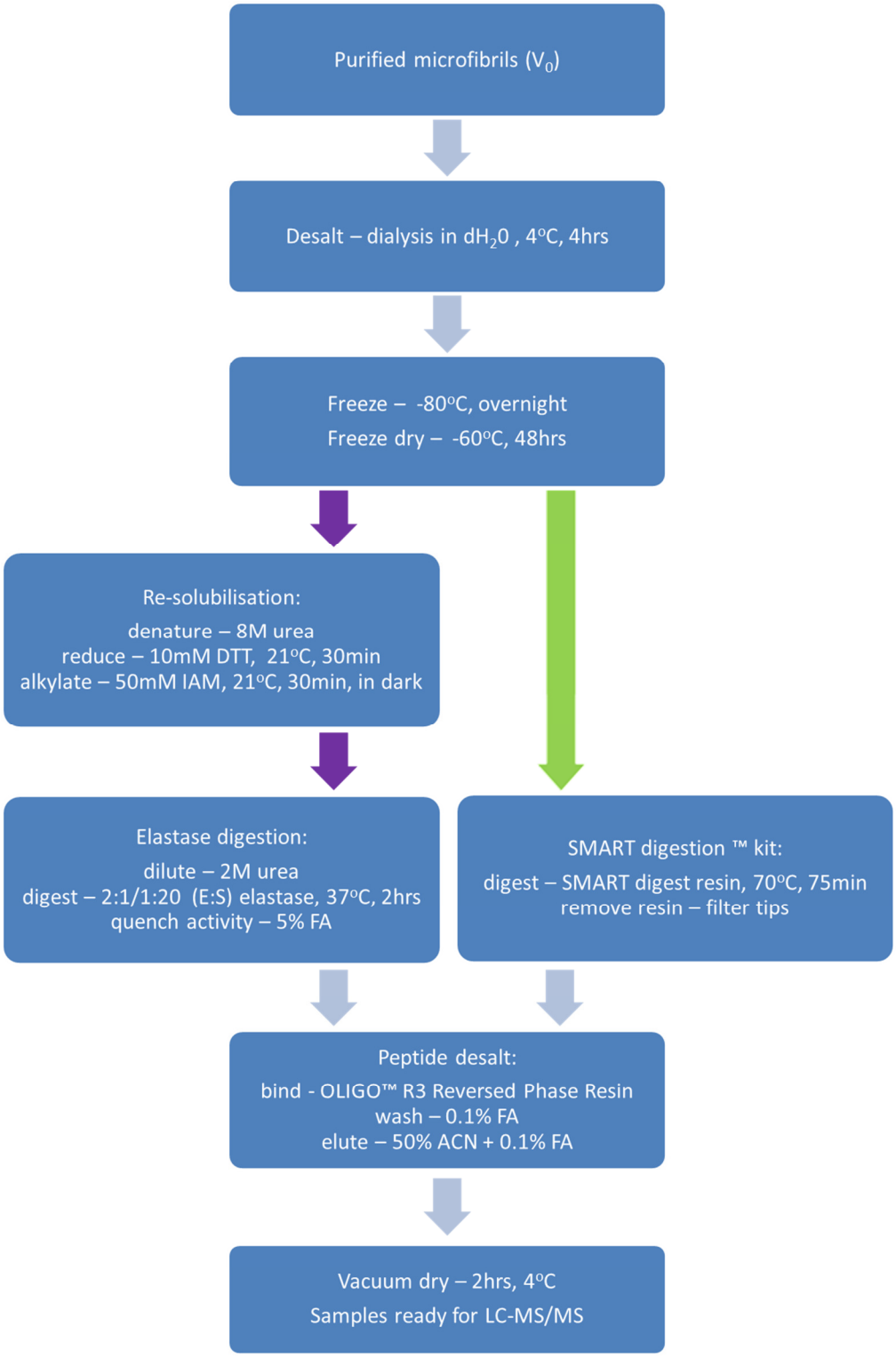

Figure 2.3: Flow diagram depicting the pre-MS sample preparation used. The purple arrows represent the elastase method for the augmentation of fibrillin-1 peptide generation. The green arrow represents the SMART™ digestion method for enhanced identification of microfibril-associated proteins (which omits re-solubilisation step and proceeds directly to digestion). DTT = dithiothreitol, IAM = iodoacetamide, E:S = enzyme to substrate ratio, FA = formic acid, ACN = acetonitrile.

2.3.2 Elastase digestion method

The elastase digestion method was developed to enhance peptide generation of proteins strongly bound within fibrillin and collagen VI microfibrils such as fibrillin-1 and COL6A3 (**Fig. 2.3**, purple path). This was achieved through the harsh resolubilisation of microfibrils (denaturation, reduction and alkylation) and the addition of porcine elastase, a nonspecific enzyme with a high activity in comparison to conventionally used trypsin (Doucet and Overall 2011; Rietschel *et al.* 2009; Sziegoleit *et al*. 1985).

Freeze-dried samples were re-suspended in 120 µl of 0.1 M Tris-HCl, pH 8.5. Microfibril samples were denatured in 8 M urea, reduced in 10 mM dithiothreitol (DTT; Fisher Scientific; Loughborough, UK) for 30 minutes at room temperature and alkylated in 50 mM iodoacetamide (IAM) for 30 minutes at room temperature, in darkness. The solution was then diluted down to 2 M urea using 0.1 M Tris-HCl, and porcine elastase (catalogue: E2150; Sigma) added at an enzyme:substrate ratio (E:S) specified for the experiment (either 1:20 or 2:1). This was incubated at 37°C for 2 hours. Elastase activity was then quenched with 5 % (v/v) formic acid in ultrapure water and samples were transferred to Eppendorf® LoBind 1.5 ml tubes (Eppendorf; Stevenage, UK) to minimise electrostatic loss of peptides.

2.3.3 SMART Digest™ trypsin method

The SMART digestion method, using the SMART Digest™ Trypsin Kit (Thermo Fisher), was performed to further enhance the identification of microfibril-associated proteins **(Fig. 2.3)**. This kit allows the fast digestion of samples through their incubation with trypsin, immobilised on a resin, at a high temperature (70°C) (Moore and Samonig 2016; Lanshoeft *et al.* 2016; Samonig *et al.* 2016). This applied heat was sufficient to denature proteins externally decorating microfibrils, making their primary structures accessible to trypsin, but insufficient for the denaturation of components within the microfibril itself. This means highly abundant microfibril proteins such as fibrillin-1 and the collagen VI alpha chains remained insoluble. As a result, the presence of less abundant microfibril accessory proteins (normally masked) became detectable with MS.

Freeze-dried samples were re-suspended in 20 µl of ultrapure water and 180 µl of SMART Digest™ buffer added. SMART Digest™ trypsin resin was then directly added to these suspensions. The samples were then incubated with the resin at 70°C for 75 minutes. Resin was then removed using detached TELOS MicroPlate™ filter tips (Kinesis; Cheshire, UK) and samples placed in Eppendorf® LoBind 1.5 ml tubes.

2.3.4 Peptide desalting

All peptide preparations were de-salted using a reverse phase column containing 1 mg of OLIGO™ R3 Reversed Phase Resin (Thermo Fisher; **Fig. 2.3**). Resin was wetted twice with 50 µl of 50% (v/v) acetonitrile (ACN) in ultrapure water within detached TELOS filter tips. Wet solution was pipetted out of resin using a standard p1000 Gilson pipette (Gilson; Middleton, Wisconsin, USA). Resin was then washed twice in 50 µl washing solution containing 0.1% (v/v) formic acid in ultrapure water. Peptide samples were then added to the resin within the TELOS tips and flow throughs kept until the end of analysis. Peptide-bound resin was then washed twice with 100 µl of washing solution. Peptides were eluted off the resin with 100 µl of 50% ACN and 0.1% (v/v) formic acid in ultrapure water. Collected samples were then vacuum-dried in a Speed Vac (Heto-Holten; Frederiksborg, Denmark) prior to liquid chromatography-tandem mass spectrometry (LC-MS/MS) analysis.

2.4 Proteomics and data analysis

2.4.1 Mass spectrometry

All MS analysis was performed by the Biomolecular Analysis Facility in the Faculty of Biology Medicine and Health at the University of Manchester (Manchester, UK). As dictated by their protocols (Buckley 2015; Lennon *et al.* 2014), peptide mixtures were analysed by LC-MS/MS using an UltiMate® 3000 Rapid Separation LC (RSLC, Dionex Corp; Sunnyvale, CA, USA) coupled to an Orbitrap Elite™ Hybrid Ion Trap-Orbitrap mass spectrometer (Thermo Fisher Scientific; **Fig. 2.4**). Peptides were separated using a gradient from 92% A (0.1% [v/v] formic acid in water) and 8% B (0.1% [v/v] formic acid in acetonitrile) to 33% B, ran in 44 minutes at 300 nL/min, using a 250 µm x 75 mm (inner diameter 1.7 µm) CSH C_{18}, analytical column (Waters; Herts, UK). Peptides were selected for fragmentation automatically by data-dependent analysis. For trypsin-digested samples, 1+ and ≥4+ charge states were rejected. For elastase-digested samples, only ≥4+ charge states were rejected.

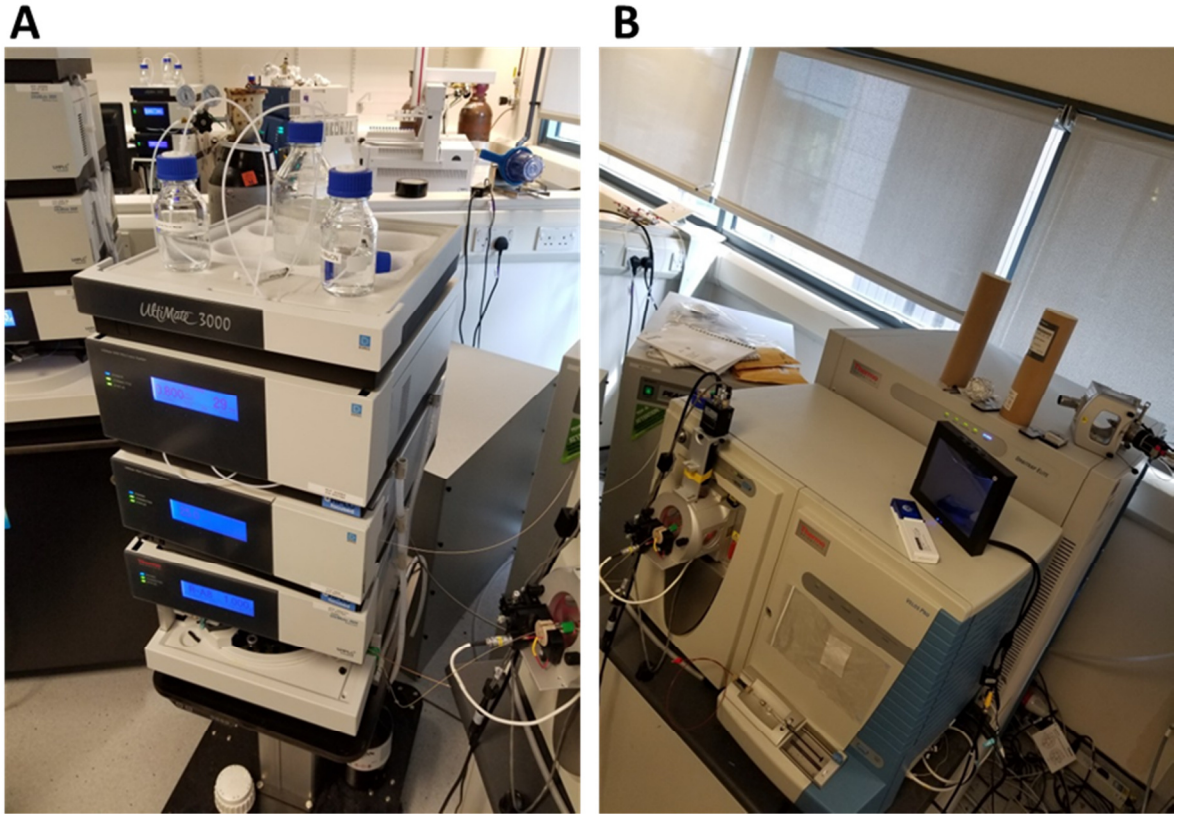

*Figure 2.4: Pictures of the LC-MS/MS instruments. An UltiMate® 3000 Rapid Separation liquid chromatographer **(A)** coupled to an Orbitrap Elite™ Hybrid Ion Trap-Orbitrap mass spectrometer **(B)** was used for all LC-MS/MS analysis.*

2.4.2 Pre-processing of raw mass spectrometry files to Mascot generic files

For a full work-flow summarising all the proteomic data analysis performed, please see **Fig. 2.5**. Raw MS spectrum files were converted to Mascot MGF files containing peak lists with associated mass and intensity values using the ExtractMSn algorithm (Thermo Fisher) under default parameters: minimum precursor mass – 400 Da; maximum precursor mass – 3500 Da; grouping tolerance – 1.4 Da; intermediate scans – 1; precursor charge – all charges; minimum scans per group – 1; minimum peaks – 10; minimum signal to noise (S/N) – 3; minimum major peaks – 5.

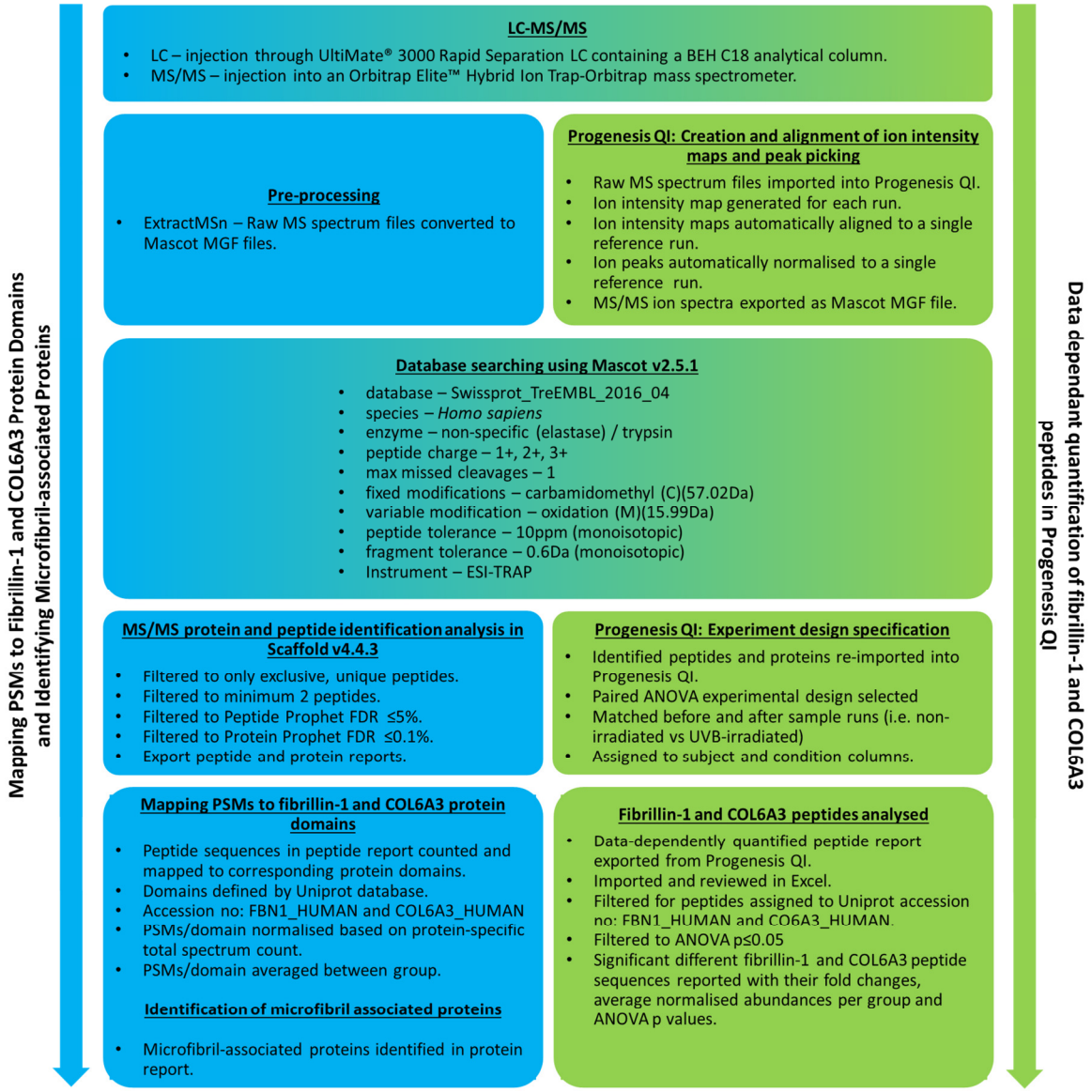

Figure 2.5: Work-flow summarising all the proteomic data analysis performed. The left blue path and associated blue text boxes detail the process of identifying peptide spectrum matches (PSMs) for fibrillin-1, COL6A3 and other fibrillin and collagen VI microfibril-associated proteins. The right green path and associated green text boxes details the process of data-dependent quantification of fibrillin-1 and COL6A3 peptides. Text boxes containing both blue and green colours detail steps pertinent to both processes.

2.4.3 Mascot-based correlation of mass spectrometry spectra with the Uniprot human database

The Mascot Daemon application v2.5.1 (Matrix Science; London, UK) was used to automate the submission of peak list MGF files to the Mascot server. The Mascot search engine then correlated the peak spectra within each file to the Uniprot human database (Swiss-Prot and TreEMBL). The Uniprot knowledgebase (Kb) is a comprehensive, freely accessible resource containing all known protein sequences and their associated functional data, curated and experimentally validated by experts worldwide (Consortium 2016). Mainly funded by the National Institute of Health, since its

creation, its proteome sequence databases have become the gold standard for MS spectra searching (Breuza *et al.* 2016).

Mascot MS/MS ion searches were performed with the following parameters: database – Swissprot_TreEMBL_2016_04; species – *Homo sapiens*; enzyme – non-specific for elastase method or trypsin for SMART digestion method; peptide charge – 1+, 2+ and 3+; max missed cleavages – 1; fixed modifications – carbamidomethyl (mass: 57.02 Da; amino acid: C); variable modification – oxidation (mass: 15.99 Da; amino acid: M); peptide tolerance – 10 ppm (monoisotopic); fragment tolerance – 0.6 Da (monoisotopic); instrument – ESI-TRAP. Mascot search results were exported as DAT files for every run performed.

2.4.4 Validation in Scaffold 4

Peptide spectrum matches (PSM) and peptide and protein identifications were generated using the Scaffold 4 software (Proteome Software; Portland, OR, USA). DAT files were imported into Scaffold 4 and peptide/protein identifications generated automatically using the following parameters: searched database – Swissprot_TreEMBL_2016_04; scoring system – LFDR scoring; protein grouping – standard experiment wide protein grouping.

From within Scaffold 4, data were filtered to report only peptides exclusive and unique to their matched proteins (with no matching ambiguity) and only proteins with a minimum of 2 identified peptides. Peptide and protein false discovery rates (FDR) were automatically calculated by Scaffold 4 using peptide and protein probabilities assigned by the Trans-Proteomic Pipeline (Sourceforge; Seattle. WA, USA) using the PeptideProphet™ (Keller *et al.* 2002) and ProteinProphet™ (Nesvizhskii *et al.* 2003) algorithms. PeptideProphet FDR was thresholded to ≤ 5 % and ProteinProphet FDR to ≤ 0.1%.

Peptide and protein reports were exported from Scaffold 4 within CSV files which were then imported into Microsoft Excel (Microsoft Office, Microsoft; Manchester, UK) for further analysis of identified peptides and proteins.

2.4.5 Analysis of microfibril-associated proteins

Microfibril-associated protein presence was identified within the protein reports generated by Scaffold 4. Lists of detected proteins were manually searched for known fibrillin and collagen VI microfibril-associated proteins (see reviews: (Thomson *et al.* 2018) and (Cescon *et al.* 2015)) as

well as those proposed by Cain *et al.* (2009) in their fibrillin-1 recombinant fragment molecular fishing study. Identified proteins were then reported alongside their PSMs.

2.4.6 Mapping peptide spectrum matches to fibrillin-1 and collagen VI α3 proteins

For peptide sequence mapping onto human fibrillin-1 and COL6A3 protein domains, primary sequences and domain positions were extracted from the Uniprot database. Only information from the reviewed SwissProt designated proteins were used: accession numbers: FBN1_HUMAN (P35555) (web address: https://www.uniprot.org/uniprot/P35555) for fibrillin-1 and CO6A3_HUMAN (P12111) (web address: https://www.uniprot.org/uniprot/P12111) for COL6A3.

Similar to the peptide mapping done by Cain *et al.* (2006), the peptide sequence of each PSM was mapped to its respective protein domains of fibrillin-1 or COL6A3 (for an example, please see **Fig. 2.6**). The number of PSMs per domain was then counted for each sample. To allow comparisons across different samples (which unavoidably contain variations in protein abundance), the number of PSMs per domain were normalised across the whole experiment based on the total spectrum counts for fibrillin-1 or COL6A3 respectively (Lundgren *et al.* 2010). Normalised PSMs per domain were then averaged across each group and subsequently heat mapped onto a domain schematic of fibrillin-1 or COL6A3 to show the average peptide yield within the different structural regions of these proteins.

A

Protein name	Uniprot accession	Exclusive unique peptides	Total spectra	Peptide sequence
Fibrillin-1	FBN1_HUMAN	214	258	ACEDIDECSLPNICV
Fibrillin-1	FBN1_HUMAN	214	258	ACIDINECEL
Fibrillin-1	FBN1_HUMAN	214	258	ADGKACEDIDEC
Fibrillin-1	FBN1_HUMAN	214	258	ADGKACEDIDECSLPNIC
Fibrillin-1	FBN1_HUMAN	214	258	ADGKACEDIDECSLPNICV
Fibrillin-1	FBN1_HUMAN	214	258	AGSDINECALDPDICPNGICENLRGT
Fibrillin-1	FBN1_HUMAN	214	258	AGSDINECALDPDICPNGICENLRGTYKC
Fibrillin-1	FBN1_HUMAN	214	258	ALDPDICPNGI
Fibrillin-1	FBN1_HUMAN	214	258	ALDPDICPNGICENLRGT
Fibrillin-1	FBN1_HUMAN	214	258	CCPGWKTLPGGNQCIVPI

B

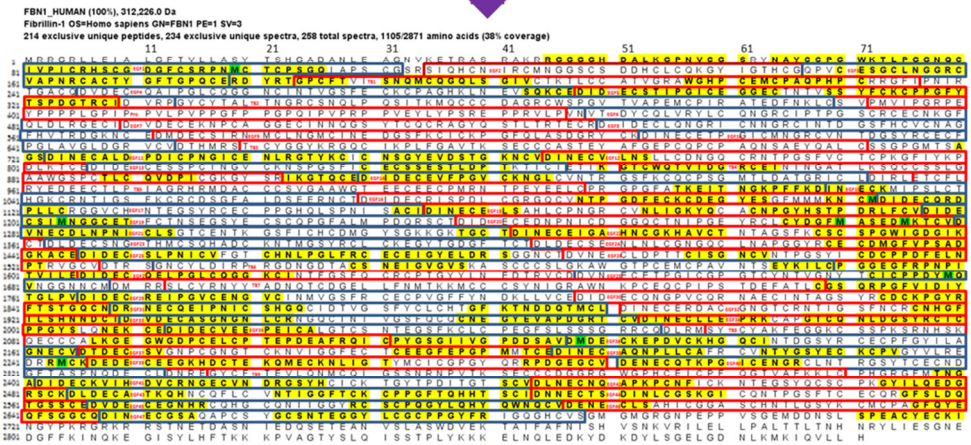

C

		Normalised PSMs				
No	Fibrillin-1 domain	Sample 1	Sample 2	Sample 3	Average	Heat map
1	N-terminal Region	0	2	2	**1**	
2	EGF-like 1	5	7	5	**6**	
3	EGF-like 2	0	0	0	**0**	
4	EGF-like 3	0	2	0	**1**	
5	TB 1	3	2	0	**2**	
6	EGF-like 4	0	2	2	**2**	
7	EGF-like 5	3	8	2	**4**	
8	TB 2	0	2	0	**1**	
9	Pro-rich	0	0	0	**0**	
10	EGF-like 6	0	0	0	**0**	

D

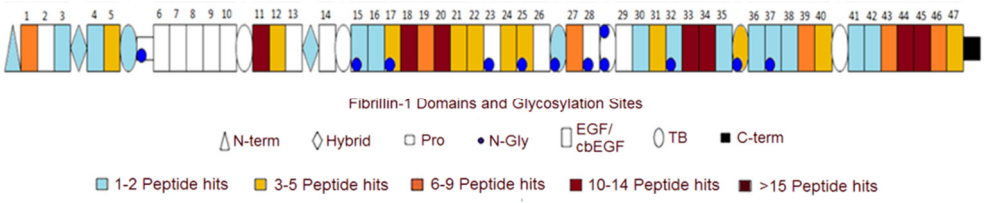

Figure 2.6: Example workflow showing the mapping of PSMs onto the domains of fibrillin-1. Fibrillin-1 peptides are identified in the peptide reports generated by Scaffold 4. This example depicts only the first ten fibrillin-1 peptide sequences identified out of 214 exclusive, unique peptides in a single sample ***(A)****. All peptides are next mapped onto the primary sequence of fibrillin-1 (highlighted yellow) overlaid with its domain positions (sequences corresponding to each domain are boxed in alternating blue and red)* ***(B)****. The number of mapped peptides is then counted per domain. The process is repeated for all samples within the group, normalised based on the total spectrum counts across the whole experiment, and averaged across the group (example shows only the first ten fibrillin-1 domains)* ***(C)****. These are subsequently heat mapped onto a domain schematic of fibrillin-1 to show the average, regional yield of peptides across its structure* ***(D)****.*

2.4.7 Data-dependent quantification of fibrillin-1 and collagen VI α3 peptides in Progenesis QI

Data-dependent peptide quantification was performed using Progenesis QI software package (Nonlinear Dynamics, Waters, Newcastle, UK; see **Fig. 2.7** for an example). Raw mass spectra files were imported and ion intensity maps were automatically generated. Ion outlines were automatically aligned by Progenesis QI to a single reference run using default settings. Ion peaks and their relative abundances were then automatically picked without filtering and normalised to a single reference run by Progenesis QI using default settings. Data were then exported as a Mascot MGF file and searched using Mascot v2.5.1 with same search parameters and on the same database as described in Section 2.4.3. This was then re-imported back into Progenesis QI where identified peptide ions were automatically matched. Normalised abundance for each peptide was calculated by Progenesis QI as the sum of the each matched peptide ion abundance (individual peptide ion abundance is equal to the sum of the intensities within the isotope boundaries).

Normalised peptide abundances, compared between matched samples, were statistically analysed within Progenesis QI using a paired (repeated measured) ANOVA test. The paired ANOVA experimental design was selected and normalised peptide abundances were compared between matched samples (i.e. non-irradiated vs. broadband UVB-irradiated). A fold change for each peptide was also calculated automatically (fold change is defined as the higher average normalised abundance of one group divided by the average normalised abundance of the second group).

Peptide quantification data were exported from Progenesis QI as a CSV file and imported in Microsoft Excel. Fibrillin-1 and COL6A3 peptides which matched to Uniprot accession numbers FBN1_HUMAN and CO6A3_HUMAN were identified and filtered to $p \leq 0.05$. Significantly different fibrillin-1 and COL6A3 peptide sequences are reported alongside their fold changes, average normalised abundances per group and paired ANOVA p values.

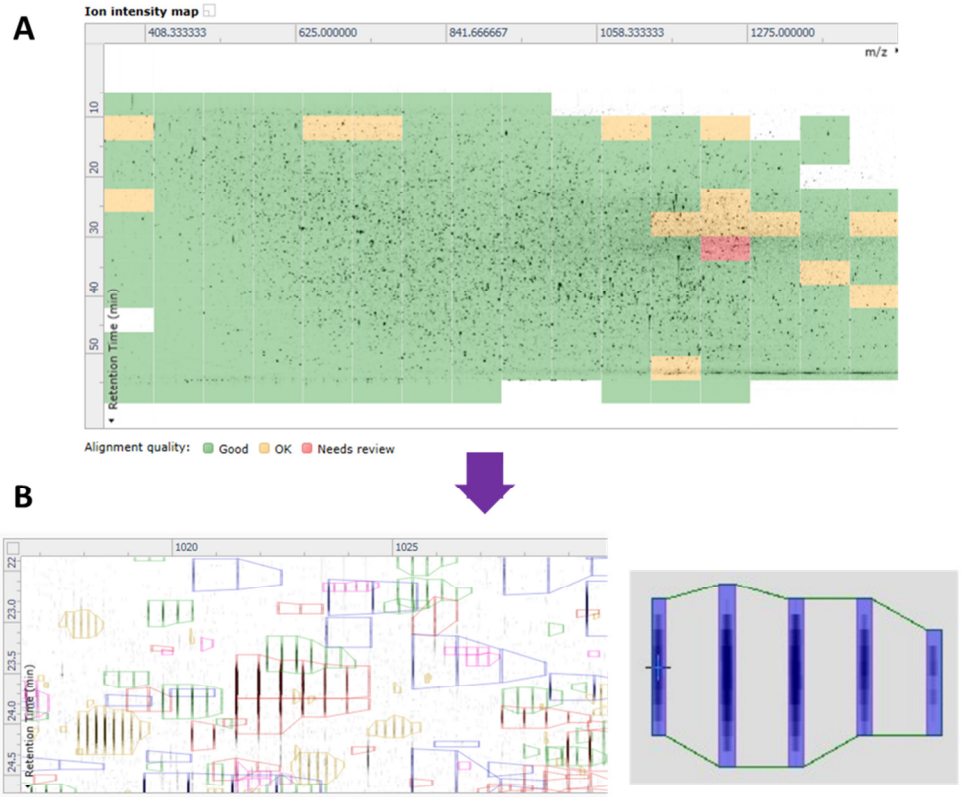

C

	Control	UVB
M79	20171206_AE_E_A01	20171206_AE_E_A03
M75	20171206_AE_E_B01	20171206_AE_E_B03
F75	20171206_AE_E_C01	20171206_AE_E_C03

D

Broadband UVB-Affected Fibrillin-1 Peptides	Fold Change	Average Norm. Abundance		Anova (p value)
		UVB	Control	
SLDQTGSSCEDVDECEGNHR	∞	109553	0	0.0281
LMPDQRSCTDIDECEDNPNICDGGQCT	∞	47826	0	0.0065
NCVDINEC	∞	9637	0	0.0090
TGCTDINECEIGA	18.6	278349	14945	0.0347
IIVGPDDSAVDMDECKEPDVCKH	9.15	94566	10336	0.0285
NEKCEDIDECVEEPEICAL	8.55	159126	18610	0.0414
GSGIIVGPDDSAVDMDECKEPDVC	3.31	382172	115352	0.0431
ALDPDICPNGI	1.84	222443	120605	0.0319
VDINECLLEPR	1.83	908622	497267	0.0423
LQHYQWNQCVDENEC	1.81	29351	16222	0.0026
CENLRGTYKCI	1.56	14171	9107	0.0447
CEDIDECVEEPEICA	∞	0	134280	0.0267
CRHSCGDGFCSRPNMCTCPS	-1060	93	98815	0.0027
GFMTNGADIDECKVIHDVCR	-2.28	9472	21569	0.0190

*Figure 2.7: Example workflow showing the data-dependent quantification analysis of fibrillin-1 peptides using Progenesis QI. Ion intensity maps were generated for each run and automatically aligned to a single reference run **(A)**. Ions and their abundances were automatically picked and assigned **(B)**. Individual ion abundance equalled the sum of the intensities within the isotope boundaries. Once spectra were matched to their respective protein peptides by Mascot and re-imported back into Progenesis QI, a paired ANOVA experimental design was selected. Matched before and after sample runs (non-irradiated vs broadband UVB-irradiated in this example) were assigned to subject and condition columns **(C)**. Peptide quantification data were then exported to Excel where peptides assigned to Uniprot accession no: FBN1_HUMAN were identified and filtered to $p \leq 0.05$. Significantly different fibrillin-1 peptide sequences were reported with their fold changes, average normalised abundances per group and p values **(D)**.*

2.5 Microfibril ultrastructure characterisation

2.5.1 Stub preparation for atomic force microscopy

Glass coverslips (Agar Scientific; Essex, UK) were soaked in absolute ethanol overnight, left to dry for 30 minutes and then attached to metal stubs (Agar Scientific) with clear nail varnish. One hundred µl of microfibril suspension was pipetted directly onto the coverslips and left for one minute where fibrillin and collagen VI microfibrils adsorbed to the glass surface. The solution was then removed and stub left to dry overnight. Stubs were then washed three times with 0.22 µm filtered ultrapure water and left to dry for one hour before imaging with atomic force microscopy (AFM; **Fig. 2.8**) (Hibbert *et al.* 2015; Sherratt *et al.* 2010).

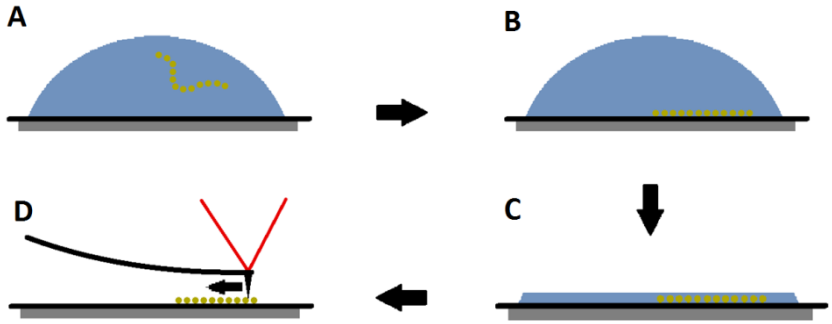

*Figure 2.8: Microfibril stub preparation for AFM. Purified microfibril extracts were pipetted directly onto coverslips **(A)** and left to adsorb for one minute **(B)**. The remaining solution was removed **(C)** and left to dry. The coverslips were then washed and dried prior to AFM **(D)**.*

2.5.2 Atomic force microscopy

Fibrillin microfibrils were imaged using peak force and Scan-Asyst® mode AFM **(Fig. 2.9 A)** using a Nanoscope IIIa Multi-mode atomic force microscope (Bruker; Santa Barbara, CA, USA) as previously described (Hibbert *et al.* 2015; Sherratt *et al.* 2005, 2010). Using a single, new Scan-Asyst® Air tip (Bruker) per sample, single fibrillin **(Fig. 2.9 B)** and collagen VI microfibrils were captured at scan rate of 0.977 Hz, at resolution of 512 pixels/line in 2 x 2 µm height scans. This gave a lateral resolution of 3.9 nm/pixel, which was high enough for ultrastructural analysis, as previously shown (Hibbert *et al.* 2015; Sherratt *et al.* 2010). Fibrillin microfibrils which were laterally associated with collagen VI microfibrils were omitted from the analysis. AFM height scans were then digitally flattened using WSxM v5.0 AFM Image Processing package (Horcas *et al.* 2007) and the height scales set to between -5 and 15 nm. These scans were then exported in text image format.

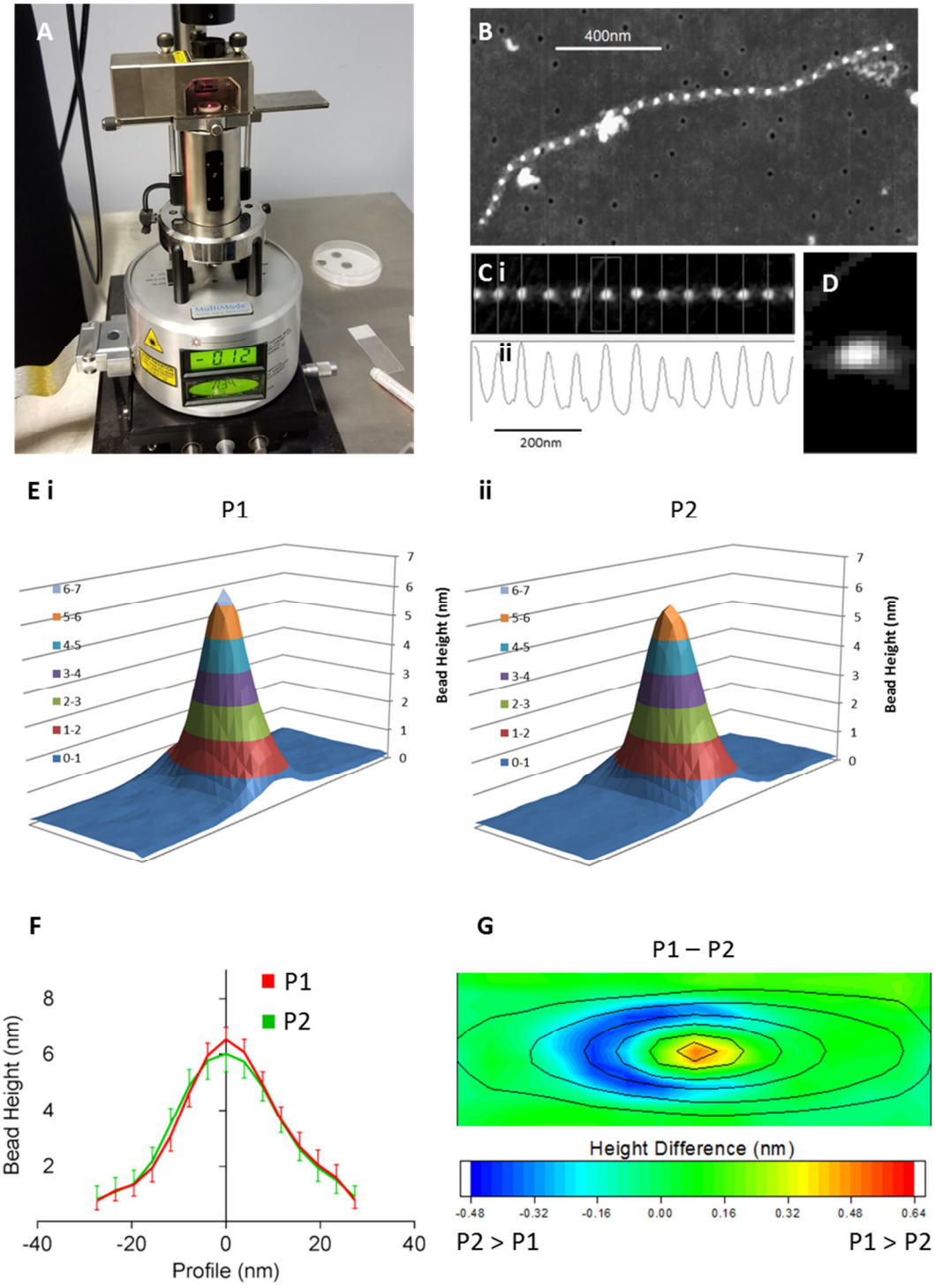

Figure 2.9: AFM characterisation of fibrillin microfibril beads. A Nanoscope IIIa Multi-mode atomic force microscope (Bruker) ***(A)*** *was used to capture fibrillin microfibrils* ***(B)*** *at a lateral resolution of 3.9 nm/pixel. These were straightened in ImageJ* ***(Ci)*** *and an axial height profile generated* ***(Cii)****. This was used to specify the centre of each bead within the microfibril (height maxima) and generate a 15 x 41 pixel height snapshot of each bead* ***(D)****. These snapshots were then averaged for each group; i.e. population 1 (P1) and P2, and a 3D height map generated* ***(Ei, ii)****. From these, axial height profiles of bead averages were generated* ***(F)*** *allowing statistical comparisons of morphologies between groups. Averaged bead snapshots from each group were also subtracted from the averaged snapshot a comparator group to show the differences in bead height. These were used to generate colour height difference heat maps overlaid with the contours of an average bead from one group* ***(G)****, allowing local differences in bead morphologies to be visualised.*

2.5.3 Fibrillin microfibril bead characterisation

The negative heights (below the glass surface) in the 2 x 2 μm height scans of individual fibrillin microfibrils were corrected by subtracting the negative background (Ratcliff and Erie 2001) using AFM Image Manipulation software developed by Sherratt *et al.* (2005) using Microsoft Visual Basic 6.0 (Redmond, WA, USA) as described previously. These were then exported as RAW files. Using ImageJ image processing program (NIH; Bethesda, MA, USA) fibrillin microfibrils were straightened using the Straighten Curved Objects plugin (Kocsis *et al.* 1991) enabling the generation of 41 pixel wide images of single, straightened assemblies **(Fig 2.9 Ci)**. This was done ensuring that the fibrillin microfibril beads fell accurately in the centre of the images (on the 21st pixel out of 41) and that the shoulder regions were always orientated to the right side of the image. LFA image processing software, developed by Sherratt *et al.* (2003) using Microsoft Visual Basic 6.0, was then used to generate an axial height profile of each straightened microfibril. Using this, the centre of each bead was specified by correlating them to their height maxima in the axial profile **(Fig. 2.9 Cii)**. This led to the generation of 15 x 41 pixel snapshots of each individual bead with the height maxima at the central pixel of the image **(Fig. 2.9 D)** which were exported to Microsoft Excel.

Using Excel, all fibrillin microfibril bead snapshots within a group (n=100 per sample, n=300 per group) were averaged and a 3D-surface graph generated for each group **(Fig. 2.9 E)**. These 3D height graphs effectively described the morphology (topography) of an average fibrillin microfibril bead within one group. From these, axial height profiles of bead averages could be generated **(Fig. 2.9 F)** allowing comparisons of morphologies between groups and descriptive and quantitative statistics to be performed. An averaged bead snapshot from one group could also be subtracted from the averaged snapshot of the second group to show the differences in heights between two average beads from each group. These were used to generate colour height difference heat maps overlaid with the contours of an average bead from one group **(Fig. 2.9 G)**. This allowed local differences in bead morphology to be visualised between two fibrillin microfibril groups.

2.5.4 Fibrillin and collagen VI microfibril periodicity analysis

Flattened 2 x 2 μm height scans (3.9 nm/pixel resolution) of single fibrillin and collagen VI microfibrils were imported into Periodicity and Angles software package developed by Sherratt *et al.* (2003) using Microsoft Visual Basic 6.0. The bead to bead distance (in nm) was then measured within the program by zooming into the beads (windows icon button + plus button on keyboard) and specifying the centre of each bead, as previously described (Sherratt *et al.* 2005) **(Fig. 2.10)**. The

periodicity measurements were then exported to Microsoft Excel and an average calculated per group (n=500 per sample, n=1500 per group) allowing the periodicity to be statistically compared.

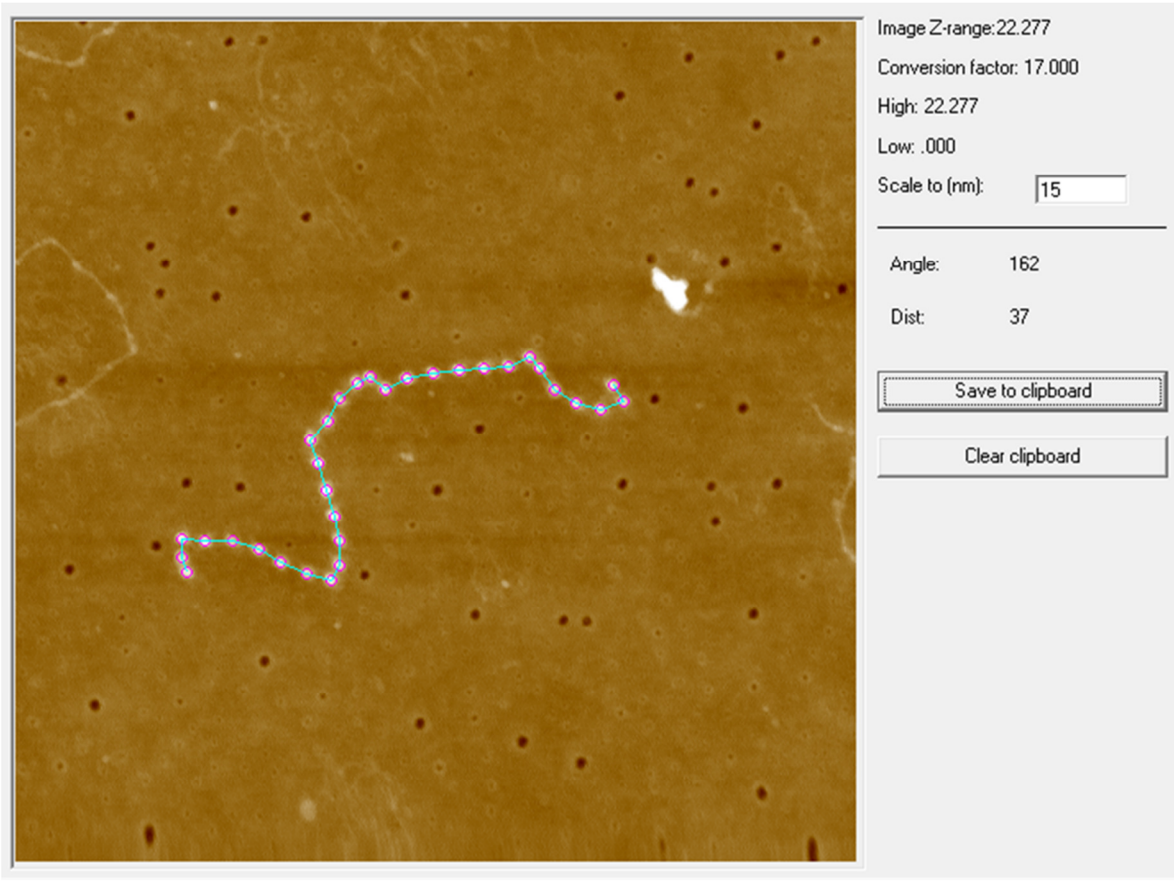

Fibrillin microfibril periodicity (nm)			
45.55	58.72	63.59	68.22
58.07	62.99	58.07	59.63
60.64	63.59	65.48	65.48
59.63	57.68	65.48	66.41
61.76	47.04	59.75	54.83
36.01	34.94	58.59	42.97
55.93	55.52	40.22	37.06
58.72	61.14	60.64	

Figure 2.10: Periodicity measurements of a fibrillin microfibril. Flattened 2 x 2 µm height scans of single microfibrils were imported into Periodicity and Angles software package and the centre of each bead specified within the program. This automatically generated the bead to bead distance measurements (in nm) which were exported to Microsoft Excel.

2.5.5 Microfibril ultrastructure statistical analyses

All microfibril ultrastructure statistical comparisons were performed using GraphPad Prism statistics software (GraphPad Software Incorporated; La Jolla, California, USA). Only differences of $p \leq 0.05$ were considered significant.

For fibrillin microfibril bead statistical comparisons, 100 beads were measured per individual sample. Statistical analyses were performed on all beads measured across a group of triplicate repeats (N=3; n=300). Central beads heights were statistically analysed using Mann-Whitney U tests and cumulative frequency distributions using Kolmogorov-Smirnov tests. Axial height profiles **(i.e. Fig. 2.9 F)** were statistically analysed using Bonferroni-corrected multiple comparisons tests.

For fibrillin and collagen VI microfibril periodicity statistical comparisons, 500 measurements were taken per individual samples. Statistical analyses were performed on all measurements across a group of triplicate repeats (N=3; n=1500). Periodicities were statistically analysed using Mann-Whitney U tests and cumulative frequency distributions of periodicities using Kolmogorov-Smirnov tests.

2.6 Ultraviolet irradiation

Triplicate samples of purified microfibril suspensions were vortexed and split into three matched groups: control, broadband UVB-irradiated and solar simulated radiation (SSR)-irradiated. All suspensions (2 ml volumes) were irradiated within uncapped 35 mm x 10 mm polystyrene cell culture dishes (Corning, Flintshire, UK).

2.6.1 Broadband ultraviolet-B irradiation

Broadband UVB-designated microfibril suspensions were irradiated with a broadband UVB spectrum as previously described (Sherratt *et al.* 2010) using two 20 W Phillips TL-12 tubes (Eindhoven, The Netherlands) with an emission wavelength range of 270 – 400 nm (peak output of 313 nm; **Fig. 2.11**). Before each experiment, the UVB waveband irradiance was first measured using a UVX radiometer (UVR Products, Upland, CA, USA) fitted with a UVX31 broadband UVB detector. An associated calibration factor (equal to 0.63) had already been pre-calculated via measurement of spectral outputs using a double grating spectroradiometer (Bentham Instruments Ltd., Reading, UK), calibrated to National Physical Laboratory (Teddington, UK) standards. By multiplying the UVX meter reading with the associated calibration factor, an absolute irradiance value was calculated in mW/cm^2:

$$\text{UVX radiometer reading} \times \text{calibration factor} = \text{irradiance } (mW/cm^2)$$

The irradiation time, equivalent to a dose of 100 mJ/cm^2 was then calculated by dividing the dose by the irradiance in a standard power calculation:

Dose (mJ/cm^2) / irradiance (mW/cm^2) = time (sec)

Suspensions were irradiated simultaneously, in triplicate: placed in the centre and at a vertical distance of 16 cm from the source, at room temperature. A UVB dose of 100 mJ/cm^2 using the TL-12 was equivalent to a dose of 13.2 mJ/cm^2 of erythemally-weighted UVR. This was calculated based on an erythema-weighting conversion factor reported by McKenzie *et al.* (2004).

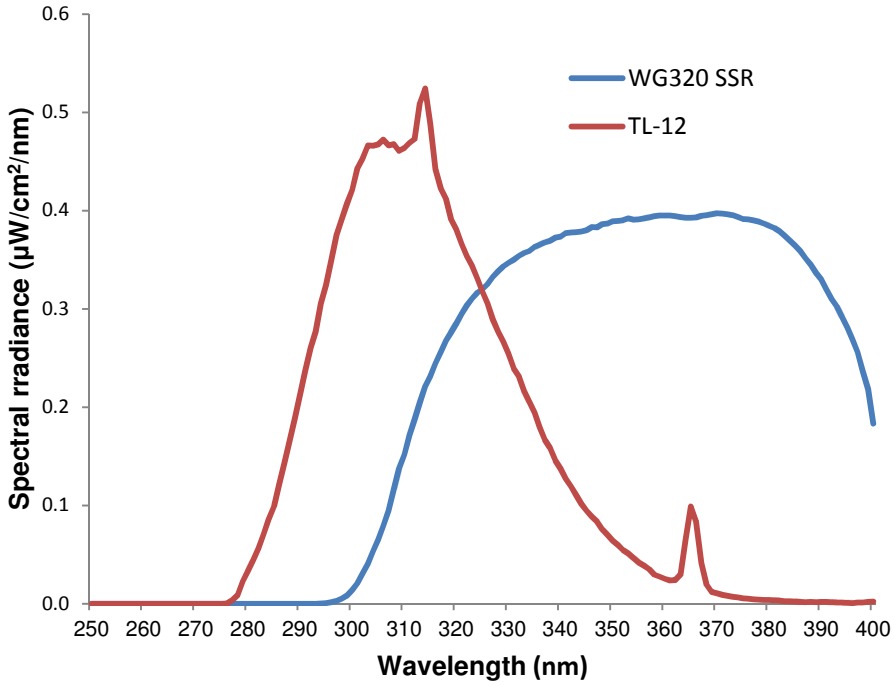

Figure 2.11: Spectral output of the UVB (TL-12) and SSR (Solar Simulator with full spectrum WG320 filter) sources used in UV irradiation experiments. The spectral irradiance for both sources is shown between the wavelengths of 250 and 400 nm. Spectral output data was kindly provided by Dr Sarah Hibbert.

2.6.2 Solar simulated irradiation

SSR-designated microfibril suspensions were irradiated using a Solar Simulator (Applied Photophysics, Cambridge, UK) as previously described (Hibbert *et al.* 2017, 2015). This is comprised of a xenon arc lamp light source fitted with a WG320 SSR filter (Schott, Stafford, UK). The spectral output was comprised of ~5% UVB and ~95% UVA **(Fig. 2.11)**. As with broadband UVB, irradiance was measured using a UVX radiometer; however, this time fitted with a UVX36 full spectrum detector. As before, a calibration factor (equal to 2.88) had been pre-calculated using spectroradiometer spectral output measurements calibrated to National Physical Laboratory standards. The irradiation time was then calculated using the same aforementioned equations and suspensions were irradiated in triplicate with a dose of 30 J/cm^2, at a vertical distance of 20 cm

from the source, at room temperature. An SSR dose of 30 J/cm^2 using a full spectrum WG320 filter was equivalent to 213.4 mJ/cm^2 of erythemally-weighted UVR. This was calculated based on an erythema-weighting conversion factor specific to the UV spectrum of the Solar Simulator fitted with the WG320 filter.

2.7 Skin histology and elastosis quantification

2.7.1 Tissue cryosectioning

Abdominal, forearm and buttock biopsies from middle-aged donors were re-embedded in optimal cutting temperature compound (OCT) embedding matrix (CellPath; Powys, UK) and frozen at -80°C. Cryosectioning was performed by Dr Abigail Langton and Mrs Poonam Halai using a Bright OTF 5000 (Bright Instruments; Bedfordshire, UK) cryostat fitted with a 190 mm microtome blade (Bright Instruments). Embedded samples were orientated and mounted onto a sectioning chuck and clamped within the cryostat. The thickness of the sections was set to 5 μm. Three serial sections were collected onto each Superfrost Ultra-Plus Adhesion slide (Thermo). These were stored at -80°C prior to Weigert's resorcin fuchsin staining.

2.7.2 Weigert's resorcin fuchsin staining

To compare the extent of solar elastosis between abdominal, forearm and buttock skin, elastic fibres in cryosections were stained with Weigert's resorcin-fuchsin elastin staining solution (Merck; Darmstadt, Germany) (Proctor and Horobin 1988).

Cryosection-adsorbed slides were left to defrost at room temperature for 5 minutes and then submerged and fixed in 4% (w/v) paraformaldehyde (PFA) in PBS, at room temperature for 10 minutes. These were then washed twice in 0.1 M Tris-HCl (pH 7.8) for 5 minutes each time. Sections were lightly rinsed with ultrapure water and then submerged in Weigert's elastin staining solution for 10 minutes at room temperature. These were then lightly rinsed twice with 100% industrial methylated spirits (IMS). Staining quality was checked using brightfield microscopy (a dark purple colour meant that the stain had effectively absorbed into the tissue). Sections were lightly rinsed with ultrapure water and then dehydrated in graded IMS: 70% (v/v), then 100%, then in fresh 100% again, 5 minutes per step and then twice in xylene for 10 minutes each, all performed at room temperature. Slides were then mounted using DPX (a mixture of distyrene, plasticizer and xylene) embedding media (Thermo) and stored at room temperature.

2.7.3 Microscopy and imaging

Weigert's stained abdominal, forearm and buttock skin sections were imaged in brightfield using an Olympus BX53 advanced research microscope (Olympus; Essex, UK) fitted with an Olympus DP73 camera and controlled by Olympus cellSens v1.15 imaging software. Three images were taken per section at two magnifications (six images total). Twenty times (20 x) magnification captured an image size of 352 μm x 264 μm at a resolution of 0.22 μm/pixel with an exposure time of 1.176 ms and 10 x magnification captured an image size of 704 μm x 528 μm at a resolution of 0.44 μm/pixel with an exposure time on 0.313 ms. Images were saved as TIFF files.

2.7.4 Elastic fibre quantification

Elastic fibre abundances in abdominal, forearm and buttock skin was quantified by measuring the percentage area of elastic fibre presence in Weigert's stained tissue sections, at a given depth, using ImageJ. Elastic fibre presence was assessed at three dermal depths of 50 μm, 100 μm and 300 μm, measured from the DEJ.

Images were imported as TIFF virtual stacks into ImageJ and stacked to standard RGB images. The scale was set to 0.22 μm/pixel for images at 20x magnification and 0.44 μm/pixel for images at 10x magnification. Vertical lines of length equating to the dermal depths assessed (50 μm, 100 μm, or 300 μm) were then inserted into the images and placed equidistantly throughout, with the tops of the lines aligned to the DEJs **(Fig. 2.12 A)**. Areas encompassing the DEJs (tops of the lines) and the bottoms of the lines were then free-drawn. Only elastic fibres within these areas, and therefore only up to the choses dermal depths, were quantified.

Percentage areas of elastic fibres, within areas drawn, were measured automatically by thresholding the images within ImageJ so pixels with a deep purple colour (stained elastic fibres) were coloured red and the rest coloured white **(Fig. 2.12 B)**. Images were thresholded by brightness using "Threshold Colour": thresholding method - moments, threshold colour – white, colour space – hue, saturation and brightness. Brightness was thresholded to between an ImageJ-assigned scale of 186 and 255 in all images. Hues and saturations were not thresholded (kept at 0-255 scale). All coloured pixels were then converted to a single red colour: images were converted to 8-bit greyscale and all grey pixels coloured red using "Threshold" and selecting the red colour. Elastic fibre abundances were measured within ImageJ as a percentage of red pixels within the areas drawn: measurements were set to include area, area fraction, and set to threshold. Percentages measured were then copied to and further analysed using Microsoft Excel.

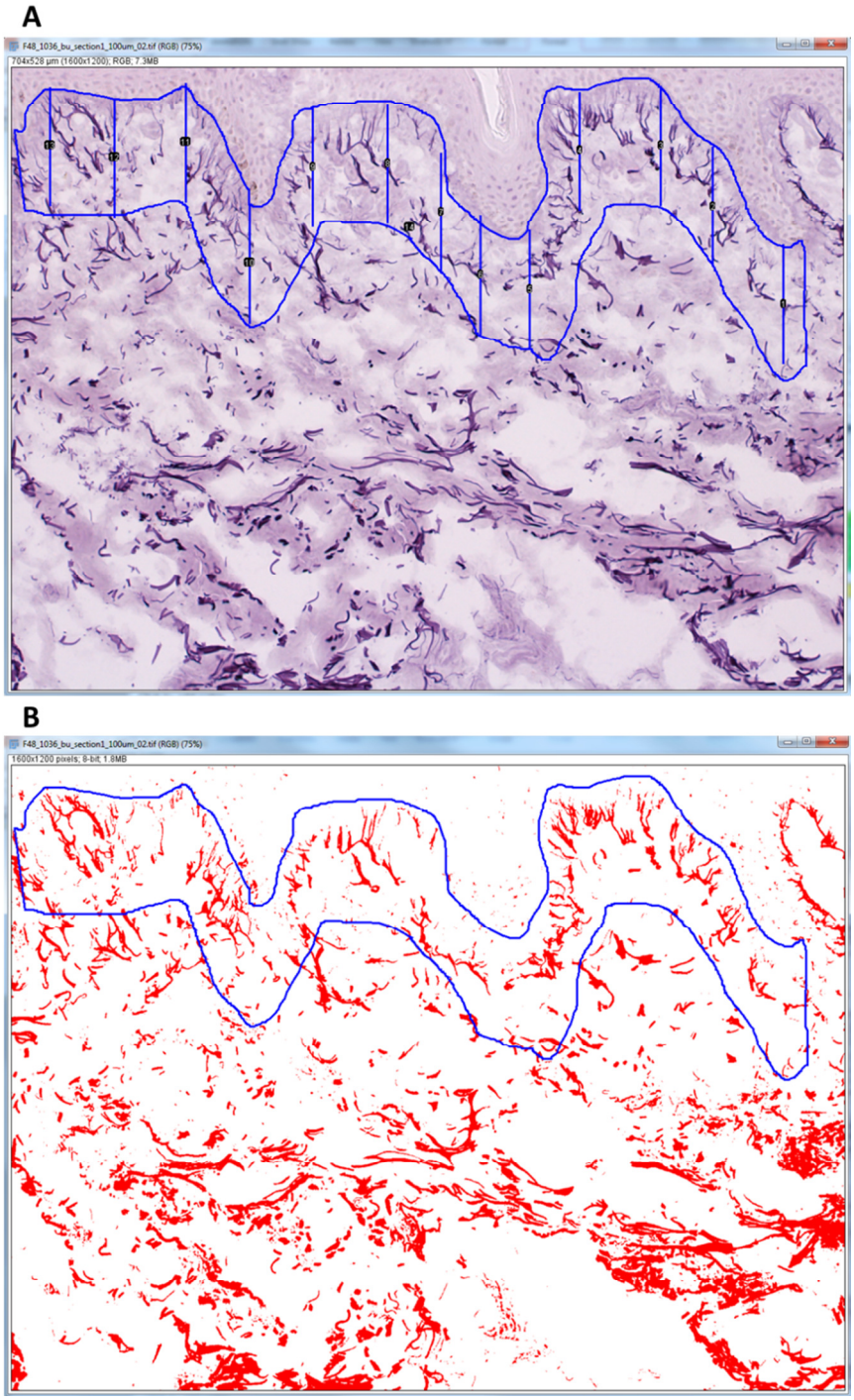

*Figure 2.12: Quantification method used to measure percentage area of elastic fibres at a depth of 100 µm. Vertical lines, 100 µm in length, were inserted into the images and placed roughly equidistantly, with the tops of the lines carefully aligned to the DEJ. An area encompassing the DEJ (tops of the lines) and the bottoms of the lines was then free-drawn **(A)**. Only elastic fibres within these areas, and therefore only within dermal depth of 100 µm, were quantified. Percentage areas of elastic fibres, within areas drawn, were measured automatically by thresholding the images within ImageJ so pixels with a deep purple colour (stained elastic fibres) were coloured red and the rest coloured white **(B)**. Elastic fibre presences were measured within ImageJ as a percentage of red pixels within the areas drawn.*

2.7.5 Histology statistical analysis

All percentage area elastic fibre statistical comparisons were performed using GraphPad Prism. Only differences of $p \leq 0.05$ were considered significant. All graphs generated represent error bars as standard deviation. The percentage area of elastic fibres (for each depth: 50 μm, 100 μm and 300 μm) was assessed for three groups (abdominal and matched forearm and buttock skin) with four individuals per group. Percentage area was measured in three images per section and three sections per individual. These nine measurements were then averaged to give a single measurement of elastic fibre area per sample at a single depth. Elastic fibres were analysed between matched forearm and buttock groups using paired t tests and between unmatched abdominal vs. buttock and abdominal vs. forearm groups using unpaired t tests (N=4). Tests were Bonferroni corrected for multiple comparisons.

Chapter 3: Optimised digestion methods for the proteomic characterisation of human tissue microfibrils

This methods paper was written with the Journal of Proteome Research in mind. I conceived, designed and performed all experiments, analysed all the data, prepared the figures and wrote the paper. Dr David Knight and Dr Ronan O'Cualain of the Biological Mass Spectrometry Core Facility in the Faculty of Biology, Medicine and Health at the University of Manchester (Manchester, UK) provided technical assistance for all LC-MS/MS. Professor Clair Baldock contributed to the preparation and interpretation of **Figure 3.3**.

Optimised digestion methods for the proteomic characterisation of human tissue microfibrils

Alexander Eckersley[1], Rachel EB Watson[2,5], David Knight[3], Ronan O'Cualain[3], Christopher EM Griffiths[2,5], Clair Baldock[1,4], Michael J Sherratt[1]*

[1]Division of Cell Matrix Biology & Regenerative Medicine, [2]Division of Musculoskeletal & Dermatological Sciences, [3]School of Biological Sciences, [4]The Wellcome Trust Centre for Cell-Matrix Research, Faculty of Biology, Medicine and Health, The University of Manchester and [5]NIHR Manchester Biomedical Research Centre, Central Manchester University Hospitals NHS Foundation Trust, Manchester Academic Health Science Centre, Manchester, UK

*** Corresponding Author**: Dr Michael J Sherratt

Address: 1.529 Stopford Building, The University of Manchester,

Oxford Rd, Manchester, M13 9PT, UK;

Telephone: +44 (0)161 275 1439;

Fax: +44 (0)161 275 5171;

Email: michael.sherratt@manchester.ac.uk

3.1 Abstract

Characterising the composition of supramolecular extracellular matrix (ECM) components like fibrillin and collagen VI microfibrils is difficult due to their large size and insolubility. Cain *et al.* (2006) revealed that proteomics has the potential to do this; however, the effective generation of peptides for LC-MS/MS remains challenging. To enhance the proteomic analysis of these components, we optimised two pre-MS preparation protocols: the elastase and SMART™ digestion methods. The elastase method successfully increased the generation of fibrillin-1 peptides from single ciliary body (CB) microfibril purifications, leading to a primary coverage of over 30% and revealed regions of the protein previously uncharacterised by proteomics. Additionally, despite the relatively low abundance of collagen VI microfibrils in human CB, the elastase method also led to the successful detection and proteomic characterisation of the collagen VI alpha-3 chain. The method also yielded abundant generation of fibrillin-1 and collagen VI alpha-3 peptides from a human skin microfibril preparation. Furthermore, the elastase method also led to the identification of co-purifying microfibril-associated proteins: annexins V and II, MFAPs 2, 4 and 5, collagen IV, vimentin, nidogen-1, laminin β2, βig-H3, and EMILIN-1. The SMART™ method enhanced the detection of additional associated proteins: versican, hyaluronan link-1, prelamin A/C and lumican. These approaches could aid in the interpretation of ECM assemblies and in the detection of age- and disease-related damage.

Keywords: proteomics, fibrillin, collagen VI, microfibrils, mass spectrometry, composition

3.2 Introduction

Many components of the extracellular matrix (ECM) exist as long-lived supramolecular structures (Stenhouse and Baxter 1977; Shapiro *et al.* 1991; Verzijl, DeGroot, Thorpe, *et al.* 2000). As a result, the use of conventional biochemical or structural analyses for the characterisation of their molecular composition can be challenging. Gel electrophoresis, for instance, is ill-suited to resolving large multimeric protein assemblies without first disassociating or fragmenting its components (Reinhardt *et al.* 1996; Reinhardt *et al.* 1997; Whiteman and Handford 2003). Additionally, ultrastructural analysis techniques like atomic force and electron microscopy allow the visualisation of structural features, but not the identification of individual protein components (Baldock *et al.* 2003, 2001; Godwin *et al.* 2017; Hibbert *et al.* 2015; Kielty *et al.* 1991; Sherratt *et al.* 2007, 2010, 2004).

Two such supramolecular assemblies are the fibrillin and collagen VI microfibrils. Fibrillin microfibrils function in conjunction with elastin, as elastic fibres in organs and tissues such as skin, arteries, ligaments and lungs where they confer elasticity (see review: Kielty *et al.* 2002). These microfibrils can also function independently of elastin as anchoring oxytalan fibres in the papillary dermis (Cotta-Pereira *et al.* 1976) and as ciliary zonules in the eye (Shi *et al.* 2013). In addition to their mechanical roles, fibrillin microfibrils sequester the homeostatic cytokine transforming growth factor beta (TGF-β), through their interaction with latent TGF-β binding proteins (LTBPs) (Raghunath *et al.* 1998), and bone morphogenetic proteins (BMPs) (Gregory *et al.* 2005; Sengle *et al.* 2008) within the ECM. Disruption of this functionality is associated with profound pathological consequences (Neptune *et al.* 2003). In contrast, the functions of collagen VI microfibrils are less well-defined. Their proposed function is to anchor cells within the matrix (Pfaff *et al.* 1993; Stallcup *et al.* 1990) and maintain its organisation through the vast network it forms with other matrix proteins (see review: Cescon *et al.* 2015). Disruptions in these interactions are known to induce autophagy (Grumati *et al.* 2010; Irwin *et al.* 2003).

It is clear that both microfibrillar networks can potentially interact with a wide variety of proteins (see reviews: Cescon *et al.* 2015 and Kielty *et al.* 2005). Fibrillin microfibrils interact with the microfibril-associated proteins (MFAPs) -2 (Jensen *et al.* 2001), -4 (Pilecki *et al.* 2016) and -5 (Hanssen *et al.* 2004) which play key roles in their assembly (Marson *et al.* 2005). Other ECM components, such as the proteoglycans versican, hyaluronan (Isogai *et al.* 2002) and perlecan (Tiedemann *et al.* 2005) also interact directly with fibrillin-1 whilst the basement membrane proteins

nidogen-1 and laminin β2 interact with fibrillin microfibrils through perlecan (Tiedemann *et al.* 2005). Finally, other fibrillin microfibril-associated proteins, such as the elastin microfibril interface proteins (EMILINs) (Colombatti *et al.* 2000) exist as a link between the fibrillin microfibril and elastin within elastic fibres. Although many fibrillin microfibril-associated proteins have been identified, there are potentially more interactions which remain undiscovered. Molecular fishing experiments have revealed a number of potential associated proteins (Cain *et al.* 2009) such as vimentin, annexins V/II, TGF-β-induced ig-H3 (βig-H3) and lamin-A/C.

Collagen VI microfibrils have been shown to interact specifically with ECM components such as collagen IV (Kuo *et al.* 1997) and lumican (Chakravarti *et al.* 1998). However, since both collagen VI and fibrillin microfibrils are commonly co-purified from connective tissues (Kielty *et al.* 1998), many of their binding interactions overlap. Hyaluronan (Specks *et al.* 1992) and MFAP2 (Finnis and Gibson 1997), are known to interact directly with collagen VI as well as fibrillin microfibrils. Additionally, nidogen-1 and laminin are known associated proteins of collagen IV (Aumailley, Wiedemann, *et al.* 1989). It is possible, therefore, that collagen VI may co-purify with these two proteins, via this interaction. As a result, the identification and attribution of these interactions to either microfibrillar species and the role they play in the ECM, remains challenging.

In common within other ECM assemblies, fibrillin and collagen VI microfibrils are thought to be long-lived (Sell and Monnier 2010; Shapiro *et al.* 1991) making them prone to the accumulation of damage through post-translational modifications (PTMs; oxidation, protease-mediated degradation, mechanical damage and ultraviolet radiation; UVR) (Sell and Monnier 2010; Ashworth, Murphy, *et al.* 1999; Watson *et al.* 1999; Sherratt *et al.* 2010; Veidal *et al.* 2011; Verzijl, DeGroot, Thorpe, *et al.* 2000). The difficulties in characterising the molecular composition of large ECM assemblies such as fibrillin and collagen VI microfibrils makes it necessary to develop novel proteomic approaches. However, to date only a single published proteomic study, performed over ten years ago by Cain *et al.* (2006), has endeavoured to characterise human tissue fibrillin microfibril composition. In this, they succeeded in analysing and mapping the peptide yield of its main component, fibrillin-1 and effectively identified the presence of three known interacting proteins (annexins II, V and MFAP2). However, whilst Cain *et al.* (2006) effectively demonstrated that mass spectrometry (MS)-based proteomic approaches have the potential to identify the protein composition of these supramolecular ECM assemblies, the generation of peptides from fibrillin-1 and associated proteins remained challenging due to their large megadalton size (Baldock *et al.* 2001), insolubility (Chang *et al.* 2016) and high number of crosslinks (Marson *et al.* 2005).

In this study, we present two novel methods of pre-MS sample preparation: elastase digestion and SMART digestion™, for the improved generation of fibrillin and collagen VI microfibril peptides and their microfibril-associated proteins from human ciliary body (CB) and skin, which led to their improved compositional analysis via liquid chromatography tandem MS (LC-MS/MS). By comparing these methods and results to previous published data by Cain *et al.* (2006), we further demonstrate the potential of proteomics for the compositional characterisation of large, supramolecular ECM assemblies from human tissues. We also demonstrate that resultant peptide mapping may potentially be used to gain novel insights into the fibrillin-1 supramolecular organisation within its microfibril.

3.3 Experimental procedures

3.3.1 Study design and method development strategy

All chemicals were sourced from Sigma-Aldrich Co. Ltd (Poole, UK) unless stated otherwise. With highly disulphide bonded proteins (such as the fibrillins), pre-MS sample preparation usually involves reduction using a redox reagent such as dithiothreitol (DTT) (Cleland 1964; Loo *et al.* 1990) followed by alkylation with an agent such as iodoacetamide (IAM) (Anfinsen and Haber 1961; Yen *et al.* 2000). Typically, these re-solubilisation steps are followed by proteolytic digestion with trypsin, a highly specific enzyme which cleaves solely at the carboxyl end of lysine and arginine (Olsen *et al.* 2004), allowing for the generation of peptides which can be detected via MS at high confidence (Link *et al.* 1999). This trypsinisation method was trialled on purified human ciliary zonule (CZ) microfibrils by Cain *et al.* (2006) in the first fibrillin microfibril proteomics study (**Fig. 3.1**, Cain *et al.* 2006 pathway). To improve upon the achievements of this previously published effort, two pre-MS sample preparation methods were developed and trialled on purified human CB and skin microfibrils.

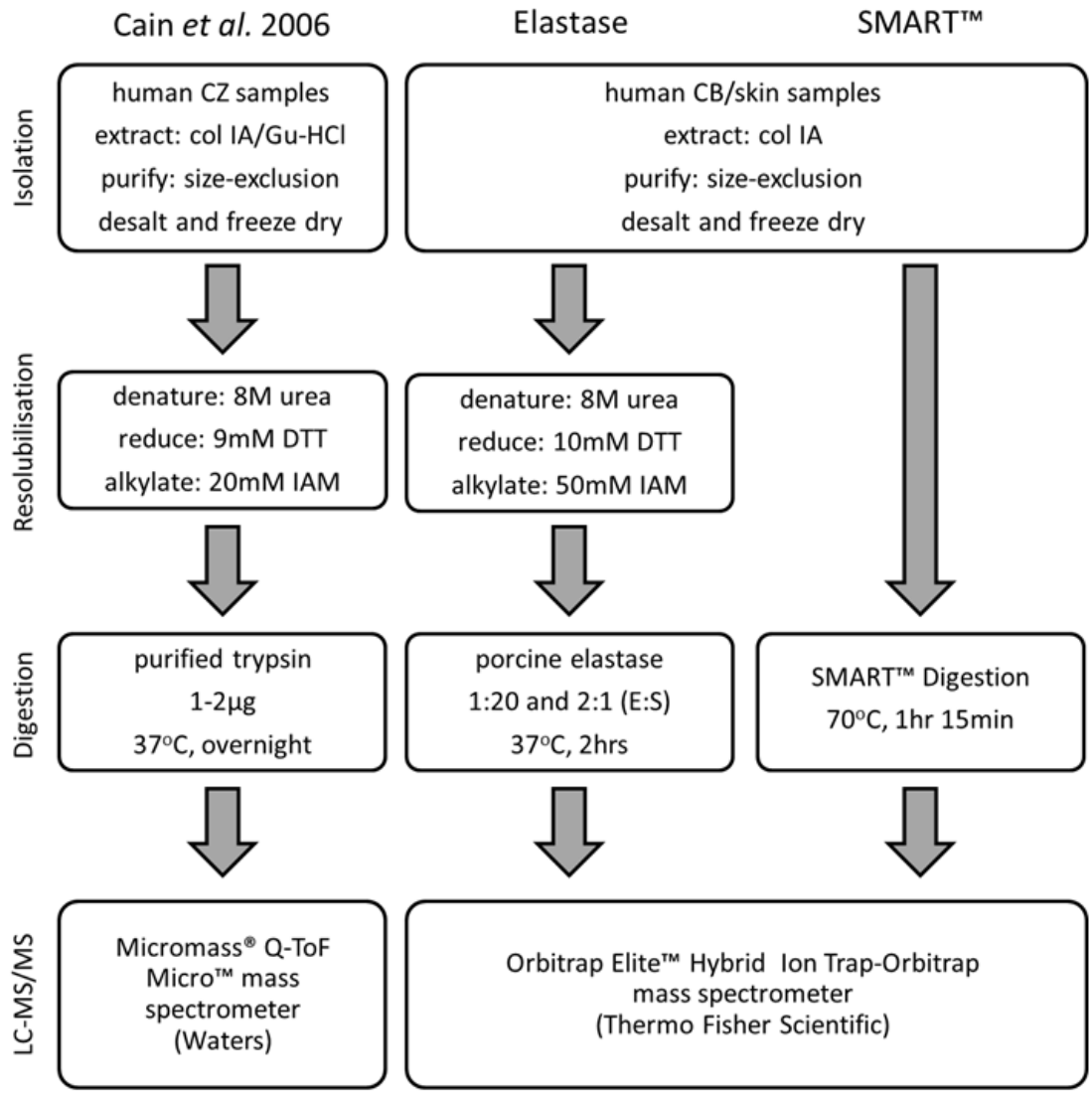

Figure 3.1: Workflow comparing the two pre-MS sample preparation methods developed in this study to the methods employed by Cain et al. *(2006). In their 2006 proteomics study of fibrillin microfibril composition, Cain* et al*, describe using either bacterial collagenase IA or guanidine hydrochloride (Gu-HCl) to extract microfibrils from human ciliary zonule (CZ) samples prior to purification using size-exclusion chromatography (Cain* et al. *2006). By comparison, we extracted microfibrils from human CB and skin solely using bacterial collagenase IA digestion. Microfibril peptide generation by Cain* et al. *was achieved by re-solubilisation via denaturation in 8 M urea, reduction in 9 mM DTT and alkylation in 20 mM IAM, prior to overnight digestion in 1-2 µg of trypsin, at 37°C. In our elastase method, microfibril extracts were more thoroughly re-solubilised and digested than those by Cain* et al. *through denaturation in 8 M urea, reduction in 10 mM DTT and alkylation in 50 mM IAM followed by digestion in porcine elastase at 37°C for 2 hours. An enzyme to substrate ratio (E:S) of 1:20 was trailed and then increased to 2:1 to maximise protein primary sequence and domain coverage. In our SMART™ Digestion method, resolubilisation was omitted and microfibril extracts were added directly to the SMART™ Digest kit and digested at 70°C for 1 hour 15 minutes to maximise the identification of microfibril-interacting proteins. LC-MS/MS was performed by Cain* et al. *in 2006 using an older generation Micromass® Q-ToF Micro™ mass spectrometer (Waters; Newcastle, UK), whereas ours was performed using a new generation Orbitrap Elite™ Hybrid Ion Trap-Orbitrap mass spectrometer (Thermo).*

To effectively unmask and digest regions deep within microfibril ultrastructure and improve upon the generation of peptides from core microfibril components, a higher concentration of DTT and IAM was used (**Fig. 3.1**, elastase method pathway) than by Cain *et al.* (2006). Additionally, porcine elastase (Sigma catalogue # E1250), a highly active enzyme, less specific than trypsin (preferentially cleaving at leucine, isoleucine, alanine, serine, valine and glycine) (Rietschel *et al.* 2009; Sziegoleit *et al.* 1985) was trialled. To demonstrate improvements in primary sequence and domain coverages, enzyme:substrate ratios (E:S) of 1:20 and 2:1 were both trialled.

In order to enhance peptide generation from proteins which co-purify with fibrillin and collagen VI microfibrils, and improve upon the number of microfibril-associated proteins identified by Cain *et al.* (2006), a second method was developed (**Fig 3.1**, SMART™ method pathway). Here, re-solubilisation was omitted (to target only loosely bound interacting proteins) and the SMART Digestion™ kit (Thermo Fisher Scientific; Paisley, UK) was used for peptide generation. This method allows the rapid digestion of the sample through a column of immobilised trypsin, in thermally denaturing conditions (70°C) (Moore and Samonig 2016). The immobilisation of the enzyme on the column prevents self-digestion (Nord *et al.* 1956; del Val *et al.* 2002), whose peptides can mask the presence of less abundant proteins and render them undetectable by MS (Gingras *et al.* 2005). This method was used, therefore, to allow the detection of less abundant, loosely bound proteins which decorate the outside of fibrillin and collagen VI microfibrils.

Finally, to instrumentally enhance the detection of microfibril peptides compared to Cain *et al.* (2006), all LC-MS/MS on microfibril extracts was performed using a new generation Orbitrap Elite™ Hybrid Ion Trap-Orbitrap mass spectrometer (Thermo Fisher Scientific; Paisley, UK), in contrast to Cain *et al.* (2006) who used an older generation Micromass® Q-ToF Micro™ mass spectrometer (Waters; Herts, UK).

3.3.2 Human tissue and materials

Human donor eye tissue was acquired in accordance with the Human Tissue Act via the Manchester Eye Bank, within 24 hours of corneal retrieval (for corneal transplant services). The use of this tissue for was approved by the University of Manchester ethics committee (ethics ref: 11305). In each case, the CB was dissected prior to snap freezing in liquid nitrogen and storage at -80°C.

The human abdominal skin sample was acquired via the University of Manchester Skin Health Biobank (MSHB). The MSHB is conducted in accordance with the Declaration of Helsinki 1964 (revised Seoul 2008) and the European Medicines Agency Note for Guidance on Good Clinical Practice. North West 5 Research Committee has approved this biobank (Research Ethics Committee reference 09/H1010/10). The sample was snap frozen in liquid nitrogen and stored at -80°C.

3.3.3 Fibrillin and collagen VI microfibril extraction and purification

CB and skin tissue samples were minced and placed in a 2 ml aliquot of buffer containing 400 mM NaCl, 50 mM Tris-HCl and 1mM $CaCl_2$, at pH7.4. Bacterial collagenase IA (1 mg) was added to a 2 ml aliquot of the same buffer containing 0.01 mM PMSF (phenylmethane sulphonyl fluoride) and 0.03 mM NEM (N-Ethylmaleimide). Tissue was digested and stirred on a rotary mixer for 4 hours at room temperature (Kielty *et al.* 1991; Sherratt *et al.* 2010). Post-digestion, mixtures were centrifuged at 5000 g for five minutes and the supernatant subjected to size exclusion chromatography on a GE HiScale 16/40 column containing Sepharose® Cl4B beads at 0.5 ml/min in 50 mM Tris-HCl (pH 7.4), 400 mM NaCl on an ÄKTA Prime Plus Liquid size-exclusion Chromatography System (GE Healthcare; Little Chalfont, UK). Fractions were collected based on spectrophotometric absorbance at 280 nm. Both fibrillin and collagen VI microfibrils co-purify and were enriched in the void volume peak (Kielty *et al.* 1991; Sherratt *et al.* 2010). Following purification, microfibril isolations were desalted via dialysis in 0.22 µm filtered ultrapure water using a Slide-A-Lyzer™ MINI Dialysis Devices (Thermo Scientific) for 4 hours at 4°C. Samples were then frozen at -80°C prior to freeze-drying at -60°C for a minimum of 48 hours. Samples were stored at -80°C until their use in LC-MS/MS experiments.

3.3.4 Elastase digestion for microfibril peptide generation

The elastase method was developed and trialled for enhanced microfibril peptide generation **(Fig. 3.1)**. Freeze dried samples were re-suspended in 0.1 M Tris-HCl, pH 8.5. Proteins were denatured in 8 M urea, reduced in 10 mM DTT for 30 minutes at room temperature and alkylated using 50 mM IAM for 30 minutes at room temperature, in darkness. The solution was then diluted to 2 M urea, and porcine elastase added at an E:S ratio of 1:20 or 2:1. This was incubated at 37°C for 2 hours. Elastase activity was quenched with 5% (v/v) formic acid in ultrapure water. Samples were desalted using OLIGO™ R3 Reversed Phase Resin (Thermo) and vacuum dried prior to LC-MS/MS analysis.

3.3.5 SMART Digestion™ for enhanced microfibril-associated protein peptide generation

The SMART™ method was trialled to enhance the peptide generation of loosely bound microfibril-associated proteins (**Fig. 3.1**, SMART™ method pathway). Freeze-dried samples were re-suspended in ultrapure water and digested for 75 minutes using a SMART Digest™ kit (Thermo Scientific), as per the manufacturer's instructions. Samples were then desalted and vacuum dried prior to LC-MS/MS.

3.3.6 Mass spectrometry

All LC-MS/MS was performed by the Biological Mass Spectrometry Core Facility in the Faculty of Biology, Medicine and Health at the University of Manchester (Manchester, UK). As dictated by their protocols (Buckley 2015; Lennon *et al.* 2014) vacuum dried samples were analysed using an UltiMate® 3000 Rapid Separation liquid chromatographer (Dionex Corp; Sunnyvale, CA, USA) and an Orbitrap Elite™ Hybrid Ion Trap-Orbitrap mass spectrometer (Thermo Fisher Scientific). Peptide mixtures were separated using a gradient from 92% A (0.1% formic acid [v/v; FA] in water) and 8% B (0.1% [v/v] FA in acetonitrile) to 33% B, in 30 minutes at 300 nL/min, using a 250 mm x 75µm i.d. 1.7 µm BEH C18, analytical column (Waters). Peptides were selected for fragmentation automatically by data-dependent analysis.

3.3.7 Mass spectrometry data analysis

Mass spectra were extracted using extract_msn (Thermo Fisher Scientific) correlated against the Uniprot human database (Consortium 2016) using Mascot (Matrix Science; London, UK).

Search parameters were: species - Homo sapiens; enzyme - non-specific for elastase, trypsin for SMART Digest™; fixed modifications - carbamidomethyl (57.02 Da on C); variable modification – oxidation (15.99 Da on M); peptide tolerance - 10 ppm (monoisotopic); fragment tolerance - 0.6 Da (monoisotopic); searched database: Swissprot_TreEMBL_2016_04 database (152,544 entries).

Mascot identifications generated ware analysed using Scaffold 4 (Proteome Software; Portland, OR, USA). Only exclusive, unique peptide counts are reported. False discovery rate (FDR) was calculated by Scaffold using protein and peptide probabilities assigned by the Trans-Proteomic Pipeline and the Protein Prophet™ (Nesvizhskii *et al.* 2003) and Peptide Prophet™ (Keller *et al.* 2002) algorithm (Sourceforge; Seattle. WA, USA). Peptide Prophet FDR was thresholded to ≤ 5% and Protein Prophet FDR was thresholded to ≤ 0.1% (min 2 peptides) for every dataset.

3.4 Results and discussion

3.4.1 Elastase digestion enhances fibrillin-1 peptide generation compared to previously published efforts

In their 2006 publication, Cain *et al.* proteomically identified fibrillin-1 in human CZ purifications (Cain *et al.* 2006). By combining data from 13 separate sample runs, they achieved a total primary sequence coverage of 30% and a total domain coverage of 64% of the fibrillin-1 protein structure **(Fig. 3.2)**. However, two regions of fibrillin-1, near the N-terminal region (blue arrow) and at the C-terminal region (green arrow), remained largely undetected and uncharacterised. In contrast, a single human CB sample, prepared using our elastase method (E:S ratio of 1:20; without pooling or data combining), led to the detection of 78 fibrillin-1 peptides, covering 25% of the primary sequence and 57% of its protein domains (**Fig. 3.2**; full protein list in **Supplemental Table 3.1**). A higher elastase E:S ratio of 2:1 further increased the primary sequence and domain coverages of fibrillin-1 to 33% and 76% respectively from another single human CB sample run (**Fig. 3.2**; full protein list in **Supplemental Table 3.2**), higher than the total coverages achieved by Cain *et al. (*2006), for a combined 13 separate sample runs. Furthermore, this optimised E:S ratio also led to the detection of the C-terminal regions of fibrillin-1 which remained previously undetected by Cain *et al.* (2006) (**Fig. 3.2**, green arrow). Further reproducibility tests for this optimised E:S ratio on two additional CB samples consistently resulted in a fibrillin-1 primary sequence coverage of ≥ 30% **(Supplemental Tables 3.3 and 3.4)**. Additionally, similar primary and domain coverages were achieved when applied to human skin (**Fig. 3.2**; full protein list in **Supplemental Table 3.5**). These improvements can likely be attributed to both the optimised elastase method and to advances in MS technology over the last decade (see review: Byron *et al.* 2013).

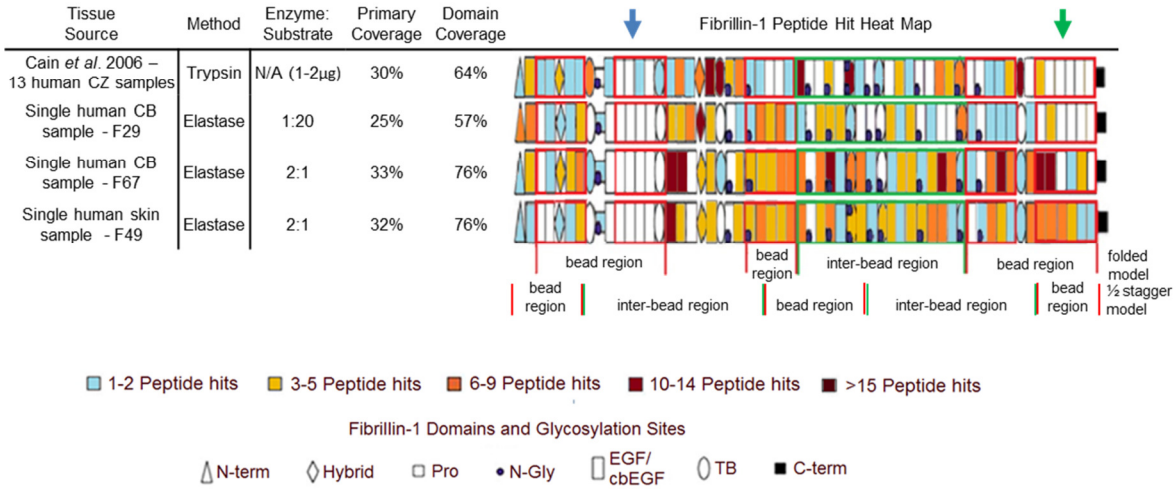

Figure 3.2: The optimised elastase method led to improved primary and domain coverage of fibrillin-1 compared with previous published efforts by Cain et al. *(2006). As done in their publication, fibrillin-1 PSMs (Peptide Prophet FDR ≤ 5%) were counted for each protein domain and heat-mapped. By combining the data of 13 separate sample runs, Cain* et al. (2006) *achieved a total fibrillin-1 primary coverage of 30% and total domain coverage of 64%. Comparatively, even at a low E:S ratio of 1:20, the elastase method led to a similar fibrillin-1 primary and domain coverage (25% and 57% respectively) to Cain* et al.'s *study, but on a single human CB sample run, without any pooling or data combining. At an increased E:S of 2:1, elastase successfully generated a primary and domain coverage greater than had been achieved Cain* et al. *for both a single human CB microfibril extract (F67) and a single human skin microfibril extract (F49). This optimised E:S ratio also successfully generated peptides from a C-terminal region which Cain* et al. *failed to identify and which had been previously unyielding (green arrow). Interestingly, there appears to be a region on the N-terminal side of fibrillin-1 which elastase was incapable of generating detectable peptides (blue arrow).*

3.4.2 Regions of fibrillin-1 devoid of peptide spectrum matches may reveal clues about the supramolecular organisation of the microfibril

Both Cain *et al.* (2006) and the use of 1:20 E:S ratio of elastase failed to generate abundant peptides from a region at the C-terminal end of fibrillin-1, between domains EGF43 and EGF47 (**Fig 3.2**, green arrow). An increased E:S ratio (2:1), however, led to the successful generation of peptides from this region. Another region, at the N-terminal side of fibrillin-1, between domains EGF6 and TB2 (blue arrow) was consistently devoid of PSMs regardless of the E:S ratio of elastase used. The lack of peptide generation from these two regions of fibrillin-1 may reveal insights into its supramolecular organisation within the microfibril **(Fig. 3.3)**.

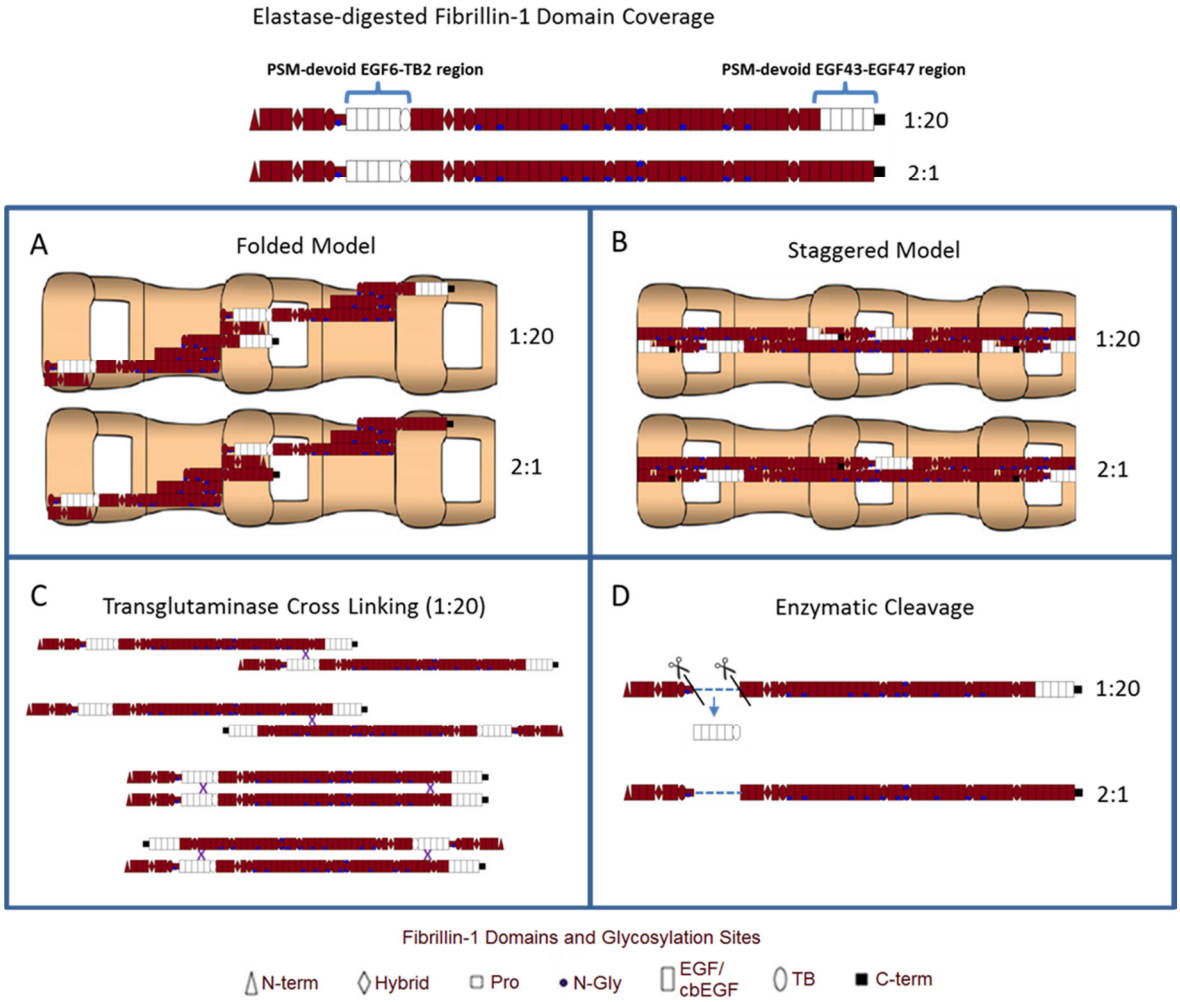

*Figure 3.3: Possible scenarios explaining the lack of peptides generated from two fibrillin-1 regions. At a 1:20 E:S ratio of elastase, two regions (one between EGF6 and TB2 and another between EGF43 and EGF47) failed to generate abundant peptides (white) compared to the rest of fibrillin-1's domains (dark red). At a 2:1 E:S ratio of elastase, the EGF43-EGF47 region successfully generated peptides; however, the EGF6-TB2 region remained unyielding. Four possible explanations for this are explored. The folded model of fibrillin-1 supramolecular organisation within the microfibril **(A)** places both regions within the bead region. This indicates that as the E:S of elastase is increased, more of the fibrillin microfibril bead may have been digested, uncovering previously masked regions deep within the quaternary structure. The staggered model **(B)** places the EGF43-EGF47 region within the bead and the EGF6-TB2 region at the shoulder of the fibrillin microfibril bead. It is possible that the shoulder region may have been over-digested (past the point of peptide detection at high confidence) due to a higher enzyme exposure than other, more masked regions. Two transglutaminase crosslinks have been reported within fibrillin-1 domains EGF9 (falling within the EGF6-TB2 region) and EGF40. From this, four possible alignments of two fibrillin-1 monomers were suggested by Qian and Glanville (1997) **(C)**. It is possible that the strength of this crosslink may prevent the effective elastase digestion of the EGF6-TB2 region, leading to the lack of peptide generation observed. Finally, it is possible that the EGF6-TB2 region may have been enzymatically cleaved during the microfibril extraction process **(D)**.*

Two major models of fibrillin-1 alignment within the microfibril have been proposed: the folded model (Baldock *et al.* 2001, 2006) and the staggered model (Kuo *et al.* 2007; Reinhardt, Keene, *et al.* 1996) (see reviews: Jensen and Handford 2016 and Kielty *et al.* 2005). When applied to the folded model **(Fig. 3.3 A)**, both PSM-devoid fibrillin-1 regions align to the microfibril bead. The observation that peptides are detected from the EGF43-EGF47 region only when the E:S ratio of elastase is increased from 1:20 to 2:1 but not from the EGF6-TB2 region suggests they may be enzyme-resistant as a direct result of their location within the densely packed microfibril bead (Kielty, Baldock, *et al.* 2002). It is possible that, as the E:S ratio increases, more of these regions within the bead are unmasked, leading to the generation of peptides. When applied to the staggered model **(Fig. 3.3 B)**, the PSM-devoid EGF43-EGF47 region of fibrillin-1 also aligns to the microfibril bead region. The consistently PSM-devoid, EGF6-TB2 region however, aligns within the microfibril shoulder region. Previous AFM and electron microscopy imaging of fibrillin microfibrils suggests that its shoulder and inter-bead region would be more readily digested than the more globular, compact and highly crosslinked bead region (Ashworth, Murphy, *et al.* 1999; Kuo *et al.* 2007). As such, the EGF6-TB2 region may have been subjected to over-digestion, even at a low E:S ratio, leading to the generation of peptides too small for either MS detection or for confident database spectra correlation using Mascot.

Although the lack of peptides from these two fibrillin-1 regions could be due to their organisation within the microfibril, there are other credible explanations. For instance, two transglutaminase crosslinks have been observed in fibrillin-1 (Qian and Glanville 1997), one of which lies in the middle of the PSM-devoid, EGF6-TB2 region **(Fig. 3.3 C)**. As such, the presence of this crosslink may have prevented the effective digestion of this region, which would explain the lack of peptides detected. PSMs and MS have been used previously in an attempt to detect transglutaminase crosslinking between a fibrillin-1 recombinant fragment and tropoelastin (Rock *et al.* 2004). Two glutamine-containing peptide sequences were successfully detected from within fibrillin-1 recombinant fragments alone but not from within fragment-tropoelastin heterodimers. As a result, these two sequences were described as likely candidates for the location of a crosslink. These two peptides, however, were only six and twelve amino acids in length, which indicates that that the presence of a transglutaminase crosslink could limit the proteomic detection of a protein sequence of only a few amino acids. As a result, it seems unlikely that a transglutaminase crosslink within fibrillin-1 would, by itself, have prevented the generation of peptides from the entire 262 amino acid-long EGF6-TB2 region.

Another possibility for the lack of PSMs at the EGF6-TB2 region of fibrillin-1 is that it may have been cleaved off by the bacterial collagenase enzyme used in the microfibril extraction process **(Fig. 3.3 D)**. The notion that this enzymatic extraction may be damaging the microfibril structure was put forward when the use of bacterial collagenase led to the loss of certain immunoreactive domains of the fibrillin microfibril (Kuo *et al.* 2007), compared to those which were extracted using guanidine hydrochloride (Gu-HCl). However, the lack of presence of this region due to enzymatic cleavage seems unlikely since, if the confidence threshold is lowered, two PSMs were detected within this region, one at 54% peptide identification probability and another at 76%.

3.4.3 Elastase digestion allows the detection of collagen VI from human ciliary body and enhances the peptide coverage of collagen VI alpha 3 chain from human skin

As well as fibrillin-1, the elastase digestion method (1:20) also successfully liberated 29 collagen VI alpha-3 (COL6A3) peptides from the same single human CB microfibril extract, resulting in a primary sequence coverage of 10% (**Fig. 3.4**; full protein list in **Supplement Table 3.1**). Since collagen VI has a very limited distribution within the CB, as previously shown histologically (Rittig *et al.* 1990), this indicates the potential of the elastase method in the detection of low abundance ECM structures.

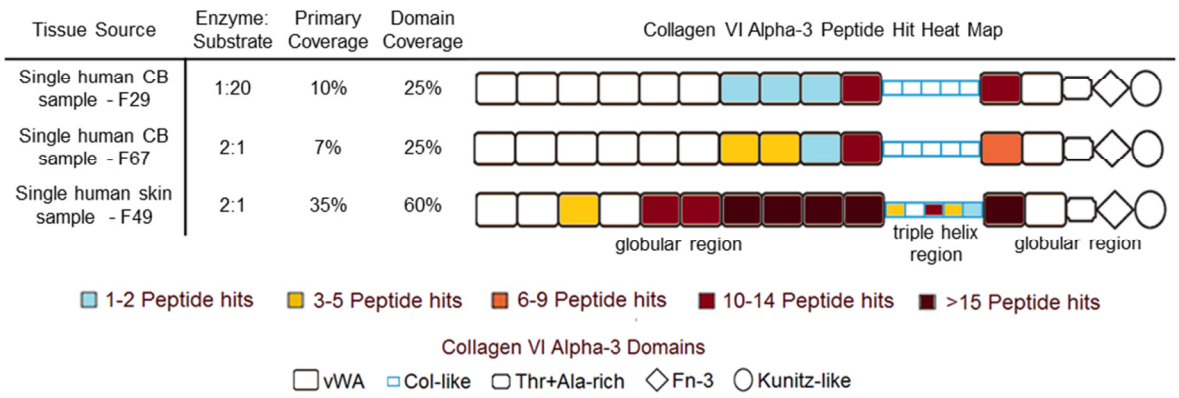

Figure 3.4: The elastase method successfully generated detectable COL6A3 peptides from human CB, despite it being a relatively collagen VI-poor tissue. As done with fibrillin-1, PSMs (Peptide Prophet FDR ≤ 5%) were heat mapped to their respective COL6A3 protein domains. The elastase method led to the successful detection of peptides from both globular regions of the COL6A3 protein, derived from human CB (F29 and F67). In contrast to fibrillin-1, increasing the E:S ratio, however, did not increase the primary or domain coverage. However, when performed on a human skin microfibril extract (F49) (a collagen VI-rich tissue source: Watson et al. *2001), an E:S ratio of 2:1 led to a high primary and domain coverage of COL6A3 and allowed the successful identification of the triple helix region as well as both globular regions.*

Increasing the E:S of elastase from 1:20 to 2:1 did not improve either the primary sequence or domain coverages of COL6A3 for CB-derived collagen VI microfibrils **(Fig. 3.4)**. However, elastase digestion of microfibril purifications from skin, where collagen VI is much more abundant (Watson *et al.* 2001), resulted in a detection of 302 COL6A3 unique peptides with a 35% primary sequence coverage and 60% domain coverage (**Fig. 3.4**; full protein list in **Supplemental Table 3.5**). PSMs were mapped to both globular regions of the protein (domains N1-N6, N8 and C1) and to the triple helical region. Additionally, 174 unique peptides were detected for COL6A1 with a primary coverage of 48% and 224 unique peptides for COL6A2 with a primary coverage of 50% **(Supplementary Table 3.5)**.

Much like for fibrillin microfibrils, only a single study has attempted the proteomic analysis of purified collagen VI microfibrils. While analysing the supramolecular organisation of the alpha chains within these microfibrils, using single particle electron microscopy, Beecher *et al.* (2011) also performed LC-MS/MS on purified extracts from bovine cornea. Using a conventional trypsin-based method similar to Cain *et al.* (2006), Beecher *et al.* (2011) detected 40 COL6A3, 14 COL6A2 and 13 COL6A1 PSMs from one sample. In contrast, we successfully detected 302, 224 and 174 PSMs, respectively, from a single sample run using our elastase method on human skin-derived microfibril extracts **(Supplementary Table 3.5)**. They also achieved a COL6A3 primary coverage of only 16% compared to our improved 35% **(Fig. 3.4)**. Comparisons between our COL6A3 primary sequence coverage and theirs revealed a major improvement in peptide coverage of all COL6A3 domains except N7 and N9, which are likely to be spliced out in skin (Dziadek *et al.* 2002). Overall, the elastase method improved both the peptide yield of collagen VI microfibrils and the primary and domain coverage of its alpha-3 chain.

3.4.4 Elastase and SMART™ digestion method enhance the detection of microfibril-associated proteins compared to previously published efforts

In their 2006 study, Cain *et al.* (2006) only identified a total of three known fibrillin microfibril-associated proteins, annexins V, II and MFAP2 **(Table 3.1)**, from a combination of 11 human CZ sample runs. In contrast, our elastase method, led to the successful detection of ten known fibrillin microfibril-interacting proteins, which co-purified with microfibrils extracted from a single human CB sample (**Table 3.1**; Full protein lists in **Supplemental Table 3.6**). These include annexins V, II and MFAP2 (as identified by Cain *et al.*) plus MFAP5, vimentin and βig-H3. The elastase method also led to the successful detection of MFAP4, nidogen-1, EMILIN-1 and laminin β2; however, these

yielded only 2-3 detected peptides. The SMART™ method led to the successful identification of an additional three fibrillin microfibril-interacting proteins from the same human CB extract: versican, hyaluronan link-1 and prelamin-A/C, which elastase had failed to generate. Furthermore, a higher number of vimentin (18), nidogen-1 (5) and laminin β2 (16) unique peptides were detected using the SMART™ method compared to elastase.

			Peptide Spectrum Matches	
Identified Associates	**Interacts with**	**Cain *et al.* 2006 (3)**	**Elastase (11)**	**SMART™ (10)**
Annexin V	Fibrillin	✓	74	17
Annexin II	Fibrillin	✓	52	17
MFAP2	Both	✓	5	
Collagen IV (α2)	Collagen VI		4	
Vimentin	Fibrillin		11	18
Nidogen-1	Both		2	5
Laminin β2	Both		3	15
βig-H3	Fibrillin		4	5
MFAP4	Fibrillin		2	
MFAP5	Fibrillin		7	
EMILIN-1	Fibrillin		2	
Versican	Fibrillin			3
Hyaluronan link-1	Both			3
Prelamin-A/C	Fibrillin			3
Lumican	Collagen VI			2

Table 3.1: The elastase and SMART™ methods resulted in a higher detection of microfibril-associated proteins than previous published efforts by Cain et al. *(2006). This list compares the known fibrillin microfibril-interacting proteins identified by Cain* et al. *(2006), to the ones identified using our optimised elastase (red) and SMART™ methods (blue) by LC-MS/MS (Protein Prophet FDR ≤ 0.1%, Peptide Prophet FDR ≤ 5%). Whether they interact with fibrillin, collagen VI or both and their respective number of PSMs is also shown (for our results only). From a combination of 11 human CZ sample runs, Cain* et al. *successfully identified only 3 known fibrillin microfibril-associated proteins in total. In contrast, the elastase and SMART™ digestion methods, separately performed on a single human CB (F73) microfibril extract, led to the identification of 13 known fibrillin microfibril-associated proteins as well as 6 known collagen VI microfibril-associated proteins. The elastase method appeared to enhance the detection of microfibril-associated proteins thought to be tightly bonded to the structure (i.e. the MFAP family) whereas the SMART™ method appeared to enhance the detection of weakly interacting proteins (i.e. versican and hyaluronan). Collectively, the elastase and SMART™ methods led to an enhanced detection of known microfibril-associated proteins compared to previous published efforts.*

With regards to collagen VI microfibril-associated proteins **(Table 3.1)**, MFAP2, nidogen-1, laminin β2 and hyaluronan all co-interact with both fibrillin and collagen VI microfibrils. However, collagen IV (α2) and lumican, which interact exclusively with collagen VI microfibrils were also detected, even despite the CB being a collagen VI-poor tissue (Rittig *et al.* 1990).

Collectively, the elastase and SMART™ methods led to the successful identification of 15 known fibrillin and/or collagen VI microfibril-associated proteins. However, several candidate associated proteins can be hypothesised from the protein lists generated from human CB **(Supplemental Table 3.6)**. Molecular fishing experiments previously identified annexin V and II as potential fibrillin microfibril-associated proteins through their binding to recombinant fragments of fibrillin-1 (Cain *et al.* 2009). This study corroborates this further by showing co-purification of these two proteins with native whole CB-derived fibrillin microfibrils **(Table 3.1)**. Interestingly, however, elastase digested- and SMART™ digested-microfibrils yielded several other co-purified annexins (I, IV, VI, VII and XI). This indicates that the annexins may play a wide role in fibrillin microfibril biology. Interestingly, talin-1 and actin were also identified. Cells constantly and plastically network their intracellular actin cytoskeleton with the ECM through their membranes via talin-1 (Wang *et al.* 2009). The sarcoglycans also play a similar role in linking the actin cytoskeleton of sarcomeric cells to the ECM (see review: (Holt and Campbell 1998)) and these were also detected. To summarise, it is possible that these microfibrils are pulling out a network of linked, co-purifying proteins, all of which may functionally interact with these assemblies and play an important role in their ability to influence cell behaviour and mechanics.

Interestingly, recent whole tissue proteomics of human ciliary zonule performed by De Maria *et al.* (2017) also report the presence of all the fibrillin microfibril-associated proteins identified in this study except βig-H3, MFAP4 and hyaluronan link-1. Additionally, they identified abundant LTBP2 from human ciliary zonule, which this study failed to detect in human CB. Since their proteomic analysis was performed solely on whole tissue, it may be that either the enzymatic extraction process or the purification procedure used in this study may have stripped LTBP2 from the fibrillin microfibrils. The advantage of this size-exclusion chromatography-purified microfibril proteomic analysis over whole tissue however, is that we can state with a high confidence that the associated proteins seen and hypothesised from our analysis must have been bound to either fibrillin or collagen VI microfibrils. Although De Maria *et al.* (2017) successfully detected these proteins using trypsin as a pre-MS peptide generation method, they did so by pooling together 4 ciliary zonule samples from different individuals and subjecting the material to a 12 hours trypsinisation step. The elastase and SMART™ digestion methods developed in this study only require a 1-2 hour digestion and were both performed on a single CB sample from one individual, without pooling. As a result, these methods can be effectively used to compare the proteomics of fibrillin microfibrils between different individuals.

3.4.5 Conclusion

The use of the developed elastase and SMART™ methods for the enhanced peptide generation of microfibrils, and their associated proteins, has allowed the structure and the composition of these macromolecular ECM components to be further scrutinised. Coupled with ultrastructural analysis via AFM, these proteomic methods may make it possible to assess whether microfibrils are invariant between tissues. It also allows the further study into the loss (Watson *et al.* 1999), deregulation and degeneration (Langton *et al.* 2010; Sherratt *et al.* 2010) of fibrillin microfibrils in response to cutaneous photoageing (Langton *et al.* 2010; Watson *et al.* 1999) and disease (Giampietro *et al.* 2002; Hartner *et al.* 2006). Additionally, it is possible that these pre-MS sample preparation methods can also be used to effectively generate peptides from other large, macromolecular proteins such as collagen fibrils (Hansen and Bruckner 2003), mucins (Nielsen *et al.* 1997) and titin (Granzier and Labeit 2004) which may be of further interest to the ECM field.

3.5 Acknowledgements

This study was fully funded by a programme Grant from Walgreens Boots Alliance, Nottingham, UK. The Wellcome Trust Centre for Cell-Matrix Research, University of Manchester is supported by core funding from the Wellcome Trust (088785/Z/09/Z). CEMG is a Senior Investigator at the National Institute for Health Research. CEMG and REBW are supported in part by the NIHR Manchester Biomedical Research Centre.

3.6 Author contributions

AE conceived, designed, performed all experiments, analysed all the data, prepared the figures and wrote the paper. MJS supervised and coordinated the study and contributed to the preparation of the figures and editing of the paper. REBW and CEMG contributed to the study design and to the editing of the paper. DK and ROC provided technical assistance for LC-MS/MS and contributed to the editing of the paper. CB contributed to the editing of the paper and to the preparation and interpretation of **Figure 3.3**. All authors contributed to the editing of the paper.

3.7 Conflict of interest

The authors declare that they have no conflicts of interest with the contents of this article. Walgreens Boots Alliance has approved this manuscript's submission but exerted no editorial control over the content.

3.8 Supplementary information

All Supplementary Tables have been uploaded to the online data repository Mendeley Data and can be accessed by copying and pasting the following link:

https://data.mendeley.com/datasets/7t8hxk7bwb/draft?a=45c5494a-55e9-49b8-9ac6-b505a148e07e

Supplementary Table 3.1: Full protein list for Elastase 1to20 CB F29
Supplementary Table 3.2: Full protein list for Elastase 2to1 CB F67
Supplementary Table 3.3: Full protein list for Elastase 2to1 variation test 1 CB F73
Supplementary Table 3.4: Full protein list for Elastase 2to1 variation test 2 CB F72
Supplementary Table 3.5: Full protein list for Elastase 2to1 Skin F49
Supplementary Table 3.6: Combined full protein list for Elastase and SMART CB F73 Associated Protein trial

Chapter 4: Structural and compositional diversity of fibrillin microfibrils in human tissues

This paper was published in the Journal of Biological Chemistry on the 6th April 2018 (Eckersley *et al.* 2018). I conceived, designed and performed all experiments, analysed all the data, prepared the figures and wrote the paper. Dr Suzanne Pilkington isolated the primary fibroblasts from human skin, used in this study. Dr David Knight and Dr Ronan O'Cualain of the Biological Mass Spectrometry Core Facility at the University of Manchester provided technical assistance for all LC-MS/MS performed.

Note: The methods paper presented in the last chapter **(chapter 3)** remains unpublished. As a result, in this published manuscript, **Figure 4.1** consists of a combination of **Figure 3.2** and **Table 3.1** from the last chapter. This was done to introduce the reader to the developed pre-mass spectrometry sample preparation methods. All remaining figures and tables within this chapter contain original work pertinent to **chapter 4** only.

Structural and compositional diversity of fibrillin microfibrils in human tissues

Alexander Eckersley[1], Kieran T. Mellody[1], Suzanne M. Pilkington[2], Christopher E.M. Griffiths[2,5], Rachel E.B. Watson[2,5], Ronan O'Cualain[3], Clair Baldock[1,4], David Knight[3], Michael J. Sherratt[1*]

From the [1]Division of Cell Matrix Biology & Regenerative Medicine, [2]Division of Musculoskeletal & Dermatological Sciences, [3]School of Biological Sciences, [4]The Wellcome Trust Centre for Cell-Matrix Research, Faculty of Biology, Medicine and Health, The University of Manchester and [5]NIHR Manchester Biomedical Research Centre, Central Manchester University Hospitals NHS Foundation Trust, Manchester Academic Health Science Centre, Manchester, UK

Running Title: *Structural diversity in human tissue fibrillin microfibrils*

*To whom correspondence should be addressed: Michael J. Sherratt: 1.529 Stopford Building, The University of Manchester, Oxford Rd, Manchester, M13 9PT, UK; michael.sherratt@manchester.ac.uk; Tel. +44 (0)161 275 1439; Fax. +44 (0)161 275 5171.

Keywords: Fibrillin microfibril, collagen VI, extracellular matrix, skin, eye, fibroblast, proteomics, atomic force microscopy, AFM, protein structure

4.1 Abstract

Elastic fibres comprising fibrillin microfibrils and elastin are present in many tissues, including the skin, lung, and arteries where they confer elasticity and resilience. Although fibrillin microfibrils play distinct and tissue-specific functional roles, it is unclear whether their ultrastructure and composition differ between elastin-rich (skin) and elastin-poor (ciliary body and zonule) organs or after *in vitro* synthesis by cultured cells. Here, we used atomic force microscopy, which revealed that the bead morphology of fibrillin microfibrils isolated from the human ciliary body differs from those isolated from the skin. Using newly developed pre-MS preparation methods and LC-MS/MS, we detected tissue-specific regions of the fibrillin-1 primary structure that were differentially susceptible to proteolytic extraction. Comparing tissue- and culture-derived microfibrils, we found that dermis and dermal fibroblast fibrillin microfibrils differ in both bead morphology and periodicity and also exhibit regional differences in fibrillin-1 proteolytic susceptibility. In contrast, collagen VI microfibrils from the same dermal or fibroblast samples were invariant in ultrastructure (periodicity) and protease susceptibility. Finally, we observed that skin- and ciliary body-derived microfibril suspensions were enriched in elastic fibre– and basement membrane–associated proteins, respectively. LC-MS/MS also identified proteins (such as calreticulin and protein disulphide isomerase) that are potentially fundamental to fibrillin microfibril biology, regardless of their tissue source. Fibrillin microfibrils synthesised in cell culture lacked some of these key proteins (MFAPs -2, -4 and fibrillin-2). These results showcase the structural diversity of these key extracellular matrix assemblies, which may relate to their distinct roles in the tissues where they reside.

4.2 Introduction

Extracellular matrices (ECM) are commonly comprised of a diverse array of assemblies which make key contributions to tissue mechanics and cell-mediated homeostasis. Some of these assemblies, such as the fibrillar collagens and the elastic fibres, are large, insoluble and supra-macromolecular. Some are markedly long-lived (Shapiro *et al.* 1991; Verzijl, DeGroot, Thorpe, *et al.* 2000); laid down early in development where they persist and undergo a process of maturation (Parry *et al.* 1978; Sherratt *et al.* 1997) and subsequent age and disease related accumulation of damage (Sell and Monnier 2010). During these processes, the ultrastructure of these assemblies can be tissue specific (Parry *et al.* 1978). Therefore, although these ECM assemblies are present in multiple tissues, they may exhibit distinct development-mediated ultrastructures which have evolved to fulfil their unique functionality.

Elastic fibres (which are comprised of fibrillin microfibrils and elastin; Kielty, Sherratt, *et al.* 2002), are present in many tissues including skin (Watson *et al.* 1999), lungs (Wright 1961), arteries (Wagenseil and Mecham 2009) and ligaments (Kielty *et al.* 1991) where they play a major role in conferring elasticity and resilience (Kielty, Sherratt, *et al.* 2002). The fibrillin microfibril, along with elastin, is a key component of the elastic fibre and adopts a bead-on-a-string appearance (Baldock *et al.* 2001) when extracted and viewed with atomic force microscopy (AFM) and electron microscopy (EM). Additionally, these microfibrils exist also as stand-alone assemblies, forming candelabra-like structures (Cotta-Pereira *et al.* 1976) (see review Naylor *et al.* 2011) in the papillary dermis. They also play a role in tissue homeostasis, sequestering and storing the latent forms of members of the TGF-β (Kaartinen and Warburton 2003; Neptune *et al.* 2003) and BMP family (Sengle *et al.* 2008). In eyes, fibrillin microfibrils play a very different architectural role to skin. They form the ciliary zonules: stand-alone suspensory ligaments which connect the lens capsule to the ciliary muscle (Ashworth *et al.* 2000; Godwin *et al.* 2018; Hiraoka *et al.* 2010). These zonules come under tensile stress as the ciliary muscle exerts a strain to deform the lens during accommodation (Burd *et al.* 1999). Although fibrillin microfibrils appear structurally and compositionally similar in mammalian tissues and cell culture systems, and retain a bead-like structure (and presence of the main component: fibrillin-1) throughout different tissues (Baldock *et al.* 2001), little is known whether they have evolved to be distinct in each. Only two studies have shown that fibrillin microfibril ultrastructure is tissue- and developmentally-dependent: In 1997, we showed that inter-tissue differences in mass and periodicity (inter-bead distance) exist in microfibrils derived from bovine foetal aorta and skin (Sherratt *et al.* 1997). We also showed that fibrillin microfibrils undergo

a process of post-translational maturation as their mass increased during foetus development. Lu *et al.* (2006) also reported similar differences in bead morphology between bovine adult aorta- and ciliary zonule-derived fibrillin microfibrils.

Since fibrillin microfibrils are present in a variety of tissues, the different roles they play may be reflected in the ultrastructure they adopt. These inter-tissue comparisons have never been made in human, or between fibrillin microfibrils sourced from ciliary body (CB) and skin, where they play very different architectural and mechanical roles. Additionally, the fibrillin microfibril's biomolecular composition has never been compared between tissues. Although their ultrastructure has been extensively studied using AFM (Hibbert *et al.* 2015; Sherratt *et al.* 2007, 2010) and EM (Baldock *et al.* 2001; Sakai *et al.* 1986; Sherratt *et al.* 2007), characterisation of the biomolecular composition through conventional biochemical approaches such as gel electrophoresis can be problematic due to their large size and insolubility. As a consequence, it is necessary to develop proteomic approaches to characterise fibrillin microfibril composition.

Recently, De Maria *et al.* (2017) performed whole tissue proteomics on dissected human ciliary zonules, and effectively characterised the zonular proteome. However, to date, only a single published proteomic study, performed by Cain *et al.* (2006), attempted to characterise both the structure and composition of fibrillin microfibrils purified from human tissue. Through liquid chromatography tandem mass spectrometry (LC-MS/MS), Cain *et al.* (2006) achieved a 30% primary coverage of fibrillin-1 and identified several microfibril-associated proteins such as microfibril-associated protein (MFAP) -2. They demonstrated that mass spectrometry (MS)-based proteomic approaches have the potential to identify the proteins involved in these supramolecular ECM assemblies. However, they observed that peptide generation from the core fibrillin-1 proteins, and their interacting proteins, was challenging due to their large size and high number of crosslinks (Marson *et al.* 2005). Since this study took place, over ten years ago, advances have been made in mass spectrometer technology allowing greater resolving power with expanded functionalities (Schilling *et al.* 2015). Coupled with improved sample preparation, we believe that these proteomic approaches can be enhanced further to allow effective inter-tissue comparisons of fibrillin microfibril composition and structure.

In this study, we optimised two effective methods of pre-MS sample preparation: elastase digestion and SMART digestion™, for the enhanced generation of fibrillin peptides and their microfibril-associated proteins. This led to their improved compositional analysis via LC-MS/MS, compared to

Cain *et al.* (2006). We go on to test differences between the ultrastructure (bead morphology and inter-bead periodicity) using AFM and biomolecular composition (fibrillin-1 structural, enzymatic susceptibly and associated protein presence) using MS of fibrillin microfibrils isolated from human eye (CB), human skin and cultured human dermal fibroblasts (HDFs). Since collagen VI microfibrils co-purify with fibrillin microfibrils in skin- and HDF-derived samples, we use them as a comparative control. We perform these analyses to test the following hypotheses:

1. Fibrillin microfibril ultrastructure and composition is tissue-dependent.
2. Culture-derived, newly synthesised fibrillin microfibril ultrastructure and composition is distinct from that of native, mature, tissue-sourced microfibrils.

4.3 Results and discussion

4.3.1 Elastase digestion methods enhance fibrillin-1 peptide generation and, combined with SMART™ digestion methods, enhance the detection of microfibril-associated proteins

To improve the generation of peptides from core microfibril components, porcine elastase, a highly active and non-specific enzyme (which preferentially cleaves leucine, isoleucine, alanine, serine, valine and glycine) (Rietschel *et al.* 2009; Sziegoleit *et al.* 1985) was used instead of conventional trypsin-based methodologies (see review Hustoft *et al.* 2012). For human CB-derived fibrillin microfibrils, this method, along with the use of a latest-generation mass spectrometer, led to an improved primary coverage (33%) and domain coverage (76%) of fibrillin-1, compared to that achieved by Cain *et al.* (2006) (30% primary, 64% domain) **(Fig. 4.1 A)** and, for the first time, the identification of peptides from the C-terminal region of fibrillin-1 (orange arrow). A similar primary sequence and domain coverage was achieved when applied to human skin. Crucially, this improved coverage was achieved by the digestion and LC-MS/MS of single CB and skin samples whereas Cain *et al.* (2006) reported a total primary sequence coverage of 30% from peptides identified in 13 separately prepared human, Gu-HCl and/or trypsin treated ciliary zonule samples.

In order to improve peptide generation from proteins which co-purify with the microfibril, SMART™ digestion was used. Collectively, the elastase and SMART™ digestion methods led to the successful identification of 13 known microfibril-associated proteins **(Fig. 4.1 B)** from human CB. These include annexin V, annexin II, and MFAP2, identified by Cain *et al.* (2006).

A

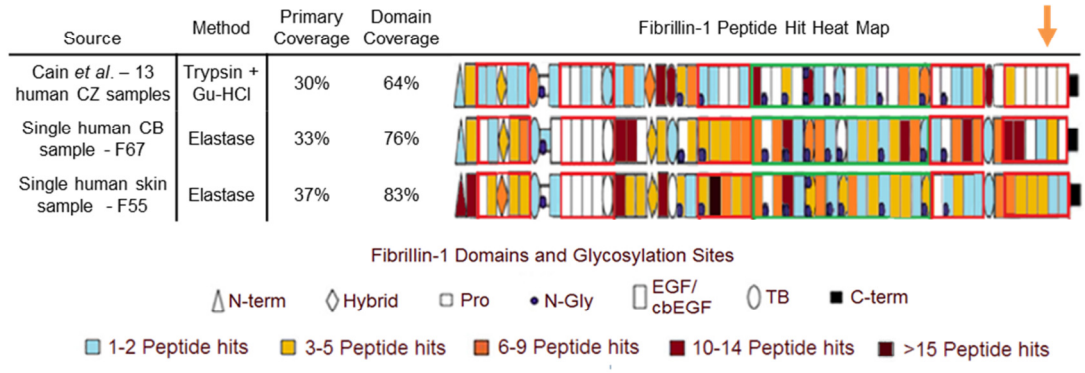

B

		Peptide Spectrum Matches	
Identified Associates	Cain *et al.* 2006 (3)	Elastase (10)	SMART™ (9)
Annexin V	✓	74	17
Annexin II	✓	52	17
MFAP2	✓	5	
Vimentin		11	18
Nidogen-1		2	5
Laminin β2		3	16
βig-H3		4	5
MFAP4		2	
MFAP5		7	
EMILIN-1		2	
Versican			3
Hyaluronan link-1			3
Prelamin-A/C			3

Figure 4.1: Elastase and SMART™ methods led to the improved detection of fibrillin-1 and improved identification of microfibril-associated proteins. The ability of the elastase method to produce peptides of fibrillin-1 from a *single human CB sample (female age 67 – F67) and a single human skin sample (F55) is compared to the efforts made by Cain* et al. *(2006)* ***(A)****. As done by Cain* et al, (*2006) peptide spectrum matches (PSMs) (Peptide Prophet FDR ≤ 5%) were counted for each respective fibrllin-1 domain and heat mapped. Our method led to a greater primary coverage and domain coverage from a single sample run than Cain* et al.*, whose coverages were achieved from 13 separate sample runs. Peptides from the C-terminal region of fibrillin-1 were also successfully detected (orange arrow) which Cain* et al. *failed to identify. The known fibrillin microfibril-interacting protein identified by Cain* et al. *(green) are compared with those identified by elastase and SMART™ methods (Protein Prophet FDR ≤ 0.1%, Peptide Prophet FDR ≤ 5%)* ***(B)****. The elastase method (red) and SMART™ method (blue) were both performed on the same human CB microfibril extract (F73). The elastase method appears to enhance the detection of fibrillin microfibril-associated proteins thought to be tightly bonded to the structure (ie. the MFAP family) whereas the SMART™ method appears to enhance the detection of weakly interacting proteins (ie. versican and hyaluronan proteins). Collectively, these methods led to an enhanced detection of known associated proteins compared to Cain* et al. (*2006).*

4.3.2 Fibrillin microfibril bead morphology is tissue-dependent

The fibrillin microfibril is composed predominantly of fibrillin-1 (approximately 8 monomers per single bead and inter-bead repeat) with a total mass of ~2.5 MDa per repeat (Baldock *et al.* 2001). The average periodicity and bead width has been approximated to 56 nm and 19 nm respectively (for detailed breakdown of microfibril dimensions see: Baldock *et al.* 2001). Our data showed that fibrillin microfibril populations derived from human eye (CB) had a significantly higher central bead heights than those derived from human skin **(Fig 4.2 Ai)**. Central bead height frequency distributions indicate that the majority of eye-derived fibrillin microfibrils had larger beads than skin-derived **(Fig. 4.2 Aii)**. Additionally, axial height profiles showed that although eye-derived fibrillin microfibrils beads are significantly higher within a ~10 nm radius of the centre, they were significantly lower at the shoulder region, ~20 nm from the peak (**Fig. 4.2 Aiii**, orange arrow) than skin-derived. These height differences in bead morphology are further exemplified in the contour heat map **(Fig. 4.2 Aiv)** where eye-derived fibrillin microfibrils appear to have a more pronounced bead with a lower shoulder region than skin. Between beads, however, there was no significant difference in the periodicities of fibrillin microfibril populations derived from eye and skin **(Fig. 4.2 Bi, ii)**.

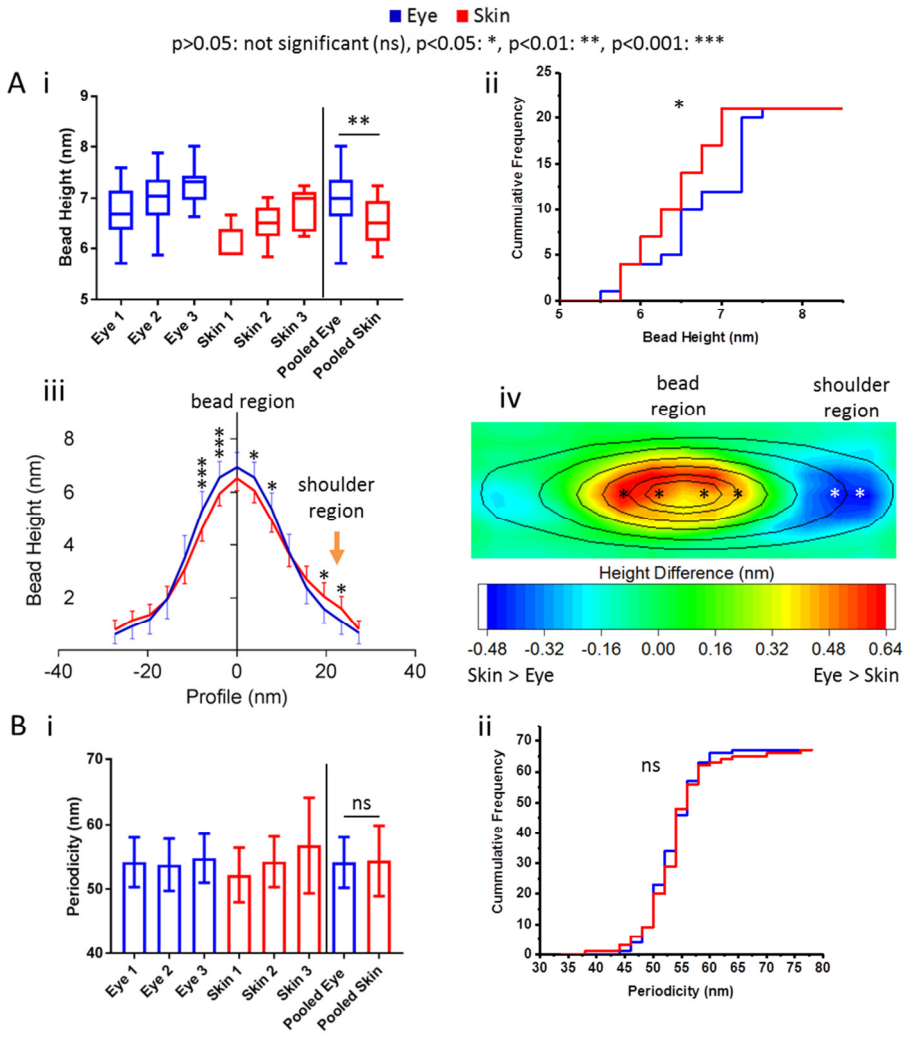

*Figure 4.2: Fibrillin microfibril ultrastructure is tissue-source dependent. Eye-derived fibrillin microfibril central bead heights were significantly higher (n=100 repeats, averaged per microfibril; n=300 repeats pooled) than skin-derived (p=0.0023, Mann-Whitney U) (**Ai**; data = median, IQR and range). Cumulative frequency distributions of central bead height (averaged per microfibril, n=21 pooled) indicate a large population of eye-derived fibrillin microfibrils with significantly larger beads (p=0.0423; Kolmogorov-Smirnov) than skin-derived **(Aii)**. Axial bead profiles show that, although skin-derived fibrillin microfibril beads are significantly smaller, within ~10 nm of the bead peak, than eye-derived (**Aiii**; data = mean and SD; Bonferroni multiple comparison test), they also have significantly higher slopes at the shoulder regions than eye-derived (orange arrow). This may suggest that skin-derived fibrillin microfibril beads have a different volume distribution than that of eye-derived. To visualise these differences in bead morphology, AFM height maps of skin-derived fibrillin microfibril beads were averaged and subtracted from that of eye-derived. The resulting height differences are represented as a heat map overlaid with the average height contour of the eye-derived beads **(Aiv)**. Significant differences seen in the axial profile panel were also added. The biggest differences in bead morphology were around the central peak where eye-derived beads were higher than skin and at the shoulder region where skin-derived beads were higher than eye. There was no significant difference between the periodicities of eye- and skin-derived fibrillin microfibrils (p=0.9737; Mann-Whitney U, n=500 repeats, averaged per microfibril; n=1500 repeats pooled) **(Bi**, data = mean and SD) nor between their cumulative frequency distributions (p=0.8580; Kolmogorov-Smirnov, averaged per microfibril, n=67 pooled) **(Bii)**.*

Many past studies exclusively used differences in periodicity to gauge ultrastructural differences in fibrillin microfibrils (Ashworth, Murphy, *et al.* 1999; Hibbert *et al.* 2017, 2015; Kielty *et al.* 1995; Kielty, Raghunath, *et al.* 1998) and other fibrillar components of the ECM (Erickson *et al.* 2013; Fang, Goldstein, *et al.* 2012; Fang, Liroff, *et al.* 2012; Hibbert *et al.* 2015). However, not only does the majority of the fibrillin microfibril's mass rest within the bead, much of microfibril's functionality is thought to be mediated via the interaction between the bead and its associated proteins (Henderson *et al.* 1996; Isogai *et al.* 2003, 2002; Thomson *et al.* 2018). Our data showed that eye-derived fibrillin microfibril beads differed in morphology in comparison to skin-derived, but periodicity did not. By omitting analysis of the microfibril bead, these studies may have missed some key ultrastructural changes linked to health and disease.

The ultrastructural variances seen between the beads of adult human eye- and skin-derived fibrillin microfibrils are similar to those we observed previously (Sherratt *et al.* 1997) where differences were detected in bead mass of microfibrils from bovine foetal skin and aorta. Lu *et al.* (2006) also detected differences in bead morphology, including the shoulder regions, from bovine adult ciliary zonule and aorta.

4.3.3 Fibrillin-1 derived from human eye and skin exhibit inter-tissue, regional differences in elastase susceptibility

To further compare and substantiate the ultrastructural differences seen between CB and skin fibrillin microfibrils, it was necessary to look at their biomolecular composition (fibrillin-1 structure and known microfibril-associated protein presence). Previous studies have used differences to fibrillin-1's susceptibility to proteolysis to gauge abnormalities in fibrillin microfibril structure (Gayraud *et al.* 2000) and function (Reinhardt *et al.* 1997; Reinhardt, Ono, *et al.* 2000). It is possible that the fibrillin-1 structure may exhibit regional differences in proteolytic susceptibilities depending on its tissue of origin.

LC-MS/MS-detected peptide hit patterns (Cain *et al.* 2006) indicate several regions of human eye-derived fibrillin-1 **(Fig. 4.3)** with differing susceptibilities to elastase in comparison to skin-derived (green brackets). These regional differences indicate that, not only are fibrillin microfibrils ultrastructurally variable between tissues, their fibrillin-1 structural composition may also be as well. Collectively, it suggests that these supramolecular assembles may have evolved distinct ultrastructures and compositions in order to cope with their different architectural, mechanical and biochemical roles in their respective tissues of origin. It is possible that the presence of different cell

types within each tissue may have contributed to these differences. Baldwin *et al.* showed that the epithelial-mesenchymal state of retinal pigment epithelial (RPE) cells influenced their ability to assemble fibrillin microfibrils (Baldwin *et al.* 2014). Although fibroblasts (mesenchymal cells) are thought to be responsible for microfibril deposition (Long and Tranquillo 2003; Milewicz *et al.* 1992; Sakai *et al.* 1986), it remains unknown whether epithelial cells contribute to fibrillin microfibril synthesis *in vivo* (Haynes *et al.* 1997). It is also unclear whether populations of fibroblasts from different tissues exhibit differences in epithelial-mesenchymal states as shown in RPE cells (Baldwin *et al.* 2014). It is possible, therefore, that different cell types (or cells in different states) may synthesise fibrillin microfibrils with localised differences in structure.

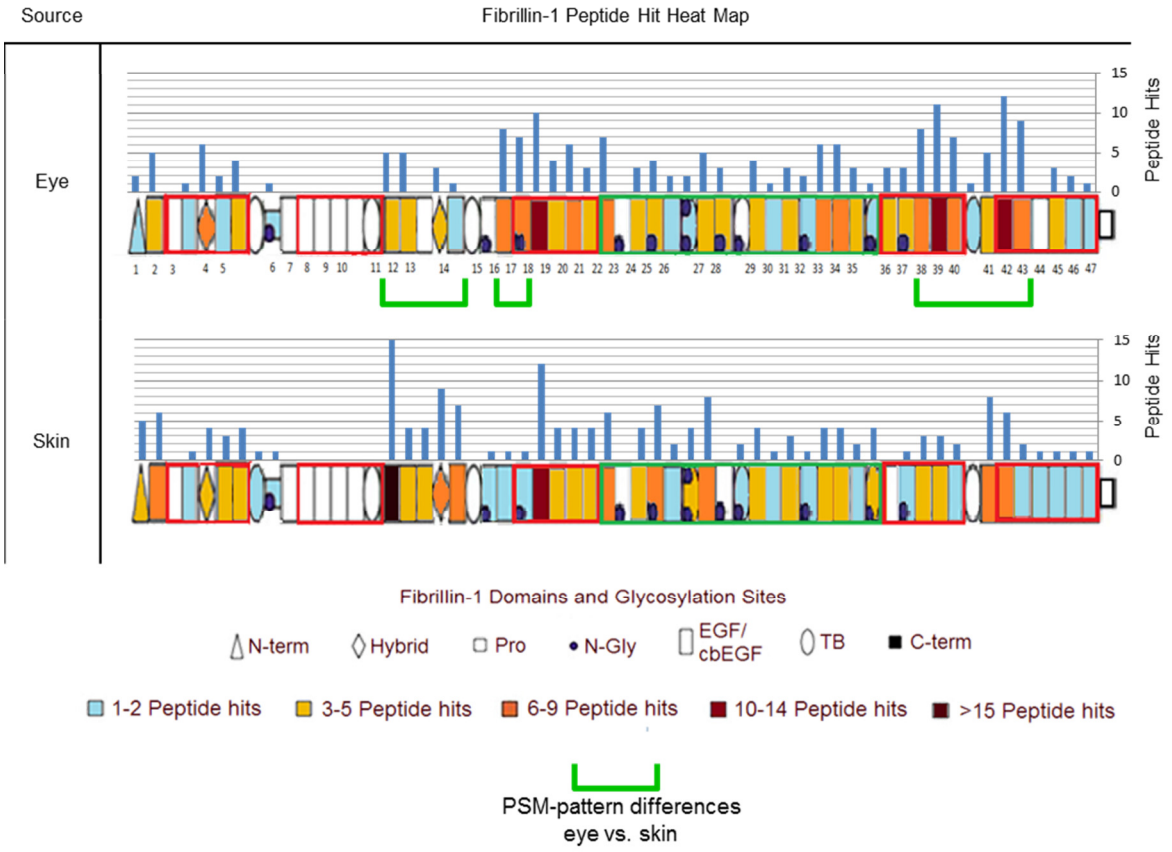

Figure 4.3: Eye-derived fibrillin-1 exhibits different regional patterns of elastase susceptibility compared to skin-derived. LC-MS/MS-detected fibrillin-1 PSMs (Peptide Prophet FDR ≤ 5%) were counted for each respective protein domain, per sample (N=3), averaged (normalised based total spectrum count), and subsequently heat mapped to their corresponding domain. Eye-derived fibrillin-1 yielded more peptides between epidermal growth factor-like domains (EGF) 38 and EGF43 than skin-derived (53 total from eye-derived versus 24 total from skin-derived) (green brackets). Eye-derived fibrillin-1 also yielded more peptides at EGF16 and EGF17 than skin-derived (15 vs. 2), however, it yielded less peptides between EGF11 and EGF14 (14 vs. 39).

So far, we have demonstrated fibrillin microfibril ultrastructure and fibrillin-1 regional susceptibility is tissue-dependent. These differences may also relate to microfibril post-translational maturation in

development. To study this, we applied the same analysis to newly synthesised fibrillin microfibrils derived from cultured HDFs and compared it to skin fibrillin microfibrils, derived *ex vivo.*

4.3.4 Newly synthesised, HDF-derived fibrillin microfibrils exhibit marked differences in ultrastructure compared to skin-derived

Cultured HDF-derived, newly synthesised, fibrillin microfibrils had a significantly lower central bead heights than human skin-derived **(Fig. 4.4 Ai)**. Additionally, central bead height frequency distributions indicate a sub-population of cultured HDF-derived fibrillin microfibrils with smaller beads than human skin-derived (**Fig. 4.4 Aii**, orange arrow). Average axial height profiles indicate that, although skin fibrillin microfibril beads have a significantly larger central peak height than cultured HDF-derived microfibrils, the reverse is true on the slopes of the beads (opposite to the shoulder region) (**Fig. 4.4 Aiii**, purple arrow). This difference in bead morphology is further shown in the contour heat map **(Fig. 4.4 Aiv)**. Skin-derived beads have a higher peak with a more pronounced slope (except near the shoulder region) than HDF-derived beads. This indicates that beads of newly synthesised fibrillin microfibrils from cultured-HDFs have a different morphology those derived from human skin.

Cultured HDF-derived fibrillin microfibrils also exhibited significantly higher periodicities in comparison to skin-derived **(Fig. 4.4 Bi)**. Periodicity frequency distributions also show a large population of cultured HDF-derived fibrillin microfibrils with significantly higher periodicities than skin-derived **(Fig. 4.4 Bii)**.

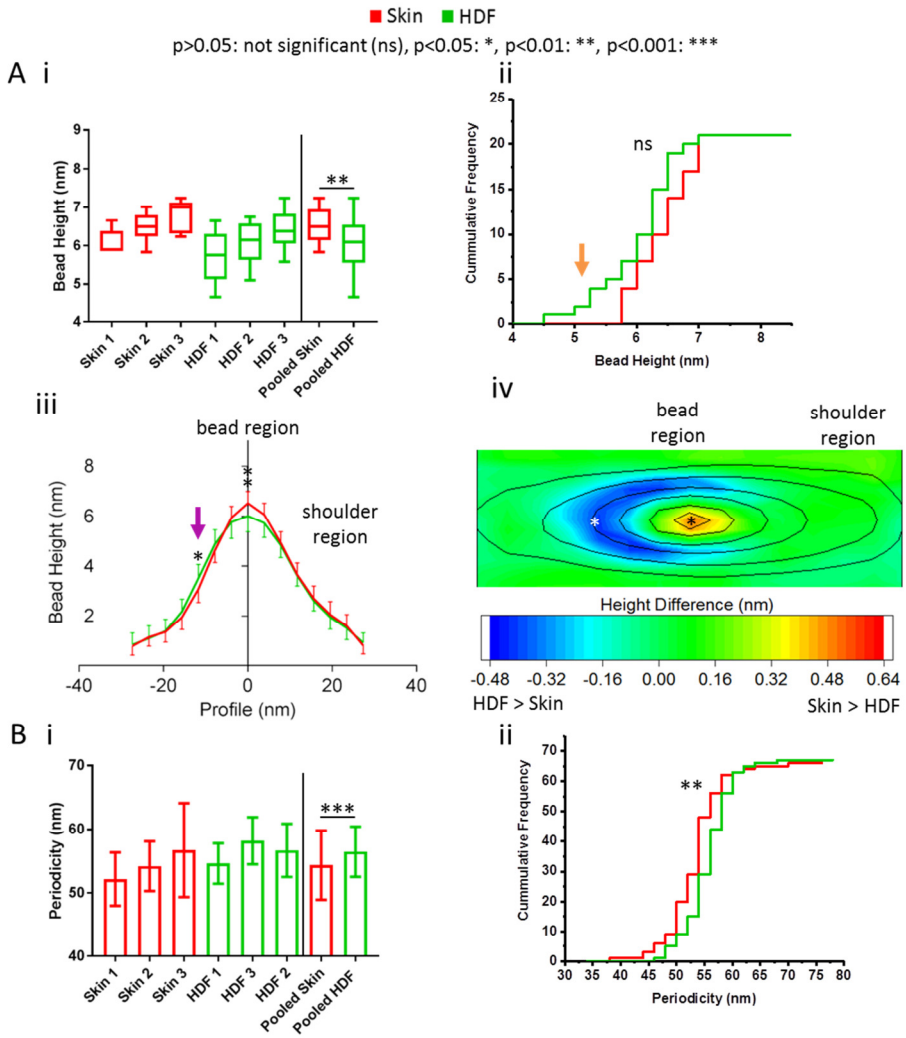

*Figure 4.4: Newly synthesised, HDF-derived fibrillin microfibril ultrastructure is significantly different than native skin-derived. HDF-derived microfibrils had significantly lower central bead heights (n=100 repeats, averaged per microfibril; n=300 repeats pooled) than skin derived- (p=0.0038, Mann-Whitney U) (**Ai**; data = median, IQR and range). Cumulative frequency distributions of central bead height were not significantly different (p=0.1938, Kolmogorov-Smirnov; averaged per microfibril, n=21 pooled), however, they indicate a sub-population of HDF-derived microfibrils with smaller beads than skin-derived (**Aii**; orange arrow). Axial bead profiles (**Aiii**; data = mean and SD) show that skin-derived fibrillin microfibril beads are significantly higher than HDF-derived beads close to the central peak and significantly lower than HDF-derived beads at the slope opposite the shoulder region (purple arrow; Bonferroni multiple comparison test; n=300 repeats pooled, averaged per microfibril). These changes in bead morphology are reflected in the height difference contoured heat map **(Aiv)** (height maps of HDF-derived fibrillin microfibril beads were averaged and subtracted from that of skin-derived and subsequently heat mapped; the contour height of the average skin bead was overlaid). Skin beads were higher than HDF beads only near the central peaks whereas HDF beads had higher slopes around the peaks (except near the shoulder region). HDF-derived fibrillin microfibrils exhibit significantly higher periodicities (n=500 repeats, averaged per microfibril; n=1500 repeats pooled) compared to skin-derived (p=0.0004, Mann Whitney U) (**Bi**; data = mean and SD). Cumulative frequency distributions also indicate a large population of HDF-derived fibrillin microfibril with significantly higher periodicities **(Bii)** in comparison to skin-derived (p=0.0051; Kolmogorov-Smirnov, averaged per microfibril, n=67 pooled).*

Similar differences in fibrillin microfibril bead morphology and periodicity have been previously reported in three cases. The first is between tissues where we showed that bovine foetal aorta fibrillin microfibrils had a higher bead mass and a lower periodicity than those derived from skin (Sherratt *et al.* 1997) and where Lu *et al.* (2006) also reported that aorta-derived fibrillin microfibrils had differing bead morphologies and a higher periodicity compared to those from bovine zonules. The second is during developmental microfibril maturation where we also showed that the gradual increase in foetal fibrillin microfibril bead mass and the gradual decrease in periodicity correlated with gestation time (Sherratt *et al.* 1997). The third is during photoageing where two studies highlighted the structural susceptibility of fibrillin microfibrils to UV irradiation. We showed that a low-dose UVB irradiation of both HDF- and human skin-derived fibrillin microfibrils directly led to the marked loss and re-distribution of their bead mass and a significant increase in their periodicity (Sherratt *et al.* 2010). Since then our group has also showed that physiological doses of both solar simulated radiation (SSR) (~5% UVB and ~95% UVA) and pure UVA led to a significant decrease in the periodicity of HDF-derived fibrillin microfibrils (Hibbert *et al.* 2015).

Although these fibrillin microfibril ultrastructural differences have been reported between tissues, during maturation and in photodamage, this study has identified them between microfibrils derived *in vitro,* from primary fibroblasts (natively found in human skin) and those derived *ex vivo*, directly from human skin. It is possible, therefore, that 1) the fibrillin microfibrils generated by HDFs are structurally immature in comparison to native microfibrils sourced from skin (either through lack of development or through the cell culture process) or that 2) the native skin-derived microfibrils have accumulated structural damage during ageing in comparison to those newly synthesised from HDFs. The ageing process would be more intrinsic than extrinsic (photoageing) since abdominal skin is relatively photoprotected compared to forearm skin used in previous photoageing studies (Watson *et al.* 1999). Since elastic fibre production is commonly thought to be fibroblast-driven (Long and Tranquillo 2003; Milewicz *et al.* 1992; Sakai *et al.* 1986), these changes may have profound implication for skin regenerative therapies, especially if they are linked to developmental maturation or ageing.

4.3.5 Fibrillin-1 derived from newly synthesised, HDF fibrillin microfibrils exhibit regional differences in elastase susceptibility compared to skin-derived.

LC-MS/MS-detected peptide hit patterns (Cain *et al.* 2006) indicate that several regions of human skin-derived fibrillin-1 **(Fig. 4.5)** with differing susceptibilities to elastase in comparison to HDF-

derived (purple brackets). The observations that: 1) these regions of cultured HDF-derived fibrillin-1 have a different structurally susceptibility to elastase than skin-derived and that 2) HDF-derived fibrillin microfibrils have different ultrastructures compared to skin **(Fig. 4.4)**, all support the possibility that either newly synthesised fibrillin microfibrils, derived from HDFs, are structurally immature compared to the more developmental (Zhang *et al.* 1994), long-lived (Shapiro *et al.* 1991) microfibrils from skin or that the skin-derived fibrillin microfibrils are exhibiting signs of ageing in comparison to those newly synthesised from cells.

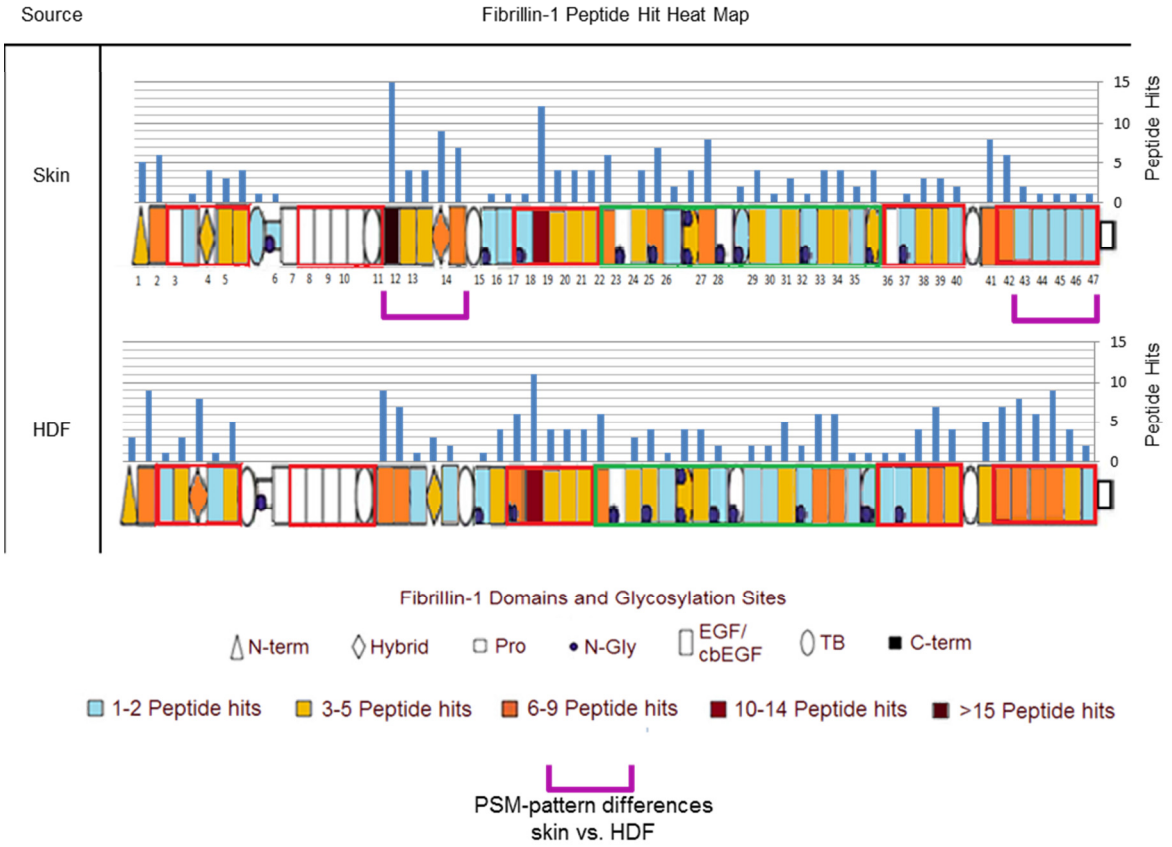

Figure 4.5: Fibrillin-1, derived from newly synthesised, HDF fibrillin microfibrils exhibits different regional patterns of elastase susceptibility compared to skin-derived. LC-MS/MS-detected fibrillin-1 PSMs (Peptide Prophet FDR≤5%) were counted for each respective protein domain, per sample (N=3), averaged (normalised based total spectrum count), and subsequently heat mapped to their corresponding domain. Skin-derived fibrillin-1 yielded less peptides from the last five domains at the C-terminal region: between EGF43 and EGF47 (6 vs. 29) than HDF-derived, however, skin-derived yielded more peptides between EGF11 and EGF14 (39 vs. 22) than HDF-derived (purple brackets).

It is possible that these long-lived (Shapiro *et al.* 1991), skin-derived fibrillin microfibrils may have accumulated age-related damage through the formation of oxidative crosslinks (Wang *et al.* 2014) (see review: Stadtman 1992) induced by the long-term exposure to reactive oxygen species (ROS) in tissue and also via the accrual of advanced-glycation end products on fibrillin-1 (Atanasova *et al.*

2009) (see review: Goldin *et al.* 2006). This process may have led to a differential susceptibility to enzyme digestion, and to an accrual of sugar on the surface of the bead, which would explain the variations in bead morphology.

4.3.6 HDF and skin-derived collagen VI microfibril structure is conserved compared to the fibrillin microfibril

Like the fibrillin microfibril, tissue collagen VI microfibrils are long-lived (Sell and Monnier 2010), supramolecular, beaded assemblies (Baldock *et al.* 2003). Both microfibrillar species are highly abundant in connective tissue (Kielty, Hanssen, *et al.* 1998) and, as such, regularly co-purify (Hibbert *et al.* 2015; Kielty, Hanssen, *et al.* 1998). This allowed us to a make a useful comparison between periodicity differences in collagen VI microfibrils and periodicity differences of fibrillin microfibrils in the same skin- and HDF-derived samples. However, because collagen VI microfibril beads are relatively small in comparison to fibrillin microfibril beads (Hibbert *et al.* 2015), unfortunately, AFM resolution was not good enough to assess differences in collagen VI bead morphology. Encouragingly though, the optimised elastase method generated sufficient collagen VI alpha-3 (COL6A3) peptides **(Supplemental Figure 4.1)** to enable its regional susceptibility to elastase to also be compared to fibrillin-1. These comparisons allow us to differentiate whether the changes seen so far, between newly synthesised fibrillin microfibrils in culture and those derived in tissue, extrapolate to another predominating component of the ECM.

The periodicity and elastase susceptibility differences seen between HDF- and skin-derived fibrillin microfibrils **(Figs. 4.4 B and 4.5)** are a stark contrast to that in collagen VI microfibrils within the same samples **(Fig. 4.6)**. Newly synthesised, cultured HDF-derived collagen VI microfibril periodicities were not significantly different to that of skin collagen VI microfibrils, derived *ex vivo* **(Fig. 4.6 Ai)**. In addition, no distinctly different sub-populations of collagen VI microfibrils were seen when looking at periodicity cumulative frequency distributions of cultured HDF- and skin-derived collagen VI microfibrils **(Fig. 4.6 Aii)**. In fact, both distributions follow almost the same pattern, suggesting there is very little difference in the periodicity of collagen VI microfibrils from these two sources, unlike the fibrillin microfibril **(Fig. 4.4 B)**.

LC-MS/MS-detected peptide hit patterns, in response to elastase digestion of COL6A3 **(Fig. 4.6 B)**, were similar at the triple helix region (Baldock *et al.* 2003), at the N1-N4 region and at the C1 domain of both skin- and HDF-derived samples. This is, again, in contrast to fibrillin-1 which did exhibit regional differences in response to elastase digestion **(Fig. 4.5)**. However, domains N5, N6

and N8 yielded many more peptides from skin-derived COL6A3 than from cultured HDF-derived **(Fig 4.6 B)**. Alternative splicing of COLA3 has been previously shown both in mice and in humans (Dziadek *et al.* 2002) and isoforms of this COL6A3 lacking domains N5 and N7-N10 has previously been identified in human cell lines (Beecher *et al.* 2011; Dziadek *et al.* 2002). It is possible, therefore, that cultured HDFs are also synthesising collagen VI microfibrils which are lacking these domains which would explain the reduction in peptide hits seen from these regions in the HDF-derived preparations compared to skin.

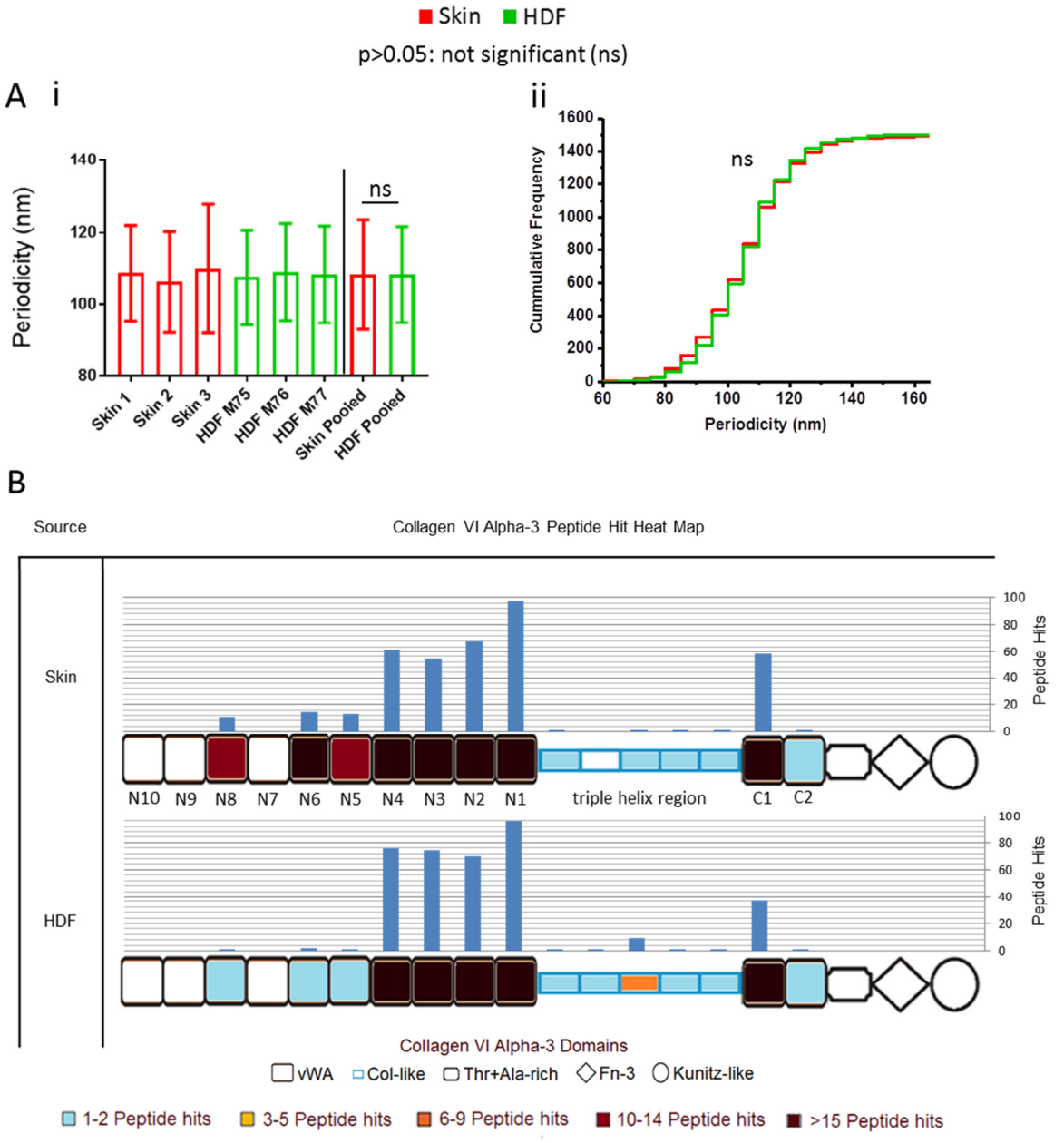

*Figure 4.6: HDF- and skin-derived collagen VI microfibril ultrastructure, and its susceptibility to elastase, is predominantly invariant. There was no significant difference in the periodicities of HDF-derived (n=500 repeats / sample, averaged per repeat; n=1500 repeats in pooled data) and skin-derived (p=0.6310, Mann-Whitney U) collagen VI microfibrils (**Ai**; data = mean and SD). Additionally, there was no significant difference between periodicity cumulative frequency distributions of HDF- and skin-derived collagen VI microfibrils (p=0.2656, Kolmogorov-Smirnov) **(Aii)**. LC-MS/MS-detected collagen VI alpha-3 (COL6A3) peptide sequences (Peptide Prophet FDR ≤ 5%) were counted for each respective protein domain, per sample (N=3), averaged (normalised based total spectrum count), and subsequently heat mapped to their corresponding domain **(B)**. There were similar PSM-patterns between skin- and HDF-derived COL6A3 in all regions except at domain N5,N6, and N8 which yielded more peptides from skin-derived (39 total) than HDF-derived (four total). This analysis could not be effectively performed on eye-derived samples, due to low abundance of collagen VI microfibrils.*

Previously, we showed that collagen VI microfibril ultrastructure (periodicity) is resistant to both UVA and SSR whereas fibrillin microfibril ultrastructure is susceptible (Hibbert *et al.* 2015). Additionally Watson *et al.* (2001) demonstrated that collagen VI microfibril distribution is unaffected in photoaged skin also in contrast to fibrillin microfibrils in elastic fibres which are markedly reduced in photoaged skin (Watson *et al.* 1999). Kielty *et al.* (1993) also reported that skin-derived collagen VI microfibril ultrastructure was indistinguishable at each stage bovine foetal development unlike fibrillin microfibril ultrastructure which is (Sherratt *et al.* 1997). The observations made in this study, that newly synthesised, HDF-derived collagen VI microfibrils are structurally similar to the long-lived microfibrils derived from tissue, corroborates evidence that they are resistant to age-related damage accumulation and that their ultrastructure may not undergo the developmental process of maturation seen in other components of the ECM. These findings are divergent in comparison to the degradation seen in fibrillin microfibrils in ageing and to their maturation process (Sherratt *et al.* 1997) and accentuate the complexity of the fibrillin microfibril in tissue development and ageing and the robustness of the collagen VI microfibril in comparison.

4.3.7 Differences in the presence of co-purifying microfibril-associated proteins may provide insight into tissue functions of fibrillin microfibrils

So far, differences have been observed in both the ultrastructure of fibrillin microfibrils and their fibrillin-1 regional susceptibility to elastase, derived, *ex vivo,* from eye and skin and *in vitro* from cultured HDFs. The fibrillin microfibril's function is tied to the network it forms with a wide variety of proteins within the ECM (see references in **Table 4.1**). It is possible, therefore, that gauging the presence of these associated proteins may provide insight into the role they play within a specific tissue and into the underlying composition of the fibrillin microfibril.

		Microfibril-Associated Protein Presence		
	Published Interaction	Eye	Skin	HDF
Annexin A2	Cain *et al.* 2009	***	***	***
Annexin A5	Cain *et al.* 2009	***	***	***
Vimentin	Cain *et al.* 2009	***	***	***
Protein disulphide-isomerase	Meirelles *et al.* 2016	***	***	***
Calreticulin	Ashworth, Kelly *et al.* 1999	***	***	***
MFAP5 (MAGP2)	Penner *et al.* 2002	**	***	***
βig-h3	Cain *et al.* 2009	*	***	***
Versican	Isogai *et al.* 2002	*	***	***
MMP14	Ashworth, Murphy *et al.* 1999	*	**	***
Prelamin-A/C	Cain *et al.* 2009	*	*	**
Vitronectin	Dahlbäck *et al.* 1990	***	**	
MFAP2 (MAGP1)	Trask *et al.* 2000	**	**	
MFAP4	Pilecki *et al.* 2016	*	***	
Fibrillin-2	Zhang *et al.* 1994	*	**	
Laminin β2	Tiedemann *et al.* 2005	***		*
SERBP1	Cain *et al.* 2009	*		*
IGFBP7	Cain *et al.* 2009	*		*
Fibulin-2	Reinhardt *et al.* 1996		**	**
Laminin α5	Tiedemann *et al.* 2005	***		
Nidogen-1	Tiedemann *et al.* 2005	**		
Perlecan	Tiedemann *et al.* 2005	**		
Hyaluronan link protein 1	Ohno-Jinno *et al.* 2008	*		
LTBP2	Hirani *et al.* 2007	*		
Elastin	Sakai *et al.* 1986		*	
Fibulin-1	Roark *et al.* 1995		*	
EMILIN-2	Schiavinato *et al.* 2016		*	
Fibronectin 1	Sabatier *et al.* 2009			***
Thrombospondin 1	Cain *et al.* 2009			***
MMP2	Ashworth, Murphy *et al.* 1999			**
MMP3	Ashworth, Murphy *et al.* 1999			*
Decorin	Trask *et al.* 2000			*

Peptide hit score	
>15	***
6-14	**
2-5	*

Table 4.1: A list of published fibrillin microfibril-associated proteins identified in eye, skin and HDF microfibril samples. Proteins, detected using LC-MS/MS (Protein Prophet FDR ≤ 0.1%), along with their peptide hit score (sum of N=3) are shown.

Within the eye, skin and HDF microfibril purifications, a large variety of known fibrillin microfibril-associated proteins were identified using LC-MS/MS **(Table 4.1)**. A large proportion of these associated proteins, were uniquely detected in either tissue. Four proteins key to elastic fibre biology were identified in skin. The elastic fibre component elastin (Sakai *et al.* 1986); Elastin

microfibril interface-located protein (EMILIN)-2, key to the microfibril's deposition onto elastic fibres (Schiavinato *et al.* 2016); fibulin-1 (Roark *et al.* 1995), which exists as an interface between elastin and the fibrillin microfibril; and fibulin-2 (Reinhardt, Sasaki, *et al.* 1996), which co-localises with elastic fibres *in vivo* . This indicates that fibrillin microfibrils play a dominating role as an elastic fibre component in skin. Conversely, four basement membrane proteins were identified in eye-microfibril samples: perlecan, which was shown to connect fibrillin microfibrils directly to basal laminas, along with two laminins and nidogen-1 which bind to perlecan itself (Tiedemann *et al.* 2005). This indicates that fibrillin microfibrils play a major role in linking basement membranes within the CB epithelium of the eye.

The advantage of size-exclusion chromatography-purified microfibril proteomic analysis over whole tissue is that we can state with high confidence that the associated proteins identified must have been bound to the fibrillin microfibrils. Many of the proteins (fibrillin-2, MFAP2, MFAP5 and LTBP2) which directly co-purified with eye-derived microfibrils **(Table 4.1)** were the same as those found in the human zonule proteome published by De Maria *et al.* (2017). Two of these proteins, metalloproteinase inhibitor 3, (TIMP3) and alpha-2 macroglobulin (A2M) were also identified in these suspensions **(Supplementary Table 4.1)**, however, they had no previously published interactions with fibrillin microfibrils. Since these proteins (TIMP3 in particular) were two of the most abundant protease inhibitors found in their whole zonule proteome, they could be newly identified associated proteins of the fibrillin microfibrils. However, some of De Maria *et al.* (2017)'s most abundant glycoproteins (emilin-1 and hemicentin-1) identified in their zonule proteome did not co-purify with our eye-derived fibrillin microfibrils. It could be that these proteins do not associate with the microfibrils directly, or that the enzymatic extraction process and purification procedures stripped them from the microfibrils.

Many of the detected fibrillin microfibril-associated proteins were shared between tissues **(Table 4.1)**. This may provide key insight into identifying the integral components, fundamental to fibrillin microfibril assembly and function, regardless of the tissue of origin. For instance the molecular chaperone calreticulin and the disulphide bond-forming protein disulphide isomerase (PDI) , both of which are involved in the correct intracellular dimerisation of fibrillin-1 (Ashworth, Kelly, *et al.* 1999) were identified in skin, eye and HDF microfibril samples. The microfibrils tested in this study were purified via size-exclusion chromatography which separates structures of high molecular weight (MDa) from those of lower (KDa). This means the void volumes used should be enriched with only

mature, fibrillin and collagen VI microfibrils of varying lengths. Theoretically, immature forms of fibrillin-1, already bound to calreticulin and PDI, may have associated to these mature microfibrils. However, the N-terminus and C-terminus of immature fibrillins are cleaved by furin (at positions 44 and 1732 respectively) (Lonnqvist *et al.* 1998; Reinhardt, Gambee, *et al.* 2000) only after secretion from the cell (Jensen *et al.* 2014). In all samples tested, LC-MS/MS failed to detect any peptides corresponding to these cleaved chains. This suggests that immature fibrillin-1 was not detected in any of the samples tested. As such, it is likely that the intracellular proteins calreticulin and PDI were released from lysed cells where they then associated to the mature fibrillin microfibrils. Although these two intracellular proteins wouldn't associate with mature microfibrils naturally, the co-purification we see in our samples exemplifies the high affinity of these proteins to fibrillin-1 which accentuates their importance in microfibril assembly.

The MFAPs -5, -2 and -4 were also identified in microfibril samples from both tissues. MFAPs -4 and -5 are both instrumental to the proper formation and organisation of elastic fibres (Penner *et al.* 2002; Pilecki *et al.* 2016) by interacting and co-localising with fibrillin-1, tropoelastin and the crosslinking enzyme desmosine as well as promoting tropoelastin self-assembly on top of fibrillin microfibrils. MFAP2 (also known as MAGP-1) binds strongly to fibrillin microfibrils (Gibson *et al.* 1989; Trask *et al.* 2000) and was found to interact directly with both TGF-β and BMP-7 (Weinbaum *et al.* 2008). Disrupting this interaction in mice, leads to a marked increase in TGF-β signalling attributed to the loss of its sequestration into the fibrillin microfibril network (Walji *et al.* 2016). As such, MFAP2 plays a key role in modulating fibrillin-growth factor signalling. Fibrillin-2, a key component of maturing fibrillin microfibrils in developing elastic (Mariencheck *et al.* 1995) and non-elastic (Yamanouchi *et al.* 2012) tissues, was also identified in microfibril preparations from both eye and skin. It is likely that these fibrillin microfibril-associated proteins were identified from both tissues because of the fundamental role they play fibrillin microfibril assembly and function.

Fibrillin-2 and MFAPs -2 and -4, which were identified in both eye- and skin-derived microfibril samples, were not detected in cultured HDF-derived microfibril samples. The observation that all three HDF-derived fibrillin microfibril purifications lacked detection of fibrillin-2, MFAP2 and MFAP4 compared to tissue-derived, indicates the possibility that these microfibrils may be immature and functionally impaired in 1) forming mature fibrillin microfibrils, 2) forming elastic fibres and 3) modulating growth factor signalling. The differences seen in the ultrastructure and presence of key associated proteins, observed in cell-derived fibrillin microfibrils compared to tissue-derived, could

be due to the limitations of the cell culture model itself. Removing HDFs from their native, homeostatic environments could have contributed directly to the formation of immature and possibly defective fibrillin microfibrils. Many studies have exclusively used cell culture-derived microfibrils to elucidate their functional role in the ECM (Kielty and Shuttleworth 1993; Kinsey *et al.* 2008; Trask *et al.* 2000). The differences seen in this study demonstrates a problem with this approach as functional observations based on cell-derived fibrillin microfibrils may not necessarily reflect that seen in native tissue.

The distinct profiles seen between HDF- and skin-derived fibrillin microfibrils may have also contributed to the differences bead morphology. MFAP2, for instance, binds to the fibrillin microfibril bead directly (Henderson *et al.* 1996). As a consequence, it is possible that the redistribution of HDF-derived microfibril bead height compared to skin-derived **(Fig. 4.4 Aiv)** may be due to the loss of these associated proteins from the surface.

4.3.8 Conclusion

This study has found that fibrillin microfibril bead morphology and fibrillin-1 regional proteolytic susceptibility is tissue-source dependent. Additionally, this study observed that newly synthesised fibrillin microfibrils derived from HDFs had a different bead morphology and periodicity compared to native skin-microfibrils. This indicated that these newly synthesised microfibrils may be structurally immature in comparison to those developmentally formed in tissue or that they may lack the structure-altering damage accumulation seen in microfibrils from aged tissue. Additionally, this study demonstrated that collagen VI microfibrils, derived from HDFs and skin, are relatively invariable in periodicity and in regional elastase susceptibility, in comparison to the fibrillin microfibril. Finally, this study found that analysing the presence of the fibrillin microfibril-associated proteins within skin, eye and HDF-derived samples provides insight into the role they play in the elastic fibre, and the basement membrane. Additionally, it allowed the potential identification of proteins which could be fundamental to fibrillin microfibril biology regardless of their tissue-source and the observation that newly-synthesised microfibrils from cell culture lacked some of these proteins.

Although the loss and deterioration of the fibrillin microfibril network in response to chronic photoageing has been observed immunohistochemically (Watson *et al.* 1999), the effects on fibrillin microfibril ultrastructure, fibrillin-1 protease susceptibility and associated protein composition has

yet to be studied. The techniques and methodology used in this tissue and culture comparison would be well suited to this goal.

4.4 Experimental procedures

4.4.1 Study design

Microfibrils were extracted and purified from adult human: 1) eye (CB) (N=3: M74 = male aged 74 years, F79, F76), 2) abdominal skin (N=3: F49, F55, F56) and 3) cultured human dermal fibroblasts (HDF) (N=3: M75, M76, M77). The ultrastructure of these purified fibrillin microfibrils (bead morphology and bead-bead periodicity), from these three different sources, was measured and compared using AFM **(Fig. 4.7)**. The regional susceptibility of the fibrillin-1 domain structure to elastase digestion was measured and compared by counting the average number of LC-MS/MS detected PSMs from each domain. Finally, the presence of known microfibril-associated proteins was detected and compared for each of these purifications using LC-MS/MS.

Collagen VI microfibrils, which are also present in these purifications, were treated as a control and their periodicity, and COL6A3 regional susceptibility to elastase compared to that of the fibrillin microfibrils in the same samples.

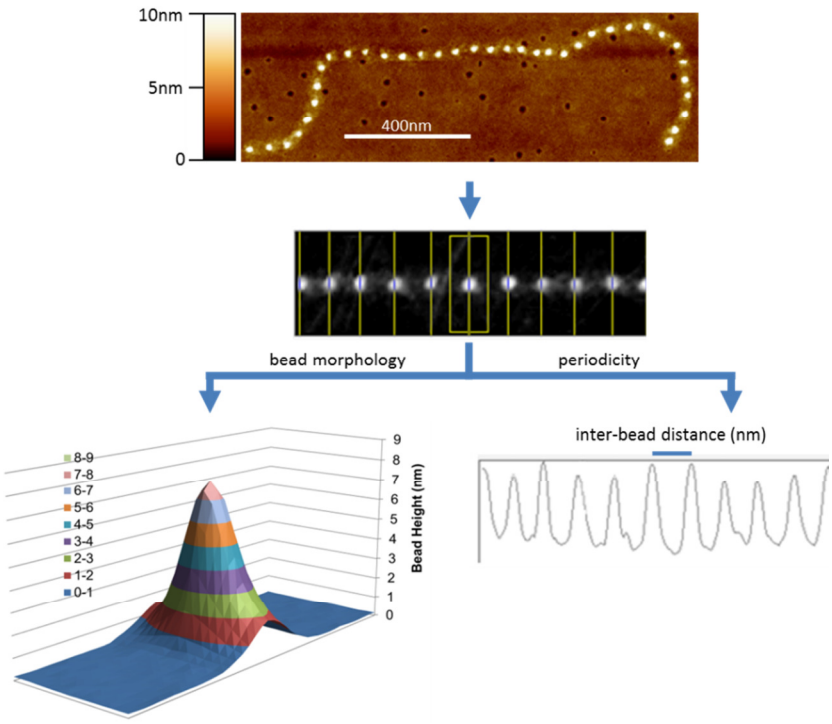

Figure 4.7: Ultrastructural measurements of the fibrillin microfibril, performed with AFM. Fibrillin microfibrils adopt a beads-on-a-string appearance when viewed with AFM. The height maps generated were used to measure and compare the bead morphology and the periodicity (inter-bead distance) of eye (CB)-, skin- and HDF-derived fibrillin microfibrils.

4.4.2 Reagents and human tissue and cell acquisition

All chemicals were sourced from Sigma-Aldrich Co. Ltd (Poole, UK) unless stated otherwise. This study is conducted in accordance with the European Medicines Agency Note for Guidance on Good Clinical Practice and the Declaration of Helsinki 1964 (revised Seoul 2008). The use of human donor eye tissue was approved by the University of Manchester ethics committee (ethics ref#11305). Tissue was received within 24 hours of corneal dissection (for corneal transplant services) from the Manchester Eye Bank, in accordance with the Human Tissue Act. The CB was carefully dissected from each tissue sample followed by snap freezing in liquid nitrogen and storage at -80°C.

Human abdominal skin samples were acquired from the University of Manchester Skin Health Biobank (MSHB). This biobank was approved by the North West 5 Research Committee (ref: 09/H1010/10). Samples were snap frozen in liquid nitrogen and stored at -80°C.

Primary HDFs were cultivated from skin biopsies taken from donor photoprotected buttock. The use of this skin was approved by North West Research Ethics Committee (ref# 14415) where all donors gave written and informed consent. All incubations and cultures were performed at 37°C (5% CO_2). Biopsies were incubated in HBSS (Fisher Scientific, Loughborough, UK) with 10% (v/v) PluriSTEM™ Dispase II solution, overnight. The dermis was then dissected and minced prior to incubation in fibroblast media: DMEM (Fisher Scientific, Loughborough, UK) containing 10% foetal calf serum (FCS), 1% L-glutamine, 1% amphotericin and 1% penicillin-streptomycin (Pen-Strep; Gibco, Paisley, UK) (all v/v). Tissue samples were then cultured with weekly fibroblast media changes until HDFs could be observed on sample plates.

4.4.3 Microfibril isolation and purification

Human eye and skin tissue samples were minced and added to a 2 ml aliquot of salt buffer (50 mM Tris-HCl, 400 mM NaCl and 1 mM $CaCl_2$; pH 7.4). 1mg of bacterial collagenase IA, 0.01 mM phenylmethylsulfonyl fluoride (PMSF) and 0.03 mM N-ethylmaleimide (NEM) was then added to the tissue which digested on a rotary mixer for 4 hours at room temperature (Hibbert *et al.* 2015; Kielty *et al.* 1991).

Post-confluent (passage 2) HDFs were maintained for 5 weeks in DMEM + GlutaMAX (Fisher Scientific, Loughborough, UK) containing 10% (v/v) FCS and 50 µg/ml of Pen-Strep. HDFs were then washed with phosphate buffered saline (PBS) and 2 ml of salt buffer was added directly to the

culture flasks. 1 mg of bacterial collagenase IA, 0.01 mM PMSF and 0.03 mM NEM was then added and digested on an orbital shaker for 2 hours at room temperature.

Microfibril purification was achieved using an ÄKTA Prime Plus Liquid Chromatography System (GE Healthcare; Little Chalfont, UK). Post-digestion, tissue- and HDF-derived samples were centrifuged at 5000g for 5 min and supernatant was ran within a column buffer (which was comprised of 50 mM Tris-HCl and 400 mM NaCl at pH 7.4), through a GE HiScale 16/40 column containing Sepharose® Cl2B beads (Sigma-Aldrich Co. Ltd), at 0.5 ml/min. Co-purifying fibrillin and collagen VI microfibrils were enriched in the void volume peak where fractions were collected based on spectrophotometric absorbance at 280 nm (Hibbert *et al.* 2015; Kielty *et al.* 1991). Aliquots of the purification were kept for AFM, and rest were desalted in 0.22 µm filtered ultrapure water using a Slide-A-Lyzer™ MINI Dialysis Devices (Thermo Fisher Scientific; Paisley, UK) for 4 hours at 4°C. Samples were subsequently frozen at -80°C and freeze-dried at -60°C for 48 hours prior to storage at -80°C until their use in MS experiments.

4.4.4 Microfibril peptide generation using elastase and SMART™ digestion prior to mass spectrometry

To enhance fibrillin-1 peptide generation, half of the freeze dried samples were re-suspended in 0.1 M Tris-HCl, pH 8.5. Proteins were denatured in 8 M urea, reduced in 10 mM dithiothreitol (DTT) for 30 minutes at room temperature and alkylated using 50 mM iodoacetamide (IAM) for 30 minutes at room temperature, in darkness. The solution was then diluted down to 2 M urea, and elastase (Catalogue # E1250) added at a 2:1 enzyme to substrate ratio. This was incubated at 37°C for 4 hours. Elastase activity was then quenched with 5% (v/v) formic acid in ultrapure water.

To enhance microfibril-associated protein peptide generation, the other half of the freeze-dried samples were re-suspended in ultrapure water and directly digested for 75 minutes using a SMART Digest™ kit (Thermo Scientific), which allows the fast digestion of the sample through immobilised trypsin beads, at a high, denaturing temperature (70°C) (Moore and Samonig 2016), as per the manufacturer's instructions. All samples were then desalted using Oligo R3 resin (Thermo) beads and vacuum dried prior to MS analysis.

4.4.5 Mass spectrometry

All MS was performed by the Biological Mass Spectrometry Core Facility in the Faculty of Biology, Medicine and Health at the University of Manchester (Manchester, UK). As dictated by their

protocols (Buckley 2015; Lennon *et al.* 2014): vacuum dried samples were analysed by LC-MS/MS using an UltiMate® 3000 Rapid Separation LC (Dionex Corp; Sunnyvale, CA, USA) and an Orbitrap Elite mass spectrometer (Thermo Fisher Scientific). Peptide mixtures were separated using a gradient from 92% A (0.1% [v/v] formic acid [FA] in water) and 8% B (0.1% [v/v] FA in acetonitrile) to 33% B, in 30 minutes at 300 nL min^{-1}, using a 250 mm x 75 µm i.d. 1.7 mM BEH C18, analytical column (Waters). Peptides were selected for fragmentation automatically by data-dependent analysis.

4.4.6 Mass spectrometry data analysis

Mass spectra were extracted using extract_msn (Thermo Fisher Scientific) correlated against the Uniprot human database (Consortium 2016) using Mascot v2.5.1 (Matrix Science; London, UK).

Search parameters were: species - Homo sapiens; enzyme – trypsin for SMART™ digested samples and non-specific for elastase digested samples; max missed cleavages – 1; fixed modifications - carbamidomethyl, mass – 57.02 Da, AA – C; variable modification – oxidation, mass – 15.99 Da, AA – M; peptide tolerance - 10 ppm (monoisotopic); fragment tolerance - 0.6 Da (monoisotopic); searched database: the SwissProt_2016_04 database (152,544 protein entries).

Data generated was validated using Scaffold (Proteome Software; Portland, OR, USA). Only exclusive, unique peptide counts are reported. False discovery rate (FDR) was calculated by Scaffold using protein and peptide probabilities assigned by the Trans-Proteomic Pipeline and the Protein Prophet™ (Nesvizhskii *et al.* 2003) and Peptide Prophet™ (Keller *et al.* 2002) algorithm (Sourceforge; Seattle. WA, USA). Peptide Prophet FDR was thresholded to ≤ 5% and Protein Prophet FDR was thresholded to ≤ 0.1% (minimum 2 peptides) for every dataset.

The MS proteomics data have been deposited to the ProteomeXchange Consortium via the PRIDE (Vizcaíno *et al.* 2016) partner repository with the dataset identifier PXD008450 and 10.6019/PXD008450.

4.4.7 Microfibril atomic force microscopy

Glass coverslips were soaked in absolute ethanol overnight then attached to metal stubs with clear nail varnish. Samples were pipetted directly onto the coverslips and left for 1 minute so microfibrils could adsorb to the surface. Liquid was removed and stub left to dry overnight. Stubs were washed three times with ultrapure water and left to dry before being scanned using AFM. Fibrillin and collagen VI microfibrils were imaged using peak force and Scan-Asyst® mode on a Multimode 8 atomic force microscope (Bruker; Billerica, MA, USA), as previously described (Hibbert *et al.* 2015;

Sherratt *et al.* 2010). Using a single, new Scan-Asyst® Air tip (Bruker), single fibrillin microfibrils were captured at 512 pixels/line in 2 x 2 µm scans. This gave a resolution of 3.9 nm/pixel, which was deemed high enough for fibrillin microfibril ultrastructural analysis. Fibrillin microfibrils which were laterally associated with collagen VI microfibrils were omitted from the analysis.

Scans were digitally flattened using WSxM v5.0 AFM Image Processing package (Horcas *et al.* 2007) and exported in text image format. Height was corrected by subtracting negative background (Ratcliff and Erie 2001). Using ImageJ (NIH; Bethesda, MA, USA), fibrillin microfibrils were straightened using the Straighten Curved Objects plugin (Kocsis *et al.* 1991) enabling the generation of 41 pixel wide images of single straightened fibrillin microfibrils **(Fig. 4.7)**. LFA image processing software, developed by our group using Microsoft Visual Basic 6.0 as previously described (Sherratt *et al.* 2003), was then used to specify the location of the maximum height of each bead and create a 15 x 41 pixel snapshot of each individual bead with the height maxima at the central pixel of the image. Maximum bead height and morphology were taken from these snapshots. Fibrillin microfibril periodicity was measured using Periodicity and Angles software package developed by our group using Microsoft Visual Basic 6.0 as previously described (Sherratt *et al.* 2005).

4.5 Acknowledgments

This study was funded by a programme Grant from Walgreens Boots Alliance, Nottingham, UK. The Wellcome Trust Centre for Cell-Matrix Research, University of Manchester is supported by core funding from the Wellcome Trust (088785/Z/09/Z). CB and MJS acknowledge the support of the BBSRC (Ref: BB/N015398/1). The content is solely the responsibility of the authors and does not necessarily represent the official views of the National Institutes of Health.

4.6 Conflict of interest

The authors declare that they have no conflicts of interest with the contents of this article. Walgreens Boots Alliance has approved this manuscript's submission but exerted no editorial control over the content.

4.7 Author contributions

AE conceived, designed, performed all experiments, analysed all the data, prepared the figures and wrote the paper. MJS supervised and coordinated the study and contributed to the preparation of the figures and writing of the paper. SMP contributed to the isolation of primary fibroblasts from

human skin and KTM contributed to their cell culture. REBW and CEMG contributed to the study design and to the editing of the paper. DK and ROC provided technical assistance and support for all LC-MS/MS. CB contributed to the editing of the paper and interpretation of the results. All authors contributed to the editing of the paper.

4.8 Supplementary information

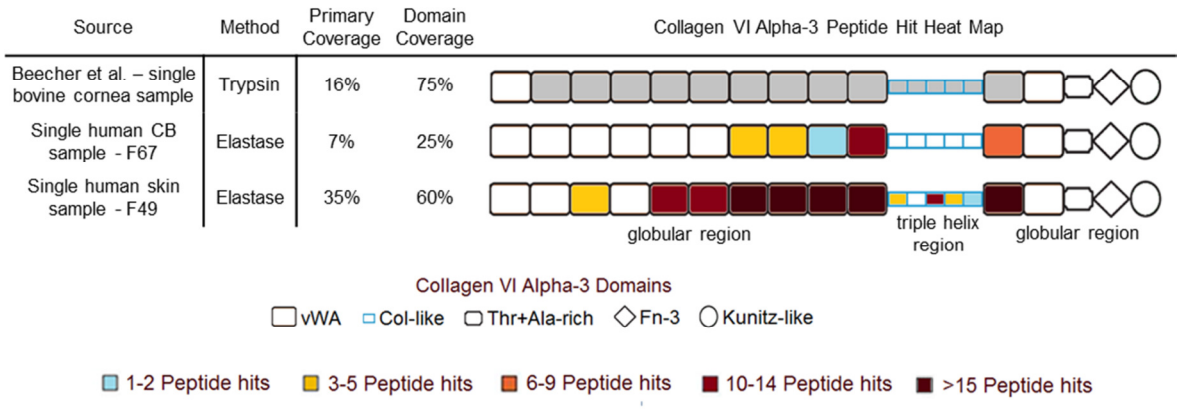

Supplemental Figure 4.1: The elastase method and advances in MS technology led to the improved detection of COL6A3 peptides. The ability of the elastase method to produce COL6A3 peptides from a single human CB sample (F67) and single human skin sample (F49) is compared to efforts made by Beecher et al. *(2011) from a single bovine cornea sample. Beecher* et al. *identified COL6A3 peptides from von Willebrand A domains (vWA) N1-N9 of N-terminal globular region, C1 of the C-terminal globular region and from the triple-helix domain (coloured grey since number of peptide hits was unreported). Since the CB is a collagen VI-poor region in comparison to cornea, our methods only detected peptides from vWA domains N1-N4 and C1 of the globular regions from the human CB-microfibril extract (F67) leading to a lower primary coverage than that by Beecher* et al. *However, when our methods were applied to human skin (F49), a collagen VI-rich tissue, we achieved a COL6A3 primary coverage which was more than double that of Beecher* et al. *(2011) .*

The Supplementary Table has been uploaded to the online data repository Mendeley Data and can be accessed by copying and pasting the following link:

https://data.mendeley.com/datasets/7t8hxk7bwb/draft?a=45c5494a-55e9-49b8-9ac6-b505a148e07e

Supplementary Table 4.1: Full protein list for all eye skin and HDF samples

Chapter 5: Molecular fingerprints of photodamage in human extracellular matrix assemblies

This paper was written with the Journal of Molecular Biology in mind. I conceived, designed and performed all experiments, analysed all the data, prepared the figures and wrote the paper. Dr Suzanne Pilkington isolated the primary fibroblasts from human skin, used in this study. Dr David Knight, Dr Ronan O'Cualain and Ms Emma-Jayne Keevill of the Biological Mass Spectrometry Core Facility in the Faculty of Biology, Medicine and Health at the University of Manchester (Manchester, UK) provided technical assistance for all LC-MS/MS.

Molecular fingerprints of photodamage in human extracellular matrix assemblies

Alexander Eckersley[1], Matiss Ozols[1], Ronan O'Cualain[3], Emma-Jayne Keevill[3], April R Foster[2], Suzanne M Pilkington[2], David Knight[3], Christopher EM Griffiths[2,4], Rachel EB Watson[2,4], Michael J Sherratt[1]

[1]Division of Cell Matrix Biology & Regenerative Medicine, [2]Division of Musculoskeletal & Dermatological Sciences, [3]School of Biological Sciences, Faculty of Biology, Medicine and Health, The University of Manchester and [4]NIHR Manchester Biomedical Research Centre, Central Manchester University Hospitals NHS Foundation Trust, Manchester Academic Health Science Centre, Manchester, UK

Running Title: Molecular foci of photodamage in human extracellular matrix

Corresponding Author: Dr Michael Sherratt

Address: 1.529 Stopford Building, The University of Manchester,

Oxford Rd, Manchester, M13 9PT, UK;

Telephone: +44 (0)161 275 1439;

Fax: +44 (0)161 275 5171;

Email: michael.sherratt@manchester.ac.uk

Keywords: Fibrillin microfibril, collagen VI microfibril, extracellular matrix, skin, fibroblast, ultraviolet, photodamage, ageing, proteomics, mass spectrometry (MS), atomic force microscopy (AFM), protein structure

5.1 Abstract

Photoageing in skin is commonly recognised histologically by architectural remodelling of dermal extracellular matrix components. Whilst these techniques are powerful, they are ill-suited to identifying molecular damage in these long-lived assemblies. Previously, we have shown that, in contrast to collagen VI microfibrils, the ultrastructure of fibrillin microfibrils (a key elastic fibre component) is susceptible to physiological doses of ultraviolet radiation (UVR). However, the molecular locations of UVR-induced damage within fibrillin-1, and potentially collagen VI alpha-3 (COL6A3) monomers, remain unknown. Using recently developed proteomic methods, this study aimed to locate UV-susceptible foci within the fibrillin-1 and COL6A3 proteins. Fibrillin and collagen VI microfibrils were co-purified from cultured human dermal fibroblasts and irradiated with either broadband UVB or solar simulated radiation (SSR). Ultrastructural damage was assessed using atomic force microscopy (AFM): fibrillin microfibril bead height and periodicity were significantly altered by both SSR- and UVB irradiation whereas collagen VI microfibril ultrastructure was not. UVR-induced molecular damage was confirmed by proteolytic peptide generation with elastase followed by liquid chromatography tandem mass spectrometry (LC-MS/MS). UV irradiation consistently enhanced the total yield of digested fibrillin-1 but not COL6A3 peptides. Furthermore, peptides characteristic of UV exposure were repeatedly identified for both fibrillin and collagen VI microfibrils. Mapping these peptides revealed that UVR exposure increased regional susceptibility within the fibrillin-1 structure to protease-mediated proteolysis. This allowed the identification of UV-susceptible foci within a key dermal assembly on a molecular scale. This proteomic approach has the potential to facilitate the rapid, protein-specific identification of differential molecular fingerprints of photodamage in key extracellular matrix proteins.

5.2 Introduction

Skin photoageing is characterised microscopically by the reorganisation of the dermal extracellular matrix (ECM) (see reviews: Naylor *et al.* 2011 and Tsoureli-Nikita *et al.* 2006) in response to chronic exposure to ultraviolet (UV) radiation (Montagna *et al.* 1989). The profound downstream consequences of this process include alterations to tissue elasticity, mechanics and homeostasis (Langton *et al.* 2017) which are thought to play contributory roles in the appearance of deep wrinkles (Warren *et al.* 1991). However, the precise molecular pathways driving this remain to be defined.

Remodelling of the elastic fibre network (which is comprised of fibrillin microfibrils and elastin (see review: (Kielty, Sherratt, *et al.* 2002)), has proved to be a sensitive indicator of both photoageing (Watson *et al.* 1999; Warren *et al.* 1991) and repair (Watson *et al.* 2009). These assemblies are remarkably long-lived, with a turnover close to the average human lifetime (Shapiro *et al.* 1991). As a consequence, they are expected to accumulate UV-induced structural and molecular damage. Photoageing can be histologically characterised by the loss of fibrillin microfibrils at the papillary dermis (Watson *et al.* 1999). However, the presence of cumulative molecular damage, which may impair structural and biochemical functionality (Kaartinen and Warburton 2003; Sengle *et al.* 2008), has yet to be demonstrated.

UV radiation, which reaches the Earth's surface, consists of approximately 5% high energy UVB (wavelength 280-315 nm) and 95% low energy UVA (315-400 nm) (El Ghissassi *et al.* 2009). The absorption of these short-wave photons by photosensitive biomolecules can cause photochemical reactions in amino acid residues (Bensasson *et al.* 1993) leading to the direct photo-degradation of protein (e.g. via the dissolution of di-sulphide bonds; Mozziconacci *et al.* 2010), or creation of new crosslinks (Itri *et al.* 2016). Additionally, it is thought that this absorption may also lead to the formation of reactive oxygen species (ROS), capable of further degrading protein structure via oxidation of amino acids (Stadtman 1992; Wondrak *et al.* 2006).

The fibrillin microfibril is a large macromolecular assembly which resembles beads on a string with a characteristic ~56 nm periodicity (Baldock *et al.* 2001; Eckersley *et al.* 2018; Hibbert *et al.* 2015, 2017; Sakai *et al.* 1986; Sherratt *et al.* 2007, 2010). Previously, we have shown that low-dose irradiation of isolated, purified, cell-derived fibrillin microfibrils by either broadband UVB (Sherratt *et al.* 2010) or solar simulated radiation (SSR: 95% UVA + 5% UVB) (Hibbert *et al.* 2015, 2017) causes quantifiable changes to microfibril ultrastructure. It is likely, therefore, that the degeneration

of the fibrillin microfibril network observed histologically during photoageing (Watson *et al.* 1999) may be due to an accumulation of molecular damage. This, however, has yet to be demonstrated experimentally.

Other dermal ECM assemblies, such as collagens are equally as long-lived as their elastic fibre counterparts (Verzijl, DeGroot, Oldehinkel, *et al.* 2000; Verzijl, DeGroot, Thorpe, *et al.* 2000) yet some, such as collagen VI microfibrils, undergo minimal architectural remodelling in photoaged skin (Watson *et al.* 2001). In common with fibrillin microfibrils, collagen VI microfibrils also play important biochemical roles: anchoring cells to the matrix (Stallcup *et al.* 1990) and interacting with numerous ECM components (Kuo *et al.* 1997; Specks *et al.* 1992; Tillet *et al.* 1994). They also form beaded macromolecular, assemblies which can be visualised using AFM (Eckersley *et al.* 2018; Hibbert *et al.* 2015; Sherratt *et al.* 2004) and EM (Baldock *et al.* 2003; Godwin *et al*. 2017; Kielty *et al.* 1991). However, in contrast to fibrillin, collagen VI microfibrils contain relatively few UV-absorbing amino acid residues (chromophores) and are resistant to UVR-induced ultrastructural damage *in vitro* (Hibbert *et al.* 2015). Although collagen VI microfibrils appear ultrastructurally and histologically resistant to UVR exposure compared to fibrillin, their irradiation may still induce molecular damage which could impact on tissue function. Additionally, the molecular mechanisms behind the differential susceptibility of collagen VI and fibrillin microfibrils to UVR remain to be determined.

Molecular damage can be characterised by conventional biochemical techniques such as gel-electrophoresis; however, the high molecular weights and insolubility of these microfibrillar ECM assemblies makes this approach challenging (Baldock *et al.* 2001; Sakai *et al.* 1986). Recently, however, we have demonstrated that proteomics can be used to effectively detect regional and compositional differences in the susceptibility of fibrillin and collagen VI microfibrils to elastase (Eckersley *et al.* 2018). By mapping liquid chromatography tandem mass spectrometry (LC-MS/MS) derived peptide spectrum matches (PSMs) of fibrillin-1 and collagen VI alpha-3 (COL6A3) to their corresponding domain structures, we demonstrated tissue-specific local differences in structure within these assemblies on a monomeric molecular scale.

In this study, we aimed to use these recently developed proteomic methods (Eckersley *et al.* 2018) to determine if UV exposure (both broadband UVB and SSR) induces molecular damage in co-purified suspensions of fibrillin and collagen VI microfibrils. These can be detected by mass spectrometry (LC-MS/MS) as characteristic peptide "fingerprints" from within fibrillin-1 and COL6A3

monomers. By isolating microfibrils from cultured primary human dermal fibroblasts (HDFs), we ensured sufficient yield of newly synthesised, non-UVR exposed assemblies drawn from a homogenous population for study. By subjecting these suspensions to UVR exposure *in vitro,* and subsequent analysis with AFM and LC-MS/MS, we tested the hypothesis that physiological doses of UVR induce localised and differential molecular changes in fibrillin and collagen VI microfibril protease susceptibility.

5.3 Results and Discussion

5.3.1 Fibrillin microfibril ultrastructure is susceptible to both broadband UVB and solar simulated radiation

Prior to LC-MS/MS analysis, broadband UVB- and SSR-induced damage to fibrillin microfibrils was assessed using AFM. Both broadband UVB and SSR caused quantifiable changes to fibrillin microfibril ultrastructure. Broadband UVB irradiation caused significant increases to fibrillin microfibril periodicity **(Fig. 5.1 Ai)**. Additionally, broadband UVB-irradiated fibrillin microfibrils had significantly higher central bead heights **(Fig. 5.1 Aii)** as well as significant changes in bead morphology compared to non-irradiated microfibrils. According to axial bead profiles, broadband UVB-irradiated fibrillin microfibril beads were higher along the entire bead profile when compared to non-irradiated **(Fig. 5.1 Aiii)**. Interestingly, contour heat mapping of bead height differences revealed that broadband UVB irradiation caused microfibril beads to increase in volume along its entire ultrastructure with the largest differences seen on the slopes surrounding the peaks **(Fig. 5.1 Aiv)**. The less energetic wavelengths in SSR were less damaging to fibrillin microfibril ultrastructure than those from broadband UVB. Although SSR caused significant increases in both fibrillin microfibril periodicities **(Fig. 5.1 Bi)** and central bead heights **(Fig. 5.1 Bii)** compared to unirradiated, it induced only minimal changes to axial height profiles **(Fig. 5.1 Biii)**. Contour heat mapping of bead height differences, however, did indicate measurable differences close to the central peak **(Fig. 5.1 Biv)**.

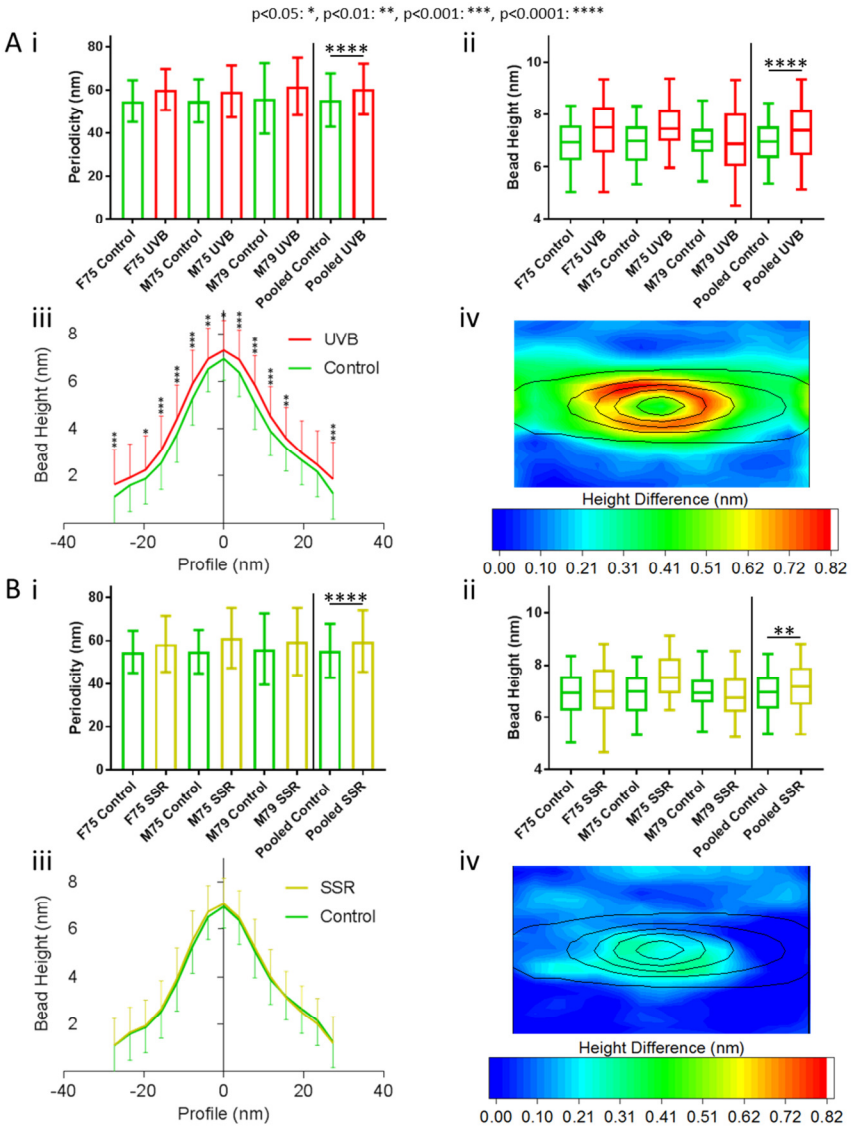

*Figure 5.1: Fibrillin microfibril ultrastructure was affected by both broadband UVB and SSR. UVB-irradiated microfibril periodicities were significantly higher (n=500 repeats, n=1500 pooled) than those of control (p<0.0001, Mann-Whitney U) (**Ai**; data = mean and SD). Additionally, central bead heights were also significantly higher in UVB-irradiated microfibrils (n=100 repeats, n=300 repeats pooled) than in control (p<0.0001, Mann-Whitney U) (**Aii**; data = median, IQR and range). The axial profiles of UVB-irradiated microfibril beads were also significantly higher along the entire central bead axis than those of control (Bonferroni multiple comparison test) (**Aiii**; data = mean and SD). In order to visualise UVR-induced changes in bead morphology, AFM height maps of control microfibril beads were averaged and subtracted from that of UVB-irradiated microfibril beads. UVB-induced changes in morphology can be observed throughout the bead but primarily along its slopes (~10nm radius from the peak) **(Aiv)**. Fibrillin microfibril ultrastructure was less affected by SSR **(B)**. SSR-irradiated microfibril periodicities were significantly higher than those of control (p<0.0001, Mann-Whitney U) (**Bi**; data = mean and SD). Central bead heights were also significantly higher in SSR-irradiated fibrillin microfibrils compared to control (p=0.0061, Mann-Whitney U) (**Bii**; data = median, IQR and range). However, axial profiles of SSR-irradiated fibrillin microfibril beads did not differ significantly from those of control (Bonferroni multiple comparison test) (**Biii**; data = mean and SD). Heat mapped height differences between SSR-irradiated and control show only small changes in bead morphology near central peak and along one of the lateral slopes **(Biv)**.*

The changes in fibrillin microfibril periodicity seen in response to both SSR and broadband UVB irradiation are consistent with previous studies (Hibbert *et al.* 2015, 2017; Sherratt *et al.* 2010). However, changes to bead morphology using AFM height mapping have not previously been demonstrated. Using STEM, we reported previously that broadband UVB caused a loss of mass within the beads of both skin- and cell-derived fibrillin microfibrils (Sherratt *et al.* 2010). Our AFM height mapping, however, showed an increase in bead volume. Collectively these observations suggest that exposure to UVR induced structural changes which result in a loss of microfibrillar material (either from fibrillin-1 or associated proteins) and, consequentially, to a reduced packing density (Baldock *et al.* 2006, 2001; Kuo *et al.* 2007; Reinhardt, Keene, *et al.* 1996; Sherratt *et al.* 2003), and hence an increased bead volume.

5.3.2 Collagen VI microfibril ultrastructure is largely resistant to SSR- and UVB-induced damage

AFM quantification showed that collagen VI microfibril ultrastructure was resistant to remodelling by both broadband UVB and SSR radiation **(Fig. 5.2)**. Neither broadband UVB **(Fig. 5.2 A)** nor SSR **(Fig. 5.2 B)** was able to cause measurable changes to collagen VI microfibril periodicity. Although we have previously shown that collagen VI microfibril ultrastructure is resistant to SSR in contrast to fibrillin microfibrils (Hibbert *et al.* 2015), here we demonstrate that these assemblies are as resistant to higher energy broadband UVB as they are to SSR. Since, in skin, collagen VI microfibrils are predominantly distributed in the upper papillary dermis, near the dermal-epidermal junction (Watson *et al.* 2001), they are likely subjected to both UVA and UVB wavebands, *in vivo* (Hibbert *et al.* 2015). Therefore, their resistance to may be inherent to their fundamental function and may explain the lack of change observed in collagen VI microfibril distribution in photoaged versus photoprotected skin (Watson *et al.* 2001).

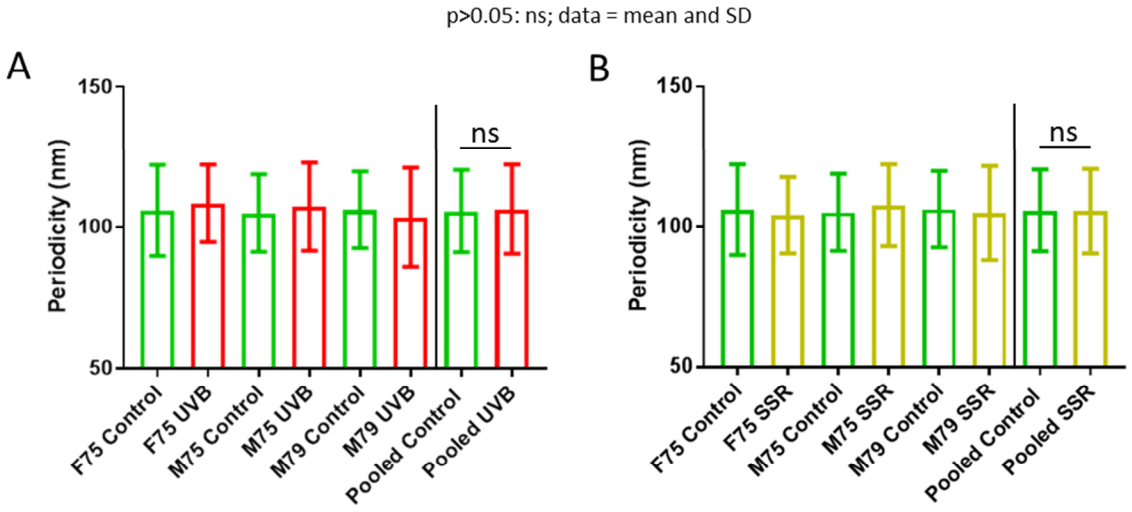

Figure 5.2: Broadband UVB and SSR did not induce changes to collagen VI microfibril periodicity. Periodicities of broadband UVB-irradiated collagen VI microfibrils (n=500 repeats, n=1500 repeats pooled) were not significantly different compared those of control (p=0.1811, Mann-Whitney U) ***(A)****. SSR also failed to induce measurable changes to collagen VI microfibril periodicity* ***(B)****. SSR-irradiated collagen VI microfibril periodicities were not significantly different compared to those of control (p=0.9778, Mann-Whitney U).*

Although collagen VI microfibrils appear resistant to UVR, ultrastructurally (*in vitro)* (Hibbert *et al.* 2015), and to photoageing histologically (*in vivo)* (Watson *et al.* 2001), molecular-scale changes may still be present which AFM is unable to resolve. Additionally, although two models of fibrillin microfibril supramolecular organisation exist (Baldock *et al.* 2001, 2006; Kuo *et al.* 2007; Reinhardt, Keene, *et al.* 1996), uncertainties regarding the packing of fibrillin-1 within the microfibril still remain (see reviews: Jensen and Handford 2016 and Kielty *et al.* 2005). It is still unclear, therefore, whether specific regions of fibrillin-1 are targeted by UV exposure. By measuring the propensity of these UVR-damaged fibrillin and collagen VI microfibrils to proteolytically yield fibrillin-1 and COL6A3 peptides using LC-MS/MS, we can assess whether damage exists on a molecular scale.

5.3.3 UVR exposure enhances the elastase-mediated detection and yield of fibrillin-1 peptides

Total numbers of LC-MS/MS-derived fibrillin-1 peptide spectrum matches (PSMs) were consistently higher for SSR-irradiated and broadband UVB-irradiated fibrillin microfibril samples than for un-irradiated samples **(Fig. 5.3)**. SSR irradiation led to a mean increase of 24% in the number of fibrillin-1 PSMs compared to unirradiated (103 vs. 83) **(Fig. 5.3 Bi)** whereas broadband UVB irradiation led to a mean 55% increase compared to control (129 vs. 83) **(Fig. 5.3 Bii)**. This increase in fibrillin-1 PSMs from irradiated microfibril samples may be due to changes in fibrillin microfibril ultrastructure. The ultrastructural damage observed in these microfibrils, (characterised

in this study by increased bead morphometry and increased periodicity **(Fig. 5.1)** and previously as a loss of bead mass (Sherratt *et al.* 2010)), may increase the accessibility of elastase to previously buried (cryptic) cleavage sites.This elastase-mediated peptide yield positively correlates with the energy of the incident radiation: high energy broadband-UVB induced more ultrastructural damage and increased the proteolytic susceptibility of fibrillin-1 than lower energy SSR.

A

Fibrillin-1 Exclusive Unique Peptides Identified (FDR≤5%)					
	Control	SSR		Broadband UVB	
	PSMs	PSMs	Fold Change vs. Control	PSMs	Fold Change vs. Control
M79	43	47	1.09	72	1.67
M75	170	214	1.26	200	1.18
F75	37	48	1.30	116	3.14

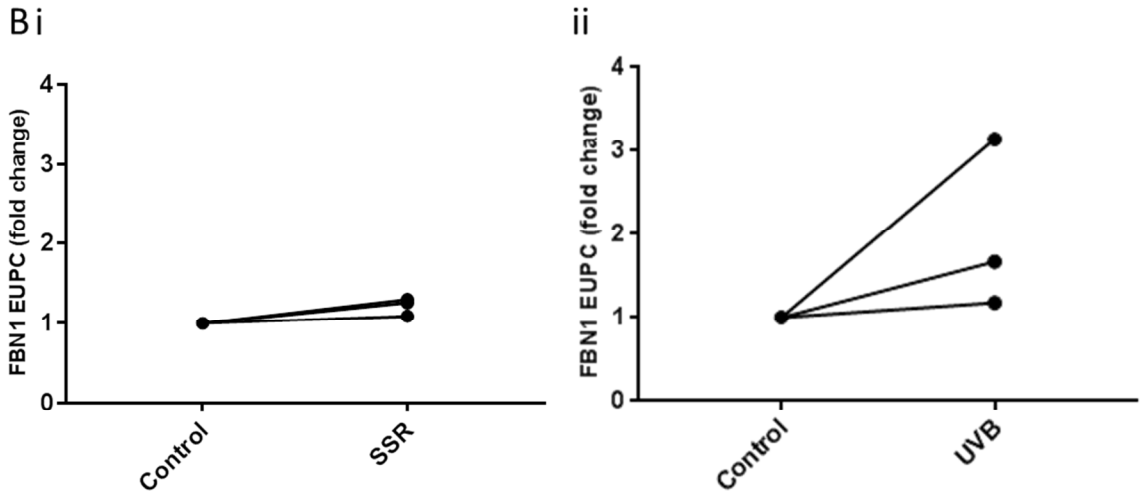

Figure 5.3: UV exposure led to an increase in the overall proteolytic susceptibility of fibrillin-1. PSMs for SSR- and broadband UVB-irradiated fibrillin-1 per individual and their fold changes in comparison to control fibrillin-1 are shown (Peptide Prophet FDR ≤ 5%) ***(A)****. SSR irradiation of fibrillin-1 led to a small but consistent increase in fibrillin-1 peptide identification (1.22 average fold change) for all three replicates* ***(Bi)****. Broadband UVB irradiation led to an even larger increase in fibrillin-1 peptide identification (2.00 average fold change)* ***(Bii)****.*

Data-dependent quantification revealed a number of fibrillin-1 peptides which were significantly different in relative abundance in broadband UVB-irradiated or SSR-irradiated fibrillin microfibril samples compared to non-irradiated **(Fig. 5.4)**. Although SSR-irradiated suspensions yielded a higher number of UVR-specific fibrillin-1 peptides than broadband UVB (21 vs 14), UVB-irradiated samples contained more peptides with fold changes ≥ ±5 (8 vs 6). Additionally, a higher proportion of these fibrillin-1 peptides were significantly increased in broadband UVB-irradiated samples (78%: 11 out of 14) than in SSR-irradiated samples (52%: 11 out of 21). This is perhaps again related to the more severe damage caused by broadband UVB to the fibrillin microfibril

ultrastructure than SSR. Crucially, this experiment identified 7 UVR-specific fibrillin-1 peptides which were significantly enriched in both broadband UVB- and SSR-irradiated fibrillin microfibril samples (**Fig. 5.4**, top table). These shared peptides may serve as useful peptide "fingerprints" of UV damage to fibrillin microfibrils, regardless of UV source used.

Shared broadband UVB- and SSR-Affected Peptides

IIVGPDDSAVDMDECKEPDVCKH
ALDPDICPNGI
VDINECLLEPR
CENLRGTYKCI
CEDIDECVEEPEICA
CRHSCGDGFCSRPNMCTCPS
GFMTNGADIDECKVIHDVCR

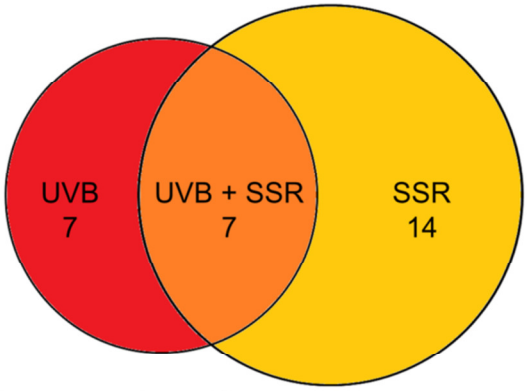

Broadband UVB-Affected Peptides	Fold Change	Average Norm. Abundance		Anova (p value)
		UVB	Control	
SLDQTGSSCEDVDECEGNHR	**∞**	**109553**	**0**	**0.0281**
LMPDQRSCTDIDECEDNPNICDGGQCT	**∞**	**47826**	**0**	**0.0065**
NCVDINEC	**∞**	**9637**	**0**	**0.0090**
TGCTDINECEIGA	**18.6**	**278349**	**14945**	**0.0347**
IIVGPDDSAVDMDECKEPDVCKH	**9.15**	**94566**	**10336**	**0.0285**
NEKCEDIDECVEEPEICAL	**8.55**	**159126**	**18610**	**0.0414**
GSGIIVGPDDSAVDMDECKEPDVC	3.31	382172	115352	0.0431
ALDPDICPNGI	1.84	222443	120605	0.0319
VDINECLLEPR	1.83	908622	497267	0.0423
LQHYQWNQCVDENEC	1.81	29351	16222	0.0026
CENLRGTYKCI	1.56	14171	9107	0.0447
CEDIDECVEEPEICA	**∞**	**0**	**134280**	**0.0267**
CRHSCGDGFCSRPNMCTCPS	**-1060**	**93**	**98815**	**0.0027**
GFMTNGADIDECKVIHDVCR	-2.28	9472	21569	0.0190

SSR-Affected Peptides	Fold Change	Average Norm. Abundance		Anova (p value)
		SSR	Control	
NEDTRVCDDVNECETPGI	**21.1**	**19214**	**908**	**0.0298**
GGFTCKCPPGFTQHHT	**17.8**	**40018**	**2242**	**0.0103**
NEKCEDIDECVEEPEICAL	**5.18**	**96336**	**18610**	**0.0492**
ALDPDICPN	2.97	58817	19832	0.0243
STGQCNDRNECQEIPNICSHGQ	2.25	191532	85274	0.0171
TNGKPFFKDINEC	2.12	26531	12506	0.0065
CEDIDECSLPNICV	1.77	338058	191357	0.0130
CKCPPGFYTSPDGT	1.76	204517	115978	0.0216
CVDINECLLEPRK	1.71	3138759	1838253	0.0395
CGPGYQRRPDGEGCVDENECQTKPGICENG	1.48	2098177	1417177	0.0023
IIVGPDDSAVDMDECKEPDVC	1.43	897450	628911	0.0208
CRHSCGDGFCSRPNMCTCPS	**-∞**	**0**	**296388**	**0.0029**
GFQYEQFSGGCQDINECGS	**-∞**	**0**	**80459**	**0.0117**
RPDGEGCVDENECQTKPG	**-86.3**	**2053**	**177403**	**0.0402**
GFMTNGADIDECKVIHDVCR	-3.05	7075	21569	0.0227
GYRCECDMGFVPSADGKACEDIDECSLPNIC	-2.16	87767	189477	0.0199
GMGMGRGNPEPPVSGEMDDNSLSPEACYE	-1.83	64134	117116	0.0364
AGSDINECALDPDICPNGICENLRGTYKC	-1.66	1755799	2917105	0.0255
AGSDINECALDPDICPNGICENLRGTYKCI	-1.46	583834	853005	0.0213
GSDINECALDPDICPNGICENLRGTYK	-1.43	600269	859731	0.0096
AGSDINECALDPDICPNGICENLRGTYK	-1.40	5805329	8121980	0.0133

Figure 5.4: Data-dependent peptide quantification revealed significant changes in the relative abundance of specific fibrillin-1 peptide sequences post-UV exposure. Fourteen fibrillin-1 peptides in broadband UVB-irradiated microfibril samples and 21 in SSR-irradiated samples were significantly increased (red) or decreased (blue) in relative abundance compared to control samples. Their peptide sequences, fold changes relative to the control group (fold changes ≥ ±5 are bold and underlined), average normalised abundances and p values are shown (Progenesis multivariate paired ANOVA). Seven of these fibrillin-1 peptides are shared between SSR- and broadband UVB-irradiated groups (top table). Broadband UVB-irradiated samples yielded more fibrillin-1 peptides with fold changes ≥ ±5 (bold + underlined) than SSR-irradiated samples (8 vs. 6).

5.3.4 UVR exposure of collagen VI microfibrils has no effect on total collagen VI alpha-3 peptide yield but did liberate SSR- and broadband UVB-specific peptides

In contrast to fibrillin-1, total numbers of LC-MS/MS-derived COL6A3 PSMs **(Fig. 5.5)** changed negligibly for SSR-irradiated **(Fig. 5.5 Bi)** and broadband UVB-irradiated **(Fig. 5.5 Bii)** microfibril samples compared to unirradiated samples (average 1% decrease for both SSR and broadband UVB). Therefore, *in vitro* UVR exposure has minimal impact on collagen VI ultrastructure **(Fig. 5.2)** and protease susceptibility **(Fig. 5.5)** whilst chronic *in vivo* exposure to UVR does not affect collagen VI architecture in human dermis (Watson *et al.* 2001). We have suggested previously that this resistance may be mediated by the relatively low abundance of UV chromophore amino acids in collagen VI alpha chains compared to fibrillin-1 (Hibbert *et al.* 2015). However, as with fibrillin-1, data-dependent quantification revealed a number of COL6A3 peptides which were significantly different in relative abundance in both broadband UVB- and SSR-irradiated microfibril samples compared to non-irradiated **(Fig. 5.6)**. Once again, although SSR-irradiated samples yielded a higher number of significantly different COL6A3 peptides than those irradiated with broadband UVB (17 vs 13), UVB-irradiated samples had more peptides with fold changes ≥ ±5 (4 vs 1). Again mirroring the results for fibrillin-1, a larger proportion of these COL6A3 peptides were significantly increased in broadband UVB-irradiated samples (54%: 7 out of 13) than in SSR-irradiated samples (29%: 5 out of 17), likely due to the UVB waveband being more energetic than SSR. As with fibrillin-1, a number of these identified COL6A3 peptide sequences were shared between both UVB- and SSR-irradiated microfibril samples.

A

Collagen VI Alpha-3 Exclusive Unique Peptides Identified					
	Control	SSR		Broadband UVB	
	PSMs	PSMs	Fold Change vs. Control	PSMs	Fold Change vs. Control
M79	107	94	0.88	89	0.83
M75	111	120	1.08	116	1.05
F75	23	23	1.00	25	1.09

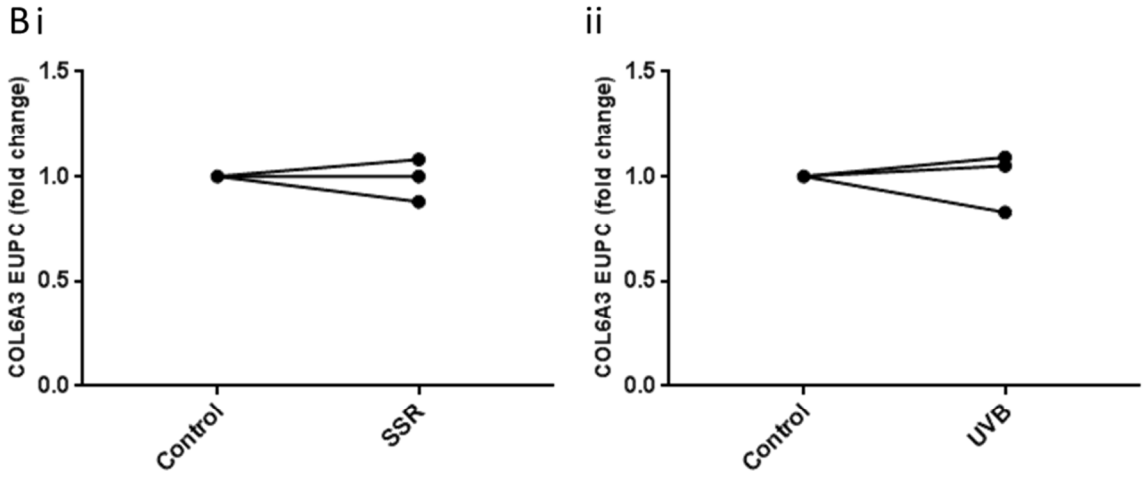

Figure 5.5: UV exposure did not cause changes to the overall proteolytic susceptibility of COL6A3. PSMs for SSR- and broadband UVB-irradiated COL6A3 per individual and their fold changes in comparison to control COL6A3 are shown (Peptide Prophet FDR ≤ 5%) ***(A)****. In contrast to fibrillin-1, both SSR-* ***(Bi)*** *and broadband UVB irradiation* ***(Bii)*** *failed to cause any consistent change in the number of COL6A3 peptides identified (average change = 0.99 for both SSR and UVB).*

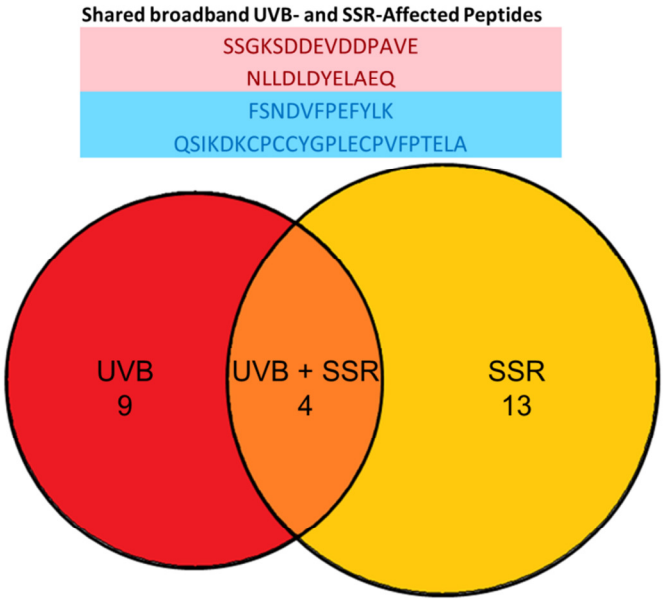

Broadband UVB-Affected Peptides	Fold Change	Average Norm. Abundance		Anova (p value)
		UVB	Control	
HLEFGRGF	**∞**	**24549**	**0**	**0.0129**
DSKRKSVLLDKI	**∞**	**5653**	**0**	**0.0352**
SSGKSDDEVDDPAVE	**11.9**	**76844**	**6488**	**0.0182**
GPPGLIGEQGI	2.39	116046	48583	0.0373
ELPNIEERI	1.98	25963	13114	0.0125
NLLDLDYELAEQ	1.76	55729	31711	0.0077
IMNSFGPSAATPAPPGVDTPPP	1.30	147351	112957	0.0085
NIFKRPLGS	**-25.4**	**3094**	**78492**	**0.0229**
CNLDVILGFDGSRDQNV	-2.81	52201	146774	0.0191
QSIKDKCPCCYGPLECPVFPTELA	-2.06	56600	116581	0.0473
FSNDVFPEFYLK	-1.94	7429	14433	0.0242
LHDAMHETLCPGVTDAA	-1.52	782919	1193796	0.0482
TFRELPSLEQKLLTPI	-1.16	1062348	1228918	0.0009

SSR-Affected Peptides	Fold Change	Average Norm. Abundance		Anova (p value)
		SSR	Control	
QFSDTPVTEF	2.10	31011	14751	0.0076
GFGSWRPS	1.89	130241	68764	0.0467
FLIDSSEGVRPDGFA	1.60	173707	108297	0.0152
QFSNDVFPEF	1.38	359011	259305	0.0393
FDFDEYQPEM	1.26	3071218	2442213	0.0009
RNIDSEEVGKIA	**-281**	**282**	**79206**	**0.0393**
KDKCPCCYGPLECPVFPTELA	-2.62	100330	262774	0.0080
QSIKDKCPCCYGPLECPVFPTELA	-2.33	50058	116581	0.0306
CLDICNIDPSCGFGSWRPS	-2.28	262432	599284	0.0389
FVSEIVDTVYEDGDSIQV	-2.25	48105	108419	0.0144
FDFDEYQPEMLEKF	-1.67	137429	228944	0.0242
FDFDEYQPEMLEK	-1.53	1204900	1838735	0.0131
SGKSDDEVDDPAVELKQFGVAPF	-1.33	880973	1174088	0.0348
SSGKSDDEVDDPAVELKQFGVAPF	-1.31	2850021	3722273	0.0064
SNDVFPEFYLK	-1.29	221486	285740	0.0110
DLDYELAEQLDNIAEKA	-1.21	517895	624977	0.0414
SSGKSDDEVDDPAVELKQFGVAPFT	-1.18	124364	146578	0.0417

Figure 5.6: Data-dependent peptide quantification revealed significant changes in the relative abundance of specific COL6A3 peptide sequences post-UV exposure. Thirteen COL6A3 peptides in broadband UVB-irradiated microfibril samples and 17 in SSR-irradiated samples were significantly increased (red) or decreased (blue) in relative abundance compared to control samples. Their peptide sequences, fold changes relative to the control group (fold changes ≥ ±5 are bold and underlined), average normalised abundances and p values are shown (Progenesis multivariate paired ANOVA). Four of these COL6A3 peptides are shared between SSR- and broadband UVB-irradiated groups. As with fibrillin-1, broadband UVB-irradiated samples yielded more COL6A3 peptides with fold changes of over 5 (bold and underlined) than SSR-irradiated samples (4 vs. 1).

Although a number of significantly different COL6A3 peptides were affected by both SSR and broadband UVB **(Fig. 5.6)**, only five (four for UVB and only one for SSR) had fold changes ≥ ±5 compared to the 14 identified from fibrillin-1 **(Fig. 5.4)** (eight for UVB and six for SSR). Fibrillin-1

also yielded a higher number of significantly different peptides which were shared between broadband UVB- and SSR-irradiated samples (seven) as compared to COL6A3 (four). These observations indicate that, with fibrillin-1, more UVR-specific peptides are detected than with COL6A3, once again indicating a divergence of UV susceptibility as noted previously, ultrastructurally (Hibbert *et al.* 2015) and histologically (Watson *et al.* 2001), however this time on a molecular scale.

The identification of UVR-specific peptides from both fibrillin-1 and COL6A3 demonstrate the capability and potential of MS for the detection of molecular photodamage within key dermal ECM assemblies. Additionally, the total numbers of detected fibrillin-1 and COL6A3 peptides correlate with the scale of ultrastructural damage observed in the microfibrils by AFM as well as their chromophore amino acid content (Hibbert *et al.* 2015). Finally, data-dependent quantification of MS-detected peptides provides a more sensitive method for detecting UVR damage than either ultrastructure **(Fig. 5.2)** (Hibbert *et al.* 2015) or histology (Watson *et al.* 2001), since UVR-specific COL6A3 peptides were identified in both broadband UVB- and SSR-irradiated microfibril isolates. This enables the identification of UV damage within collagen VI microfibrils on a molecular scale, previously undetectable using conventional methods, which could potentially impact on their function in tissue.

The use of peptide degradation products in the detection of disease is not a novel concept: oncopeptidomics is a growing field which attempts to use the LC-MS/MS detection of peptide biomarkers as a diagnostic tool for tumour presence (Schwab 2011; Tammen 2011) (see review: (Diamandis 2006)). Additionally, the LC-MS/MS detection of peptide degradation products has been used to identify biomarkers of Fanconi syndrome (Cutillas *et al.* 2003), inflammation (Weathington *et al.* 2006) and even allergies (Careri *et al.* 2007). This is not the first time UVR exposure has been shown to increase the susceptibility of an ECM assembly to protease-mediated proteolysis; Menter *et al.* (2003) previously demonstrated that the UV irradiation of murine collagen I significantly increased its susceptibility to proteolysis by bacterial collagenase.

5.3.5 Fibrillin-1 structure exhibits regional foci of UV susceptibility in contrast to collagen VI alpha-3 which was less susceptible

Menter *et al.* (2003) went on to suggest that the regional susceptibility of collagen I to UVR may be dependent on its superstructure and the supramolecular organisation of its protein components. In an attempt to identify this in our microfibril assemblies, fibrillin-1 PSMs and significantly different,

data-dependently quantified peptides from SSR-irradiated and broadband UVB-irradiated samples were mapped to the protein domain structure and compared **(Fig. 5.7)**. Interestingly, mapped differences in fibrillin-1 PSMs per domain, compared to control, were remarkably consistent between fibrillin microfibrils separately irradiated with either SSR or broadband UVB, with many of the same patterns exhibited. The largest regional differences, consistent within both SSR- and broadband UVB-irradiated fibrillin-1, can be seen between the N-terminal domain and epidermal growth factor-like (EGF) domain 1 and within EGF22, both with sharp increases in PSM numbers in both regions, and between EGFs 33 and 34 with a sharp decrease in PSM number. Encouragingly, many of the peptides with significant differences in abundance coincide with regions exhibiting the largest differences in PSMs compared to control. As previously shown, the fluctuation in peptides identified within these different regions of fibrillin-1 are indicative of the propensity of elastase to yield peptides specifically at these molecular locations (Eckersley *et al.* 2018). The changes seen here are most likely, directly related to the disruption of protein folding within the tertiary structure via the dissolution of bonds by UV, evidenced further by the direct changes seen in fibrillin microfibril ultrastructure. These fluctuations in fibrillin-1 structural susceptibility to elastase indicate that, although UV damage appears spread throughout the majority of the fibrillin-1 domain structure, regional foci of this damage can be detected consistently for both SSR and broadband UVB sources of UV. Additionally, a large region of increased PSMs close to the C-terminus, between EGFs 42-45, can be seen exclusively in broadband UVB-irradiated fibrillin-1 compared to control, and not in SSR-irradiated. This could be related to the greater damage caused by broadband UVB to the fibrillin microfibril ultrastructure compared to SSR.

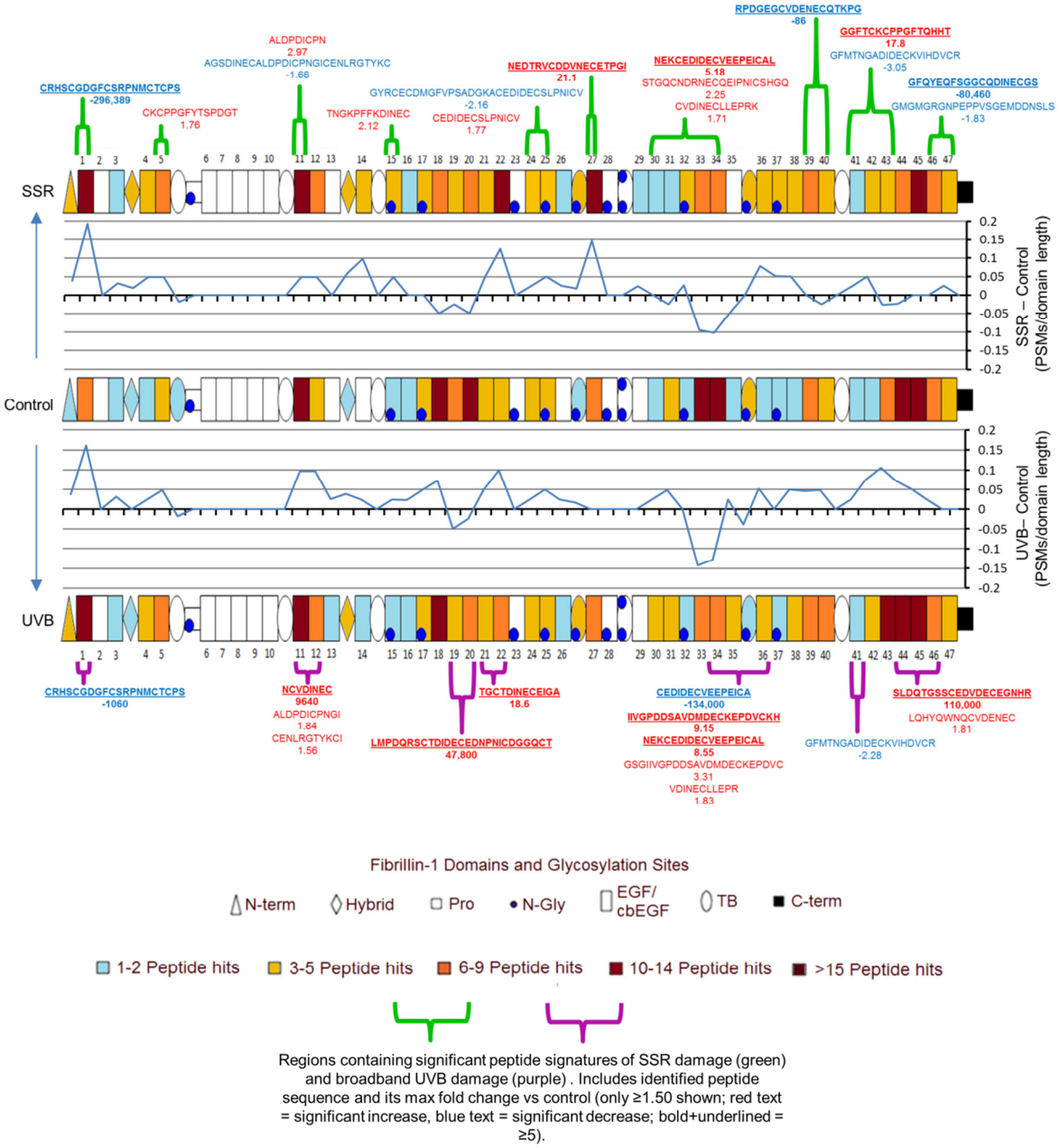

Figure 5.7: SSR and broadband UVB exposure leads to changes in the proteolytic susceptibility of specific protein regions within fibrillin-1. LC-MS/MS identified fibrillin-1 peptide sequences (PSMs: peptide prophet FDR ≤ 5%) were counted for each respective protein domain, normalised based on total spectrum count and subsequently heat mapped. The PSM number corresponding to each broadband UVB- and SSR-irradiated fibrillin-1 domain were then subtracted from the counts of control and divided by the domain's primary sequence length to show regional fluctuations in elastase susceptibility. Significantly different peptide sequences shown in ***Fig. 5.5*** *and their fold changes are also mapped. UV-induced damage to fibrillin-1 is spread throughout the structure, although the N-terminal region (N-term domain + EGF1) and EGFs 22, 33-34 and 43-45 appear the most affected. The pattern of changes seen throughout the fibrillin-1 structure is consistent in many regions, regardless of the UV irradiation method used (SSR or broadband UVB).*

As with fibrillin-1, COL6A3 PSMs and significantly different peptides from SSR-irradiated and broadband UVB-irradiated microfibril samples were also mapped to the protein domain structure and compared **(Fig. 5.8)**. Consistent with the previous UV-resistance seen in collagen VI microfibril ultrastructure compared to fibrillin (Hibbert *et al.* 2015), COL6A3 had much lower regional fluctuations in PSM number compared to fibrillin-1 **(Fig. 5.7)** on the same scale. The largest regional changes in COL6A3 PSM number were at von Willebrand factor type A (vWA) domains N2 and N4.

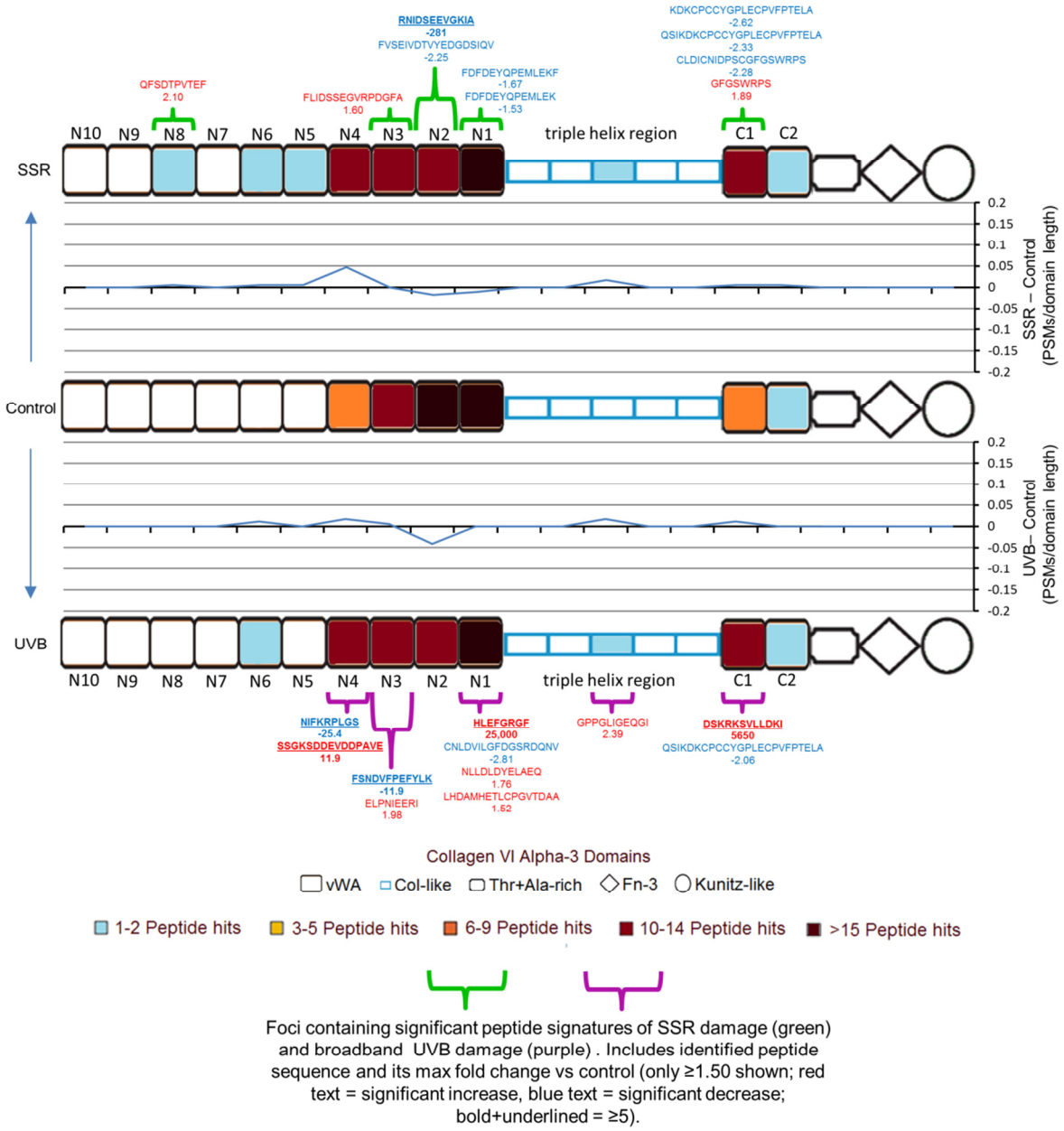

Figure 5.8: SSR and broadband UVB exposure leads to only minimal changes in the proteolytic susceptibility of specific protein regions within COL6A3. LC-MS/MS identified COL6A3 peptide sequences (PSMs: peptide prophet FDR ≤ 5%) were counted for each respective protein domain, normalised based on total spectrum count and subsequently heat mapped. The PSM number corresponding to each broadband UVB- and SSR-irradiated COL6A3 domain were then subtracted from the counts of control and divided by the domain's primary sequence length to show regional fluctuations in elastase susceptibility. Significantly different peptide sequences shown in ***Fig. 5.7*** *and their fold changes are also mapped. Regional UV damage to COL6A3 was limited, with the highest changes in PSMs/domain length mapping to the N4 (vWA) domain for SSR-irradiated and N2 domain for broadband UVB-irradiated.*

The structural alterations identified in this study may have downstream effects on fibrillin-1 function in photoexposed tissue. One of the main foci of UV damage in the fibrillin-1 structure for both SSR- and broadband UVB-irradiated samples was at the N-terminal region **(Fig. 5.7)**. Fibrillin microfibril

assembly involves the homotypic interaction between the N-terminal region and C-terminal regions of fibrillin-1 (Marson *et al.* 2005). It is possible that these polymeric associations between fibrillin-1 within the microfibril become disrupted post-irradiation with UV which may have caused the characteristic ultrastructural changes within the bead and inter-bead regions. Additionally, key elastic fibre proteins elastin and microfibril-associated glycoprotein 1 (MAGP1), which promotes elastin deposition onto microfibrils, both bind strongly to the N-terminal region of fibrillin-1 (Jensen *et al.* 2001; Rock *et al.* 2004). This compromise in fibrillin microfibril structure, and perhaps its ability to interact with key elastic fibre proteins, may affect the integrity and function of elastic fibres within the dermis.

As network-forming ECM assemblies, fibrillin-1 within native microfibrils associates with a variety of proteins in the dermis. Additionally, a large number of these known fibrillin microfibril-associated proteins also interact exclusively with the N-terminal region of fibrillin-1. Fibrillin microfibrils have the ability to store the important homeostatic cytokines TGFβ (Kaartinen and Warburton 2003; Neptune *et al.* 2003), through their interactions with LTBPs (see review: Rifkin 2005) and BMPs (Gregory *et al.* 2005; Sengle *et al.* 2008) via direct association to the N-terminal regions of fibrillin-1 (Ono *et al.* 2009; Sengle *et al.* 2008). Additionally, fibulins-2, -4 and -5, which play a major role in elastogenesis (Kadoya *et al.* 2005; Kobayashi *et al.* 2007; McLaughlin *et al.* 2006), versican, which plays a major role in ECM assembly and cellular interactions (see review: (Wight 2002)) and ADAMTSs-10 and -6 which are instrumental to microfibril assembly and matrix stability (see review: Hubmacher and Apte 2015) all interact specifically with the N-terminal region of fibrillin-1 (Cain *et al.* 2016; Choudhury *et al.* 2009; Isogai *et al.* 2002; Kutz *et al.* 2011; Ono *et al.* 2009). It is possible that the UV-mediated disruption of the N-terminal region may have a profound impact, not only in the degeneration of elastic fibre integrity, but importantly on tissue homeostasis and function on a wider scale.

5.3.6 Differences in fibrillin-1 and collagen VI alpha-3 chromophore content may account for an overall divergence in UV susceptibility

Of the 20 amino acids, three have the ability to absorb UVB and UVA wavebands: tryptophan, tyrosine and double-bonded cysteine (cystine) (Bensasson *et al.* 1993). This has led to the hypothesis that these chromophores are the ones most responsible for the direct photodegradation of proteins in UV-exposed tissues. In previous studies, we showed that the UV susceptibility of a dermal ECM assembly correlates with its total chromophore content (% of these three amino acids)

within four different assemblies: fibrillin microfibrils (fibrillin-1: 16.4%), fibronectin (fibronectin-1: 8.54%), type I collagen (α1 and α2 chains: 0.32%) and collagen VI microfibrils (α1,α2 and α3 chains: 3.66%) (Hibbert *et al.* 2015; Sherratt *et al.* 2010).

To determine whether visualising these differences in chromophore content at the domain level, between fibrillin-1 and COL6A3, could give us new insight into their UV susceptibilities and whether the regional fluctuations of UV damage seen within the fibrillin-1 domain structure also correlated with its chromophore content, we heat mapped the percentage chromophore to their corresponding protein domains **(Fig. 5.9)**. The majority of fibrillin-1 domains (all except for one hybrid domain, the proline-rich domain and three TGFβ-binding (TB) domains) had a chromophore content of above 7.5% with an average of ~10%. In contrast, all COL6A3 domains except for the Kunitz-like domain (not present in microfibrils as it is cleaved prior to assembly, alongside the fibronectin-like domain (Aigner *et al.* 2002)) had a chromophore content below 7.5% with an average of ~3%. This likely indicates that the UV-susceptibility of fibrillin-1 is much greater than that of COL6A3, and may explain why the overall damage to fibrillin-1 seen by LC-MS/MS **(Fig. 5.3)** was higher than that of COL6A3 **(Fig. 5.5)**. The effect of this susceptibility would likely have caused the higher ultrastructural damage see to the fibrillin microfibrils **(Fig. 5.1)** compared to collagen VI microfibrils **(Fig. 5.2)**.

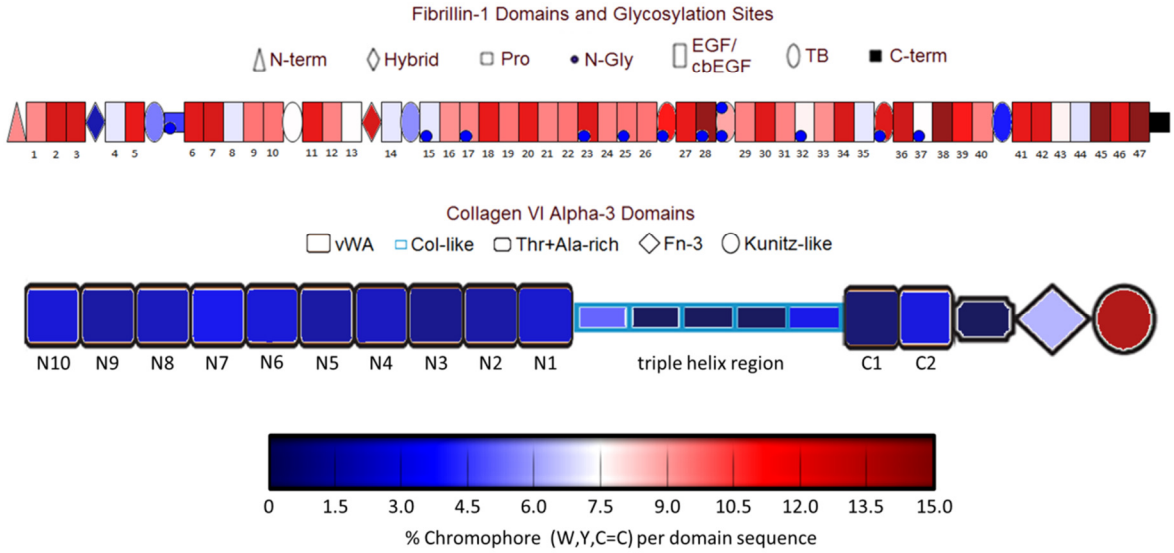

Figure 5.9: The chomophoric amino acid content of fibrillin-1 and COL6A3. To gauge the overall structural susceptibility of the fibrillin-1 and COL6A3 primary sequences to UV, the number of chromophoric amino acids (tryptophans, tyrosines and double-bonded cysteines) were counted for each domain and represented as a heat mapped percentage of chromophore content per domain. The majority of fibrillin-1 domains exhibit a chromophore content of between 9% and 15% whereas all COL6A3 domains, except the Kunitz-like, exhibit a content of below 6%.

Although this may explain the overall susceptibility of fibrillin-1 to UV, compared to COL6A3, it does not explain the regional foci of UV damage seen within its structure **(Fig. 5.7)**. The largest regional damage for both SSR-irradiated and broadband UVB-irradiated fibrillin-1 was observed at the N-terminal region (N-terminal domain + EGF1), at EGF22 and at EGFs 33-34. Although the chromophore content of all of these domains is above 9%, the domains with the largest differences in PSM numbers did not directly correlate with those with the highest chromophore content. However, these regional concentrations of UV-associated peptides suggest that damage is not stochastic, despite the distribution of chromophores. The reason behind this may lie with the way regional damage has been measured using LC-MS/MS. The changes to fibrillin microfibrils caused by UV (i.e. alterations within the bead) may, in turn, change the accessibility of these different proteinaceous regions to the peptide generating elastase. This means that any UV-induced regional changes in peptide numbers would likely correlate to changes in the higher-order tertiary and quaternary structure of fibrillin-1, within the microfibril, rather than that of its primary structure. This would mean that, although the concentrations of chromophores in different regions of fibrillin-1 may be important for the primary sequence susceptibility, the UV-induced damage measured here by LC-MS/MS, likely relates instead to the regions of fibrillin-1 exposed to proteolytic digestion.

This is still important, as it indicates the areas of the microfibril which are most affected by UV on a molecular scale.

5.3.7 Conclusion

In this study, we successfully identified broadband UVB- and SSR-susceptible regions within the fibrillin-1 monomer of human fibrillin microfibrils. We effectively demonstrated that, although the quantity of damage to the fibrillin-1 structure and to the fibrillin microfibril ultrastructure correlates with the type of UV exposure (broadband UVB or SSR), many of these molecular foci are conserved between UV sources. Additionally, by comparing these to the COL6A3 monomer within co-purifying collagen VI microfibrils, we confirmed their UV-resistance on a monomeric level. However, through data-dependent quantification, we detected UVR-specific peptides from COL6A3 arising post-irradiation, indicating that this monomer is susceptible at least on a molecular scale. Furthermore, we showed that differences in chromophore content between fibrillin-1 and COL6A3 may account for the overall divergence in UV susceptibility. However, the domain mapped chromophore content of fibrillin-1 did not correlate with its regional foci of UV damage, which indicated that the changes observed are likely due to tertiary and quaternary structural alterations rather than to the primary structure.

The discoveries made in this study forward the limited fundamental understanding we have of the photodamaging effects of UV to dermal proteins. A great potential emerging from of this study is the identification of specific peptide “fingerprints” of fibrillin-1 and COL6A3 damage shared between microfibrils separately irradiated with broadband UVB and SSR. Should these be detected within chronically photoaged microfibrils, they could serve as an early marker of the photoageing process. Additionally, these were seen in two biochemically unrelated proteins suggesting that such signatures may be ubiquitous in other ECM components. These experiments also indicate the potential of LC-MS/MS as a method of identifying historical molecular damage due to direct UVR and possibly ROS and protease.

5.4 Materials and Methods

5.4.1 Study design

Fibrillin and collagen VI microfibrils were extracted and purified from cultured primary human dermal fibroblasts (n=3; M79 (male aged 79 years), M75 and F75). Matched samples were split into three; one group was irradiated with a 30 J/cm^2 dose of SSR (95% UVA, 5% UVB) (Hibbert *et*

al. 2015), another with a 100 mJ/cm^2 of broadband UVB (Sherratt *et al.* 2010) and the third was kept as control (un-irradiated). Quantitative ultrastructural measurement of fibrillin microfibril bead morphology and periodicity (inter-bead distance) and of collagen VI microfibril periodicity was performed and compared using AFM. Fibrillin-1 and COL6A3 regional susceptibility to elastase digestion in response to UV irradiation was assessed by mapping the number of LC-MS/MS-detected PSMs and significantly different peptides (data-dependently quantified) to their respective protein domains. Regional differences were compared between UV-irradiated (broadband UVB or SSR) and control, un-irradiated.

5.4.2 Reagents and cell acquisition

Chemicals were sourced from Sigma-Aldrich Co. Ltd (Poole, UK) unless otherwise stated. This study was performed in accordance with the European Medicines Agency Note for Guidance on Good Clinical Practice and the Declaration of Helsinki 1964 (revised Seoul 2008). The use of human skin in this study was approved by North West Research Ethics Committee (ref# 14415). Donors gave written and informed consent prior to the collection of punch biopsies. Primary dermal fibroblasts were cultivated from skin biopsies taken from human donor photoprotected buttock. Incubations and cell cultures were conducted at 37^{o}C (5% CO_2). Biopsies were incubated overnight in HBSS (Fisher Scientific, Loughborough, UK) containing 10% (v/v) PluriSTEM™ Dispase II solution. The dermis was separated from the epidermis, minced and further incubated in fibroblast DMEM media (Fisher Scientific, Loughborough, UK) containing 10% foetal calf serum (FCS), 1% amphotericin, 1% penicillin-streptomycin (Pen-Strep; Gibco, Paisley, UK) and 1% L-glutamine (all v/v). Fibroblast media was changed weekly until cells could be observed on sample plates.

5.4.3 Microfibril extraction and purification

HDFs were cultured until confluent and maintained for a further five weeks in DMEM, high glucose, GlutaMAX™ Supplement (Fisher Scientific, Loughborough, UK) containing 10% (v/v) FCS and 50 µg/ml of Pen-Strep. Cells were then washed with phosphate buffered saline (PBS) within their culture flasks. 2 ml of salt buffer (400 mM NaCl, 50 mM Tris-HCl and 10 mM $CaCl_2$ at pH 7.4) containing 1 mg of bacterial collagenase IA and protease inhibitors: 0.01 mM phenylmethylsulfonyl fluoride (PMSF) and 0.03 mM N-ethylmaleimide (NEM) was then added directly to the culture flasks. These were digested on an orbital shaker for two hours at room temperature.

Microfibrils were purified using size-exclusion chromatography via the ÄKTA Prime Plus Liquid Chromatography System (GE Healthcare; Little Chalfont, UK) as previously described (Eckersley

et al. 2018; Hibbert *et al.* 2015; Sherratt *et al.* 2010). After digestion with bacterial collagenase IA, HDF-derived mixtures were centrifuged at 5000 g for five minutes. The supernatants were injected and ran at 0.5 ml/min within a column buffer (50 mM Tris-HCl and 400 mM NaCl at pH 7.4) through a GE HiScale 16/40 column containing Sepharose® Cl2B beads (Sigma-Aldrich Co. Ltd). Fractions containing both fibrillin and collagen VI microfibrils were collected based on spectrophotometric absorbance at 280 nm and were enriched in the void volume peak.

5.4.4 Microfibril suspension UV irradiation

Purified microfibril suspensions were split into three matched groups: control, broadband UVB-irradiated and SSR-irradiated. All suspensions (2 ml volumes) were irradiated within uncapped 35 mm x 10 mm polystyrene cell culture dishes (Corning, Flintshire, UK).

As previously described (Hibbert *et al.* 2015) SSR-designated suspensions were irradiated using a Solar Simulator (Applied Photophysics, Cambridge, UK) which is comprised of a xenon arc lamp light source fitted with a WG320 SSR filter (Schott, Stafford, UK). Double grating spectroradiometer (Bentham Instruments Ltd., Reading, UK), calibrated to National Physical Laboratory (Teddington, UK) standards, was used to measure SSR spectral outputs. Irradiance was measured using a UVX radiometer (UVR Products, Upland, CA, USA) fitted with a UVX36 full spectrum detector which was calibrated against the aforementioned spectroradiometer spectral output measurements. Suspensions were exposed to a dose of 30 J/cm^2 (25 minutes and 30 seconds exposure time, irradiance = 19.6 mW/cm^2) at a vertical distance of 20 cm from the source, at room temperature.

As previously described, (Sherratt *et al.* 2010) broadband UVB-designated microfibril suspensions were irradiated with a broadband UVB spectrum using two 20 W Phillips TL-12 tubes (Eindhoven, The Netherlands) with an emission wavelength range of 270–400 nm (peak output of 313 nm). UVB waveband irradiance was measured using a UVX radiometer fitted with a UVX31 UVB detector calibrated using a double grating spectroradiometer to National Physical Laboratory standards. Suspensions were exposed to a dose of 100 mJ/cm^2 (4 minutes 54 seconds exposure time, irradiance = 0.34 mW/cm^2) at the centre of, and at a vertical distance of 16 cm from the source, at room temperature.

Aliquots of each sample were kept for ultrastructural analysis using AFM, and remaining suspensions were desalted in 0.22 µm filtered ultrapure water using Slide-A-Lyzer™ MINI Dialysis Devices (Thermo Fisher Scientific; Paisley, UK) for 4 hours at 4°C. Desalted samples were frozen

at -80°C and subsequently freeze-dried at -60°C for 48 hours. These were stored at -80°C until their use in MS experiments.

5.4.5 Microfibril atomic force microscopy

Glass coverslips were immersed in absolute ethanol overnight and then attached to magnetic AFM stubs using clear nail varnish. Microfibril suspensions were pipetted directly onto the coverslips and left for one minute for the assemblies to adsorb to the glass surface. The majority of fluid was removed and the coverslip left to dry overnight. Coverslips were washed three times with ultrapure water to remove crystalized salt and left to dry prior to their use in AFM. As described previously (Eckersley *et al.* 2018; Sherratt *et al.* 2007), fibrillin and collagen VI microfibrils were scanned using peak force in Scan-Asyst® mode on a Multimode 8 atomic force microscope (Bruker; Billerica, MA, USA). Using new Scan-Asyst® Air tips (Bruker), fibrillin and collagen VI microfibrils were captured in a 2 x 2 µm scan area at a resolution of 512 pixels/line. This produced a resolution of 3.9 nm/pixel, which was high enough for ultrastructural analysis as previously described (Eckersley *et al.* 2018; Hibbert *et al.* 2015; Sherratt *et al.* 2010).

WSxM v5.0 AFM Image Processing package (Horcas *et al.* 2007) was used to digitally flatten each scan which were then exported in text image format. Height was subsequently corrected by subtracting negative background (Ratcliff and Erie 2001; Eckersley *et al.* 2018). Images (41 pixels wide) of single straightened fibrillin microfibrils were generated using the Straighten Curved Objects plugin (Kocsis *et al.* 1991) in ImageJ (NIH; Bethesda, MA, USA). The image processing software: LFA, which was developed using Microsoft Visual Basic 6.0 by our group as described previously (Eckersley *et al.* 2018; Sherratt *et al.* 2003), was used to specify the height maxima of each fibrillin microfibril bead. This generated 15 x 41 pixel snapshots of individual beads with the central pixel of the images corresponding to the centre of a single bead. Fibrillin microfibril bead height and morphology was measured and analysed using these snapshots. Fibrillin and collagen VI microfibril periodicity (inter-bead distance) was measured using the software package, Periodicity and Angles, developed by our group using Microsoft Visual Basic 6.0, as previously described (Eckersley *et al.* 2018; Hibbert *et al.* 2015; Sherratt *et al.* 2005). A single measurement consisted of the distance from the centre of one bead to the centre of another.

5.4.6 Microfibril fibrillin-1 and COL6A3 peptide generation using elastase digestion prior to mass spectrometry

As described previously (Eckersley *et al.* 2018), the freeze dried microfibril purifications were re-suspended and denatured in 8 M urea. Suspensions were then reduced by adding 10 mM dithiothreitol (DTT) for 30 minutes at room temperature and further alkylated using 50 mM iodoacetamide (IAM) in darkness, also for 30 minutes at room temperature. The suspension was then diluted to a concentration of 2 M urea using Tris-HCl buffer (100 mM Tris-HCl at pH 8.5), and porcine elastase (Catalogue # E1250) then added (2:1, enzyme:substrate ratio). Samples were digested at 37°C for four hours after which enzyme activity was then quenched using 5% (v/v) formic acid in ultrapure water. Peptide samples were then desalted using OLIGO R3 Reversed-Phase Resin beads (Thermo Fisher Scientific) and vacuum dried.

5.4.7 Mass spectrometry

LC-MS/MS was performed by the Biological Mass Spectrometry Core Facility in the Faculty of Biology, Medicine and Health at the University of Manchester (Manchester, UK). As previously described in their protocols (Buckley 2015; Eckersley *et al.* 2018; Lennon *et al.* 2014): vacuum dried peptide samples were analysed via LC-MS/MS using an UltiMate® 3000 Rapid Separation LC (Dionex Corp; Sunnyvale, CA, USA) and an Orbitrap Elite mass spectrometer (Thermo Fisher Scientific). Peptide mixtures were separated using a 250 mm x 75 µm i.d. 1.7 mM BEH C18, analytical column (Waters, Hertfordshire, UK) on a gradient of 92% A (0.1% [v/v] formic acid in water) and 8% B (0.1% [v/v] formic acid in acetonitrile) to 33% B. These were run for 60 minutes with a flow rate of 300 nL/min. Peptides were automatically picked for fragmentation via data-dependent analysis.

5.4.8 Mass spectrometry data analysis

For peptide spectrum matching, mass spectra were extracted using extract_msn (Thermo Fisher Scientific). Mascot v2.5.1 (Matrix Science; London, UK) was used to correlate the spectra against the Swissprot_2016_04 database (152,544 protein entries) (Consortium 2016) with the following search parameters: species - Homo sapiens; enzyme – non-specific (elastase); max missed cleavages – 1; fixed modifications - carbamidomethyl, mass – 57.02 Da, AA – C; variable modification – oxidation, mass – 15.99 Da, AA – M; peptide tolerance - 10 ppm (monoisotopic); fragment tolerance - 0.6 Da (monoisotopic). The PSMs reported were generated using Scaffold (Proteome Software; Portland, OR, USA). Only exclusive, unique peptide counts are reported for

every dataset. FDR was calculated by Scaffold using protein and peptide probabilities assigned using the Trans-Proteomic Pipeline and the Peptide Prophet™ (Keller *et al.* 2002) algorithm (Sourceforge; Seattle. WA, USA). Peptide Prophet FDR was thresholded to ≤ 5% for every dataset.

Data-dependent peptide quantification was performed using Progenesis QI (Nonlinear Dynamics, Waters; Newcastle, UK). Raw mass spectra files were imported and aligned using default settings. Data was then searched using Mascot v2.5.1 with same search parameters and on the same database as described earlier. This was then re-imported back into Progenesis QI where identified peptides and proteins were automatically matched. Raw abundance for each peptide was calculated by Progenesis QI as the sum of the each matched peptide ion abundance (individual peptide ion abundance defined as the sum of the intensities within the isotope boundaries) and normalised to a single run. Normalised peptide abundances were compared between matched samples (control vs. broadband UVB and control vs SSR) and a fold change for each peptide calculated automatically (fold change defined as the higher average normalised abundance of one group divided by the average normalised abundance of the second group). Normalised peptide abundances compared between matched samples were statistically analysed within Progenesis QI using a paired ANOVA.

Peptide quantification data was exported from Progenesis QI to Excel (Microsoft Office, Microsoft, Manchester, UK). Only fibrillin-1 peptides which matched to Uniprot (Consortium 2016) accession number FBN1_HUMAN and COL6A3 peptides which matched to CO6A3_HUMAN, and which filtered to $p \leq 0.05$, are reported.

5.5 Acknowledgments

This study was funded by a programme grant from Walgreens Boots Alliance, Nottingham, UK. Professor Christopher Griffiths and Professor Rachel Watson are supported in part by the NIHR Manchester BRC. We would like to thank Dr Nigel Hodgson of the BioAFM facility at the University of Manchester for his help and guidance regarding the AFM performed in this study. The content in this study is solely the responsibility of the authors and does not necessarily represent the official views of the National Institutes of Health.

5.6 Conflict of Interest

The authors declare that they have no conflicts of interest with the contents of this article. Walgreens Boots Alliance has approved this manuscript's submission but exerted no editorial control over the content.

5.7 Author Contributions

AE conceived, designed, performed all experiments, analysed all the data, prepared the figures and wrote the paper. MJS supervised, coordinated the study and contributed to the preparation of the figures and writing of the paper. MO contributed to the chromophoric amino acid content mapping of COL6A3 and fibrillin-1 **(Fig. 5.9)**. SMP contributed to the isolation of primary human dermal fibroblasts from skin and ARF contributed to their cell culture. REBW and CEMG contributed to the study design. DK, EJK and ROC provided technical assistance and support for all LC-MS/MS performed. All authors contributed to the editing of the paper.

Chapter 6: Characterising the molecular photosusceptibility of human skin microfibrils

The writing of this manuscript is intended as a Brief Communication to the Journal of Molecular Biology. The journal requirements indicate that the text should be continuous throughout, with methods described within the figure legends. However, in keeping with the rest of thesis and for the benefit of the reader, the contents have been reformatted to a traditional manuscript format. I conceived, designed and performed all experiments, analysed all the data, prepared the figures and wrote the paper. Dr Abigail K Langton and Mrs. Poonam Halai performed all the tissue cryosectioning for this study. Dr David Knight, Dr Ronan O'Cualain and Ms. Emma-Jayne Keevill of the Biological Mass Spectrometry Core Facility at the University of Manchester provided technical assistance for all LC-MS/MS performed.

Characterising the molecular photosusceptibility of human skin microfibrils

Alexander Eckersley[1], Matiss Ozols[1], Abigail K Langton[2], Poonam Halai[2], Ronan O'Cualain[3], Emma-Jayne Keevill[3], David Knight[3], Christopher EM Griffiths[2,4], Rachel EB Watson[2,4], Michael J Sherratt[1]*

[1]Division of Cell Matrix Biology & Regenerative Medicine, [2]Division of Musculoskeletal & Dermatological Sciences, [3]School of Biological Sciences, Faculty of Biology, Medicine and Health, The University of Manchester and [4]NIHR Manchester Biomedical Research Centre, Central Manchester University Hospitals NHS Foundation Trust, Manchester Academic Health Science Centre, Manchester, UK

*** Corresponding Author**: Dr Michael J Sherratt

Address: 1.529 Stopford Building, The University of Manchester, Oxford Rd, Manchester, M13 9PT, UK;

Telephone: +44 (0)161 275 1439;

Fax: +44 (0)161 275 5171;

Email: michael.sherratt@manchester.ac.uk

6.1 Abstract

Studies of fibrillin and collagen VI microfibril dermal architecture and ultrastructure have highlighted the differential susceptibilities of these important extracellular matrix assemblies to photoageing and UV-induced photodamage. Recently, using proteomic approaches, we successfully identified foci of this photodamage within fibrillin-1 and collagen VI alpha-3 (COL6A3) monomers of both these microfibrillar assemblies. However, this study was performed on microfibrils isolated from primary human dermal fibroblast (HDFs). Previously, we also showed that human skin-derived fibrillin microfibrils differed both in ultrastructure (bead morphology and periodicity) and in molecular composition (fibrillin-1 regional susceptibility and presence of associated proteins) compared to those which were HDF-derived. As a result, we aimed to confirm whether or not the molecular photosusceptibility identified in HDF-derived fibrillin and collagen VI microfibrils translated to those of human skin. We first confirmed that abdominal skin was sufficiently photoprotected for use in experiments and proceeded to extract and co-purify both fibrillin and collagen VI microfibrils which were subsequently irradiated with broadband UVB (100 mJ/cm^2).

Contrary to previous work on HDF-derived microfibrils, analysis of LC-MS/MS peptide spectrum matches (PSMs) failed to adequately detect structural changes in the proteolytic susceptibility of fibrillin-1, in response to broadband UVB irradiation. Encouragingly, data-dependent quantification revealed ten significantly different fibrillin-1 peptides, two of which matched peptide signatures previously identified in HDF-derived isolations. We propose that the high UV-susceptibility of one of the peptide signature, corresponding to EGF11, may be particularly important since mutations in this domain are known to cause classical Marfan syndrome.

Corroborating the previous work on HDF-derived microfibrils, PSM analysis of COL6A3 structure confirmed its overall resistance to broadband UVB irradiation. Despite this, data-dependent quantification revealed twenty-four significantly changed COL6A3 peptides, ten of which matched peptide signatures of UV previously identified in HDF-derived microfibrils. Since these peptides all correspond to the double bead of the collagen VI microfibril, we propose that this region may be the site most susceptible to ultrastructural damage by UV.

Keywords: Fibrillin, collagen VI, microfibril, proteomics, structure, ultraviolet, photodamage

6.2 Introduction

Photoageing in skin is an extrinsic process caused by periodic exposure to ultraviolet (UV) radiation over an individual's lifetime (see review: Naylor *et al.* 2011). Clinically, photoaged skin is exemplified by deep wrinkles, hyperpigmentation (Griffiths *et al.* 1992) and the loss of tissue elasticity and compliance (Langton *et al.* 2017). Histologically, it is characterised both by the aberrant deposition of elastin, known as solar elastosis (Bernstein *et al.* 1995; Chen *et al.* 1986), and by the loss of fibrillin microfibrils (Watson *et al.* 1999), resulting in the degeneration of the elastic fibre architecture. As long-lived (Shapiro *et al.* 1991), macromolecular extracellular matrix (ECM) assemblies, fibrillin microfibril degeneration is considered to be a result of damage accumulation. This is thought to occur either directly, through absorption of UV energy by chromophoric amino acids, or indirectly, through oxidation by UV-induced reactive oxygen species (ROS; see review: Watson *et al.* 2014) Previous work has shown that exposure of physiological doses of UV to fibrillin microfibrils *in vitro,* can cause quantifiable changes to its beaded ultrastructure (Hibbert *et al.* 2015, 2017; Sherratt *et al.* 2010; **chapter 5, Fig 5.1**). In contrast, other ECM assembles, such as collagen VI microfibrils, seem comparatively unaffected by both the photoageing process (Watson *et al.* 2001) and by UV irradiation *in vitro* (Hibbert *et al.* 2015; **chapter 5 Fig. 5.2**). Although it is clear that the ultrastructures of these two ECM assemblies are differentially susceptible to UV irradiation, the molecular locations of this damage within the fibrillin-1 monomer and how this differs from a collagen VI alpha chain (namely α3), remained unknown.

Using a recently developed liquid chromatography tandem mass spectrometry (LC-MS/MS)–based proteomic approach (Eckersley *et al.* 2018; **chapters 3 and 4**), we demonstrated that UV irradiation of primary human dermal fibroblast (HDF)-derived fibrillin and collagen VI microfibrils consistently enhanced the total yield of peptides (peptide spectrum matches: PSMs) from digested fibrillin-1, but not from collagen VI-alpha-3 (COL6A3) **(chapter 5, Figs 5.3 and 5.5)**. Furthermore, we showed that peptide signatures characteristic of UV exposure were repeatedly identified for both microfibrillar assemblies **(chapter 5, Figs 5.4 and 5.6)**. Mapping both the PSMs and these peptide signatures also revealed that UV radiation exposure increases regional susceptibility of the fibrillin-1 protein structure to proteolysis by elastase **(chapter 5, Fig 5.7)**.

This study led to the identification of UV-susceptible foci within the fibrillin microfibril, on a molecular scale. However, it was performed on a structurally homogenous population of microfibrils, derived from culturing a single primary cell type (HDFs). Previously, we have also

shown that human skin-derived fibrillin microfibrils differ both in ultrastructure and in molecular composition compared to HDF-derived microfibrils (Eckersley *et al.* 2018; **chapter 4**). HDF-derived fibrillin microfibrils had different bead morphologies and longer mean periodicities than skin-derived fibrillin microfibrils **(chapter 4, Fig 4.4)**. Additionally, HDF-derived fibrillin-1 contained two protein regions of differential susceptibility to elastase-mediated proteolysis: between epidermal growth factor-like (EGF) domains 11 and 14 (within N-terminal half) and between EGFs 43 and 47 (within the C-terminal end; **chapter 4, Fig 4.5)**. Finally, HDF-derived fibrillin microfibrils lacked key accessory proteins fibrillin-2 and microfibril-associated proteins (MFAPs) 2 and 4 **(chapter 4, Table 4.1)**.

Since HDF-derived fibrillin microfibrils differ in ultrastructure and composition to skin-derived microfibrils (Eckersley *et al.* 2018; **chapter 4**), in this study, we aimed to confirm if the molecular photosusceptibility identified in HDF-fibrillin microfibrils **(chapter 5)** was also evident for microfibrils isolated from human skin. Unfortunately, the 3 - 6 mm donor biopsies from anatomical sites conventionally used to study photoageing, such as photoexposed forearm and photoprotected buttock (Watson *et al.* 1999), yielded insufficient microfibrils required for this type of proteomic analysis. However, previous work has shown that human donor abdominal skin samples were suitable (Eckersley *et al.* 2018; **chapter 4**). Prior to microfibril extraction and proteomics, we first confirmed histologically that abdominal skin samples were relatively photoprotected in comparison to photoexposed forearm, and were similar to photoprotected buttock in regards to their elastic fibre content and organisation. We then went on to assess whether broadband UVB exposure induced molecular damage in suspensions of fibrillin and collagen VI microfibrils, co-extracted from human abdominal skin.

6.3 Materials and Methods

6.3.1 Human tissue and materials

Chemicals were sourced from Sigma-Aldrich Co. Ltd (Poole, UK) unless otherwise stated. Human skin was collected from middle-aged donors (females ages 42-60; mean = 49) with informed and written consent. The use of forearm and buttock biopsies was approved by The University of Manchester Research Ethics Committee 3 (ref: UREC 15464). Abdominal skin samples were acquired via the University of Manchester Skin Health Biobank (MSHB). North West 5 Research Committee has approved this biobank (ref: 09/H1010/10). Samples were bisected, one half snap frozen (for LC-MS/MS) and one half embedded in Optimal Cutting Temperature compound (OCT;

CellPath; Powys, UK) and snap frozen (for histology). All samples were stored at -80°C prior to experimentation.

6.3.2 Tissue cryosectioning and Weigert's staining

Tissue (buttock, abdominal and forearm) was cryosectioned at a thickness of 5 μm (OTF cryostat; Bright Instruments, Bedfordshire, UK). Three serial sections were collected per slide and stored at -80°C prior to Weigert's staining.

The extent of solar elastosis between abdominal, buttock and forearm skin, was assessed using Weigert's resorcin-fuchsin elastin staining (Merck; Darmstadt, Germany) (Proctor and Horobin 1988; Tsuji *et al.* 1986). Cryosections were fixed in 4% [w/v] paraformaldehyde (PFA) in PBS and then submerged in Weigert's elastin staining solution, each step for 10 minutes at room temperature. Stained sections were dehydrated in graded industrial methylated spirit (IMS) (70% [v/v], then twice with 100%), cleared in xylene (5 minutes per step at room temperature) and then permanently mounted (DPX).

6.3.3 Imaging and elastic fibre quantification

Weigert's stained skin sections were imaged using brightfield microscopy. Elastic fibre abundance was quantified by measuring the percentage area of elastic fibres in Weigert's stained tissue sections, at a three dermal depths (within 50 μm, 100 μm, and 300 μm, measured from the dermal-epidermal junction: DEJ), using ImageJ (NIH; Bethesda, MA, USA). Percentage areas of elastic fibres, within areas encompassing these depths, were measured automatically by thresholding the images by brightness using "Threshold Colour" between an ImageJ-assigned scale of 186 and 255 in all images. All coloured pixels, corresponding to the purple stained elastic fibres were then converted to a single colour and all other pixels were coloured white. Elastic fibre abundances were measured within ImageJ as a percentage of coloured pixels within the areas.

Statistical comparisons were performed using GraphPad Prism (GraphPad Software Incorporated; La Jolla, California, USA). Only differences of $p \leq 0.05$ were considered significant. The percentage area of elastic fibres, for each depth, was assessed for three groups (abdominal and matched forearm and buttock skin) with four individuals per group. Percentage area was measured in three images per section and three sections per individual, and then averaged. Elastic fibres were analysed between matched forearm and buttock groups using paired t tests and between

unmatched abdominal vs. buttock and abdominal vs. forearm groups using unpaired t tests (N=4). Tests were Bonferroni corrected for multiple comparisons.

6.3.4 Fibrillin and collagen VI microfibril extraction and purification

Fibrillin and collagen VI microfibrils were extracted and purified as previously described (Eckersley *et al.* 2018; Hibbert *et al.* 2015; Kielty *et al.* 1991; Sherratt *et al.* 2010). Human abdominal tissue samples were digested with bacterial collagenase IA in 50 mM TBS buffer (400 mM NaCl, 1 mM $CaCl^2$, 0.01 mM phenylmethane sulphonyl fluoride and 0.03 mM N-Ethylmaleimide; pH 7.4) for four hours at room temperature. Mixtures were centrifuged and the supernatant subjected to size exclusion chromatography on a GE HiScale 16/40 column containing Sepharose® Cl4B beads at on an ÄKTA Prime Plus Liquid size-exclusion Chromatography System (GE Healthcare; Little Chalfont, UK). Void volume fractions were collected based on spectrophotometric absorbance at 280 nm.

6.3.5 Broadband UV irradiation of microfibril isolations

Isolated microfibril suspensions were split into two groups; one group was irradiated with a dose of 100 mJ/cm^2 of broadband UVB as described previously (Sherratt *et al.* 2010) and the second was kept as control (unirradiated). Suspensions were irradiated within uncapped 35 mm x 10 mm polystyrene cell culture dishes (Corning, Flintshire, UK). Broadband UVB-designated microfibril suspensions were irradiated with a broadband UVB spectrum using two 20 W Phillips TL-12 tubes (Eindhoven, The Netherlands) with an emission wavelength range of 270 – 400 nm. UVB waveband irradiance was measured using a UVX radiometer fitted with a UVX31 UVB detector calibrated to National Physical Laboratory standards. As with previous work on HDF-derived microfibrils **(chapter 5)**, suspensions were exposed to a dose of 100 mJ/cm^2 (4 minutes 38 seconds exposure time, irradiance = 0.36 mW/cm^2) at the centre of, and at a vertical distance of 16 cm from the source, at room temperature. All samples were desalted in 0.22 µm filtered ultrapure water using Slide-A-Lyzer™ MINI Dialysis Devices (Thermo Fisher Scientific; Paisley, UK) for 4 hours at 4°C. Desalted samples were frozen at -80°C and freeze dried at -60°C for 48 hours. These were stored at -80°C.

6.3.6 Fibrillin-1 and COL6A3 peptide generation using elastase digestion prior to LC-MS/MS

As described previously (Eckersley *et al.* 2018), freeze dried microfibril purifications were re-suspended and denatured in 8 M urea, reduced in 10 mM dithiothreitol (DTT) and alkylated in 50 mM iodoacetamide (IAM) in darkness, each step for 30 minutes at room temperature. The

suspension was then diluted to a concentration of 2 M urea using 100mM TBS (pH 8.5), and porcine elastase (Catalogue # E1250) then added (2:1, enzyme:substrate ratio). Samples were digested at 37°C for 4 hours after which enzyme activity was then quenched using 5% (v/v) formic acid in ultrapure water. Peptide samples were then desalted using OLIGO R3 Reversed-Phase Resin beads (Thermo Fisher Scientific) and vacuum dried.

6.3.7 Mass spectrometry

All LC-MS/MS was performed by the Biological Mass Spectrometry Core Facility in the Faculty of Biology, Medicine and Health at the University of Manchester (Manchester, UK). As dictated by their protocols (Buckley 2015; Lennon *et al.* 2014): vacuum dried samples were analysed using an UltiMate® 3000 Rapid Separation liquid chromatographer (Dionex Corp; Sunnyvale, CA, USA) and an Orbitrap Elite™ Hybrid Ion Trap-Orbitrap mass spectrometer (Thermo Fisher Scientific). Peptide mixtures were separated using a gradient from 92% A (0.1% [v/v] formic acid in water) and 8% B (0.1% [v/v] formic acid in acetonitrile) to 33% B, in 30 minutes at 300 nL/min, using a 250 mm x 75 µm i.d. 1.7 µm BEH C18, analytical column (Waters; Hertfordshire, UK). Peptides were selected for fragmentation automatically by data-dependent analysis.

6.3.8 Mass spectrometry data analysis

As described previously, (Eckersley *et al.* 2018), for peptide spectrum matching, mass spectra were extracted using extract_msn (Thermo Fisher Scientific). Mascot v2.5.1 (Matrix Science; London, UK) was used to correlate the spectra against the Swissprot_2016_04 database (152,544 protein entries) with the following search parameters: species - Homo sapiens; enzyme – non-specific; max missed cleavages – 1; fixed modifications - carbamidomethyl, mass – 57.02 Da, AA – C; variable modification – oxidation, mass – 15.99 Da, AA – M; peptide tolerance - 10 ppm (monoisotopic); fragment tolerance - 0.6 Da (monoisotopic). PSMs reported were validated using Scaffold (Proteome Software; Portland, OR, USA). Only exclusive, unique peptide counts are reported for every dataset. False discovery rate (FDR) was calculated by Scaffold using protein and peptide probabilities assigned using the Trans-Proteomic Pipeline and the Peptide Prophet™ (Keller *et al.* 2002) algorithm (Sourceforge; Seattle. WA, USA). Peptide Prophet FDR was thresholded to ≤ 5% for every dataset.

Data-dependent peptide quantification was performed using Progenesis QI (Nonlinear Dynamics, Waters) as described previously **(chapter 5)**. Raw mass spectra files were aligned using default settings. Data was then searched using Mascot v2.5.1 with same search parameters and on the

same database as described earlier and identified peptides and proteins were automatically matched by Progenesis QI. Normalised peptide abundances were compared between matched samples (control vs. broadband UVB) and a fold change for each peptide calculated automatically. Normalised peptide abundances, compared between matched samples, were statistically analysed within Progenesis QI using a paired ANOVA. Only fibrillin-1 peptides which matched to Uniprot (Consortium 2016) accession number FBN1_HUMAN and COL6A3 peptides which matched to CO6A3_HUMAN, and which filtered to $p \leq 0.05$, are reported.

Fibrillin-1 and COL6A3 regional susceptibility to elastase digestion in response to UV irradiation was assessed by mapping the number of LC-MS/MS-detected PSMs and significantly different peptides (data-dependently quantified) to their respective protein domains. Regional differences were compared between broadband UVB-irradiated and control.

6.4 Results and Discussion

6.4.1 Abdominal skin is sufficiently photoprotected for use in microfibril UV irradiation experiments.

Prior to microfibril extraction, the photoageing status of middle-aged abdominal skin samples was assessed by characterising elastic fibre presence in abdominal skin and comparing with photoexposed forearm and photoprotected buttock samples. Visually, photoexposed forearm skin sections exhibited marked solar elastosis, as expected (Mitchell 1967; Chen *et al.* 1986; Raimer *et al.* 1986) with higher levels of aberrant amorphous masses of deposited elastin, in comparison to both abdominal and photoprotected buttock skin sections **(Fig. 6.1; Supplemental Fig. 6.1)**. Elastic fibres seen in abdominal skin sections had a similar, organised architecture (running parallel to the DEJ, in the reticular dermis) to that in photoprotected buttock (Cotta-Pereira *et al.* 1976).

Quantification of elastic fibre abundance (% coverage) indicated no significant differences between abdominal skin and photoprotected buttock skin of middle-aged donors, regardless of the dermal depth of assessment **(Fig. 6.1; Supplemental Fig. 6.2)**. Photoexposed forearm skin however, where solar elastosis was visually widespread, had significantly higher abundances of elastic fibres in comparison to both abdominal and photoprotected buttock skin. Since abdominal skin elastic fibre abundance and architecture resembled that of photoprotected buttock, it suggests that abdominal skin is likely a suitable source of UV-naïve fibrillin and collagen VI microfibrils, permitting their use in subsequent irradiation experiments.

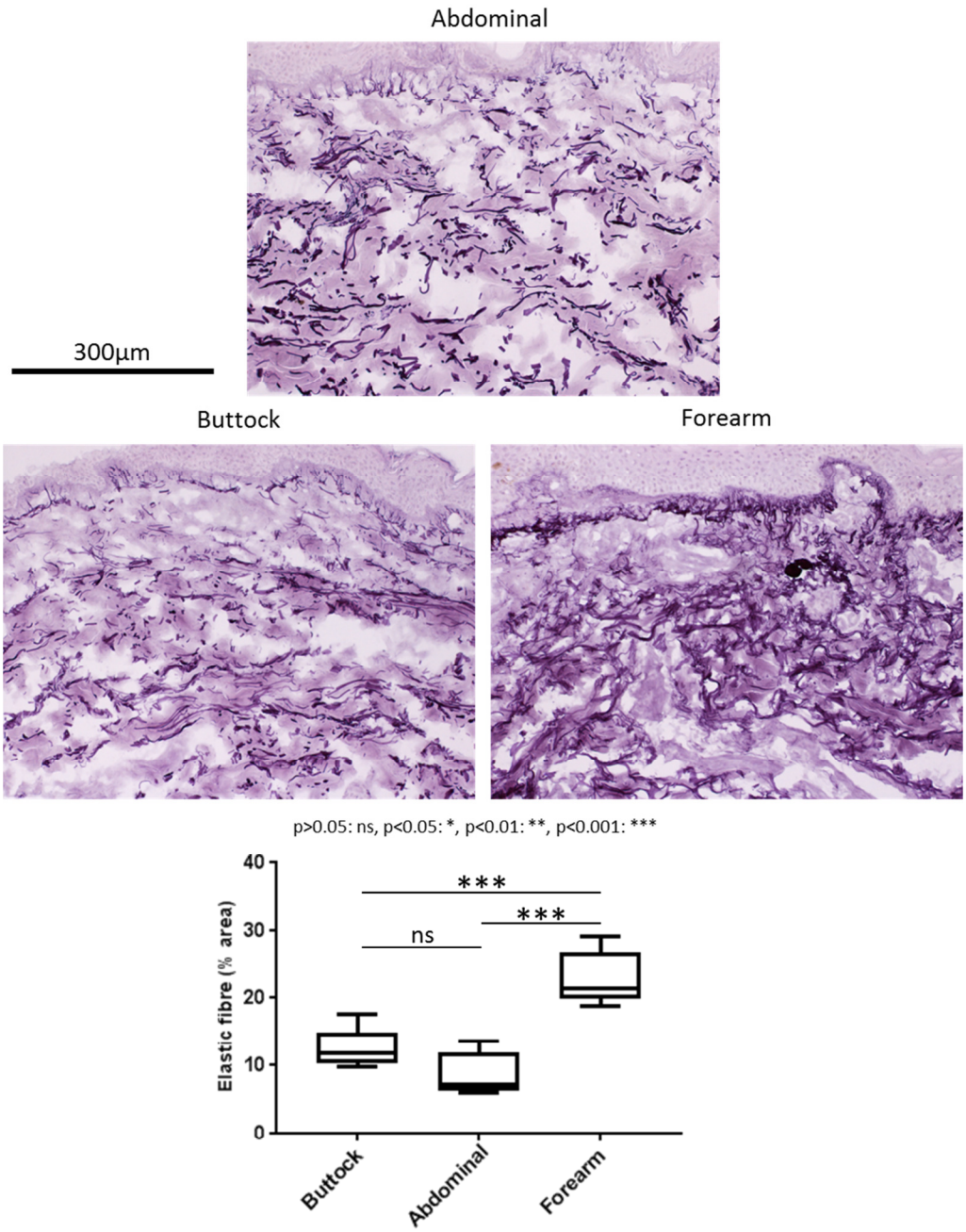

Figure 6.1: Solar elastosis and elastic fibre abundance was compared in Weigert's stained abdominal, forearm and buttock skin cryosections. Marked elastosis was clearly seen in photoexposed forearm sections whereas both abdominal and photoprotected buttock exhibited no signs of this hallmark of advanced photoageing (example buttock and forearm sections from a 46 year old female, F46; abdominal from F49). Elastic fibre abundance in abdominal skin sections was quantified and compared to that of photoexposed forearm and photoprotected buttock (n=4; data = median, IQR and range). Within an area encompassing a depth of up to 300 µm immediately below the DEJ, percentage elastic fibres in abdominal skin sections was not significantly different than in photoprotected buttock sections (p=0.0973; unpaired t test). In contrast, the elastic fibre abundances in photoexposed forearm skin sections were significantly higher than in photoprotected body sites (abdominal, p=0.0003, unpaired t test; buttock, p=0.0002, paired t test; all tests Bonferroni corrected for multiple comparisons).

6.4.2 Peptide spectrum match analysis revealed only limited UV-induced damage to skin-derived fibrillin-1 structure, which is likely due to tissue-specific variation in microfibril assembly.

Broadband UVB irradiation of abdominal skin-derived microfibril suspensions failed to cause consistent increases in the number of fibrillin-1 peptides identified **(Fig. 6.2 Ai, ii)**. This stands in contrast to our previous work on HDF-derived microfibrils where broadband UVB irradiation led to a consistent increase in fibrillin-1 PSMs **(chapter 5, Fig. 5.3)**. Despite this, data-dependent quantification of fibrillin-1 peptides revealed a number of peptide sequences which were either significantly increased or decreased as a consequence of broadband UVB irradiation **(Fig. 6.2 B)**. However, their fold changes were relatively low in comparison to our previous work on HDF-derived microfibrils. Previously, more than half of identified HDF-derived fibrillin-1 peptide signatures of broadband UVB had fold changes greater than 5 **(chapter 5, Fig 5.4)**, whereas fold changes calculated for these abdominal skin-derived fibrillin-1 peptide signatures all equalled 1.62 or below **(Fig. 6.2 B)**. Encouragingly, however, two sequences in particular: TGCTDINECEI and GSDINECALDPDICPN (**Fig. 6.2 B**, bold and underlined) match peptide sequences which had also significantly changed in HDF-derived, UV-irradiated fibrillin-1 **(chapter 5, Fig 5.4)**. These two common peptide signatures may indicate specific sites where fibrillin-1 is most vulnerable to UV-induced damage.

A i

Fibrillin-1 Exclusive Unique Peptides Identified			
	Control	UVB	
	PSMs	PSMs	Fold Change
F44	118	154	1.31
F49	122	114	0.93
F60	150	156	1.04
F56	163	161	0.99

ii

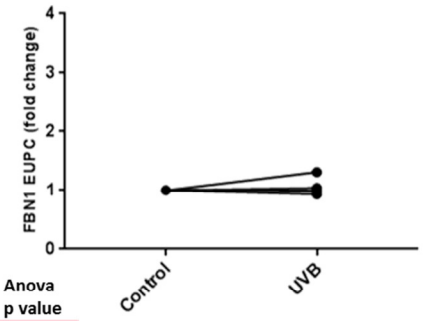

B

UVB-Affected Fibrillin-1 Peptides	Fold Change	Anova p value
CNHGFILS	1.29	0.0223
NCMDIDECQRDPLLCRG	-1.62	0.0421
CKEGYTGDGFTCT	-1.60	0.0175
CEDIDECSLPNIC	-1.52	0.0316
TGCTDINECEI	-1.46	0.0110
AVGLDGRVCVD	-1.41	0.0291
SYICDCPPDFELNPT	-1.38	0.0226
GSDINECALDPDICPN	-1.32	0.0032
ADGKACEDIDECSLPNIC	-1.20	0.0306
GQCRNTPG	-1.15	0.0481

C

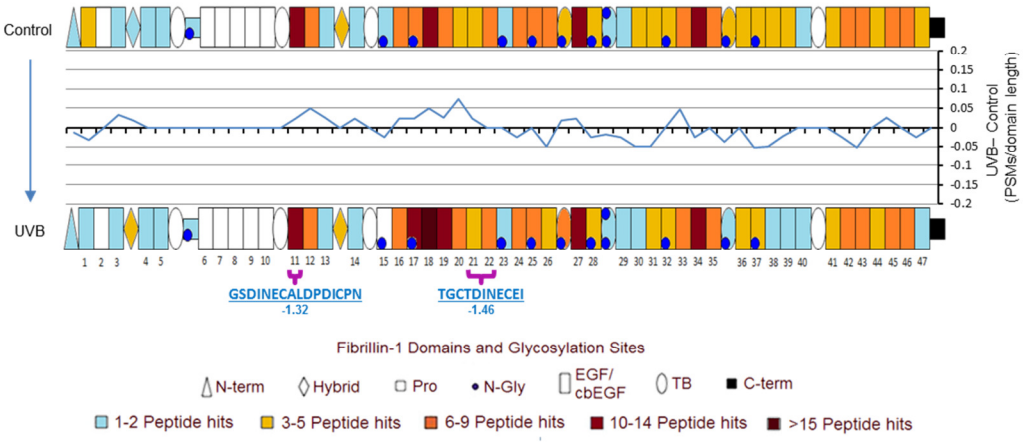

Figure 6.2: Despite PSM analysis detecting only limited UV-induced damage to skin fibrillin-1 structure, data-dependent analysis did reveal significant changes in specific peptides. PSMs for broadband UVB-irradiated fibrillin-1 per individual and their fold changes in comparison to control are shown (Peptide Prophet FDR ≤ 5%) ***(Ai)****. Broadband UVB irradiation failed to cause any consistent change in the number of fibrillin-1 PSMs identified (average fold change = 1.07)* ***(Aii)****. However, data-dependent peptide quantification did reveal ten fibrillin-1 peptides in irradiated microfibril samples which had significantly changed in relative abundance compared to control samples* ***(B)*** *(increase = red, decrease = blue). Their peptide sequences alongside their fold changes and p values are shown (n=4; multivariate paired ANOVA). Two of these match UV-specific peptide signatures which had been previously identified in UV irradiated HDF microfibrils (bold and underlined). To analyse regional fluctuations in peptide yield within the fibrillin-1 protein structure, PSMs were counted for each respective domain, normalised based on total spectrum count and subsequently heat mapped* ***(C)****. PSM counts corresponding to each broadband UVB fibrillin-1 domain were then subtracted from the counts of the control and divided by each domain's primary sequence length to show regional fluctuations in elastase susceptibility. Significantly different peptide sequences which matched previous HDF results (****B,*** *bold and underlined) and their fold changes are also mapped (****C****, purple bracket). UV-induced damage to fibrillin-1 structure was limited, with only small regional differences in peptide yield.*

Comparisons of PSM count maps of fibrillin-1 domains (as done in **chapter 5, Fig. 5.7**) indicate only minimal changes in the regional susceptibility of fibrillin-1 to elastase digestion, as a consequence of broadband UVB irradiation **(Fig. 6.2 C)**. Abdominal skin-derived fibrillin-1 exhibited only discreet fluctuations in PSMs per domain, especially in comparison to the previous study performed on HDF-derived fibrillin-1 **(chapter 5, Fig 5.7)**. Previously, broadband UVB irradiation of HDF-derived fibrillin-1 resulted in large changes in peptide yields near the N-terminal (EGF1) and C-terminal (EGFs 42 - 47) regions and, more focally, at EGF domains 22, 33 and 34 **(chapter 5, Fig 5.7)**, whereas, on the same PSMs/domain length scale, irradiation of abdominal skin-derived fibrillin failed to induce similar peptide yield patterns in these regions **(Fig. 6.2 C)**. The largest regional change in abdominal skin-derived fibrillin-1 peptide yield appears to be at EGF20 (0.07 change in PSMs/domain length change) **(Fig. 6.2 C)**; however, when compared to the previous study, the largest domain changes to HDF-derived fibrillin-1 peptide yields were nearly double this (EGF1 = 0.16 and EGF33 = 0.14 change in PSMs/domain length) **(chapter 5, Fig. 5.7)**.

The two UV-specific fibrillin-1 peptide sequences: GSDINECALDPDICPN and TGCTDINECEI, which had significantly changed in both skin-derived and HDF-derived microfibril isolations correspond to EGF11 and between EGFs 21 and 22, respectively (**Fig. 6.2 C**, purple brackets). It is possible either that fibrillin-1 may be particularly UV-susceptible at these sites or that unfolding in other regions masks or unmasks these sites, changing their exposure to elastase. The folded model of supramolecular organisation of fibrillin-1 within the microfibril (Baldock *et al.* 2001, 2006) places these domains at the interface between the bead and inter-bead regions of the microfibril, with EGF11 placed specifically within the shoulder region. Ultrastructural susceptibility of both these regions have been shown previously, since fibrillin microfibril periodicity (Hibbert *et al.* 2015, 2017; Sherratt *et al.* 2010*;* **chapter 5, Fig 5.1**) and bead morphology (Sherratt *et al.* 2010; **chapter 5, Fig 5.1**) change significantly in response to UV irradiation *in vitro.* As such, it is possible that UV damage (either direct or via induced ROS) at the sites of these two peptide sequences may have been partly responsible for these ultrastructural changes. Interestingly, not only do mutations in EGF11 (also known as calcium binding-EGF7) cause classical Marfan syndrome (Hayward *et al.* 1994), they also change the proteolytic susceptibility of recombinant fragments containing this mutant domain (Kirschner *et al.* 2011). This clearly fits with our observations where UV-induced damage to EGF11 also caused changes in its proteolytic susceptibility, resulting in a significantly decreased yield of the GSDINECALDPDICPN peptide fragment. If mutations to EGF11 cause

Marfan syndrome, it is possible that UV-induced changes to this domain may lead to similar downstream disruptions to function.

This proteomics approach only managed to detect very limited UV-induced molecular damage to abdominal skin-derived fibrillin-1 **(Fig. 6.2)**. This is in stark contrast to HDF-derived fibrillin-1 where this analysis not only detected an increase in overall protease susceptibility in response to UV irradiation **(chapter 5, Fig 5.3)**, but also identified regional foci of damage within the protein domain structure **(chapter 5, Fig. 5.7)**. It is unlikely that the results in this study allude to skin-derived fibrillin microfibrils being more resistant to UV than HDF-derived. Both HDF- and skin-derived fibrillin-1 contain the same number of UV-sensitive chromophoric amino acids and previous studies clearly demonstrate similar changes microfibril ultrastructure from both sources, in response to direct UV irradiation *in vitro* (Hibbert *et al.* 2015; Sherratt *et al.* 2010). The reasons behind this discrepancy are more likely due to inherent differences in structural variability within fibrillin microfibril populations derived from skin compared to populations derived from a single cell type.

Previously, we showed that human abdominal skin-derived fibrillin microfibrils differed both in ultrastructure and in molecular composition to HDF-derived (Eckersley *et al.* 2018; **chapter 4**). We hypothesised that these differences may be due to sub-population variability in the structures of skin-derived microfibrils. These assemblies are long-lived (Shapiro *et al.* 1991) and their ultrastructure is known to vary depending on a tissues developmental stage (Sherratt *et al.* 1997). Additionally, keratinocytes have been shown to synthesise fibrillin microfibrils, *in vitro* (Haynes *et al.* 1997) and the epithelial-mesenchymal states of cells affect their ability to synthesise these assemblies (Baldwin et al. 2014). As a result, different cell types may be synthesising fibrillin microfibrils *in vivo*, and their assembly may vary as a consequence. Furthermore, histology has clearly shown the presence of different functional sub-populations of these assemblies: those that are elastin-associated as part of the elastic fibre system in the reticular dermis (Suwabe *et al.* 1999) and those that are stand-alone oxytalan fibres in the upper papillary dermis (Cotta-Pereira *et al.* 1976; Watson *et al.* 1999). Since we have shown previously that functionally-distinct fibrillin microfibrils are demonstrably different in ultrastructure and composition, in different tissues, (Eckersley *et al.* 2018) **(chapter 4, Figs. 4.2 and 4.3)**, it is possible different sub-populations within the same tissue may be present as well. To conclude, these observations indicate that fibrillin microfibrils isolated from abdominal skin may have dynamic ultrastructures and compositions which vary according to their maturation states (Sherratt *et al.* 1997), the cell types which synthesised

them (Baldwin *et al.* 2014; Haynes *et al.* 1997) and their function (Cotta-Pereira *et al.* 1976; Eckersley *et al*. 2018). As a result, proteomics was unable to detect UV-induced molecular damage within a mixed population of fibrillin microfibrils, with varying structures. This is in contrast to HDF-derived, which are synthesised from a single cell type and, therefore, more invariant.

6.4.3 Despite peptide spectrum match analysis confirming overall resistance of skin-derived COL6A3 structure to broadband-UVB, data-dependent quantification revealed numerous COL6A3 peptide signatures of UV, previously identified in HDF microfibrils

Broadband UVB irradiation of abdominal skin-derived microfibril suspensions failed to cause consistent increases in the number of COL6A3 peptides identified **(Fig. 6.3 Ai, ii)**. This suggests that, as with HDF-derived microfibrils **(chapter 5, Fig. 5.5)**, UV exposure has minimal impact on abdominal skin collagen VI microfibril protease susceptibility. Despite this, data-dependent quantification of peptides revealed 24 COL6A3 peptide sequences which had significantly changed in abundance in response to broadband UVB irradiation **(Fig. 6.3 Bi, ii)**. However, only two out of these 24 peptide signatures had fold changes ≥ 5. In contrast, previous broadband UVB irradiation of HDF-derived microfibrils yielded four out of 13 COL6A3 peptides with fold changes ≥ 5 **(chapter 5, Fig 5.6)**. This indicates that broadband UVB induced significant changes to abdominal skin derived-COL6A3 which were less pronounced than in HDF-derived COL6A3. Encouragingly, out of these 24 peptide signatures of UV, ten (**Fig. 6.3 Bi, ii**; bold and underlined) successfully matched sequences identified in HDF-derived, UV-irradiated COL6A3 **(chapter 5, Fig 5.6)**. As with fibrillin-1, these may reflect sites where COL6A3 is most vulnerable to UV-induced damage.

A i

COL6A3 Exclusive Unique Peptides Identified			
	Control	UVB	
	PSMs	PSMs	Fold Change
F44	271	273	1.01
F49	301	284	0.94
F60	299	299	1
F56	233	217	0.93

ii

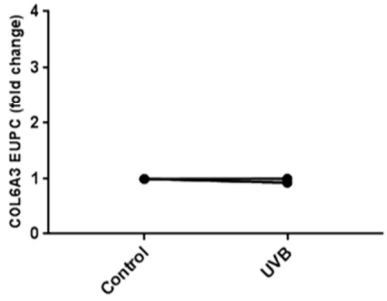

B i

UVB-Affected COL6A3 Peptides	Fold Change	Anova p value
IDSSEGVRPDGFA	2.35	0.0053
KSVLLDKI	2.30	0.0328
AVPIGIGIG	2.21	0.0207
QVLVLISA	1.86	0.0292
LFVKSAGSRIEDGVPQ	1.61	0.0434
IDGSQSAGPEF	1.44	0.0201
IMNSFGPS	1.41	0.0287
FLLDGSIN	1.38	0.0007
GFAGGELA	1.38	0.0399
LHDAMHETLCPGVTDAA	1.37	0.0120
LQPLPSPGVGGKRDVV	1.36	0.0441
KQFGVAPFT	1.32	0.0427
YEDGDSIQVG	1.20	0.0225
DGSQSAGPEF	1.16	0.0203
FVITGGKSVEDAQ	1.10	0.0077

ii

UVB-Affected COL6A3 Peptides	Fold Change	Anova p value
GRDLTDFLENVLTCHV	-26.6	0.0344
ANTPSGPVEAFDFDEYQPEMLEKFR	-18.5	0.0402
LIERLVDYLDVGFDTT	-3.42	0.0328
RAAGSDVDIDMA	-2.02	0.0095
RDLTDFLENVLT	-1.88	0.0484
NDVFPEF	-1.72	0.0230
DLDYELA	-1.51	0.0368
FRELPSLEQK	-1.41	0.0274
CSGQRGDRGPIGSIGPKGIPGEDG	-1.27	0.0196

C

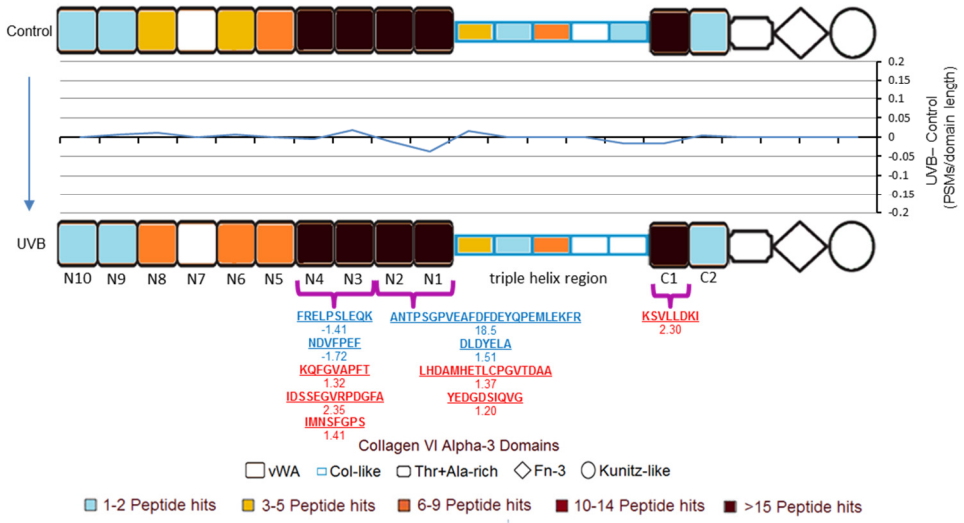

Figure 6.3: Despite PSM analysis confirming resistance of skin COL6A3 structure to broadband-UVB, data-dependent quantification revealed numerous COL6A3 peptide signatures of UV damage. PSMs for broadband UVB-irradiated COL6A3 per individual and their fold changes in comparison to control are shown (Peptide Prophet FDR ≤ 5%) ***(Ai)****. As with fibrillin-1, broadband UVB irradiation failed to cause any consistent change in the number of COL6A3 PSMs identified (average fold change = 0.97)* ***(Aii)****. However, data-dependent peptide quantification revealed 24 COL6A3 peptides in broadband UVB-irradiated microfibril samples which had significantly changed (****Bi****, increased = red;* ***Bii****, decreased = blue) in relative abundance compared to control samples (n=4; multivariate paired ANOVA). Of these, ten matched peptide signatures previously identified as in HDF-derived microfibrils (bold and underlined). As done for fibrillin-1, COL6A3 PSMs were counted per protein domain, normalised based on total spectrum count heat mapped* ***(C)****. PSM counts corresponding to each broadband UVB COL6A3 domain were then subtracted from the counts of the control and divided by each domain's primary sequence length to show regional fluctuations in elastase susceptibility. Significantly different peptide sequences which matched previous HDF results* ***(B)*** *are also mapped (****C****, purple bracket). UV damage to COL6A3 structure was also limited, with even smaller regional differences in peptide yield than to fibrillin-1 structure.*

When comparing PSM count maps of COL6A3 domains, broadband UVB caused minimal changes in the regional susceptibility of abdominal COL6A3 to elastase digestion **(Fig. 6.3 C)**, as with fibrillin-1 **(Fig. 6.2 C)**. This corroborates the observations following broadband UVB irradiation of HDF-derived microfibril isolations, where COL6A3 also exhibited only discreet fluctuations PSMs per protein domain **(chapter 5 Fig. 5.8)**.

The ten COL6A3 peptide sequences which had significantly changed in both skin-derived and HDF-derived microfibril isolations, mapped to vWA (A-domains of von Willibrand factor) domains N1-N4 and C1 (**Fig. 6.3 C**, purple brackets). These correspond to the double bead region of the collagen VI microfibril (specifically on either side of the triple helix regions) (Baldock *et al.* 2003; Chu *et al.* 1989; Furthmayr *et al.* 1983). Interestingly, this suggests that the double beads of the collagen VI microfibril may be the most UV-susceptible regions of this assembly. This is an important observation, as our previous ultrastructural studies of UV-irradiated collagen VI microfibrils have focused solely on changes affecting periodicity (the inter-bead region). Although we showed that collagen VI microfibril periodicity remains unaffected by UV irradiation (Hibbert *et al.* 2015; **chapter 5, Fig 5.2**), it is possible that by neglecting the ultrastructural analysis of the bead we may have missed a key region of UV-susceptibility within this assembly.

Surprisingly, UVB irradiation of abdominal skin-derived microfibrils yielded a higher number of significantly different COL6A3 peptides, many with larger fold changes, **(Fig. 6.3 Bi, ii)** than fibrillin-1 peptides **(Fig. 6.2B)**. This is in contradiction to the observations made for HDF-derived microfibril isolations **(chapter 5)** and to previous studies which have shown that collagen VI microfibrils exhibit marked resistance both to photodamage (Hibbert *et al.* 2015) **(chapter 5, Fig 5.2)**, and to photoageing (Watson *et al.* 2001), in comparison to fibrillin microfibrils **(chapter 5, Fig 5.1)** (Hibbert *et al.* 2015; Watson *et al.* 1999). The reason behind this may be due to collagen VI microfibrils having a more conserved, invariant structure in comparison to fibrillin microfibrils. We previously showed that collagen VI microfibrils from abdominal skin did not differ in ultrastructure and COL6A3 structure in comparison to HDF-derived assemblies **(chapter 4, Fig. 4.6)** whereas co-purifying fibrillin microfibrils did **(chapter 4, Figs. 4.4 and 4.5)** (Eckersley *et al.* 2018). This suggests that collagen VI microfibril populations isolated from skin do not vary as greatly in structure compared to fibrillin microfibrils. This means that, whereas sub-population variability in fibrillin microfibril structure would limit the ability of LC-MS/MS to detect UV-induced molecular damage in fibrillin-1,

this would not be the case for collagen VI microfibrils and COL6A3. This would explain why LC-MS/MS detected a higher number of significantly different COL6A3 peptides than fibrillin-1 peptides in abdominal skin microfibril isolations.

6.4.4 Conclusion

Contrary to our previous work on HDF-derived microfibrils **(chapter 5)**, PSM analysis failed to adequately detect broadband UVB damage within the fibrillin-1 structure of microfibrils isolated from *ex vivo* abdominal skin. We propose that this is due to structural variability within skin-derived fibrillin microfibril populations which is rendering any UV-induced changes undetectable with PSM analysis. This is an important consideration, as these results may show that sub-populations of fibrillin microfibrils vary in structure and composition within the same tissue and further demonstrates the dynamic nature of these assemblies. Encouragingly however, data-dependent quantification revealed a number of UV-specific peptides, whose abundances had significantly changed in response to irradiation. Two of these successfully matched peptide signatures of UV, identified previously in HDF-derived microfibril isolations **(chapter 5)**. One of these peptides corresponded to EGF11 within the fibrillin-1 structure. We proposed that the higher UV-susceptibility of EGF11 may be particularly important due to its association with Marfan syndrome.

As seen in previous work on HDF-derived microfibrils **(chapter 5)**, PSM analysis of COL6A3 structure confirmed its overall resistance to broadband UVB-radiation. Despite this, as with fibrillin-1, data-dependent quantification revealed a number COL6A3 peptide sequences which had significantly changed in abundance in response to this irradiation. Ten of these successfully matched peptide signatures of UV in HDF-derived COL6A3 **(chapter 5)**. Since these peptides all correspond to the double bead region of the collagen VI microfibril, we propose that this region may be the site of most susceptible to ultrastructural damage by UV. This is important, since the effects of UV irradiation on the double bead region of collagen VI has never been previously assessed.

Proteomic analysis of skin-derived microfibrils was wholly successful for collagen VI but not for fibrillin, probably due to differences in sub-population structural variation. Since we know, historically, that fibrillin microfibrils are UV-susceptible, had these assemblies been less dynamic in structure, it is likely we could have identified many more significantly different UV-specific fibrillin-1 peptides in common with those of HDF-derived, as done successfully for COL6A3. We also anticipate we would have seen regional fluctuations in fibrillin domain-mapped PSMs similar to that seen for HDF-derived. To conclude, due to the proposed variability in skin-derived fibrillin

microfibrils, cell culture may be the most appropriate way to proteomically analyse UV-induced damage to this assembly. Regardless, data-dependent quantification was still able to detect significant UV-induced changes in specific fibrillin-1 and COL6A3 peptide sequences common to both human skin-derived microfibrils and HDF-derived microfibrils. Encouragingly, it indicates that this proteomic approach has the potential to define molecular fingerprints of UV damage not just in fibrillin and collagen VI microfibrils but in a panel of ECM components. As such, it may be able to characterise and reveal the molecular photosusceptibility of the whole dermal proteome, enhancing our understanding of the mechanisms behind skin photoageing and the role UV plays in its progression.

6.5 Acknowledgements

This study was fully funded by a programme Grant from Walgreens Boots Alliance, Nottingham, UK. CEMG is a Senior Investigator at the National Institute for Health Research. CEMG and REBW are partly supported by the NIHR Manchester Biomedical Research Centre.

6.6 Author Contributions

AE conceived, designed and performed all experiments, analysed all the data, prepared the figures and wrote the paper. MJS supervised and coordinated the study and contributed to the preparation of the figures and editing of the paper. MO aided in the mapping of peptide spectrum matches onto the domains structures of fibrillin-1 and COL6A3. AKL and PH performed all cryosectioning of skin tissue. REBW and CEMG contributed to the study design and to the editing of the paper. DK, ROC and EJK provided technical assistance for LC-MS/MS and contributed to the editing of the paper.

6.7 Conflict of Interest

The authors declare that they have no conflicts of interest with the contents of this article. Walgreens Boots Alliance has approved this manuscript's submission but exerted no editorial control over the content.

6.8 Supplemental Information

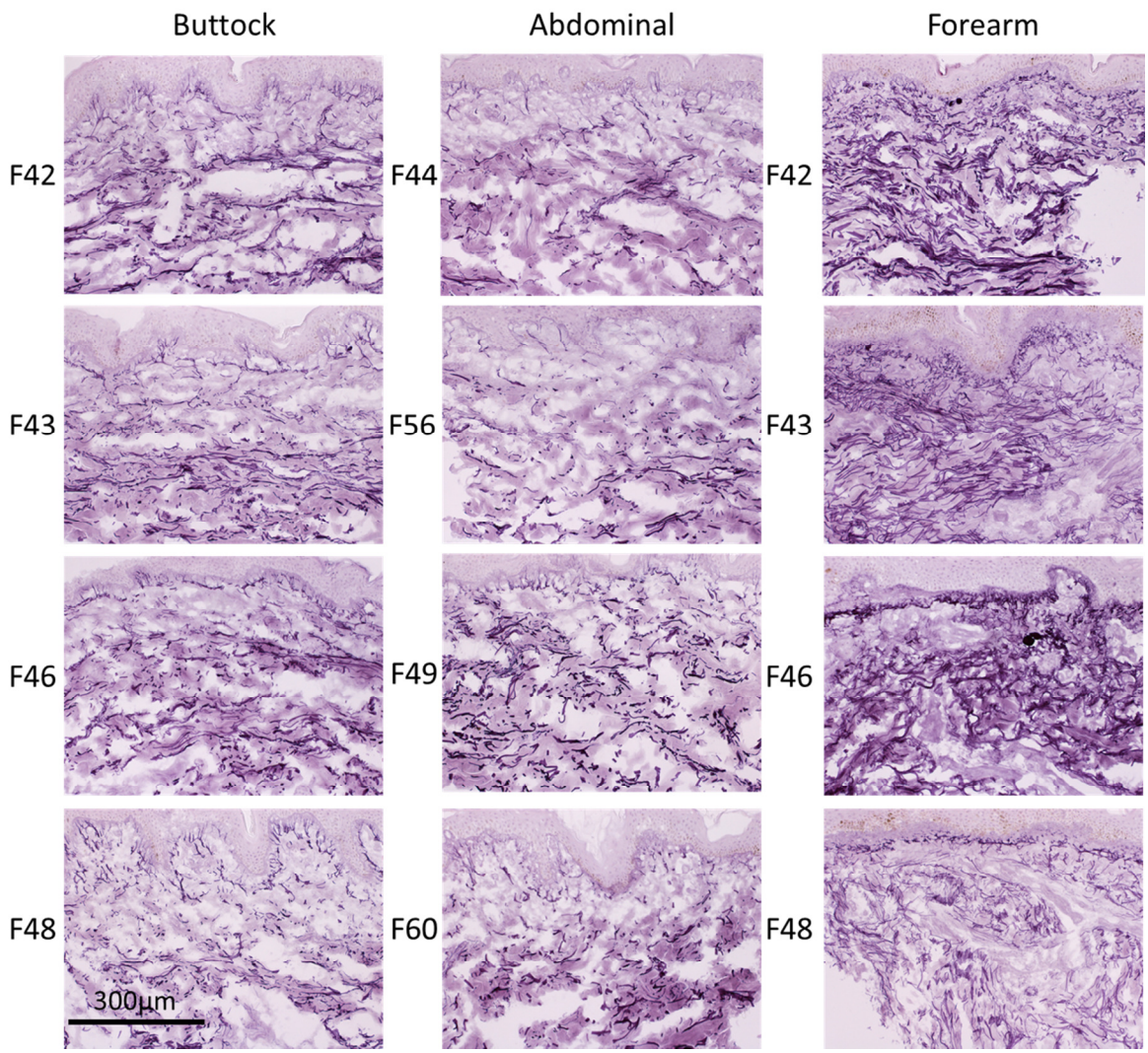

Supplemental Figure 6.1: Extent of solar elastosis compared in Weigert's stained abdominal, forearm and buttock skin cryosections. Marked elastosis was clearly seen in photoexposed forearm sections whereas both abdominal and photoprotected buttock exhibited no signs of this hallmark of advanced photoageing.

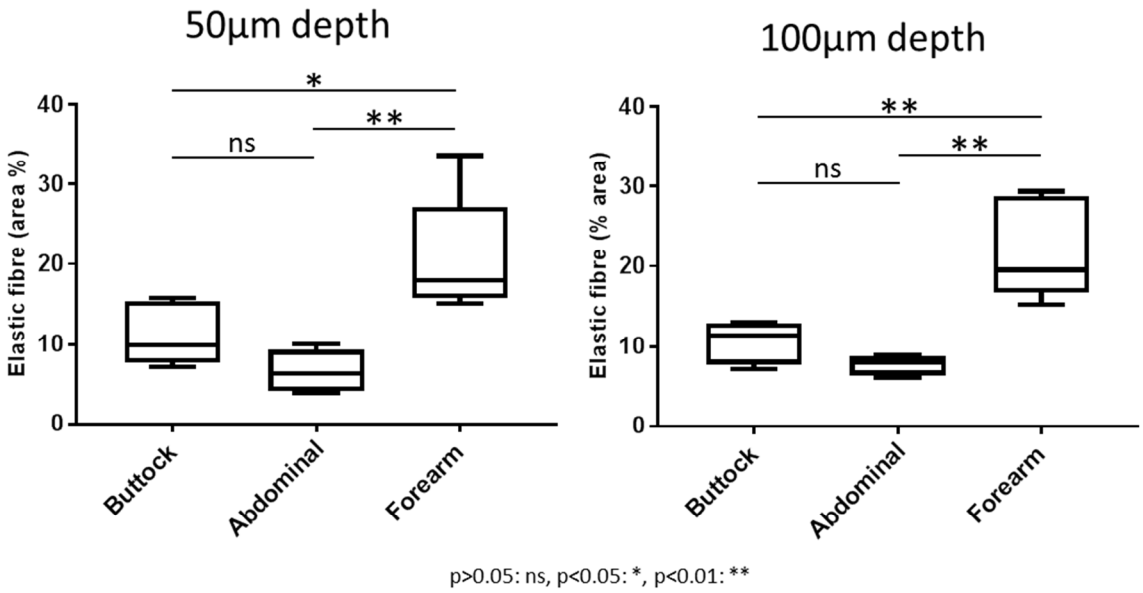

Supplemental Figure 6.2: Elastic fibre abundance in abdominal skin resembles that of photoprotected buttock more than photoexposed forearm. Elastic fibre abundance in abdominal skin sections was also compared to that of photoexposed forearm and photoprotected buttock (n=4; data = median, IQR and range), at dermal depths of 50 µm and 100 µm below the DEJ. Within these areas, percentage elastic fibres in abdominal skin sections were not significantly different than in photoprotected buttock sections (50 µm, p=0.0648; 100 µm, p=0.0640; unpaired t tests). In contrast, elastic fibre abundance in photoexposed forearm skin was significantly higher than in abdominal skin (50 µm, p=0.0040; 100 µm, p=0.0011; unpaired t tests). As expected, elastic fibre abundance was significantly higher in photoexposed forearm sections than in photoprotected buttock sections (50 µm, p=0.0290; 100 µm, p=0.0088; paired t tests; all tests Bonferroni corrected for multiple comparisons).

Chapter 7: Discussion and Future Perspectives

7.1 Summary of Thesis

The fibrillin microfibril is a large supramolecular ECM assembly (Baldock *et al.* 2001) whose versatility enables the fulfilment of a plethora of roles in different tissues, both as a stand-alone component (Godwin *et al.* 2018; Hiraoka *et al.* 2010; Yamanouchi *et al.* 2012) or as a constituent of the elastic fibre (Kielty *et al.* 2002). As a consequence of their biological importance, disruption of the fibrillin microfibril network in skin during the photoageing process (Watson *et al.* 1999) is thought to be tied directly to clinical symptoms (wrinkling) (Montagna *et al.* 1989) and loss of gross tissue mechanics (elasticity and resilience) (Langton *et al.* 2010).

The all-encompassing aim of this PhD was to characterise human fibrillin microfibril structural and compositional diversity and UV-induced damage, on a molecular scale. To realise this, our first aim was to develop a unique LC-MS/MS-based proteomic approach capable of characterising differences in fibrillin-1 structure and microfibril composition **(chapter 3)**. Characterisation of fibrillin-1 structure was accomplished by optimising a sample preparation method using elastase digestion which allowed the effective generation of fibrillin-1 peptides from microfibrils isolated from eye (ciliary body) and skin tissue. This enabled the analysis of fluctuations in the protein's regional susceptibility to proteolysis, pertinent to its structure. Characterisation of fibrillin microfibril supramolecular composition was accomplished by optimising a sample preparation method using the SMART Digestion™ kit. This enabled the LC-MS/MS detection of co-purifying microfibril-associated protein peptides which the elastase method failed to yield. These proteomic methods also enabled the structural and compositional analysis of the collagen VI microfibril, another ECM assembly which frequently co-purifies with the fibrillin microfibril. Coupled with the ability to quantifiably measure ultrastructure (bead morphology and periodicity) with AFM, these approaches became powerful tools in addressing the remaining aims set out in this thesis. With it, these studies were able to show that differences in fibrillin and collagen VI microfibril ultrastructure went hand-in-hand with differences in fibrillin-1 and COL6A3 structure and composition.

Since fibrillin microfibrils played distinct biological roles in different tissues, the next aim was to answer whether or not this was reflected in their ultrastructure, fibrillin-1 structure and molecular composition **(chapter 4)**. Fibrillin microfibrils isolated from the ciliary body of eye differed not only in bead morphology and periodicity to those isolated from skin, but also in their regional susceptibility

of their fibrillin-1 monomers to proteolysis, and in the presence of functionally associated proteins. Additionally, we showed that similar differences were also present in fibrillin microfibrils derived from cultured HDFs compared to those derived from human skin. This was in contrast to co-purifying collagen VI microfibrils which did not differ in periodicity or COL6A3 structure between HDF-derived and skin-derived isolations. Finally, the data demonstrated that the presence of microfibril-associated proteins reflected the distinct functions fibrillin microfibrils played in different tissues. Ciliary body-derived fibrillin microfibrils co-purified with proteins involved in basement membrane function such as nidogen-1 and laminin (Yurchenco 2011) whereas skin-derived fibrillin microfibrils co-purified with those involved in elastic fibre function such as EMILIN-2, elastin and fibulin-1 (Colombatti *et al.* 2000; Kielty, Sherratt, *et al.* 2002; Roark *et al.* 1995). Importantly, these studies also demonstrated that HDF-derived fibrillin microfibrils lacked important microfibril-associated proteins such as fibrillin-2 and MFAPs 2 and 4, key to microfibril maturation (Zhang *et al.* 1994) and elastic fibre assembly (Jensen *et al.* 2001; Pilecki *et al.* 2016). The observations made in this study clearly demonstrate that fibrillin microfibril structure and composition is intricately tied to its tissue of origin and the roles they play within. This study was published in the Journal of Biological Chemistry (Eckersley *et al.* 2018).

Having successfully characterised the structural and compositional diversity of fibrillin microfibrils from elastin-rich (skin) and elastin-poor (ciliary body) tissues for the first time, the next aim was to assess UV-induced damage due to its association to the photoageing process in skin. Fibrillin microfibril architecture is demonstrably susceptible to the photoageing process (Watson *et al.* 1999) and, its ultrastructure, to UV-induced damage (Hibbert *et al.* 2015; Sherratt *et al.* 2010) *in vitro*, in contrast to collagen VI microfibrils which are resistant to both (Hibbert *et al.* 2015; Watson *et al.* 2001). However, the molecular effects of UV on the structure of the fibrillin-1 monomer, and how this differs to the COL6A3 monomer, remained unknown. Hence, the next aim was to characterise UV-induced damage in fibrillin and collagen VI microfibrils on an ultrastructural and molecular scale. This was initially attempted in HDF-derived isolations **(chapter 5)**, anticipating that cells would give us a suitable source of homogenous, non-UV-exposed microfibrils. In doing so, the data effectively showed that both solar simulated radiation (SSR) and broadband UVB not only induced ultrastructural changes to bead morphology and periodicity but also led to an increase in the regional susceptibility of the fibrillin-1 to proteolysis. As expected, this was in contrast to collagen VI microfibrils, which remained resistant to UV, both ultrastructurally and molecularly. Despite these differences in UV susceptibility, data-dependent quantification of fibrillin-1 and

COL6A3 revealed peptide signatures of UV-induced damage within both microfibril assemblies. These peptides significantly changed in abundance in response to both SSR and broadband UVB irradiation. In summary, this study successfully identified regional foci of UV-induced damage to the fibrillin-1 structure, common to both sources of UV irradiation (SSR and broadband UVB) for the first time. Additionally, it led to the detection of peptide signatures of UV damage from the comparatively UV-resistant collagen VI microfibrils, indicating that proteomic approaches may be more sensitive in characterising this damage than ultrastructural measurements with AFM (Hibbert *et al.* 2015).

Having successfully characterised fibrillin-1 and COL6A3 UV-induced damage in HDF-derived microfibril isolations, the next aim was to test whether this photosusceptibility translated to human skin-derived microfibrils **(chapter 6)**. However, contrary to previous work, the proteomics approaches failed to adequately characterise molecular damage to skin-derived fibrillin-1 structure, in response to broadband UVB irradiation of microfibril isolations. The structural variations in fibrillin microfibril populations from skin may have interfered with the ability to detect UV-induced damage to fibrillin-1 using this proteomic approach. Despite this, data-dependent quantification successfully identified two fibrillin-1 peptide signatures of broadband UVB damage which corresponded to signatures previously detected in the UV-irradiated HDF-derived microfibril study. Encouragingly, the resultant data confirmed the overall resistance of skin COL6A3 structure to UV-induced damage, as shown in the previous HDF study. Despite this, ten COL6A3 peptide signatures of broadband UVB-induced damage were detected which corresponded to signatures identified in the previous HDF study. This indicates that the proteomic approach was successful in characterising molecular damage in COL6A3, in contrast to fibrillin-1. This may be due to collagen VI microfibrils being comparatively less structurally variable than fibrillin microfibrils, enabling their effective proteomic analysis.

In conclusion this work successfully addressed the aims of the PhD. Through the development of novel proteomic methods and AFM, distinct fibrillin microfibril populations were structurally and compositionally characterised from two different tissues (ciliary body and skin). These novel observations enhance our understanding of this versatile supramolecular ECM assembly. Furthermore, the studies enabled the characterisation of UV-induced molecular damage within both fibrillin-1 monomers of fibrillin microfibrils and COL6A3 monomers of collagen VI microfibrils, derived from HDF culture and from *ex vivo* skin. This has potential implications for elucidating the

mechanisms of photoageing by enhancing our understanding of how these assemblies may be differentially compromised by the photoageing process, on a molecular scale. Despite this success, the limitations of this thesis and potential future directions remain to be discussed.

7.2 The supramolecular organisation of the fibrillin microfibril is the missing link between fibrillin-1 regional fluctuations in susceptibility and ultrastructure

In this work, there are three examples where differences in fibrillin microfibril ultrastructure correlated with large, regional fluctuations in proteolytic susceptibility within fibrillin-1 protein structure. This was demonstrated when ciliary body-derived microfibrils were compared to skin-derived, when skin-derived were compared to HDF culture-derived **(chapter 4)** and when UV-irradiated (either with SSR or broadband UVB) fibrillin microfibrils were compared with non-irradiated **(chapter 5)**. These three separate observations strongly suggest that proteolytic susceptibility of different protein regions of fibrillin-1 is intimately tied to fibrillin microfibril ultrastructure and, therefore, the supramolecular organisation of these monomers within. Unfortunately, this connection can only be inferred, since the supramolecular organisation of fibrillin-1 within the microfibril remains deeply contested.

Two models of fibrillin microfibril supramolecular organisation exist: the folded model (Baldock *et al.* 2001, 2006) and the staggered model (Jensen and Handford 2016; Kielty *et al.* 2005) **(chapter 1, Fig 1.8)**. Although both predict the presence of 8 fibrillin-1 monomers per microfibril repeat, they disagree on the alignment of the molecules within the structure. For example, the folded model predicts that the inter-bead region of microfibrils is putatively composed of a single protein region of fibrillin-1 (between EGF22 and TB6), whereas the staggered model predicts two (one between TB1 and EGF17 and another between EGF28 and EGF41). The disagreement in fibrillin-1 alignment between these two models means that regional fluctuations in the proteolytic susceptibility of fibrillin-1 cannot be directly related to ultrastructural differences observed in microfibril bead morphology or inter-bead distance (periodicity). Were the supramolecular organisation of fibrillin-1 within the microfibril solved, we could have directly linked the tissue-dependent molecular differences and the UV-dependent molecular changes seen in this work to the differences in ultrastructure observed. This would have informed greatly on the effect of UV-induced damaged fibrillin-1 on the assembly as a whole.

Despite this, it is possible that the principles and approaches used in this work could contribute greatly to answering the question of how fibrillin-1 is organised within the microfibril. The data

showed that fibrillin-1 protein displays marked regional variations in proteolytic susceptibility and indicated that these patterns likely relate to the organisation of fibrillin-1 within the microfibril **(chapter 3, Fig 3.3).** It is possible that cryptic protein regions of fibrillin-1, which yielded little to no peptides in response to elastase digestion, may be hidden deep within the globular regions of the microfibril ultrastructure (namely the bead). As a result, they remain masked by more superficial proteinaceous regions and therefore resistant to proteolysis. Relating these patterns to the folded and staggered models further widened the discrepancies between them. It is possible, however, that these observations could be used to help predict the alignment of fibrillin-1 within the microfibril.

Although solving the three-dimensional (3D) structure of the fibrillin-1 monomer is challenging (due to its size), structures of its component protein fragments (PF regions) have been solved using nuclear magnetic resonance (NMR) (Yadin *et al.* 2013), X-ray crystallography (Jensen *et al.* 2009; Lee *et al.* 2004) and small angle X-ray scattering (SAXS) (Baldock *et al.* 2006). Recent ongoing work by the Baldock (Professor Clair Baldock) lab at the University of Manchester is attempting to localise and align the 3D structure of these fibrillin PF regions to the 3D ultrastructure of the microfibril (Godwin *et al.* 2018). The work presented in this thesis could aid in that pursuit. Mapping the regional differences in the peptide yield of fibrillin-1, in response to elastase digestion, to these PF regions may further inform on their alignment. If the predictions are correct, PFs resistant to elastase would likely correspond to the internal regions of the microfibril, whereas susceptible PFs to external regions. This highlights the future potential of this novel proteomic approach in answering fundamental questions about fibrillin microfibril structure and assembly.

7.3 Characterisation of fibrillin microfibril composition in different tissues enables the identification of potential new associated proteins

Isolating fibrillin microfibrils directly from human ciliary body, skin and HDF culture allowed the proteomic identification of numerous co-purifying microfibril-associated proteins (Eckersley *et al.* 2018) **(chapter 4, Table 4.1)**. In doing so, it enabled the characterisation of tissue- and HDF culture-dependent differences in fibrillin microfibril composition. The identities, interactions and fibrillin-associated biological roles of proteins such as fibrillin-2 (Zhang *et al.* 1994), elastin (Sakai *et al.* 1986), the MFAPs (Penner *et al.* 2002; Pilecki *et al.* 2016; Trask *et al.* 2000), the fibulins (Reinhardt, Sasaki, *et al.* 1996; Roark *et al.* 1995), versican (Isogai *et al.* 2002) and fibronectin-1 (Sabatier *et al.* 2009) have long been known. However, this work identified a number of co-

purifying proteins whose interactions with native microfibrils had never been previously reported. As a result it could aid in determining potential new microfibril-associated proteins.

In order to distinguish whether of the presence of these co-purifying proteins are due to genuine interactions or to non-specific binding, we can compare them to those identified by molecular fishing in the Cain *et al.* (2009) study **(chapter 1, Fig. 1.16)**. Proteins which are co-identified both in native tissue microfibril isolations and by molecular fishing with PF regions of fibrillin-1 in HDF culture are likely candidates of new interactors. Five protein families fit these criteria: annexins, vimentins, βig-H3, IGFBPs and PAIs. **(Table 7.1)**.

New Associated Protein Candidates	Known ECM interactions
Annexins V, II	Both of these Ca^{2+} channels are major components of matrix vesicles. Their channel activity is stimulated by direct binding to ECM components like collagens II and X (Kirsch *et al.* 2000).
Vimentin	These intracellular intermediate filaments interact with the ECM indirectly via vimentin associated matrix adhesions (VAMs) (Ivaska *et al.* 2007).
βig-H3	An ECM molecule with a versatile role in tissue homeostasis; it interacts with numerous ECM components (Thapa *et al.* 2007).
IGFBP3, 7	These IGF binding partners modulate the cytokine's action in tissue. This can be affected by their direct interaction with fibronectin (McIntosh *et al.* 2010).
PAI-1	This protease inhibitor mediates the degradation of the ECM (Cajot *et al.* 1990)

Table 7.1: Suggested new fibrillin microfibril-associated protein candidates, selected based upon their co-identification in both the 2009 molecular fishing study (Cain et al. *2009) and the 2018 native tissue co-purification study (Eckersley* et al. *2018)* ***(chapter 4)****. This table was presented in a recent published review (Thomson* et al. *2018), which I co-authored and contributed to, and was featured in the section entitled: "Potential new associated proteins".*

Having proposed these new fibrillin microfibril-associated protein candidates, the next logical step would be to validate their interactions by dual immunofluorescence histolochemistry, using antibodies to co-localize interactions *in vivo*. Additionally, it would be useful to discover the interaction site of these proteins on the microfibril ultrastructure by potentially using immuno-gold labelling and AFM on extracted microfibrils. This would also distinguish which proteins bind specifically with fibrillin microfibrils and which with collagen VI microfibrils. Finally the use of techniques such as surface plasmon resonance and the solid phase binding assay would allow us to determine the binding strength (disassociation constants) of these proteins. In summary, the

work presented in this thesis not only enhances our knowledge of fibrillin microfibril composition in native, human tissue but also highlights the potential for the discovery of novel protein interactions key to tissue functionality.

7.4 Structural diversity of fibrillin microfibrils: from inter-tissue to intra-tissue variation

In the tissue comparison study **(chapter 4)**, we successfully demonstrated that fibrillin microfibrils derived from eye and from skin differed not only in ultrastructure (bead morphology) **(Fig. 4.2 A)**, but also in fibrillin-1 structure (regional susceptibility to proteolysis) **(Fig. 4.3)** and composition (associated protein presence) **(Table 4.1).** We attributed these inter-tissue differences to skin fibrillin microfibrils being predominantly elastic fibre-associated (Cotta-Pereira *et al.* 1976) compared to those from the ciliary body which exist as stand-alone assemblies (Godwin *et al.* 2018; Hiraoka *et al.* 2010). These results suggest that these ECM components may have evolved distinct supramolecular assemblies to cope with their different functions in tissues. However, although skin fibrillin microfibrils are predominantly elastic fibre-associated, a smaller sub-population exist as functionally distinct, stand-alone oxytalan fibres in the papillary dermis (Cotta-Pereira *et al.* 1976; Yamanouchi *et al.* 2012). If fibrillin microfibrils with different functions have evolved distinct ultrastructures and compositions, we can hypothesise that this may also be true intra-tissue, as well as inter-tissue.

Similarly, within the tissue comparison study, we also discovered that the ultrastructures **(Fig. 4.4)**, fibrillin-1 structures **(Fig. 4.5)** and compositions **(Table 4.1)** of fibrillin microfibrils isolated from human skin differed from those isolated from cultured HDFs. This is further indicative of the potential existence of structural and compositional variation between sub-populations of skin-derived fibrillin microfibrils. HDF-sourced populations, being derived from a single cell type, likely exhibit a more homogenous structure than those sourced from skin. Interestingly, frequency histograms (replotted from skin and HDF microfibril periodicity data presented in **chapter 4, Figs 4.4 B and 4.6 A**) reveal that the periodicities of skin fibrillin microfibril populations exhibit a bimodal distribution **(Fig 7.1, blue arrows)**. This is in contrast to periodicities of HDF-derived microfibrils which appear relatively unimodal in distribution and further exemplifies the potential for intra-tissue variability of fibrillin microfibrils within skin.

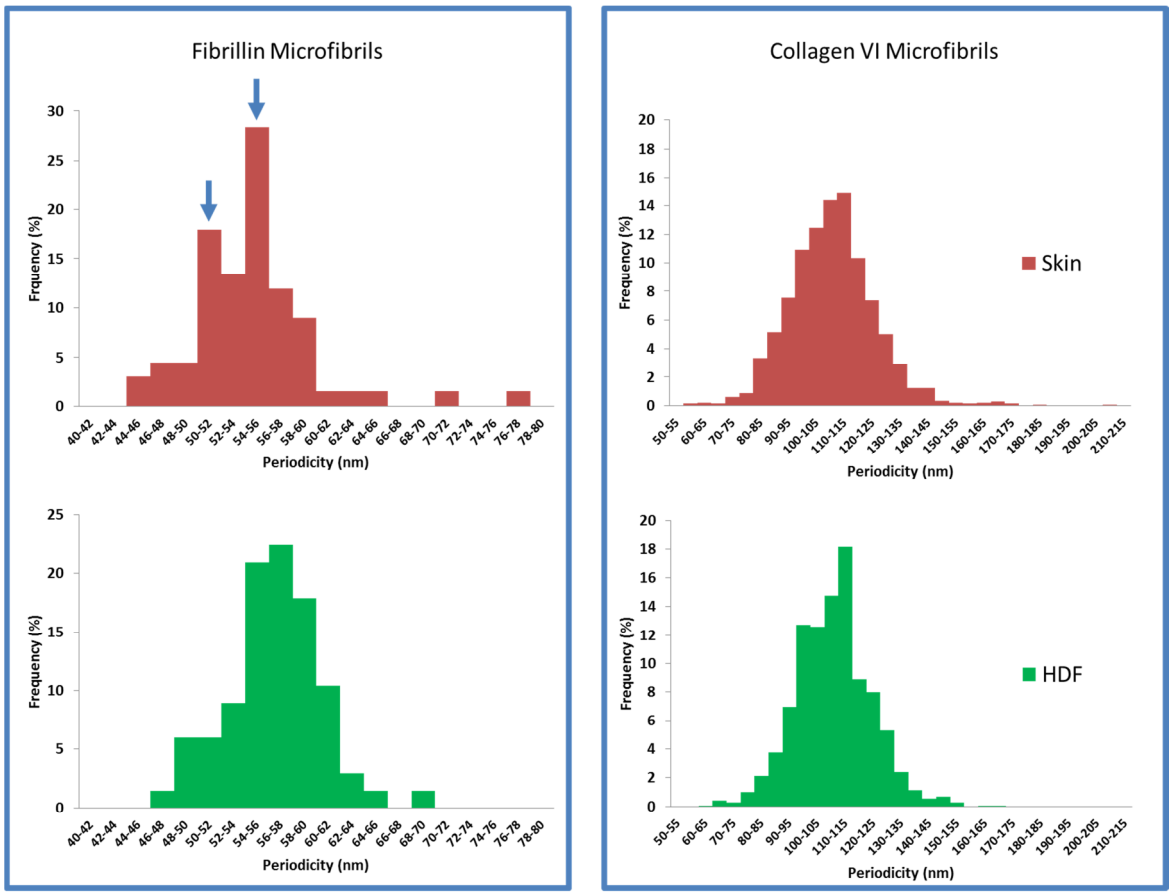

Figure 7.1: Skin-derived fibrillin microfibril periodicity exhibits a bimodal distribution. Frequency distributions were generated using fibrillin and collagen VI microfibril periodicity measurements from skin and HDF-culture isolations. Datasets were taken directly from the tissue comparison study represented previously in ***chapter 4, Figures 4.4 B and 4.6 A*** *(Eckersley* et al. *2018), and re-plotted as frequency histograms (N=3, n=1500 pooled from n=500 per individual). Periodicities of skin-derived fibrillin microfibrils appear bimodal in distribution (blue arrows), whereas HDF-derived periodicities appear unimodal. Collagen VI microfibrils periodicities, in contrast, appear unimodal in distribution regardless of whether they were sourced from skin or from HDF culture.*

The potential existence of fibrillin microfibril intra-tissue variation may also explain why LC-MS/MS-based proteomic approaches failed to effectively detect molecular photodamage to UV-irradiated skin fibrillin microfibrils **(chapter 6)**, but did so successfully in HDF-fibrillin microfibrils **(chapter 5)**. High supramolecular variability may have interfered with the ability of this approach to detect molecular scale UV-induced damage to fibrillin-1.

In contrast to fibrillin, collagen VI microfibrils do not appear to share the same degree of intra-tissue variations in structure and composition. The tissue comparison study **(chapter 4)** also showed that skin-derived collagen VI microfibrils did not differ in ultrastructure or COL6A3 structure to HDF-derived **(Fig. 4.6)**. Additionally, frequency histograms indicate that regardless of whether collagen VI microfibrils are isolated from skin or from HDFs, their periodicities remain unimodal **(Fig 7.1)**.

This may be tied to the architecture of collagen VI microfibrils in skin being relatively homogenous in comparison to that of fibrillin microfibril whose architecture exists in two states: elastic fibre associated and stand alone, oxytalan fibres.

In summary, in addition to inter-tissue diversity, this work may have also potentially revealed intra-tissue differences in fibrillin microfibril structure and composition. Interestingly, this does not seem to extend to collagen VI microfibrils, whose structures appear relatively homogenous in comparison.

7.5 Future Work

7.5.1 Bridging the gap between microfibril photodamage models and chronic photoageing

There are a number of potential future projects which could arise from, or as a continuation of, this work. Despite the success in identifying and characterising molecular-scale photodamage in UV-irradiated fibrillin microfibrils *in vitro,* these studies **(chapters 5 and 6)** fell short of bridging the gap between UV-induced damage (Hibbert *et al.* 2015; Sherratt *et al.* 2010) and chronic photoageing (Watson *et al.* 1999). This was primarily due a persistent failure to isolate sufficient microfibrils from skin biopsies (3 mm and 6 mm) for proteomic analysis. Unfortunately, this meant that the analyses performed in this work could not be applied to skin biopsies derived from photoaged forearm and photoprotected dermis; sites conventionally used to study photoageing.

Since it is likely that a large fraction of these assemblies are lost during the size-exclusion purification process, a potential solution to this problem may lay in the development of whole tissue sample preparation methods. Encouragingly, the Swift lab at the University of Manchester (Dr Joe Swift) is currently optimising new methods of protein extraction from whole murine skin. Therefore, a promising future collaboration would be to adapt these innovations to human skin. If doing so allows the sufficient yield and LC-MS/MS detection of fibrillin-1 peptides, it would successfully enable proteomic comparisons between chronically photoaged and photoprotected fibrillin microfibrils from forearm and buttock biopsies. By performing the same analyses used in this work, we could potentially compare changes in regional patterns of proteolytic susceptibility within chronically photoaged fibriilin-1 with those seen within UV-induced photodamaged fibrillin-1 **(chapters 5 and 6)**. This has the potential of elucidating a causal link between UV-induced fibrillin microfibril damage (Hibbert *et al.* 2015; Sherratt *et al.* 2010) and the loss of fibrillin microfibrils

observed during the photoageing process (Watson *et al.* 1999). As a result, it would have large implications for the skin ageing field, as this causal link has always been inferred, but never proven.

7.5.2 Gauging the effects of photodamage on microfibril-associated protein interactions

Further to our UV studies **(chapters 5 and 6)**; another promising future project may involve assessing whether UV irradiation disrupts the interactions between the microfibrils and their associated proteins. Doing so would demonstrate that UV exposure could potentially interfere with microfibril function and tissue homeostasis, providing insight into the mechanistic disruptions of the photoageing process. In the tissue comparison study **(chapter 4)**, we successfully demonstrated that fibrillin microfibrils isolated from ciliary body, skin and HDF culture had distinct compositions by showing variations in the presence of associated proteins **(Table 4.1)**, detected via LC-MS/MS. Therefore, a potential future study may include: 1) UV-irradiating fibrillin microfibrils isolated from HDF culture and skin. This would, hypothetically, disrupt the binding of associated proteins. 2) After this, re-purifying these irradiated isolations using size-exclusion chromatography, which would remove any previously-bound proteins. 3) Finally, by comparing the presence of these proteins with non-irradiated controls and consistently identifying those missing, we could deduce which interactions, and therefore which functions, are likely candidates for disruption during photoageing. Additionally, it would prove that UV has the potential to change the supramolecular composition of fibrillin microfibrils.

7.5.3 Using the proteomics to detect matrix metalloproteinase-specific damage to fibrillin microfibrils

Additional to gauging microfibril-associated protein interaction, the UV studies detailed in this work did not touch upon the effects of matrix metalloproteinase (MMP) on fibrillin microfibril degradation. In skin, the upregulation of these proteases is deeply involved in the damage of ECM components after UV-exposure (Brennan *et al.* 2003) and potentially during the photoageing process (see review: Quan *et al.* 2009). Since these enzymes are known to cleave fibrillin microfibrils (Ashworth, Murphy, *et al.* 1999), one potential future endeavour may be to characterise the peptide degradation products of MMP-digested fibrillin-1 using LC-MS/MS. Data-dependent quantification could then be used to detect significant increases of these specific peptide signatures in photoaged (forearm) and photoprotected (buttock) skin tissue. Doing so would demonstrate a direct link between the UV-induced upregulation of MMPs and ECM degradation *in vivo,* and these peptide signatures may also potentially serve as diagnostic biomarkers of excessive UV-exposure.

7.5.4 Future potential of the developed proteomic approaches

The successful characterisations of tissue-dependent differences and UV-induced molecular damage in microfibril structure was made possible through the development of novel proteomic approaches **(chapter 3)**. Future studies could use these approaches to enhance our understanding of known genetic fibrillinopathies (such as Marfan and Weill Marchesani syndromes) (Pyeritz 2000; Faivre *et al.* 2003) and collagen VI-associated pathologies (such as Belthlem and myosclerosis myopathies) (Lamandé *et al.* 1999; Merlini *et al.* 2008). These techniques have the potential to elucidate the effects of mutations on microfibril structure and composition.

Additionally, these proteomic innovations successfully allowed us to gauge regional differences in the proteolytic susceptibility of monomers from within two large supramolecular assemblies **(Figs 3.2 and 3.4)**. They also allowed the characterisation of component molecules and interactions pertinent to their compositions **(Table 3.1)**. If these approaches are able to demonstrably characterise differences in these ECM components, they can likely be applied to other large supramolecular assemblies which are difficult to characterise biochemically. One potential assembly is titin, the largest protein in the body, with a primary sequence length of 34,350 amino acids and a molecular mass of 3.8 MDa. This mega-protein is a key player in myocardial function, signalling and disease (see review: Granzier and Labeit 2004). Another potential candidate are the mucins: large glycosylated macromolecules which play a key role in the mucociliary defence of the respiratory tract, with links to asthma, chronic obstructive pulmonary diseases (COPD) and cystic fibrosis (see review: Rose and Voynow 2006). Their component isoforms range from a primary sequence length of 500 and 5500 amino acids (Uniprot). By using the developed innovations in proteomic analysis, it may be possible to characterise the structure and compositions of these assemblies and analyse potential disease-mediated changes.

7.6 Conclusion

In summary, the work showcased in this thesis has successfully addressed the four key research questions set out at the beginning of the PhD project **(thesis chapter 1.10)**: 1) We successfully improved the proteomic characterisation (fibrillin-1 coverage and associated protein detection) of isolated and purified human fibrillin microfibrils through the development of novel sample preparation methods and with advances in mass spectrometry technology; 2) We used these newly developed proteomics methods to successfully characterise tissue-specific differences in fibrillin microfibril ultrastructure, fibrillin-1 structure and molecular composition; 3) We then revealed

that UV irradiation of primary HDF-derived fibrillin microfibrils *in vitro,* causes specific changes to fibrillin-1 structure within its microfibril and finally; 4) Although validating these UV-induced changes to fibrillin-1 structure in skin-derived fibrillin microfibrils *ex vivo* was challenging, we successfully identified evidence of UV-specific peptide fingerprints which matched those shown in UV irradiated HDF microfibrils. In conclusion, this PhD successfully characterised fibrillin microfibril structural diversity and UV-induced damage. In doing so, it has made a significant contribution to the field of ECM biology and photobiology, with the prospect of future research projects arising from this endeavour.

References

Aberdam, Daniel. 2003. “Derivation of Keratinocyte Progenitor Cells and Skin Formation from Embryonic Stem Cells.” *International Journal of Developmental Biology* 48(2–3):203–6.

Abraham, Sheena, Marion J. Riggs, Kristina Nelson, Vladimir Lee, and Raj R. Rao. 2010. “Characterization of Human Fibroblast-Derived Extracellular Matrix Components for Human Pluripotent Stem Cell Propagation.” *Acta Biomaterialia* 6(12):4622–33.

Ahram, Dina, T. Shawn Sato, Abdulghani Kohilan, Marwan Tayeh, Shan Chen, Suzanne Leal, Mahmoud Al-Salem, and Hatem El-Shanti. 2009. “A Homozygous Mutation in ADAMTSL4 Causes Autosomal-Recessive Isolated Ectopia Lentis.” *The American Journal of Human Genetics* 84(2):274–78.

Aigner, Thomas, Stephan Söder, Ursula Schlötzer-Schrehardt, and Ernst Pöschl. 2002. “The C5 Domain of Col6a3 Is Cleaved off from the Col6 Fibrils Immediately after Secretion.” *Biochemical and Biophysical Research Communications* 290(2):743–48.

Alves, Rodrigo D. A. M., Jeroen A. A. Demmers, Karel Bezstarosti, Bram C. J. van der Eerden, Jan A. N. Verhaar, Marco Eijken, and Johannes P. T. M. van Leeuwen. 2011. “Unraveling the Human Bone Microenvironment beyond the Classical Extracellular Matrix Proteins: A Human Bone Protein Library.” *Journal of Proteome Research* 10(10):4725–33.

Anfinsen, Christian B. and Edgar Haber. 1961. “Studies on the Reduction and Re-Formation of Protein Disulfide Bonds.” *Journal of Biological Chemistry* 236(5):1361–63.

Antusch, Linda, Nadine Gaß, and Hans□Achim Wagenknecht. 2017. “Elucidation of the Dexter□ Type Energy Transfer in DNA by Thymine–Thymine Dimer Formation Using Photosensitizers as Artificial Nucleosides.” *Angewandte Chemie International Edition* 56(5):1385–89.

Apte, Suneel S. 2009. “A Disintegrin-like and Metalloprotease (Reprolysin-Type) with Thrombospondin Type 1 Motif (ADAMTS) Superfamily: Functions and Mechanisms.” *Journal of Biological Chemistry* 284(46):31493–97.

Ashworth, Jane L., Vicky Kelly, Richard Wilson, Adrian Shuttleworth, and Cay M. Kielty. 1999. “Fibrillin Assembly: Dimer Formation Mediated by Amino-Terminal Sequences.” *Journal of Cell Science* 112(20):3549–58.

Ashworth, Jane L., Cay M. Kielty, and David McLeod. 2000. “Fibrillin and the Eye.” *British Journal of Ophthalmology* 84(11):1312–17.

Ashworth, Jane L., Gilian Murphy, Michael J. Sherratt, Stephen D. Shapiro, Adrian Shuttleworth, and Cay M. Kielty. 1999. “Fibrillin Degradation by Matrix Metalloproteinases: Implications for Connective Tissue Remodelling.” *Biochemical Journal* 340:171–81.

Atanasova, Milena, Emiliana Konova, Tatiana Betova, and Stephan Baydanoff. 2009. “Non-Enzymatic Glycation of Human Fibrillin-1.” *Gerontology* 55(1):73–81.

Aumailley, Monique, Karlheinz Mann, Helga von der Mark, and Rupert Timpl. 1989. “Cell Attachment Properties of Collagen Type VI and Arg-Gly-Asp Dependent Binding to Its A2 (VI) and A3 (VI) Chains.” *Experimental Cell Research* 181(2):463–74.

Aumailley, Monique, Hanna Wiedemann, Karlheinz Mann, and Rupert Timpl. 1989. “Binding of Nidogen and the Laminin Nidogen Complex to Basement Membrane Collagen Type IV.” *European Journal of Biochemistry* 184(1):241–48.

Aziz, Najib, Roger Detels, Joshua J. Quint, Qian Li, David Gjertson, and Anthony W. Butch. 2016. “Stability of Cytokines, Chemokines and Soluble Activation Markers in Unprocessed Blood Stored under Different Conditions.” *Cytokine* 84:17–24.

Baldock, Clair, Abraham J. Koster, Ulrike Ziese, Matthew J. Rock, Michael J. Sherratt, Karl E. Kadler, C. Adrian Shuttleworth, and Cay M. Kielty. 2001. “The Supramolecular Organization of Fibrillin-Rich Microfibrils.” *The Journal of Cell Biology* 152(5):1045–56.

Baldock, Clair, Michael J. Sherratt, C. Adria. Shuttleworth, and Cay M. Kielty. 2003. “The

Supramolecular Organization of Collagen VI Microfibrils." *Journal of Molecular Biology* 330(2):297–307.

Baldock, Clair, Veronique Siegler, Daniel V Bax, Stuart A. Cain, Kieran T. Mellody, Andrew Marson, J. Louise Haston, Richard Berry, Ming-Chuan Wang, J. Günter Grossmann, Manfred Roessle, Cay M. Kielty, and Tim J. Wess. 2006. "Nanostructure of Fibrillin-1 Reveals Compact Conformation of EGF Arrays and Mechanism for Extensibility." *Proceedings of the National Academy of Sciences of the United States of America* 103(32):11922–27.

Baldwin, Andrew K., Stuart A. Cain, Rachel Lennon, Alan Godwin, Catherine L. R. Merry, and Cay M. Kielty. 2014. "Epithelial-Mesenchymal Status Influences How Cells Deposit Fibrillin Microfibrils." *Journal of Cell Science* 127(1):158–71.

Baldwin, Andrew K., Andreja Simpson, Ruth Steer, Stuart A. Cain, and Cay M. Kielty. 2013. "Elastic Fibres in Health and Disease." *Expert Reviews in Molecular Medicine* 15.

Barbier, Mathieu, Marie-Sylvie Gross, Mélodie Aubart, Nadine Hanna, Ketty Kessler, Dong-Chuan Guo, Laurent Tosolini, Benoit Ho-Tin-Noe, Ellen Regalado, and Mathilde Varret. 2014. "MFAP5 Loss-of-Function Mutations Underscore the Involvement of Matrix Alteration in the Pathogenesis of Familial Thoracic Aortic Aneurysms and Dissections." *The American Journal of Human Genetics* 95(6):736–43.

Bax, Daniel. V, Sarah E. Bernard, Amanda Lomas, Amanda Morgan, Jon Humphries, C. Adrian Shuttleworth, Martin J. Humphries, and Cay M. Kielty. 2003. "Cell Adhesion to Fibrillin-1 Molecules and Microfibrils Is Mediated by A5β1 and Avβ3 Integrins." *Journal of Biological Chemistry* 278(36):34605–16.

Beecher, Nicola, Alan M. Roseman, Thomas A. Jowitt, Richard Berry, Helen Troilo, Richard A. Kammerer, C. Adrian Shuttleworth, Cay M. Kielty, and Clair Baldock. 2011. "Collagen VI, Conformation of A-Domain Arrays and Microfibril Architecture." *Journal of Biological Chemistry* 286(46):40266–75.

Bensasson, Rene V, Edward J. Land, and George Truscott. 1993. *Excited States and Free Radicals in Biology and Medicine*. Tokyo.

Bernstein, Eric F., Douglas B. Brown, Frederick Urbach, Donald Forbes, Magaly Del Monaco, May Wu, Stacy D. Katchman, and Jouni Uitto. 1995. "Ultraviolet Radiation Activates the Human Elastin Promoter in Transgenic Mice: A Novel In Vivo and In Vitro Model Of Cutaneous Photoaging." *Journal Investigative Dermatology* 105(2):269–73.

Bernstein, Eric F., Yue Qiu Chen, Katsuto Tamai, Kenneth J. Shepley, Kenneth S. Resnik, Hui Zhang, Rocky Tuan, Alain Mauviel, and Jouni Uitto. 1994. "Enhanced Elastin and Fibrillin Gene Expression in Chronically Photodamaged Skin." *Journal Investigative Dermatology* 103(2):182–86.

Bhushan, Bharat, Wu Tang, and Shangying Ge. 2010. "Nanomechanical Characterization of Skin and Skin Cream." *Journal of Microscopy* 240(2):135–44.

Bidanset, Deborah J., Clyde Guidry, Lawrence C. Rosenberg, Haing U. Choi, Rupert Timpl, and Magnus Hook. 1992. "Binding of the Proteoglycan Decorin to Collagen Type VI." *Journal of Biological Chemistry* 267(8):5250–56.

Blank, Irvin H. 1952. "Factors Which Influence the Water Content of the Stratum Corneum." *Journal Investigative Dermatology* 18(6):433–40.

Bonaldo, Paolo, Paola Braghetta, Miriam Zanetti, Stefano Piccolo, Dino Volpin, and Giorgio M. Bressan. 1998. "Collagen VI Deficiency Induces Early Onset Myopathy in the Mouse: An Animal Model for Bethlem Myopathy." *Human Molecular Genetics* 7(13):2135–40.

Bonaldo, Paolo, Vincenzo Russo, Francesco Bucciotti, Roberto Doliana, and Alfonso Colombatti. 1990. "Structural and Functional Features of the. Alpha. 3 Chain Indicate a Bridging Role for Chicken Collagen VI in Connective Tissues." *Biochemistry* 29(5):1245–54.

Brennan, Meghan, Humaa Bhatti, Kamalakar C. Nerusu, Narasimharao Bhagavathula, Sewon Kang, Gary J. Fisher, James Varani, and John J. Voorhees. 2003. "Matrix Metalloproteinase 1 Is the Major Collagenolytic Enzyme Responsible for Collagen Damage in UV irradiated

Human Skin." *Photochemistry and Photobiology* 78(1):43–48.

Brenneisen, Peter, Jutta Wenk, Oliver Klotz, Meinhard Wlaschek, Karlis Briviba, Thomas Krieg, Helmut Sies, and Karin Scharffetter-Kochanek. 1998. "Central Role of Ferrous/Ferric Iron in the Ultraviolet B Irradiation-Mediated Signaling Pathway Leading to Increased Interstitial Collagenase (Matrix-Degrading Metalloprotease (MMP)-1) and Stromelysin-1 (MMP-3) MRNA Levels in Cultured Human Dermal Fibrobl." *Journal of Biological Chemistry* 273(9):5279–87.

Bressan, Giorgio M., Daniela Daga-Gordini, Alfonso Colombatti, Ines Castellani, Valeria Marigo, and Dino Volpin. 1993. "Emilin, a Component of Elastic Fibers Preferentially Located at the Elastin-Microfibrils Interface." *The Journal of Cell Biology* 121(1):201–12.

Breuza, Lionel, Sylvain Poux, Anne Estreicher, Maria Livia Famiglietti, Michele Magrane, Michael Tognolli, Alan Bridge, Delphine Baratin, and Nicole Redaschi. 2016. "The UniProtKB Guide to the Human Proteome." *Database : The Journal of Biological Databases and Curation* 2016.

Briggaman, Robert A. and Clayton E. Wheeler. 1975. "The Epidermal Dermal Junction." *Journal of Investigative Dermatology* 65(1):71–84.

Brinster, Ralph L., Serge Brunner, Xavier Joseph, and Irwin L. Levey. 1979. "Protein Degradation in the Mouse Blastocyst." *Journal of Biological Chemistry* 254(6):1927–31.

Brodsky, Barbara and Anton V. B. T. Advances in Protein Chemistry Persikov. 2005. "Molecular Structure of the Collagen Triple Helix." Pp. 301–39 in *Fibrous Proteins: Coiled-Coils, Collagen and Elastomers*. Vol. 70, edited by and J. M. S. B. T.-A. in P. C. David A. D. Parry. Academic Press.

Brown, Judith C., Karlheinz Mann, Hanna Wiedemann, and Rupert Timpl. 1993. "Structure and Binding Properties of Collagen Type XIV Isolated from Human Placenta." *The Journal of Cell Biology* 120(2):557–67.

Buckley, Michael. 2015. "Ancient Collagen Reveals Evolutionary History of the Endemic South American 'Ungulates.'" *Proceedings of the Royal Society B: Biological Sciences* 282(1806).

Bultmann-Mellin, Insa, Jeroen Essers, Paula M. van Heijingen, Harald von Melchner, Gerhard Sengle, and Anja Sterner-Kock. 2016. "Function of Ltbp-4L and Fibulin-4 in Survival and Elastogenesis in Mice." *Disease Models & Mechanisms* 9(11):1367–74.

Burd, Harvey J., Stuart J. Judge, and Mark J. Flavell. 1999. "Mechanics of Accommodation of the Human Eye." *Vision Research* 39(9):1591–95.

Burg, Michael A., Emmanuelle Tillet, Rupert Timpl, and William B. Stallcup. 1996. "Binding of the NG2 Proteoglycan to Type VI Collagen and Other Extracellular Matrix Molecules." *Journal of Biological Chemistry* 271(42):26110–16.

Burgeson, Robert E. and Angela M. Christiano. 1997. "The Dermal—epidermal Junction." *Current Opinion in Cell Biology* 9(5):651–58.

Byron, Adam, Jonathan D. Humphries, and Martin J. Humphries. 2013. "Defining the Extracellular Matrix Using Proteomics." *International Journal of Experimental Pathology* 94(2):75–92.

Cadet, Jean, Evelyne Sage, and Thierry Douki. 2005. "Ultraviolet Radiation-Mediated Damage to Cellular DNA." *Mutation Research/Fundamental and Molecular Mechanisms of Mutagenesis* 571(1–2):3–17.

Cain, Stuart A., Amanda McGovern, Elaine Small, Lyle J. Ward, Clair Baldock, Adrian Shuttleworth, and Cay M. Kielty. 2009. "Defining Elastic Fiber Interactions by Molecular Fishing: An Affinity Purification and Mass Spectrometry Approach." *Molecular & Cellular Proteomics* 8(12):2715–32.

Cain, Stuart A., Amanda Morgan, Michael J. Sherratt, Stephen G. Ball, C. Adrian Shuttleworth, and Cay M. Kielty. 2006. "Proteomic Analysis of Fibrillin-Rich Microfibrils." *Proteomics* 6(1):111–22.

Cain, Stuart A., Ewa J. Mularczyk, Mukti Singh, Teresa Massam-Wu, and Cay M. Kielty. 2016. "ADAMTS-10 and-6 Differentially Regulate Cell-Cell Junctions and Focal Adhesions."

Scientific Reports 6:35956.

Cain, Stuart A., Bertrand Raynal, Nigel Hodson, Adrian Shuttleworth, and Cay M. Kielty. 2008. "Biomolecular Analysis of Elastic Fibre Molecules." *Methods* 45(1):42–52.

Cajot, Jean-François, Jeannine Bamat, Gabriela E. Bergonzelli, Evan K. Kruithof, Robert L. Medcalf, Joëlle Testuz, and Bernard Sordat. 1990. "Plasminogen-Activator Inhibitor Type 1 Is a Potent Natural Inhibitor of Extracellular Matrix Degradation by Fibrosarcoma and Colon Carcinoma Cells." *Proceedings of the National Academy of Sciences* 87(0027-8424):6939–43.

Careri, Maria, Anthony Costa, Lisa Elviri, Jesse B. Lagos, Alessandro Mangia, Mattia Terenghi, Angela Cereti, and Perono Garoffo. 2007. "Use of Specific Peptide Biomarkers for Quantitative Confirmation of Hidden Allergenic Peanut Proteins Ara h 2 and Ara h 3/4 for Food Control by Liquid Chromatography-Tandem Mass Spectrometry." *Analytical and Bioanalytical Chemistry* 389(6):1901–7.

Carta, Luca, Lygia Pereira, Emilio Arteaga-Solis, Sui Y. Lee-Arteaga, Brett Lenart, Barry Starcher, Christian A. Merkel, Marina Sukoyan, Alexander Kerkis, and Noriko Hazeki. 2006. "Fibrillins 1 and 2 Perform Partially Overlapping Functions during Aortic Development." *Journal of Biological Chemistry* 281(12):8016–23.

Cescon, Matilde, Francesca Gattazzo, Peiwen Chen, and Paolo Bonaldo. 2015. "Collagen VI at a Glance." *Journal of Cell Science* 128(19):3525–31.

Chakraborti, Sajal, Malay Mandal, Sudip Das, Amritlal Mandal, and Tapati Chakraborti. 2003. "Regulation of Matrix Metalloproteinases. An Overview." *Molecular and Cellular Biochemistry* 253(1–2):269–85.

Chakravarti, Shukti, Terry Magnuson, Jonathan H. Lass, Karl J. Jepsen, Christian LaMantia, and Heidi Carroll. 1998. "Lumican Regulates Collagen Fibril Assembly: Skin Fragility and Corneal Opacity in the Absence of Lumican." *The Journal of Cell Biology* 141(5):1277–86.

Chang, Chia Wei, Ailsa J. Dalgliesh, Javier E. López, and Leigh G. Griffiths. 2016. "Cardiac Extracellular Matrix Proteomics: Challenges, Techniques, and Clinical Implications." *Proteomics Clinical Applications* 10(1):39–50.

Chen, Peiwen, Matilde Cescon, and Paolo Bonaldo. 2015. "Lack of Collagen VI Promotes Wound-Induced Hair Growth." *Journal of Investigative Dermatology* 135(10):2358–67.

Chen, Virginia L., Raul Fleischmajer, Elaine Schwartz, Marie Palaia, and Rupert Timpl. 1986. "Immunochemistry of Elastotic Material in Sun-Damaged Skin." *Journal Investigative Dermatology* 87(3):334–37.

Choudhury, Rawshan, Amanda McGovern, Caroline Ridley, Stuart A. Cain, Andrew Baldwin, Ming-Chuan Wang, Chun Guo, Aleksandr Mironov, Zoe Drymoussi, and Dorothy Trump. 2009. "Differential Regulation of Elastic Fiber Formation by Fibulin-4 and-5." *Journal of Biological Chemistry* 284(36):24553–67.

Chu, Mon-Li, Dorothy Conway, Te-Cheng Pan, Clinton Baldwin, Karlheinz Mann, Deutzmann, and Rupert Timpl. 1988. "Amino Acid Sequence of the Triple-Helical Domain of Human Collagen Type VI." *Journal of Biological Chemistry* 263(35):18601–6.

Chu, Mon-Li, Te-Cheng Pan, Dorothy Conway, Huey-Ju Kuo, Robert Glanville, Rupert Timpl, Karlheinz Mann, and Rainer Deutzmann. 1989. "Sequence Analysis of Alpha 1 (VI) and Alpha 2 (VI) Chains of Human Type VI Collagen Reveals Internal Triplication of Globular Domains Similar to the A Domains of von Willebrand Factor and Two Alpha 2 (VI) Chain Variants That Differ in the Carboxy Terminus." *The EMBO Journal* 8(7):1939–46.

Chu, Mon-Li, Rui-Zhu Zhang, Te-Cheng Pan, David G. Stokes, Dorothy Conway, Huey-Ju Kuo, Robert W. Glanville, Gerhard Mayer, Karlheinz Mann, and Rainer Deutzmann. 1990. "Mosaic Structure of Globular Domains in the Human Type VI Collagen Alpha 3 Chain: Similarity to von Willebrand Factor, Fibronectin, Actin, Salivary Proteins and Aprotinin Type Protease Inhibitors." *The EMBO Journal* 9(2):385–93.

Cleland, Walter. W. 1964. “Dithiothreitol, a New Protective Reagent for SH Groups” *Biochemistry* 3(4):480–82.

Collin, Gayle B., Dirk Hubmacher, Jeremy R. Charette, Wanda L. Hicks, Lisa Stone, Minzhong Yu, Jürgen K. Naggert, Mark P. Krebs, Neal S. Peachey, and Suneel S. Apte. 2015. “Disruption of Murine Adamtsl4 Results in Zonular Fiber Detachment from the Lens and in Retinal Pigment Epithelium Dedifferentiation.” *Human Molecular Genetics* 24(24):6958–74.

Colombatti, Alfonso, Roberto Doliana, Simonetta Bot, Anna Canton, Maurizio Mongiat, Gabriella Mungiguerra, Stefano Paron-Cilli, and Paola Spessotto. 2000. “The EMILIN Protein Family.” *Matrix Biology* 19(4):289–301.

Consortium, UniProt. 2016. “UniProt: The Universal Protein Knowledgebase.” *Nucleic Acids Research* 45(D1):D158–69.

Corson, Glen M., Noe L. Charbonneau, Douglas R. Keene, and Lynn Y. Sakai. 2004. “Differential Expression of Fibrillin-3 Adds to Microfibril Variety in Human and Avian, but Not Rodent, Connective Tissues.” *Genomics* 83(3):461–72.

Cotta-Pereira, Gerson, Guerra Rodrigo, and Ana S. Bittencourt-Sampaio. 1976. “Oxytalan, Elaunin, And Elastic Fibers In The Human Skin.” *Journal of Investigative Dermatology* 66(3):143–48.

Craven, Nicholas M., Rachel E. B. Watson, Carolyn J. P. Jones, Adrian Shuttleworth, Cay M. Kielty, and Christopher E. M. Griffiths. 1997. “Clinical Features of Photodamaged Human Skin Are Associated with a Reduction in Collagen VII.” *British Journal of Dermatology* 137(3):344–50.

Cutillas, Pedro R., Anthony G. W. Norden, Rainer Cramer, Alma L. Burlingame, and Robert J. Unwin. 2003. “Detection and Analysis of Urinary Peptides by On-Line Liquid Chromatography and Mass Spectrometry: Application to Patients with Renal Fanconi Syndrome.” *Clinical Science* 104(5):483–90.

Dagoneau, Nathalie, Catherine Benoist-Lasselin, Céline Huber, Laurence Faivre, André Mégarbané, Abdulrahman Alswaid, Hélène Dollfus, Yves Alembik, Arnold Munnich, and Laurence Legeai-Mallet. 2004. “ADAMTS10 Mutations in Autosomal Recessive Weill-Marchesani Syndrome.” *The American Journal of Human Genetics* 75(5):801–6.

Dahlbäck, Karin, Anne Ljungquist, Helge Löfberg, Björn Dahlbäck, Eva Engvall, and Lynn Y. Sakai. 1990. “Fibrillin Immunoreactive Fibers Constitute a Unique Network in the Human Dermis: Immunohistochemical Comparison of the Distributions of Fibrillin, Vitronectin, Amyloid P Component, and Orcein Stainable Structures in Normal Skin and Elastosis.” *Journal of Investigative Dermatology* 94(3):284–91.

Danussi, Carla, Alessandra Petrucco, Bruna Wassermann, Eliana Pivetta, Teresa Maria Elisa Modica, Lisa Del Bel Belluz, Alfonso Colombatti, and Paola Spessotto. 2011. “EMILIN1-A4/A9 Integrin Interaction Inhibits Dermal Fibroblast and Keratinocyte Proliferation.” *Journal of Cell Biology* 195(1):131–45.

Dekker, Jan, John W. A. Rossen, Hans A. Büller, and Alexandra W. C. Einerhand. 2002. “The MUC Family: An Obituary.” *Trends in Biochemical Sciences* 27(3):126–31.

Delamere, Nicholas A. 2005. “Ciliary Body and Ciliary Epithelium.” *Advances in Organ Biology* 10:127–48.

Dempsey, Edward W. and Albert I. Lansing. 1954. “Elastic Tissue.” *International Review of Cytology* 3:437–53.

Denning, Mitchell F., Yihua Wang, Brian J. Nickoloff, and Tamara Wrone-Smith. 1998. “Protein Kinase Cδ Is Activated by Caspase-Dependent Proteolysis during Ultraviolet Radiation-Induced Apoptosis of Human Keratinocytes.” *Journal of Biological Chemistry* 273(45):29995–2.

Diamandis, Eleftherios P. 2006. “Peptidomics for Cancer Diagnosis: Present and Future.” *Journal of Proteome Research* 5(9):2079–82.

Didangelos, Athanasios, Xiaoke Yin, Kaushik Mandal, Mark Baumert, Marjan Jahangiri, and

Manuel Mayr. 2010. “Proteomics Characterization of Extracellular Space Components in the Human Aorta.” *Molecular & Cellular Proteomics* 9(9):2048–62.

Dong, Chun, Joaquin M. Muriel, Sarah Ramirez, Harald Hutter, Edward M. Hedgecock, Leonid Breydo, Ilia V Baskakov, and Bruce E. Vogel. 2006. “Hemicentin Assembly in the Extracellular Matrix Is Mediated by Distinct Structural Modules.” *Journal of Biological Chemistry* 281(33):23606–10.

Doucet, Alain and Christopher M. Overall. 2011. “Broad Coverage Identification of Multiple Proteolytic Cleavage Site Sequences in Complex High Molecular Weight Proteins Using Quantitative Proteomics as a Complement to Edman Sequencing.” *Molecular & Cellular Proteomics : MCP* 10(5):1221-42.

Downing, Kristina, Vroni Knott, Jörn M. Werner, Chris M. Cardy, Iain D. Campbell, and Penny A. Handford. 1996. “Solution Structure of a Pair of Calcium-Binding Epidermal Growth Factor-like Domains: Implications for the Marfan Syndrome and Other Genetic Disorders.” *Cell* 85(4):597–605.

Dziadek, Marie, Janette S. Kazenwadel, Jaqueline A. Hendrey, Te-Cheng Pan, Rui-Zhu Zhang, and Mon-Li Chu. 2002. “Alternative Splicing of Transcripts for the Alpha3 Chain of Mouse Collagen VI: Identification of an Abundant Isoform Lacking Domains N7–N10 in Mouse and Human.” *Matrix Biology* 21(3):227–41.

Eckersley, Alexander, Kieran T. Mellody, Suzanne Pilkington, Christopher E. M. Griffiths, Rachel E. B. Watson, Ronan O’Cualain, Clair Baldock, David Knight, and Michael J. Sherratt. 2018. “Structural and Compositional Diversity of Fibrillin Microfibrils in Human Tissues.” *Journal of Biological Chemistry* 293(14):5117–33.

El-Domyati, Moetaz, Sameh Attia, Fatma Saleh, David Brown, David E. Birk, Frances Gasparro, Hecham Ahmad, and Jouni Uitto. 2002. “Intrinsic Aging vs. Photoaging: A Comparative Histopathological, Immunohistochemical, and Ultrastructural Study of Skin.” *Experimental Dermatology* 11(5):398–405.

Engvall, Eva, Helena Hessle, and George Klier. 1986. “Molecular Assembly, Secretion, and Matrix Deposition of Type VI Collagen.” *The Journal of Cell Biology* 102(3):703–10.

Erickson, Blake, Ming Fang, Joseph M. Wallace, Bradford G. Orr, Clifford M. Les, and Mark M. Banaszak Holl. 2013. “Nanoscale Structure of Type I Collagen Fibrils: Quantitative Measurement of D-spacing.” *Biotechnology Journal* 8(1):117–26.

Evanko, Stephen P., Markku I. Tammi, Raija H. Tammi, and Thomas N. Wight. 2007. “Hyaluronan-Dependent Pericellular Matrix.” *Advanced Drug Delivery Reviews* 59(13):1351–65.

Faivre, Laurence, Hélène Dollfus, Stanislas Lyonnet, Yves Alembik, André Mégarbané, John Samples, Robert J. Gorlin, Abdulrahman Alswaid, Josué Feingold, and Martine Le Merrer. 2003. “Clinical Homogeneity and Genetic Heterogeneity in Weill–Marchesani Syndrome.” *American Journal of Medical Genetics Part A* 123(2):204–7.

Fang, Ming, Elizabeth L. Goldstein, A. Simon Turner, Clifford M. Les, Bradford G. Orr, Gary J. Fisher, Kathleen B. Welch, Edward D. Rothman, and Mark M. Banaszak Holl. 2012. “Type i Collagen D-Spacing in Fibril Bundles of Dermis, Tendon, and Bone: Bridging between Nano- and Micro-Level Tissue Hierarchy.” *ACS Nano* 6(11):9503–14.

Fang, Ming, Kaitlin G. Liroff, A. Simon Turner, Clifford M. Les, Bradford G. Orr, and Mark M. Banaszak Holl. 2012. “Estrogen Depletion Results in Nanoscale Morphology Changes in Dermal Collagen.” *Journal of Investigative Dermatology* 132(7):1791–97.

Farage, Miranda A., Kenneth W. Miller, Peter Elsner, and Howard I. Maibach. 2008. “Intrinsic and Extrinsic Factors in Skin Ageing: A Review.” *International Journal of Cosmetic Science* 30(2):87–95.

Feneck, Eleanor M., Philip N. Lewis, Jim Ralphs, and Keith M. Meek. 2018. “A Comparative Study of the Elastic Fibre System within the Mouse and Human Cornea.” *Experimental Eye Research* 177:35–44.

Finnis, Merran L. and Mark A. Gibson. 1997. “Microfibril-Associated Glycoprotein-1 (MAGP-1) Binds to the Pepsin-Resistant Domain of the A3 (VI) Chain of Type VI Collagen.” *Journal of Biological Chemistry* 272(36):22817–23.

Fisher, Gary J., Subhash C. Datta, Harvinder S. Talwar, Zeng-Quan Wang, James Varani, Sewon Kang, and John J. Voorhees. 1996. “Molecular Basis of Sun-Induced Premature Skin Ageing and Retinoid Antagonism.” *Nature* 379(6563):335.

Fitzgerald, Jamie, Matthias Mörgelin, Carly Selan, Charlotte Wiberg, Douglas R. Keene, Shireen R. Lamandé, and John F. Bateman. 2001. “The N-Terminal N5 Subdomain of the A3 (VI) Chain Is Important for Collagen VI Microfibril Formation.” *Journal of Biological Chemistry* 276(1):187–93.

Fitzgerald, Jamie, Cathleen Rich, Fiona H. Zhou, and Uwe Hansen. 2008. “Three Novel Collagen VI Chains, A4 (VI), A5 (VI), and A6 (VI).” *Journal of Biological Chemistry* 283(29):20170–80.

Fleischmajer, Raul, Douglas MacDonald, Jerome S. Perlish, Robert E. Burgeson, and Larry W. Fisher. 1990. “Dermal Collagen Fibrils Are Hybrids of Type I and Type III Collagen Molecules.” *Journal of Structural Biology* 105(1–3):162–69.

Fleischmajer, Raul, Atsushi Utani, Douglas MacDonald, Jerome S. Perlish, Te-Cheng Pan, Mon-Li Chu, Motoyoshi Nomizu, Yoshifumi Ninomiya, and Yoshihiko Yamada. 1998. “Initiation of Skin Basement Membrane Formation at the Epidermo-Dermal Interface Involves Assembly of Laminins through Binding to Cell Membrane Receptors.” *Journal of Cell Science* 111(14):1929–40.

Fligiel, Suzanne E. G., James Varani, Subhash C. Datta, Sewon Kang, Gary J. Fisher, and John J. Voorhees. 2003. “Collagen Degradation in Aged/Photodamaged Skin in Vivo and after Exposure to Matrix Metalloproteinase-1 in Vitro.” *Journal of Investigative Dermatology* 120(5):842–48.

Franken, Romy, Teodora Radonic, Alexander W. den Hartog, Maarten Groenink, Gerard Pals, Marco van Eijk, Rene Lutter, Barbara J. M. Mulder, Aeilko H. Zwinderman, V. de Waard, and Maarten Groenink. 2015. “The Revised Role of TGF-beta In Aortic Aneurysms in Marfan Syndrome.” *Netherlands Heart Journal* 23(2):116–21.

Fujita, Takahiro, Eichi Tsuruga, Kaori Yamanouchi, Yoshihiko Sawa, and Hiroyuki Ishikawa. 2014. “Microfibril-Associated Glycoprotein-1 Controls Human Ciliary Zonule Development in Vitro.” *Acta Histochemica et Cytochemica* 47(1):11–17.

Furthmayr, Heinz, Hanna Wiedemann, Rupert Timpl, Erich Odermattt, and Jürgen Engel. 1983. “Electron-Microscopical Approach to a Structural Model of Intima Collagen.” *The Biochemical Journal* 211(2):303–11.

Gabriel, Luis A. R., Lauren W. Wang, Hannah Bader, Jason C. Ho, Alana K. Majors, Joe G. Hollyfield, Elias I. Traboulsi, and Suneel S. Apte. 2012. “ADAMTSL4, a Secreted Glycoprotein Widely Distributed in the Eye, Binds Fibrillin-1 Microfibrils and Accelerates Microfibril Biogenesis.” *Investigative Ophthalmology & Visual Science* 53(1):461–69.

Gara, Sudheer Kumar, Paolo Grumati, Stefano Squarzoni, Patrizia Sabatelli, Anna Urciuolo, Paolo Bonaldo, Mats Paulsson, and Raimund Wagener. 2011. “Differential and Restricted Expression of Novel Collagen VI Chains in Mouse.” *Matrix Biology* 30(4):248–57.

Gara, Sudheer Kumar, Paolo Grumati, Anna Urciuolo, Paolo Bonaldo, Birgit Kobbe, Manuel Koch, Mats Paulsson, and Raimund Wagener. 2008. “Three Novel Collagen VI Chains with High Homology to the A3 Chain.” *Journal of Biological Chemistry* 283(16):10658–70.

Garcia, Benjamin A., Mark D. Platt, Timothy L. Born, Jeffrey Shabanowitz, Norman A. Marcus, and Donald F. Hunt. 2006. “Protein Profile of Osteoarthritic Human Articular Cartilage Using Tandem Mass Spectrometry.” *Rapid Communications in Mass Spectrometry: An International Journal Devoted to the Rapid Dissemination of Up-to-the-Minute Research in Mass Spectrometry* 20(20):2999–3006.

Garhart, Christine and Vasudevan Lakshminarayanan. 2014. “Anatomy of the Eye.” *Handbook of Visual Display Technology*.

Gayraud, Barbara, Douglas R. Keene, Lynn Y. Sakai, and Francesco Ramirez. 2000. “New Insights into the Assembly of Extracellular Microfibrils from the Analysis of the Fibrillin 1 Mutation in the Tight Skin Mouse.” *The Journal of Cell Biology* 150(3):667–80.

Gelse, Kolja, Ernst Pöschl, and Thomas Aigner. 2003. “Collagens - Structure, Function, and Biosynthesis.” *Advanced Drug Delivery Reviews* 55(12):1531–46.

El Ghissassi, Fatiha, Robert Baan, Kurt Straif, Yann Grosse, Béatrice Secretan, Véronique Bouvard, Lamia Benbrahim-Tallaa, Neela Guha, Crystal Freeman, and Laurent Galichet. 2009. “A Review of Human Carcinogens—part D: Radiation.” *The Lancet Oncology* 10(8):751–52.

Giampietro, Philip F., Cathleen Raggio, and Jessica G. Davis. 2002. “Marfan Syndrome: Orthopedic and Genetic Review.” *Current Opinion in Pediatrics* 14(1):35–41.

Gibson, Mark A., Jaliya S. Kumaratilake, and Edward G. Cleary. 1989. “The Protein Components of the 12-Nanometer Microfibrils of Elastic and Nonelastic Tissues.” *Journal of Biological Chemistry* 264(8):4590–98.

Gibson, Mark A., David I. Leavesley, and Leonie K. Ashman. 1999. “Microfibril-Associated Glycoprotein-2 Specifically Interacts with a Range of Bovine and Human Cell Types via AVβ3 Integrin.” *Journal of Biological Chemistry* 274(19):13060–65.

Gingras, Anne-Claude, Ruedi Aebersold, and Brian Raught. 2005. “Advances in Protein Complex Analysis Using Mass Spectrometry.” *The Journal of Physiology* 563(Pt 1):11–21.

Godwin, Alan F., Tobias Starborg, David J. Smith, Michael J. Sherratt, Alan M. Roseman, and Clair Baldock. 2018. “Multiscale Imaging Reveals the Hierarchical Organisation of Fibrillin Microfibrils.” *Journal of Molecular Biology* 430(21):4142–55.

Godwin, Alan R. F., Tobias Starborg, Michael J. Sherratt, Alan M. Roseman, and Clair Baldock. 2017. “Defining the Hierarchical Organisation of Collagen VI Microfibrils at Nanometre to Micrometre Length Scales.” *Acta Biomaterialia* 52:21–32.

Le Goff, Carine, Fanny Morice-Picard, Nathalie Dagoneau, Lauren W. Wang, Claire Perrot, Yanick J. Crow, Florence Bauer, Elisabeth Flori, Catherine Prost-Squarcioni, and Deborah Krakow. 2008. “ADAMTSL2 Mutations in Geleophysic Dysplasia Demonstrate a Role for ADAMTS-like Proteins in TGF-β Bioavailability Regulation.” *Nature Genetics* 40(9):1119.

Goldin, Alison, Joshua A. Beckman, Ann Marie Schmidt, and Mark A. Creager. 2006. “Advanced Glycation End Products.” *Circulation* 114(6):597–605.

Goodsell, David S. 2001. “The Molecular Perspective: Ultraviolet Light and Pyrimidine Dimers.” *The Oncologist* 6(3):298–99.

Granzier, Henk L. and Siegfried Labeit. 2004. “The Giant Protein Titin a Major Player in Myocardial Mechanics, Signaling, and Disease.” *Circulation Research* 94(3):284–95.

Gregory, Kate E., Robert N. Ono, Noe L. Charbonneau, Chiu-Liang Kuo, Douglas R. Keene, Hans Peter Bächinger, and Lynn Y. Sakai. 2005. “The Prodomain of BMP-7 Targets the BMP-7 Complex to the Extracellular Matrix.” *Journal of Biological Chemistry* 280(30):27970–80.

Griffiths, Christopher E. M., Timothy S. Wang, Ted A. Hamilton, John J. Voorhees, and Charles N. Ellis. 1992. “A Photonumeric Scale for the Assessment of Cutaneous Photodamage.” *Archives of Dermatology* 128(3):347–51.

Grumati, Paolo, Luisa Coletto, Patrizia Sabatelli, Matilde Cescon, Alessia Angelin, Enrico Bertaggia, Bert Blaauw, Anna Urciuolo, Tania Tiepolo, and Luciano Merlini. 2010. “Autophagy Is Defective in Collagen VI Muscular Dystrophies, and Its Reactivation Rescues Myofiber Degeneration.” *Nature Medicine* 16(11):1313.

Handford, Penny, A. Kristina Downing, Zihe Rao, Duncan R. Hewett, Bryan C. Sykes, and Cay M. Kielty. 1995. “The Calcium Binding Properties and Molecular Organization of Epidermal Growth Factor-like Domains in Human Fibrillin-1.” *Journal of Biological Chemistry* 270(12):6751–56.

Hansen, Kirk C., Lauren Kiemele, Ori Maller, Jenean O'Brien, Aarthi Shankar, Jaime Fornetti, and Pepper Schedin. 2009. "An In-Solution Ultrasonication-Assisted Digestion Method for Improved Extracellular Matrix Proteome Coverage." *Molecular & Cellular Proteomics* 8(7):1648–57.

Hansen, Uwe, Justin M. Allen, Rachel White, Cathleen Moscibrocki, Peter Bruckner, John F. Bateman, and Jamie Fitzgerald. 2012. "WARP Interacts with Collagen VI-Containing Microfibrils in the Pericellular Matrix of Human Chondrocytes." *PloS One* 7(12).

Hansen, Uwe and Peter Bruckner. 2003. "Macromolecular Specificity of Collagen Fibrillogenesis: Fibrils of Collagens I and XI Contain a Heterotypic Alloyed Core and a Collagen I Sheath." *Journal of Biological Chemistry* 278(39):37352–59.

Hanssen, Eric, Fan Hing Hew, Emma Moore, and Mark A. Gibson. 2004. "MAGP-2 Has Multiple Binding Regions on Fibrillins and Has Covalent Periodic Association with Fibrillin-Containing Microfibrils." *Journal of Biological Chemistry* 279(28):29185–94.

Hartner, Andrea, Liliana Schaefer, Markus Porst, Nada Cordasic, Anke Gabriel, Bernd Klanke, Dieter P. Reinhardt, and Karl F. Hilgers. 2006. "Role of Fibrillin-1 in Hypertensive and Diabetic Glomerular Disease." *American Journal of Physiology-Renal Physiology* 290(6):1329–36.

Haynes, Sharon L., Adrian Shuttleworth, and Cay M. Kielty. 1997. "Keratinocytes Express Fibrillin and Assemble Microfibrils: Implications for Dermal Matrix Organization." *British Journal of Dermatology* 137(1):17–23.

Hayward, Caroline, Alison L. Rae, Mary E. M. Porteous, Lindsay J. Logie, and David J. H. Brock. 1994. "Two Novel Mutations and a Neutral Polymorphism in EGF-like Domains of the Fibrillin Gene (FBN1): SSCP Screening of Exons 15–21 in Marfan Syndrome Patients." *Human Molecular Genetics* 3(2):373–75.

Heck, Tobias, Greta Faccio, Michael Richter, and Linda Thöny-Meyer. 2013. "Enzyme-Catalyzed Protein Crosslinking." *Applied Microbiology and Biotechnology* 97(2):461–75.

Henderson, Marilyn, Roman Polewski, Joseph C. Fanning, and Mark A. Gibson. 1996. "Microfibril-Associated Glycoprotein-1 (MAGP-1) Is Specifically Located on the Beads of the Beaded-Filament Structure for Fibrillin-Containing Microfibrils as Visualized by the Rotary Shadowing Technique." *Journal of Histochemistry and Cytochemistry* 44(12):1389–97.

Hibbert, Sarah A., Patrick Costello, Clare O'Connor, Mike Bell, Christopher E. M. Griffiths, Rachel E. B. Watson, and Michael J. Sherratt. 2017. "A New in Vitro Assay to Test UVR Protection of Dermal Extracellular Matrix Components by a Flat Spectrum Sunscreen." *Journal of Photochemistry and Photobiology B: Biology* 175:58–64.

Hibbert, Sarah A., Rachel E. B. Watson, Neil K. Gibbs, Patrick Costello, Clair Baldock, Anthony S. Weiss, Christopher E. M. Griffiths, and Michael J. Sherratt. 2015. "A Potential Role for Endogenous Proteins as Sacrificial Sunscreens and Antioxidants in Human Tissues." *Redox Biology* 5:101–13.

Hirai, Maretoshi, Masahito Horiguchi, Tetsuya Ohbayashi, Toru Kita, Kenneth R. Chien, and Tomoyuki Nakamura. 2007. "Latent TGF-β-binding Protein 2 Binds to DANCE/Fibulin-5 and Regulates Elastic Fiber Assembly." *The EMBO Journal* 26(14):3283–95.

Hirani, Rena, Eric Hanssen, and Mark A. Gibson. 2007. "LTBP-2 Specifically Interacts with the Amino-Terminal Region of Fibrillin-1 and Competes with LTBP-1 for Binding to This Microfibrillar Protein." *Matrix Biology* 26(4):213–23.

Hiraoka, Mari, Ken-Ichi Inoue, Chiaki Ohtaka-Maruyama, Shunji Ohsako, Naosuke Kojima, Haruki Senoo, and Masahiko Takada. 2010. "Intracapsular Organization of Ciliary Zonules in Monkey Eyes." *The Anatomical Record* 293(10):1797–1804.

Hoch, Werner, James T. Campanelli, Sheree Harrison, and Richard H. Scheller. 1994. "Structural Domains of Agrin Required for Clustering of Nicotinic Acetylcholine Receptors." *The EMBO Journal* 13(12):2814–21.

Hogan, Michael J., Jorge A. Alvarado, and John E. Weddell. 1971. "Histology Ofthe Human Eye."

Philadelphia, WB Saunders Co 328–63.

Holt, Kathleen H. and Kevin P. Campbell. 1998. "Assembly of the Sarcoglycan Complex Insights for Muscular Dystrophy." *Journal of Biological Chemistry* 273(52):34667–70.

Hönigsmann, Herbert. 2002. "Erythema and Pigmentation." *Photodermatology, Photoimmunology & Photomedicine* 18(2):75–81.

Horcas, Ignacio, Rodrigo. Fernández, Jose M. Gómez-Rodríguez, Jaime. Colchero, Julio Gómez-Herrero, and Arturo M. Baro. 2007. "WSXM: A Software for Scanning Probe Microscopy and a Tool for Nanotechnology." *Review of Scientific Instruments* 78(1).

Horiguchi, Masahito, Tadashi Inoue, Tetsuya Ohbayashi, Maretoshi Hirai, Kazuo Noda, Lihua Y. Marmorstein, Daisuke Yabe, Kyoko Takagi, Tomoya O. Akama, and Toru Kita. 2009. "Fibulin-4 Conducts Proper Elastogenesis via Interaction with Cross-Linking Enzyme Lysyl Oxidase." *Proceedings of the National Academy of Sciences* 106(45):19029–34.

Hubmacher, Dirk and Suneel S. Apte. 2015. "ADAMTS Proteins as Modulators of Microfibril Formation and Function." *Matrix Biology* 47:34–43.

Hunter, John A. A., Eva Mcvittie, and Jacob S. Comaish. 1974. "Light and Electron Microscopic Studies of Physical Injury to the Skin II. Friction." *British Journal of Dermatology* 90(5):491–99.

Hunzelmann, Nicolas, Roswitha Nischt, Peter Brenneisen, Astrid Eickert, and Thomas Krieg. 2001. "Increased Deposition of Fibulin-2 in Solar Elastosis and Its Colocalization with Elastic Fibres." *British Journal of Dermatology* 145(2):217–22.

Hustoft, Hanne Kolsrud, Helle Malerod, Steven Ray Wilson, Leon Reubsaet, Elsa Lundanes, and Tyge Greibrokk. 2012. "A Critical Review of Trypsin Digestion for LC-MS Based Proteomics." in *Integrative Proteomics*.

Hynes, Richard O. and Alexandra Naba. 2012. "Overview of the Matrisome-An Inventory of Extracellular Matrix Constituents and Functions." *Cold Spring Harbor Perspectives in Biology* 4(1).

Imanishi, Nobuaki, Kazuo Kishi, Hak Chang, Hideo Nakajima, and Sadakazu Aiso. 2008. "Three-Dimensional Venous Anatomy of the Dermis Observed Using Stereography." *Journal of Anatomy* 212(5):669–73.

Inoue, Tadashi, Tetsuya Ohbayashi, Yusuke Fujikawa, Hideyuki Yoshida, Tomoya O. Akama, Kazuo Noda, Masahito Horiguchi, Katsuro Kameyama, Yoshio Hata, and Kanji Takahashi. 2014. "Latent TGF-β Binding Protein-2 Is Essential for the Development of Ciliary Zonule Microfibrils." *Human Molecular Genetics* 23(21):5672–82.

Irwin, William A., Natascha Bergamin, Patrizia Sabatelli, Carlo Reggiani, Aram Megighian, Luciano Merlini, Paola Braghetta, Marta Columbaro, Dino Volpin, and Giorgio M. Bressan. 2003. "Mitochondrial Dysfunction and Apoptosis in Myopathic Mice with Collagen VI Deficiency." *Nature Genetics* 35(4):367–71.

Isogai, Zenzo, Anders Aspberg, Douglas R. Keene, Robert N. Ono, Dieter P. Reinhardt, and Lynn Y. Sakai. 2002. "Versican Interacts with Fibrillin-1 and Links Extracellular Microfibrils to Other Connective Tissue Networks." *Journal of Biological Chemistry* 277(6):4565–72.

Isogai, Zenzo, Robert N. Ono, Shin Ushiro, Douglas R. Keene, Yan Chen, Roberta Mazzieri, Noe L. Charbonneau, Dieter P. Reinhardt, Daniel B. Rifkin, and Lynn Y. Sakai. 2003. "Latent Transforming Growth Factor β-Binding Protein 1 Interacts with Fibrillin and Is a Microfibril-Associated Protein." *Journal of Biological Chemistry* 278(4):2750–57.

Itri, Francesco, Daria M. Monti, Bartolomeo Della Ventura, Roberto Vinciguerra, Marco Chino, Felice Gesuele, Angelina Lombardi, Raffaele Velotta, Carlo Altucci, and Leila Birolo. 2016. "Femtosecond UV-Laser Pulses to Unveil Protein–protein Interactions in Living Cells." *Cellular and Molecular Life Sciences* 73(3):637–48.

Ivaska, Johanna, Hanna-Mari Pallari, Jonna Nevo, and John E. Eriksson. 2007. "Novel Functions of Vimentin in Cell Adhesion, Migration, and Signaling." *Experimental Cell Research*

313(10):2050–62.

Jacob, Soosan and Preethi Naveen. 2016. “Anatomy of the Cornea.” Pp. 1–11 in *Mastering Endothelial Keratoplasty*. Springer.

Jensen, Sacha A., Georgia Aspinall, and Penny A. Handford. 2014. “C-Terminal Propeptide Is Required for Fibrillin-1 Secretion and Blocks Premature Assembly through Linkage to Domains CbEGF41-43.” *Proceedings of the National Academy of Sciences* 111(28):10155–60.

Jensen, Sacha A. and Penny A. Handford. 2016. “New Insights into the Structure, Assembly and Biological Roles of 10–12 Nm Connective Tissue Microfibrils from Fibrillin-1 Studies.” *Biochemical Journal* 473(7):827-47.

Jensen, Sacha A., Sarah Iqbal, Edward D. Lowe, Christina Redfield, and Penny A. Handford. 2009. “Structure and Interdomain Interactions of a Hybrid Domain: A Disulphide-Rich Module of the Fibrillin/LTBP Superfamily of Matrix Proteins.” *Structure* 17(5):759–68.

Jensen, Sacha A., Dieter P. Reinhardt, Mark A. Gibson, and Anthony S. Weiss. 2001. “Protein Interaction Studies of MAGP-1 with Tropoelastin and Fibrillin-1.” *Journal of Biological Chemistry* 276(43):39661–66.

Jensen, Sacha A., Ian B. Robertson, and Penny A. Handford. 2012. “Dissecting the Fibrillin Microfibril: Structural Insights into Organization and Function.” *Structure* 20(2):215–25.

Kaartinen, Vesa and David Warburton. 2003. “Fibrillin Controls TGF-β Activation.” *Nature Genetics* 33(3):331–32.

Kadler, Karl E., Clair Baldock, Jordi Bella, and Raymond P. Boot-Handford. 2007. “Collagens at a Glance.” *Journal of Cell Biology* 120(12):1955–58.

Kadoya, Kuniko, Takako Sasaki, Günter Kostka, Rupert Timpl, Kyoichi Matsuzaki, Norio Kumagai, Lynn Y. Sakai, Tetsuo Nishiyama, and Satoshi Amano. 2005. “Fibulin-5 Deposition in Human Skin: Decrease with Ageing and Ultraviolet B Exposure and Increase in Solar Elastosis.” *British Journal of Dermatology* 153(3):607–12.

Kainulainen, Katariina, Leena Karttunen, Lea Puhakka, Lynn Sakai, and Leena Peltonen. 1994. “Mutations in the Fibrillin Gene Responsible for Dominant Ectopia Lentis and Neonatal Marfan Syndrome.” *Nature Genetics* 6(1):64.

Al Kaissi, Ali, Elisabeth Zwettler, Rudolf Ganger, Simone Schreiner, Klaus Klaushofer, and Franz Grill. 2013. “Musculo-Skeletal Abnormalities in Patients with Marfan Syndrome.” *Clinical Medicine Insights: Arthritis and Musculoskeletal Disorders* 6:1–9.

Kalkhof, Stefan, Sebastian Haehn, Christian Ihling, Mats Paulsson, Neil Smyth, and Andrea Sinz. 2008. “Determination of Disulfide Bond Patterns in Laminin B1 Chain N-terminal Domains by Nano-high-performance Liquid Chromatography/Matrix-assisted Laser Desorption/Ionization Time-of-flight/Time-of-flight Mass Spectrometry.” *Rapid Communications in Mass Spectrometry: An International Journal Devoted to the Rapid Dissemination of Up-to-the-Minute Research in Mass Spectrometry* 22(12):1933–40.

Kao, Alexander P., John T. Connelly, and Asa H. Barber. 2016. “3D Nanomechanical Evaluations of Dermal Structures in Skin.” *Journal of the Mechanical Behavior of Biomedical Materials* 57:14–23.

Keller, Andrew, Alexey I. Nesvizhskii, Eugene Kolker, and Ruedi Aebersold. 2002. “Empirical Statistical Model to Estimate the Accuracy of Peptide Identifications Made by MS/MS and Database Search.” *Analytical Chemistry* 74(20):5383–92.

Keski-Oja, Jorma. 1976. “Polymerization of a Major Surface-associated Glycoprotein, Fibronectin, in Cultured Fibroblasts.” *FEBS Letters* 71(2):325–29.

Kettle, Susan, Xuemei Yuan, Gabrielle Grundy, Vroni Knott, A. Kristin. Downing, and Penny A. Handford. 1999. “Defective Calcium Binding to Fibrillin-1: Consequence of an N2144S Change for Fibrillin-1 Structure and Function.” *Journal of Molecular Biology* 285(3):1277–87.

Khan, Arif O., Mohammed A. Aldahmesh, and Fowzan S. Alkuraya. 2011. “Congenital Megalocornea with Zonular Weakness and Childhood Lens-Related Secondary Glaucoma-a Distinct Phenotype Caused by Recessive LTBP2 Mutations.” *Molecular Vision* 17:2570.

Kielty, Cay M., Clair Baldock, David Lee, Matthew J. Rock, Jane L. Ashworth, and C. Adrian Shuttleworth. 2002. “Fibrillin: From Microfibril Assembly to Biomechanical Function.” *Philosophical Transactions of the Royal Society of London B: Biological Sciences* 357(1418):207–17.

Kielty, Cay M., Linda Berry, Stephen P. Whittaker, Michael E. Grant, and C. Adrian Shuttleworth. 1993. “Microfibrillar Assemblies of Foetal Bovine Skin: Developmental Expression and Relative Abundance of Type VI Collagen and Fibrillin.” *Matrix* 13(2):103–12.

Kielty, Cay M., Christine Cummings, Stephen P. Whittaker, C. Adrian Shuttleworth, and Michael E. Grant. 1991. “Isolation and Ultrastructural Analysis of Microfibrillar Structures from Foetal Bovine Elastic Tissues. Relative Abundance and Supramolecular Architecture of Type VI Collagen Assemblies and Fibrillin.” *Journal of Cell Science* 99(4):797–807.

Kielty, Cay M., Sally J. Davies, Janet E. Phillips, C. J. Jones, C. Adrian Shuttleworth, and Stephen J. Charles. 1995. “Marfan Syndrome: Fibrillin Expression and Microfibrillar Abnormalities in a Family with Predominant Ocular Defects.” *Journal of Medical Genetics* 32(1):1–6.

Kielty, Cay M., Eric Hanssen, and C. Adrian Shuttleworth. 1998. “Purification of Fibrillin-Containing Microfibrils and Collagen VI Microfibrils by Density Gradient Centrifugation.” *Analytical Biochemistry* 255(1):108–12.

Kielty, Cay M., Michael Raghunath, Linda D. Siracusa, Michael J. Sherratt, Reiner Peters, C. Adrian Shuttleworth, and Sergio A. Jimenez. 1998. “The Tight Skin Mouse: Demonstration of Mutant Fibrillin-1 Production and Assembly into Abnormal Microfibrils.” *The Journal of Cell Biology* 140(5):1159–66.

Kielty, Cay M., Michael J. Sherratt, Andrew Marson, and Clair Baldock. 2005. “Fibrillin Microfibrils.” *Advances in Protein Chemistry* 70:405–36.

Kielty, Cay M., Michael J. Sherratt, and C. Adrian Shuttleworth. 2002. “Elastic Fibres.” *Journal of Cell Science* 115(14):2817–28.

Kielty, Cay M. and C. Adria. Shuttleworth. 1993. “The Role of Calcium in the Organization of Fibrillin Microfibrils.” *FEBS Letters* 336(2):323–26.

Kinsey, Rachel, Matthew R. Williamson, Shazia Chaudhry, Kieran T. Mellody, Amanda McGovern, Seiichiro Takahashi, C. Adrian Shuttleworth, and Cay M. Kielty. 2008. “Fibrillin-1 Microfibril Deposition Is Dependent on Fibronectin Assembly.” *Journal of Cell Science* 121(16):2696–2704.

Kirkwood, Thomas B. L. 2008. “A Systematic Look at an Old Problem.” *Nature* 451(7179):644–47.

Kirsch, Thorsten, Gerald Harrison, Ellis E. Golub, and Hyun-Duck Nah. 2000. “The Roles of Annexins and Types II and X Collagen in Matrix Vesicle-Mediated Mineralization of Growth Plate Cartilage.” *Journal of Biological Chemistry* 275(45):35577–83.

Kirschner, Ryan, Dirk Hubmacher, Garud Iyengar, Jasvir Kaur, Christine Fagotto-Kaufmann, Dieter Bromme, Rainer Bartels, and Dieter P. Reinhardt. 2011. “Classical and Neonatal Marfan Syndrome Mutations in Fibrillin-1 Cause Differential Protease Susceptibilities and Protein Function.” *Journal of Biological Chemistry* 286:32810–23.

Kobayashi, Naoyuki, Günter Kostka, Jörg H. O. Garbe, Douglas R. Keene, Hans Peter Bächinger, Franz-Georg Hanisch, Dessislava Markova, Takeshi Tsuda, Rupert Timpl, and Mon-Li Chu. 2007. “A Comparative Analysis of the Fibulin Protein Family Biochemical Characterization, Binding Interactions, and Tissue Localization.” *Journal of Biological Chemistry* 282(16):11805–16.

Kocsis, Eva, Benes L. Trus, Clifford J. Steer, Margaret E. Bisher, and Alasdair C. Steven. 1991. “Image Averaging of Flexible Fibrous Macromolecules: The Clathrin Triskelion Has an Elastic Proximal Segment.” *Journal of Structural Biology* 107(1):6–14.

Kömüves, László G., Karen Hanley, Anne-Marie Lefebvre, Mao-Qiang Man, Dean C. Ng, Daniel D. Bikle, Mary L. Williams, Peter M. Elias, Johan Auwerx, and Kenneth R. Feingold. 2000. "Stimulation of PPARα Promotes Epidermal Keratinocyte Differentiation in Vivo." *Journal of Investigative Dermatology* 115(3):353–60.

Kuehl, LeRoy and Earl N. Sumsion. 1970. "Turnover of Several Glycolytic Enzymes in Rat Liver." *Journal of Biological Chemistry* 245(24):6616–23.

Kuo, Chiu-Liang, Zenzo Isogai, Douglas R. Keene, Noriko Hazeki, Robert N. Ono, Gerhard Sengle, Hans Peter Bächinger, and Lynn Y. Sakai. 2007. "Effects of Fibrillin-1 Degradation on Microfibril Ultrastructure." *Journal of Biological Chemistry* 282(6):4007–20.

Kuo, Huey-Ju, Cheryl L. Maslen, Douglas R. Keene, and Robert W. Glanville. 1997. "Type VI Collagen Anchors Endothelial Basement Membranes by Interacting with Type IV Collagen." *Journal of Biological Chemistry* 272(42):26522–29.

Kutz, Wendy E., Lauren W. Wang, Hannah L. Bader, Alana K. Majors, Kazushi Iwata, Elias I. Traboulsi, Lynn Y. Sakai, Douglas R. Keene, and Suneel S. Apte. 2011. "ADAMTS10 Protein Interacts with Fibrillin-1 and Promotes Its Deposition in Extracellular Matrix of Cultured Fibroblasts." *Journal of Biological Chemistry* 286(19):17156–67.

Lack, Jeremy, Joanne M. O'Leary, Vroni Knott, Xuemei Yuan, Daniel B. Rifkin, Penny A. Handford, and A. Kristin. Downing. 2003. "Solution Structure of the Third TB Domain from LTBP1 Provides Insight into Assembly of the Large Latent Complex That Sequesters Latent TGF-β." *Journal of Molecular Biology* 334(2):281–91.

Lamandé, Shireen R., Matthias Mörgelin, Naomi E. Adams, Carly Selan, and Justin M. Allen. 2006. "The C5 Domain of the Collagen VI A3(VI) Chain Is Critical for Extracellular Microfibril Formation and Is Present in the Extracellular Matrix of Cultured Cells." *Journal of Biological Chemistry* 281(24):16607–14.

Lamandé, Shireen R., Matthias Mörgelin, Carly Selan, G. Joost Jöbsis, Frank Baas, and John F. Bateman. 2002. "Kinked Collagen VI Tetramers and Reduced Microfibril Formation as a Result of Bethlem Myopathy and Introduced Triple Helical Glycine Mutations." *Journal of Biological Chemistry* 277(3):1949–56.

Lamandé, Shireen R., Katherine A. Shields, Andrew J. Kornberg, Lloyd K. Shield, and John F. Bateman. 1999. "Bethlem Myopathy and Engineered Collagen VI Triple Helical Deletions Prevent Intracellular Multimer Assembly and Protein Secretion." *Journal of Biological Chemistry* 274(31):21817–22.

Lamme, Evert N., Henry J. C. De Vries, Henk Van Veen, Giulio Gabbiani, Wiete Westerhof, and Esther Middelkoop. 1996. "Extracellular Matrix Characterization during Healing of Full-Thickness Wounds Treated with a Collagen/Elastin Dermal Substitute Shows Improved Skin Regeneration in Pigs." *Journal of Histochemistry and Cytochemistry* 44(11):1311–22.

Langton, Abigail K., Helen K. Graham, James C. McConnell, Michael J. Sherratt, Christopher E. M. Griffiths, and Rachel E. B. Watson. 2017. "Organization of the Dermal Matrix Impacts the Biomechanical Properties of Skin." *British Journal of Dermatology* 177(3):818–27.

Langton, Abigail K., Michael J. Sherratt, Christopher E. M. Griffiths, and Rachel E. B. Watson. 2010. "A New Wrinkle on Old Skin: The Role of Elastic Fibres in Skin Ageing." *International Journal of Cosmetic Science* 32(5):330–39.

Lanshoeft, Christian, Olivier Heudi, and Sarah Cianférani. 2016. "SMART Digest™ Compared with Pellet Digestion for Analysis of Human Immunoglobulin G1 in Rat Serum by Liquid Chromatography Tandem Mass Spectrometry." *Analytical Biochemistry* 501:23–25.

Lee, Jin Young, Yeon Kyung Kim, Jin Young Seo, Chong Won Choi, Jae Sung Hwang, Byeong Gon Lee, Ih Seop Chang, and Jin Ho Chung. 2008. "Loss of Elastic Fibers Causes Skin Wrinkles in Sun-Damaged Human Skin." *Journal of Dermatological Science* 50(2):99–107.

Lee, Stephen S. J., Vroni Knott, Jelena Jovanović, Karl Harlos, Jonathan M. Grimes, Laurence Choulier, Helen J. Mardon, David I. Stuart, and Penny A. Handford. 2004. "Structure of the Integrin Binding Fragment from Fibrillin-1 Gives New Insights into Microfibril Organization."

Structure 12(4):717–29.

Lemaire, Raphael, Julie Bayle, and Robert Lafyatis. 2006. “Fibrillin in Marfan Syndrome and Tight Skin Mice Provides New Insights into Transforming Growth Factor Beta Regulation and Systemic Sclerosis.” *Current Opinion in Rheumatology* 18(6):582–87.

Lemaire, Raphael, Julie Bayle, Robert P. Mecham, and Robert Lafyatis. 2007. “Microfibril-Associated MAGP-2 Stimulates Elastic Fiber Assembly.” *Journal of Biological Chemistry* 282(1):800–808.

Lennon, Rachel, Adam Byron, Jonathan D. Humphries, Michael J. Randles, Alex Carisey, Stephanie Murphy, David Knight, Paul E. Brenchley, Roy Zent, and Martin J. Humphries. 2014. “Global Analysis Reveals the Complexity of the Human Glomerular Extracellular Matrix.” *Journal of the American Society of Nephrology : JASN* 1–13.

Link, Andrew J., Jimmy Eng, David M. Schieltz, Edwin Carmack, Gregory J. Mize, David R. Morris, Barbara M. Garvik, and John R. Yates. 1999. “Direct Analysis of Protein Complexes Using Mass Spectrometry.” *Nature Biotechnology* 17(7):676–82.

Liu, Anguo, Pallavi Garg, Shiqi Yang, Ping Gong, Manuel A. Pallero, Douglas S. Annis, Yuanyuan Liu, Antonino Passaniti, Dean Mann, and Deane F. Mosher. 2009. “Epidermal Growth Factor-like Repeats of Thrombospondins Activate Phospholipase Cγ and Increase Epithelial Cell Migration through Indirect Epidermal Growth Factor Receptor Activation.” *Journal of Biological Chemistry* 284(10):6389–6402.

Liu, Xiaoqing, Yun Zhao, Jiangang Gao, Basil Pawlyk, Barry Starcher, Jeffrey A. Spencer, Hiromi Yanagisawa, Jian Zuo, and Tiansen Li. 2004. “Elastic Fiber Homeostasis Requires Lysyl Oxidase–like 1 Protein.” *Nature Genetics* 36(2):178.

Long, Jennifer L. and Robert T. Tranquillo. 2003. “Elastic Fiber Production in Cardiovascular Tissue-Equivalents.” *Matrix Biology* 22(4):339–50.

Lonnqvist, Lasse, Dieter P. Reinhardt, Lynn Y. Sakai, and Leena Peltonen. 1998. “Evidence for Furin-Type Activity-Mediated C-Terminal Processing of Profibrillin-1 and Interference in the Processing by Certain Mutations.” *Human Molecular Genetics* 7(13):2039–44.

Loo, Joseph A., Charles G. Edmonds, Harold R. Udseth, and Richard D. Smith. 1990. “Effect of Reducing Disulfide-Containing Proteins on Electrospray Ionization Mass Spectra.” *Analytical Chemistry* 62(7):693–98.

Lorand, Laszlo and Robert M. Graham. 2003. “Transglutaminases: Crosslinking Enzymes with Pleiotropic Functions.” *Nature Reviews Molecular Cell Biology* 4(2):140–56.

Lu, Yinhui, Michael J. Sherratt, Ming Chuan Wang, and Clair Baldock. 2006. “Tissue Specific Differences in Fibrillin Microfibrils Analysed Using Single Particle Image Analysis.” *Journal of Structural Biology* 155(2):285–93.

Lundgren, Deborah H., Sun-Il Hwang, Linfeng Wu, and David K. Han. 2010. “Role of Spectral Counting in Quantitative Proteomics.” *Expert Review of Proteomics* 7(1):39–53.

Maaß, Tobias, Christopher P. Bayley, Matthias Mörgelin, Sandra Lettmann, Paolo Bonaldo, Mats Paulsson, Clair Baldock, and Raimund Wagener. 2016. “Heterogeneity of Collagen VI Microfibrils: Structural Analysis of Non-Collagenousregions.” *Journal of Biological Chemistry* 291(10):5247–58.

De Maria, Alicia, Phillip A. Wilmarth, Larry L. David, and Steven Bassnett. 2017. “Proteomic Analysis of the Bovine and Human Ciliary ZonuleProteomic Analysis of the Ciliary Zonule.” *Investigative Ophthalmology & Visual Science* 58(1):573–85.

Mariencheck, Maria C., Elaine C. Davis, Hui Zhang, Francesco Ramirez, Joel Rosenbloom, Mark A. Gibson, William C. Parks, and Robert P. Mecham. 1995. “Fibrillin-1 and Fibrillin-2 Show Temporal and Tissue-Specific Regulation of Expression in Developing Elastic Tissues.” *Connective Tissue Research* 31(2):87–97.

Marson, Andrew, Matthew J. Rock, Stuart A. Cain, Lyle J. Freeman, Amanda Morgan, Kieran Mellody, C. Adrian Shuttleworth, Clair Baldock, and Cay M. Kielty. 2005. “Homotypic Fibrillin-

1 Interactions in Microfibril Assembly." *Journal of Biological Chemistry* 280(6):5013–21.

Martoni, Elena, Anna Urciuolo, Patrizia Sabatelli, Marina Fabris, Matteo Bovolenta, Marcella Neri, Paolo Grumati, Adele D'amico, Marika Pane, and Eugenio Mercuri. 2009. "Identification and Characterization of Novel Collagen VI Non-canonical Splicing Mutations Causing Ullrich Congenital Muscular Dystrophy." *Human Mutation* 30(5):E662–72.

Massagué, Joan. 1998. "TGF-β Signal Transduction." *Annual Review of Biochemistry* 67(1):753–91.

McDougall, Steven, John Dallon, Jonathan Sherratt, and Philip Maini. 2006. "Fibroblast Migration and Collagen Deposition during Dermal Wound Healing: Mathematical Modelling and Clinical Implications." *Philosophical Transactions. Series A, Mathematical, Physical, and Engineering Sciences* 364(1843):1385–1405.

McGrath, John A., Biljana Gatalica, Angela M. Christiano, Katsushi Owaribe, James R. McMillan, Robin A. J. Eady, and Jouni Uitto. 1995. "Mutations in the 180–kD Bullous Pemphigoid Antigen (BPAG2), a Hemidesmosomal Transmembrane Collagen (COL17A1), in Generalized Atrophic Benign Epidermolysis Bullosa." *Nature Genetics* 11(1):83.

McIntosh, Jamie, Godwin Dennison, Jeff M. P. Holly, Caroline Jarrett, Alexandra Frankow, Emily J. Foulstone, Zoe E. Winters, and Claire M. Perks. 2010. "IGFBP-3 Can Either Inhibit or Enhance EGF-Mediated Growth of Breast Epithelial Cells Dependent upon the Presence of Fibronectin." *Journal of Biological Chemistry* 285(50):38788–800.

McKenzie, Richard, Dan Smale, and Michael Kotkamp. 2004. "Relationship between UVB and Erythemally Weighted Radiation." *Photochemical & Photobiological Sciences* 3(3):252–56.

McLaughlin, Precious J., Qiuyun Chen, Masahito Horiguchi, Barry C. Starcher, J. Brett Stanton, Thomas J. Broekelmann, Alan D. Marmorstein, Brian McKay, Robert Mecham, and Tomoyuki Nakamura. 2006. "Targeted Disruption of Fibulin-4 Abolishes Elastogenesis and Causes Perinatal Lethality in Mice." *Molecular and Cellular Biology* 26(5):1700–1709.

Medzihradszky, Katalin F. 2005. "In-solution Digestion of Proteins for Mass Spectrometry." *Methods in Enzymology* 405:50–65.

Meirelles, Thayna, Thaís L. S. Araujo, Patrícia Nolasco, Ana I. S. Moretti, Maria C. Guido, Victor Debbas, Lygia V Pereira, and Francisco R. Laurindo. 2016. "Fibrillin-1 MgΔ Lpn Marfan Syndrome Mutation Associates with Preserved Proteostasis and Bypass of a Protein Disulfide Isomerase-Dependent Quality Checkpoint." *The International Journal of Biochemistry & Cell Biology* 71:81–91.

Menter, Julian M., L. M. Cornelison, L. Cannick, A. M. Patta, J. C. Dowdy, R. M. Sayre, I. K. Abukhalaf, N. S. Silvestrov, and I. Willis. 2003. "Effect of UV on the Susceptibility of Acid-Soluble Skh-1 Hairless Mouse Collagen to Collagenase." *Photodermatology Photoimmunology and Photomedicine* 19(1):28–34.

Merlini, Luciano, Elena Martoni, Paolo Grumati, Patrizia Sabatelli, Stefano Squarzoni, Anna Urciuolo, Andea Ferlini, Francesco Gualandi, and Paolo Bonaldo. 2008. "Autosomal Recessive Myosclerosis Myopathy Is a Collagen VI Disorder." *Neurology* 71(16):1245–53.

Mikesh, Leann M., Lavakumar Reddy Aramadhaka, Christopher Moskaluk, Paola Zigrino, Cornelia Mauch, and Jay W. Fox. 2013. "Proteomic Anatomy of Human Skin." *Journal of Proteomics* 84:190–200.

Milewicz, Dianna M., Reed E. Pyeritz, E. Stanley Crawford, and Peter H. Byers. 1992. "Marfan Syndrome: Defective Synthesis, Secretion, and Extracellular Matrix Formation of Fibrillin by Cultured Dermal Fibroblasts." *The Journal of Clinical Investigation* 89(1):79–86.

Mitchell, Ruth E. 1967. "Chronic Solar Dermatosis: A Light and Electron Microscopic Study of the Dermis." *Journal of Investigative Dermatology* 48(3):203–20.

Mongiat, Maurizio, Giovanni Ligresti, Stefano Marastoni, Erica Lorenzon, Roberto Doliana, and Alfonso Colombatti. 2007. "Regulation of the Extrinsic Apoptotic Pathway by the Extracellular Matrix Glycoprotein EMILIN2." *Molecular and Cellular Biology* 27(20):7176–87.

Mongiat, Maurizio, Stefano Marastoni, Giovanni Ligresti, Erica Lorenzon, Monica Schiappacassi, Roberto Perris, Sergio Frustaci, and Alfonso Colombatti. 2010. “The Extracellular Matrix Glycoprotein Elastin Microfibril Interface Located Protein 2: A Dual Role in the Tumor Microenvironment.” *Neoplasia* 12(4):294–306.

Montagna, William, Sam Kirchner, and Kay Carlisle. 1989. “Histology of Sun-Damaged Human Skin.” *Journal of the American Academy of Dermatology* 21(5 Pt 1):907–18.

Montes, Gregorio S. 1996. “Structural Biology of the Fibres of the Collagenous and Elastic Systems.” *Cell Biology International* 20(1):15–27.

Moore, Rowan and Martin Samonig. 2016. “High-Throughput, High-Resolution Peptide Maps.” *Genetic Engineering & Biotechnology News* 36(12):20–21.

Mozziconacci, Olivier, Bruce A. Kerwin, and Christian Schöneich. 2010. “Photolysis of an Intrachain Peptide Disulfide Bond: Primary and Secondary Processes, Formation of H2S, and Hydrogen Transfer Reactions.” *The Journal of Physical Chemistry B* 114(10):3668–88.

Murdoch, Lamont, Bryan A. Walker, Barry L. Halpern, Jan W. Kuzma, and Victor A. McKusick. 1972. “Life Expectancy and Causes of Death in the Marfan Syndrome.” *New England Journal of Medicine* 286(15):804–8.

Naba, Alexandra, Karl R. Clauser, and Richard O. Hynes. 2015. “Enrichment of Extracellular Matrix Proteins from Tissues and Digestion into Peptides for Mass Spectrometry Analysis.” *Journal of Visualized Experiments: JoVE* (101).

Naik, Edwina, Ewa M. Michalak, Andreas Villunger, Jerry M. Adams, and Andreas Strasser. 2007. “Ultraviolet Radiation Triggers Apoptosis of Fibroblasts and Skin Keratinocytes Mainly via the BH3-Only Protein Noxa.” *The Journal of Cell Biology* 176(4):415–24.

Naylor, Elizabeth C., Rachel E. B. Watson, and Michael J. Sherratt. 2011. “Molecular Aspects of Skin Ageing.” *Maturitas* 69(3):249–56.

Neptune, Enid R., Pamela A. Frischmeyer, Dan E. Arking, Loretha Myers, Tracie E. Bunton, Barbara Gayraud, Francesco Ramirez, Lynn Y. Sakai, and Harry C. Dietz. 2003. “Dysregulation of TGF-β Activation Contributes to Pathogenesis in Marfan Syndrome.” *Nature Genetics* 33(3):407–11.

Nesvizhskii, Alexey I., Andrew Keller, Eugene Kolker, and Ruedi Aebersold. 2003. “A Statistical Model for Identifying Proteins by Tandem Mass Spectrometry.” *Analytical Chemistry* 75(17):4646–58.

Nielsen, Peter A., Eric P. Bennett, Hans H. Wandall, Marianne H. Therkildsen, Jens Hannibal, and Henrik Clausen. 1997. “Identification of a Major Human High Molecular Weight Salivary Mucin (MG1) as Tracheobronchial Mucin MUC5B.” *Glycobiology* 7(3):413–19.

Noda, Kazuo, Branka Dabovic, Kyoko Takagi, Tadashi Inoue, Masahito Horiguchi, Maretoshi Hirai, Yusuke Fujikawa, Tomoya O. Akama, Kenji Kusumoto, and Lior Zilberberg. 2013. “Latent TGF-β Binding Protein 4 Promotes Elastic Fiber Assembly by Interacting with Fibulin-5.” *Proceedings of the National Academy of Sciences* 110(8):2852–57.

Nord, Frank F., Mark Bier, and Louis Terminiello. 1956. “On the Mechanism of Enzyme Action. LXI. The Self Digestion of Trypsin, Calcium-Trypsin and Acetyltrypsin.” *Archives of Biochemistry and Biophysics* 65(1):120–31.

Ohno-Jinno, Akiko, Zenzo Isogai, Masahiko Yoneda, Kenji Kasai, Osamu Miyaishi, Yoko Inoue, Takuya Kataoka, Jing-Song Zhao, Huili Li, and Masayuki Takeyama. 2008. “Versican and Fibrillin-1 Form a Major Hyaluronan-Binding Complex in the Ciliary Body.” *Investigative Ophthalmology & Visual Science* 49(7):2870–77.

Olin, Anders I., Matthias Mörgelin, Takako Sasaki, Rupert Timpl, Dick Heinegård, and Anders Aspberg. 2001. “The Proteoglycans Aggrecan and Versican Form Networks with Fibulin-2 through Their Lectin Domain Binding.” *Journal of Biological Chemistry* 276(2):1253–61.

Olsen, Jesper V, Shao-En Ong, and Matthias Mann. 2004. “Trypsin Cleaves Exclusively C-Terminal to Arginine and Lysine Residues.” *Molecular & Cellular Proteomics* 3(6):608–14.

Onnerfjord, Patrik, Areej Khabut, Finn P. Reinholt, Olle Svensson, and Dick Heinegard. 2012. “Quantitative Proteomic Analysis of Eight Cartilaginous Tissues Reveals Characteristic Differences as Well as Similarities between Subgroups.” *Journal of Biological Chemistry* 287(23):18913–24.

Ono, Robert N., Gerhard Sengle, Noe L. Charbonneau, Valerie Carlberg, Hans Peter Bächinger, Takako Sasaki, Sui Lee-Arteaga, Lior Zilberberg, Daniel B. Rifkin, and Francesco Ramirez. 2009. “Latent Transforming Growth Factor β-Binding Proteins and Fibulins Compete for Fibrillin-1 and Exhibit Exquisite Specificities in Binding Sites.” *Journal of Biological Chemistry* 284(25):16872–81.

Parry, David A. D., Gregory R. G. Barnes, and Allen S. Craig. 1978. “A Comparison of the Size Distribution of Collagen Fibrils in Connective Tissues as a Function of Age and a Possible Relation between Fibril Size Distribution and Mechanical Properties.” *Proceedings of the Royal Society of London - Biological Sciences* 203(1152):305–21.

Pecora, Fabio, Antonella Forlino, Benedetta Gualeni, Anna Lupi, Sofia Giorgetti, Loredana Marchese, Monica Stoppini, Ruggero Tenni, Giuseppe Cetta, and Antonio Rossi. 2007. “A Quantitative and Qualitative Method for Direct 2-DE Analysis of Murine Cartilage.” *Proteomics* 7(21):4003–7.

Penner, Akiyo S., Matthew J. Rock, Cay M. Kielty, and J. Michael Shipley. 2002. “Microfibril-Associated Glycoprotein-2 Interacts with Fibrillin-1 and Fibrillin-2 Suggesting a Role for MAGP-2 in Elastic Fiber Assembly.” *Journal of Biological Chemistry* 277(38):35044–49.

Pfaff, Martin, Monique Aumailley, Ulrich Specks, Joachim Knolle, Hans Günter Zerwes, and Rupert Timpl. 1993. “Integrin and Arg-Gly-Asp Dependence of Cell Adhesion to the Native and Unfolded Triple Helix of Collagen Type VI.” *Experimental Cell Research* 206(1):167–76.

Piha-Gossack, Adam, Wayne Sossin, and Dieter P. Reinhardt. 2012. “The Evolution of Extracellular Fibrillins and Their Functional Domains.” *PLoS ONE* 7(3):e33560.

Pilecki, Bartosz, Anne T. Holm, Anders Schlosser, Jesper B. Moeller, Alexander P. Wohl, Alexandra V Zuk, Stefanie E. Heumüller, Russell Wallis, Soren K. Moestrup, and Gerhard Sengle. 2016. “Characterization of Microfibrillar-Associated Protein 4 (MFAP4) as a Tropoelastin-and Fibrillin-Binding Protein Involved in Elastic Fiber Formation.” *Journal of Biological Chemistry* 291(3):1103–14.

Prattes, Susanne, Gerd Hörl, Astrid Hammer, Astrid Blaschitz, Wolfgang F. Graier, Wolfgang Sattler, Rudolf Zechner, and Ernst Steyrer. 2000. “Intracellular Distribution and Mobilization of Unesterified Cholesterol in Adipocytes: Triglyceride Droplets Are Surrounded by Cholesterol-Rich ER-like Surface Layer Structures.” *Journal of Cell Science* 113:2977–89.

Price, John C., Shenheng Guan, Alma Burlingame, Stanley B. Prusiner, and Sina Ghaemmaghami. 2010. “Analysis of Proteome Dynamics in the Mouse Brain.” *Proceedings of the National Academy of Sciences* 107(32):14508–13.

Proctor, Gordon B. and Richard W. Horobin. 1988. “Chemical Structures and Staining Mechanisms of Weigert’s Resorcin-Fuchsin and Related Elastic Fiber Stains.” *Biotechnic and Histochemistry* 63(2):101–11.

Proksch, Ehrhardt, Johanna M. Brandner, and Jens Michael Jensen. 2008. “The Skin: An Indispensable Barrier.” *Experimental Dermatology* 17(12):1063–72.

Pyeritz, Reed E. 2000. “The Marfan Syndrome.” *Annual Review of Medicine* 51(1):481–510.

Qian, Rui-Qing and Robert W. Glanville. 1997. “Alignment of Fibrillin Molecules in Elastic Microfibrils Is Defined by Transglutaminase-Derived Cross-Links.” *Biochemistry* 36(50):15841–47.

Quan, Taihao, Zhaoping Qin, Wei Xia, Yuan Shao, John J. Voorhees, and Gary J. Fisher. 2009. “Matrix-Degrading Metalloproteinases in Photoaging.” *The Journal of Investigative Dermatology. Symposium Proceedings / the Society for Investigative Dermatology, Inc. [and] European Society for Dermatological Research* 14(1):20–24.

Raghunath, Michael, Elizabeth A. Putnam, Timothy M. Ritty, Derek Hamstra, Elizabeth S. Park, Michael Tschodrich-Rotter, Reiner Peters, Anesh Rehemtulla, and Dianna M. Milewicz. 1999. “Carboxy-Terminal Conversion of Profibrillin to Fibrillin at a Basic Site by PACE/Furin-like Activity Required for Incorporation in the Matrix.” *Journal of Cell Science* 112(7):1093–1100.

Raghunath, Michael, Christine Unsold, Ulrich Kubitscheck, Leena Bruckner-Tuderman, Reiner Peters, and Martin Meuli. 1998. “The Cutaneous Microfibrillar Apparatus Contains Latent Transforming Growth Factor-β Binding Protein-1 (LTBP-1) and Is a Repository for Latent TGF-B1.” *Journal of Investigative Dermatology* 111(4):559–64.

Rai, Reena and Chakravarthi R. Srinivas. 2007. “Photoprotection.” *Indian Journal of Dermatology, Venereology, and Leprology* 73(2):73.

Raimer, Sharon S., Ramon L. Sanchez, Winthrope R. Hubler, and Ronald F. Dodson. 1986. “Solar Elastotic Bands of the Forearm: An Unusual Clinical Presentation of Actinic Elastosis.” *Journal of the American Academy of Dermatology* 15(4):650–56.

Ratcliff, Glen C. and Dorothy. A. Erie. 2001. “A Novel Single-Molecule Study to Determine Protein-Protein Association Constants.” *Journal of the American Chemical Society* 123(24):5632–35.

Reinhardt, Dieter P., Jay E. Gambee, Robert N. Ono, Hans Peter Bächinger, and Lynn Y. Sakai. 2000. “Initial Steps in Assembly of Microfibrils: Formation of Disulfide-Cross-Linked Multimers Containing Fibrillin-1.” *Journal of Biological Chemistry* 275(3):2205–10.

Reinhardt, Dieter P., Douglas R. Keene, Glen M. Corson, Ernst Pöschl, Hans Peter Bächinger, Jay E. Gambee, and Lynn Y. Sakai. 1996. “Fibrillin-1: Organization in Microfibrils and Structural Properties.” *Journal of Molecular Biology* 258(1):104–16.

Reinhardt, Dieter P., Robert N. Ono, Holger Notbohm, Peter K. Müller, Hans Peter Bächinger, and Lynn Y. Sakai. 2000. “Mutations in Calcium-Binding Epidermal Growth Factor Modules Render Fibrillin-1 Susceptible to Proteolysis.” *Journal of Biological Chemistry* 275(16):12339–45.

Reinhardt, Dieter P., Robert N. Ono, and Lynn Y. Sakai. 1997. “Calcium Stabilizes Fibrillin-1 against Proteolytic Degradation.” *Journal of Biological Chemistry* 272(2):1231–36.

Reinhardt, Dieter P., Takako Sasaki, Bette J. Dzamba, Douglas R. Keene, Mon-Li Chu, Walter Göhring, Rupert Timpl, and Lynn Y. Sakai. 1996. “Fibrillin-1 and Fibulin-2 Interact and Are Colocalized in Some Tissues.” *Journal of Biological Chemistry* 271(32):19489–96.

Rietschel, Benjamin, Tabiwang N. Arrey, Bjoern Meyer, Sandra Bornemann, Malte Schuerken, Michael Karas, and Ansgar Poetsch. 2009. “Elastase Digests: New Ammunition for Shotgun Membrane Proteomics.” *Molecular & Cellular Proteomics* 8(5):1029–43.

Rifkin, Daniel B. 2005. “Latent Transforming Growth Factor-β (TGF-β) Binding Proteins: Orchestrators of TGF-β Availability.” *Journal of Biological Chemistry* 280(9):7409–12.

Rittig, Michael, Elke Lütjen-Drecoll, Jürgen Rauterberg, Rudolf Jander, and Jürgen Mollenhauer. 1990. “Type-VI Collagen in the Human Iris and Ciliary Body.” *Cell and Tissue Research* 259(2):305–12.

Ritty, Timothy M., Thomas Broekelmann, Clarina Tisdale, Dianna M. Milewicz, and Robert P. Mecham. 1999. “Processing of the Fibrillin-1 Carboxyl-Terminal Domain.” *Journal of Biological Chemistry* 274(13):8933–40.

Ritz-Timme, Stefanie, I. Laumeier, and Matthew J. Collins. 2003. “Aspartic Acid Racemization: Evidence for Marked Longevity of Elastin in Human Skin.” *British Journal of Dermatology* 149(5):951–59.

Roark, Eileen F., Douglas R. Keene, Christian C. Haudenschild, Svetlana Godyna, Charles D. Little, and W. Scott Argraves. 1995. “The Association of Human Fibulin-1 with Elastic Fibers: An Immunohistological, Ultrastructural, and RNA Study.” *Journal of Histochemistry & Cytochemistry* 43(4):401–11.

Robinson, Peter N., Patrick Booms, Stefanie Katzke, Markus Ladewig, Luitgard Neumann, Monika Palz, Reinhard Pregla, Frank Tiecke, and Thomas Rosenberg. 2002. “Mutations of FBN1 and

Genotype–phenotype Correlations in Marfan Syndrome and Related Fibrillinopathies." *Human Mutation* 20(3):153–61.

Rock, Matthew J., Stuart A. Cain, Lyle J. Freeman, Amanda Morgan, Kieran Mellody, Andrew Marson, C. Adrian Shuttleworth, Anthony S. Weiss, and Cay M. Kielty. 2004. "Molecular Basis of Elastic Fiber Formation Critical Interactions and a Tropoelastin-Fibrillin-1 Cross-Link." *Journal of Biological Chemistry* 279(22):23748–58.

Roeder, Blayne A., Klod Kokini, Jennifer E. Sturgis, J. Paul Robinson, and Sherry L. Voytik-Harbin. 2002. "Tensile Mechanical Properties of Three-Dimensional Type I Collagen Extracellular Matrices with Varied Microstructure." *Journal of Biomechanical Engineering* 124(2):214–22.

Rose, Mary Callaghan and Judith A. Voynow. 2006. "Respiratory Tract Mucin Genes and Mucin Glycoproteins in Health and Disease." *Physiological Reviews* 86(1):245–78.

Saarialho-Kere, Ulpu, Erja Kerkelä, Leila Jeskanen, Annamari Ranki, Maarit Vaalamo, Taina Hasan, Richard Pierce, Barry Starcher, Riikka Raudasoja, and Aarne Oikarinen. 1999. "Accumulation of Matrilysin (MMP-7) and Macrophage Metalloelastase (MMP-12) in Actinic Damage." *Journal of Investigative Dermatology* 113(4):664–72.

Sabatelli, Patrizia, Paolo Bonaldo, Giovanna Lattanzi, Paola Braghetta, Natascha Bergamin, Cristina Capanni, Elisabetta Mattioli, Marta Columbaro, Andrea Ognibene, and Guglielmina Pepe. 2001. "Collagen VI Deficiency Affects the Organization of Fibronectin in the Extracellular Matrix of Cultured Fibroblasts." *Matrix Biology* 20(7):475–86.

Sabatier, Laetitia, Daliang Chen, Christine Fagotto-Kaufmann, Dirk Hubmacher, Marc D. McKee, Douglas S. Annis, Deane F. Mosher, and Dieter P. Reinhardt. 2009. "Fibrillin Assembly Requires Fibronectin." *Molecular Biology of the Cell* 20(3):846–58.

Saharinen, Juha, Jussi Taipale, and Jorma Keski-Oja. 1996. "Association of the Small Latent Transforming Growth Factor-beta with an Eight Cysteine Repeat of Its Binding Protein LTBP-1." *The EMBO Journal* 15(2):245–53.

Saitta, Biagio, David G. Stokes, Henrik Vissing, Rupert Timpl, and Mon-li Chu. 1990. "Alternative Splicing of the Human A2(VI) Collagen Gene Generates Multiple MRNA Transcripts Which Predict Three Protein Variants with Distinct Carboxyl Termini." *Journal of Biological Chemistry* 265(11):6473–80.

Sakai, Lynn Y., Douglas R. Keene, and Eva Engvall. 1986. "Fibrillin, a New 350-KD Glycoprotein, Is a Component of Extracellular Microfibrils." *The Journal of Cell Biology* 103(6 Pt 1):2499–2509.

Samonig, Martin, Alexander Schwahn, Ken Cook, Mike Oliver, and Remco Swart. 2016. "SMART Digest Compared to Classic In-Solution Digestion of Rituximab for in-Depth Peptide Mapping Characterization." *Application Note 1159* 1–11.

Sarrazin, Stephane, William C. Lamanna, and Jeffrey D. Esko. 2011. "Heparan Sulfate Proteoglycans." *Cold Spring Harbor Perspectives in Biology* 3(7):1–33.

Sasaki, Takako, Walter Göhring, Te-Cheng Pan, Mon-Li Chu, and Rupert Timpl. 1995. "Binding of Mouse and Human Fibulin-2 to Extracellular Matrix Ligands." *Journal of Molecular Biology* 254(5):892–99.

Sasaki, Takako, Erhard Hohenester, Rui-zhu Zhang, Susan Gotta, Marcy C. Speer, Rup Tandan, Rupert Timpl, and Mon-li Chu. 2000. "A Bethlem Myopathy Gly to Glu Mutation in the von Willebrand Factor A Domain N2 of the Collagen A3 (VI) Chain Interferes with Protein Folding." *The FASEB Journal* 14(5):761–68.

Schiavinato, Alvise, Ann-Kathrin A. Becker, Miriam Zanetti, Diana Corallo, Martina Milanetto, Dario Bizzotto, Giorgio Bressan, Marija Guljelmovic, Mats Paulsson, and Raimund Wagener. 2012. "EMILIN-3, Peculiar Member of Elastin Microfibril Interface-Located Protein (EMILIN) Family, Has Distinct Expression Pattern, Forms Oligomeric Assemblies, and Serves as Transforming Growth Factor β (TGF-β) Antagonist." *Journal of Biological Chemistry* 287(14):11498–515.

Schiavinato, Alvise, Douglas R. Keene, Alexander P. Wohl, Diana Corallo, Alfonso Colombatti,

Raimund Wagener, Mats Paulsson, Paolo Bonaldo, and Gerhard Sengle. 2016. “Targeting of EMILIN-1 and EMILIN-2 to Fibrillin Microfibrils Facilitates Their Incorporation into the Extracellular Matrix.” *Journal of Investigative Dermatology* 136(6):1150–60.

Schilling, Birgit, Brendan MacLean, Jason M. Held, Alexandria K. Sahu, Matthew J. Rardin, Dylan J. Sorensen, Theodore Peters, Alan J. Wolfe, Christie L. Hunter, and Michael J. MacCoss. 2015. “Multiplexed, Scheduled, High-Resolution Parallel Reaction Monitoring on a Full Scan QqTOF Instrument with Integrated Data-Dependent and Targeted Mass Spectrometric Workflows.” *Analytical Chemistry* 87(20):10222–29.

Schwab, Manfred, 2011. “Peptide Biomarkers BT - Encyclopedia of Cancer.” Pp. 2809–10 in. Berlin, Heidelberg: Springer Berlin Heidelberg.

Scott, Derek, Peter J. Coleman, Andrea Abiona, Dorothy E. Ashhurst, Roger M. Mason, and Jeremy R. Levick. 1998. “Effect of Depletion of Glycosaminoglycans and Non-collagenous Proteins on Interstitial Hydraulic Permeability in Rabbit Synovium.” *The Journal of Physiology* 511(2):629–43.

Segade, Fernando, Barbara Crippes Trask, Thomas J. Broekelmann, Richard A. Pierce, and Robert P. Mecham. 2002. “Identification of a Matrix-Binding Domain in MAGP1 and MAGP2 and Intracellular Localization of Alternative Splice Forms.” *Journal of Biological Chemistry* 277(13):11050–57.

Sell, David R. and Vincent M. Monnier. 2010. “Aging of Long-Lived Proteins: Extracellular Matrix (Collagens, Elastins, Proteoglycans) and Lens Crystallins.” in *Comprehensive Physiology*. John Wiley & Sons, Inc.

Sengle, Gerhard, Noe L. Charbonneau, Robert N. Ono, Takako Sasaki, Jennifer Alvarez, Douglas R. Keene, Hans Peter Bächinger, and Lynn Y. Sakai. 2008. “Targeting of Bone Morphogenetic Protein Growth Factor Complexes to Fibrillin.” *Journal of Biological Chemistry* 283(20):13874–88.

Setlow, Richard B. 1966. “Cyclobutane-Type Pyrimidine Dimers in Polynucleotides.” *Science* 153(3734):379–86.

Shapiro, Steven D., Scott K. Endicott, M. a. Province, John A. Pierce, and Edward Campbell. 1991. “Marked Longevity of Human Lung Parenchymal Elastic Fibers Deduced from Prevalence of D-Aspartate and Nuclear Weapons-Related Radiocarbon.” *Journal of Clinical Investigation* 87(5):1828–34.

Sherratt, Michael J. 2009. “Tissue Elasticity and the Ageing Elastic Fibre.” *Age* 31(4):305–25.

Sherratt, Michael J., Clair Baldock, J. Louise Haston, David F. Holmes, Carolyn J. P. Jones, C. Adrian Shuttleworth, Timothy J. Wess, and Cay M. Kielty. 2003. “Fibrillin Microfibrils Are Stiff Reinforcing Fibres in Compliant Tissues.” *Journal of Molecular Biology* 332(1):183–93.

Sherratt, Michael J., Clair Baldock, Amanda Morgan, and Cay M. Kielty. 2007. “The Morphology of Adsorbed Extracellular Matrix Assemblies Is Critically Dependent on Solution Calcium Concentration.” *Matrix Biology* 26(3):156–66.

Sherratt, Michael J., Daniel V. Bax, Shazia S. Chaudhry, Nigel Hodson, Jian R. Lu, Priya Saravanapavan, and Cay M. Kielty. 2005. “Substrate Chemistry Influences the Morphology and Biological Function of Adsorbed Extracellular Matrix Assemblies.” *Biomaterials* 26(34):7192–7206.

Sherratt, Michael J., Christopher P. Bayley, Siobhan M. Reilly, Neil K. Gibbs, Christopher E. M. Griffiths, and Rachel E. B. Watson. 2010. “Low-Dose Ultraviolet Radiation Selectively Degrades Chromophore-Rich Extracellular Matrix Components.” *Journal of Pathology* 222(1):32–40.

Sherratt, Michael J., David F. Holmes, C. Adrian Shuttleworth, and Cay M. Kielty. 1997. “Scanning Transmission Electron Microscopy MassSherratt, Michael J., David F. Holmes, C. Adrian Shuttleworth, and Cay M. Kielty. 1997. “Scanning Transmission Electron Microscopy Mass Analysis of Fibrillin-Containing Microfibrils from Foetal Elastic Tissues.” *The International Journal of Biochemistry & Cell Biology* 29(8–9):1063–70.

Sherratt, Michael J., David F. Holmes, C. Adrian Shuttleworth, and Cay M. Kielty. 2004. “Substrate-Dependent Morphology of Supramolecular Assemblies: Fibrillin and Type-VI Collagen Microfibrils.” *Biophysical Journal* 86(5):3211–22.

Shi, Yanrong, Yidong Tu, Alicia De Maria, Robert P. Mecham, and Steven Bassnett. 2013. “Development, Composition, and Structural Arrangements of the Ciliary Zonule of the Mouse.” *Investigative Ophthalmology and Visual Science* 54(4):2504–15.

Sideek, Mohamed A., Clementine Menz, Mahroo K. Parsi, and Mark A. Gibson. 2014. “LTBP-2 Competes with Tropoelastin for Binding to Fibulin-5 and Heparin, and Is a Negative Modulator of Elastinogenesis.” *Matrix Biology* 34:114–23.

Specks, Ulrich, Ulrike Mayer, Roswitha Nischt, Thomas Spissinger, Karlheinz Mann, Rupert Timpl, Jurgen Engel, and Mon-Li Chu. 1992. “Structure of Recombinant N-Terminal Globule of Type VI Collagen Oc3 Chain and Its Binding to Heparin and Hyaluronan.” *The EMBO Journal* 1(12):4281–90.

Spessotto, Paola, Roberta Bulla, Carla Danussi, Oriano Radillo, Marta Cervi, Giada Monami, Fleur Bossi, Francesco Tedesco, Roberto Doliana, and Alfonso Colombatti. 2006. “EMILIN1 Represents a Major Stromal Element Determining Human Trophoblast Invasion of the Uterine Wall.” *Journal of Cell Science* 119(21):4574–84.

Spessotto, Paola, Marta Cervi, Maria Teresa Mucignat, Gabriella Mungiguerra, Ida Sartoretto, Roberto Doliana, and Alfonso Colombatti. 2003. “B1 Integrin-Dependent Cell Adhesion to EMILIN-1 Is Mediated by the GC1q Domain.” *Journal of Biological Chemistry* 278(8):6160–67.

Stadtman, Earl R. 1992. “Protein Oxidation and Aging.” *Science* 257(5074):1220–24.

Stallcup, William B., Kimberlee Dahlin, and Patricia Healy. 1990. “Interaction of the NG2 Chondroitin Sulfate Proteoglycan with Type VI Collagen.” *The Journal of Cell Biology* 111(6):3177–88.

Stamenkovic, Ivan. 2003. “Extracellular Matrix Remodelling: The Role of Matrix Metalloproteinases.” *The Journal of Pathology: A Journal of the Pathological Society of Great Britain and Ireland* 200(4):448–64.

Stenhouse, Michael J. and Murdoch S. Baxter. 1977. “Bomb 14C as a Biological Tracer.” *Nature* 267(5614):828.

Suwabe, Hisako, Akihiko Serizawa, Hiroshi Kajiwara, Muneo Ohkido, and Yutaka Tsutsumi. 1999. “Degenerative Processes of Elastic Fibers in Sun-protected and Sun-exposed Skin: Immunoelectron Microscopic Observation of Elastin, Fibrillin-1, Amyloid P Component, Lysozyme and A1-antitrypsin.” *Pathology International* 49(5):391–402.

Sziegoleit, Andreas, Dietmar Linder, Michael Schulter, Michio Ogawa, Shunzo Nishibe, and Kenichi Fujimoto. 1985. “Studies on the Specificity of the Cholesterol-binding Pancreatic Proteinase and Identification as Human Pancreatic Elastase 1.” *European Journal of Biochemistry* 151(3):595–99.

Talwar, Harvinder S., Christopher E. M. Griffiths, Gary J. Fisher, Ted A. Hamilton, and John J. Voorhees. 1995. “Reduced Type I and Type III Procollagens in Photodamaged Adult Human Skin.” *Journal of Investigative Dermatology* 105(2):285–90.

Tamm, Ernst R. and Elke Lütjen-Drecoll. 1996. “Ciliary Body.” *Microscopy Research and Technique* 33(5):390–439.

Tammen, Harald. 2011. “Oncopeptidomics BT - Encyclopedia of Cancer.” Pp. 2632–34 in, edited by M. Schwab. Berlin, Heidelberg: Springer Berlin Heidelberg.

Thapa, Narendra, Byung-Heon Lee, and In-San Kim. 2007. “TGFBIp/Big-H3 Protein: A Versatile Matrix Molecule Induced by TGF-β.” *The International Journal of Biochemistry & Cell Biology* 39(12):2183–94.

Thomson, Jennifer, Mukti Singh, Alexander Eckersley, Stuart A. Cain, Michael J. Sherratt, and Clair Baldock. 2018. “Fibrillin Microfibrils and Elastic Fibre Proteins: Functional Interactions and Extracellular Regulation of Growth Factors.” *Seminars in Cell and Developmental*

Biology.

Tiecke, Frank, Stefanie Katzke, Patrick Booms, Peter N. Robinson, Luitgard Neumann, Maurice Godfrey, Kurt R. Mathews, Maren Scheuner, Georg Klaus Hinkel, and Rolf E. Brenner. 2001. "Classic, Atypically Severe and Neonatal Marfan Syndrome: Twelve Mutations and Genotype–phenotype Correlations in FBN1 Exons 24–40." *European Journal of Human Genetics* 9(1):13.

Tiedemann, Kerstin, Takako Sasaki, Erika Gustafsson, Walter Göhring, Boris Bätge, Holger Notbohm, Rupert Timpl, Thilo Wedel, Ursula Schlötzer-Schrehardt, and Dieter P. Reinhardt. 2005. "Microfibrils at Basement Membrane Zones Interact with Perlecan via Fibrillin-1." *Journal of Biological Chemistry* 280(12):11404–12.

Tillet, Emmanuelle, Hanna Wiedemann, Ralph Golbik, Te-Cheng Pan, Rui-Zhu Zhang, Karlheinz Mann, Mon-Li CHU, and Rupert Timpl. 1994. "Recombinant Expression and Structural and Binding Properties of A1 (VI) and A2 (VI) Chains of Human Collagen Type VI." *The FEBS Journal* 221(1):177–87.

Tobiska, Kent and Anatoliy A. Nusinov. 2005. "Status of ISO Draft International Standard for Determining Solar Irradiances (DIS 21348)." *Journal of Advanced Space Research*.

Trask, Barbara Crippes, Timothy M. Trask, Thomas Broekelmann, and Robert P. Mecham. 2000. "The Microfibrillar Proteins MAGP-1 and Fibrillin-1 Form a Ternary Complex with the Chondroitin Sulfate Proteoglycan Decorin." *Molecular Biology of the Cell* 11(5):1499–1507.

Tsoureli-Nikita, Evridiki, Rachel E. B. Watson, and Christopher E. M. Griffiths. 2006. "Photoageing: The Darker Side of the Sun." *Photochemical & Photobiological Sciences* 5(2):160–64.

Tsuji, Takuo and Toshio Hamada. 1981. "Age-Related Changes in Human Dermal Elastic Fibres." *British Journal of Dermatology* 105(1):57–63.

Tsuji, Takuo, Tetsuo Yorifuji, Yoshi Hayashi, and Toshio Hamada. 1986. "Light and Scanning Electron Microscopic Studies on Wrinkles in Aged Persons' Skin." *British Journal of Dermatology* 114(3):329–35.

Urciuolo, Anna, Marco Quarta, Valeria Morbidoni, Francesca Gattazzo, Sibilla Molon, Paolo Grumati, Francesca Montemurro, Francesco Saverio Tedesco, Bert Blaauw, and Giulio Cossu. 2013. "Collagen VI Regulates Satellite Cell Self-Renewal and Muscle Regeneration." *Nature Communications* 4:1964.

del Val, Gregorio, Frank E. Hagie, and Bob B. Buchanan. 2002. "Thioredoxin-(Dithiol-) Linked Inactivation of Elastase." *Molecular Immunology* 38(10):759–63.

Vehviläinen, Piia, Marko Hyytiäinen, and Jorma Keski-Oja. 2009. "Matrix Association of Latent TGF-beta Binding Protein-2 (LTBP-2) Is Dependent on Fibrillin-1." *Journal of Cellular Physiology* 221(3):586–93.

Veidal, Sanne Skovgård, Morten Asser Karsdal, Efstathios Vassiliadis, Arkadiusz Nawrocki, Martin Røssel Larsen, Quoc Hai Trieu Nguyen, Per Hägglund, Yunyun Luo, Qinlong Zheng, and Ben Vainer. 2011. "MMP Mediated Degradation of Type VI Collagen Is Highly Associated with Liver Fibrosis–identification and Validation of a Novel Biochemical Marker Assay." *PLoS One* 6(9).

Vernon, Hazel J., Alfred T. Lane, Linda J. Wischerath, Jonathan M. Davis, and Marilyn A. Menegus. 1990. "Semipermeable Dressing and Transepidermal Water Loss in Premature Infants." *Pediatrics* 86(3):357–62.

Verzijl, Nicole, Jeroen DeGroot, Esther Oldehinkel, R. A. Bank, S. R. Thorpe, J. W. Baynes, M. T. Bayliss, J. W. Bijlsma, F. P. Lafeber, and J. M. Tekoppele. 2000. "Age-Related Accumulation of Maillard Reaction Products in Human Articular Cartilage Collagen." *Biochemical Journal* 350(Pt 2):381–87.

Verzijl, Nicole, Jeroen DeGroot, Suzanne R. Thorpe, Ruud A. Bank, J. Nikki Shaw, Timothy J. Lyons, Johannes W. J. Bijlsma, Floris P. J. G. Lafeber, John W. Baynes, and Johan M. TeKoppele. 2000. "Effect of Collagen Turnover on the Accumulation of Advanced Glycation

End Products." *Journal of Biological Chemistry* 275(50):39027–31.

Vincourt, Jean-Baptiste, Frédéric Lionneton, Gueorgui Kratassiouk, François Guillemin, Patrick Netter, Didier Mainard, and Jacques Magdalou. 2006. "Establishment of a Reliable Method for Direct Proteome Characterization of Human Articular Cartilage." *Molecular & Cellular Proteomics* 5(10):1984–95.

Vizcaíno, Juan Antonio, Attila Csordas, Noemi del-Toro, José A. Dianes, Johannes Griss, Ilias Lavidas, Gerhard Mayer, Yasset Perez-Riverol, Florian Reisinger, and Tobias Ternent. 2016. "2016 Update of the PRIDE Database and Its Related Tools." *Nucleic Acids Research* 44(D1):D447–56.

Wagenseil, Jessica E. and Robert P. Mecham. 2009. "Vascular Extracellular Matrix and Arterial Mechanics." *Physiological Reviews* 89(3):957–89.

Walji, Tezin A., Sarah E. Turecamo, Antea J. DeMarsilis, Lynn Y. Sakai, Robert P. Mecham, and Clarissa S. Craft. 2016. "Characterization of Metabolic Health in Mouse Models of Fibrillin-1 Perturbation." *Matrix Biology* 55:63–76.

Wang, Ning, Jessica D. Tytell, and Donald E. Ingber. 2009. "Mechanotransduction at a Distance: Mechanically Coupling the Extracellular Matrix with the Nucleus." *Nature Reviews Molecular Cell Biology* 10(1):75–82.

Wang, Zhen, Brian Lyons, Roger J. W. Truscott, and Kevin L. Schey. 2014. "Human Protein Aging: Modification and Crosslinking through Dehydroalanine and Dehydrobutyrine Intermediates." *Aging Cell* 13(2):226–34.

Warren, Raphael, Vladimir Gartstein, Albert M. Kligman, William Montagna, Richard A. Allendorf, and Gregg M. Ridder. 1991. "Age, Sunlight, and Facial Skin: A Histologic and Quantitative Study." *Journal of the American Academy of Dermatology* 25(5, Part 1):751–60.

Watson, Rachel E. B., Stephen G. Ball, Nicholas M. Craven, John Boorsma, Clay L. East, Adrian Shuttleworth, Cay M. Kielty, and Christopher E. M. Griffiths. 2001. "Distribution and Expression of Type VI Collagen in Photoaged Skin." *British Journal of Dermatology* 144(4):751–59.

Watson, Rachel E. B., Neil K. Gibbs, Christopher E. M. Griffiths, and Michael J. Sherratt. 2014. "Damage to Skin Extracellular Matrix Induced by UV Exposure." *Antioxidants & Redox Signaling* 21(7):1063–77.

Watson, Rachel E. B., Christopher E. M. Griffiths, Nicholas M. Craven, C. Adrian Shuttleworth, and Cay M. Kielty. 1999. "Fibrillin-Rich Microfibrils Are Reduced in Photoaged Skin. Distribution at the Dermal-Epidermal Junction." *Journal of Investigative Dermatology* 112(5):782–87.

Watson, Rachel E. B., Sarah Ogden, Lindsay F. Cotterell, June J. Bowden, Jean Y. Bastrilles, Stephen P. Long, and Christopher E. M. Griffiths. 2009. "A Cosmetic 'anti-Ageing' Product Improves Photoaged Skin: A Double-Blind, Randomized Controlled Trial." *British Journal of Dermatology* 161(2):419–26.

Weathington, Nathaniel M., Anneke H. van Houwelingen, Brett D. Noerager, Patricia L. Jackson, Aletta D. Kraneveld, F. Shawn Galin, Gert Folkerts, Frans P. Nijkamp, and J. Edwin Blalock. 2006. "A Novel Peptide CXCR Ligand Derived from Extracellular Matrix Degradation during Airway Inflammation." *Nature Medicine* 12(3):317.

Weil, Miguel, Martin C. Raff, and Vania M. M. Braga. 1999. "Caspase Activation in the Terminal Differentiation of Human Epidermal Keratinocytes." *Current Biology* 9(7):361–65.

Weinbaum, Justin S., Thomas J. Broekelmann, Richard A. Pierce, Claudio C. Werneck, Fernando Segade, Clarissa S. Craft, Russell H. Knutsen, and Robert P. Mecham. 2008. "Deficiency in Microfibril-Associated Glycoprotein-1 Leads to Complex Phenotypes in Multiple Organ Systems." *Journal of Biological Chemistry* 283(37):25533–43.

Werner, Jörn M., Vroni Knott, Penny A. Handford, Iain D. Campbell, and A. Kristin. Downing. 2000. "Backbone Dynamics of a CbEGF Domain Pair in the Presence of Calcium1." *Journal of Molecular Biology* 296(4):1065–78.

Whiteman, Pat and Penny A. Handford. 2003. “Defective Secretion of Recombinant Fragments of Fibrillin-1: Implications of Protein Misfolding for the Pathogenesis of Marfan Syndrome and Related Disorders.” *Human Molecular Genetics* 12(7):727–37.

Wiberg, Charlotte, Dick Heinegård, Christina Wenglén, Rupert Timpl, and Matthias Mörgelin. 2002. “Biglycan Organizes Collagen VI into Hexagonal-like Networks Resembling Tissue Structures.” *Journal of Biological Chemistry* 277(51):49120–26.

Wiberg, Charlotte, Andreas R. Klatt, Raimund Wagener, Mats Paulsson, John F. Bateman, Dick Heinegård, and Matthias Mörgelin. 2003. “Complexes of Matrilin-1 and Biglycan or Decorin Connect Collagen VI Microfibrils to Both Collagen II and Aggrecan.” *Journal of Biological Chemistry* 278(39):37698–704.

Wight, Thomas N. 2002. “Versican: A Versatile Extracellular Matrix Proteoglycan in Cell Biology.” *Current Opinion in Cell Biology* 14(5):617–23.

Wilson, Richard. 2010. “The Extracellular Matrix: An Underexplored but Important Proteome.” *Expert Review of Proteomics* 7(6):803–6.

Wilson, Richard, Emma L. Norris, Bent Brachvogel, Constanza Angelucci, Snezana Zivkovic, Lavinia Gordon, Bianca C. Bernardo, Jacek Stermann, Kiyotoshi Sekiguchi, Jeffrey J. Gorman, and John F. Bateman. 2012. “Changes in the Chondrocyte and Extracellular Matrix Proteome during Post-Natal Mouse Cartilage Development.” *Molecular & Cellular Proteomics* 11(1):2224–56.

Wondrak, Georg T., Myron K. Jacobson, and Elaine L. Jacobson. 2006. “Endogenous UVA-Photosensitizers: Mediators of Skin Photodamage and Novel Targets for Skin Photoprotection.” *Photochemical & Photobiological Sciences* 5(2):215–37.

Wong, David J. and Howard Y. Chang. 2008. “Skin Tissue Engineering.” in *StemBook*. Cambridge (MA).

Woodley, David, Daniel Sauder, Mary Jane Talley, Michael Silver, Gary Grotendorst, and Eva Qwarnstrom. 1983. “Localization of Basement Membrane Components after Dermal-Epidermal Junction Separation.” *Journal of Investigative Dermatology* 81(2):149–53.

World Health Organization. 2002. “Global Solar UV Index: A Practical Guide.” *World Meteorological Organization, United Nations Environment Programme, and the International Commission on Non-Ionizing Radiation Protection* 28.

Wright, Robert R. 1961. “Elastic Tissue of Normal and Emphysematous Lungs: A Tridimensional Histologic Study.” *The American Journal of Pathology* 39(3):355–67.

Xiong, Xuepeng, Tianfu Wu, and Sangang He. 2013. “Physical Forces Make Rete Ridges in Oral Mucosa.” *Medical Hypotheses* 81(5):883–86.

Yaar, Mina and Barbara A. Gilchrest. 2007. “Photoageing: Mechanism, Prevention and Therapy.” *British Journal of Dermatology* 157(5):874–87.

Yadin, David A., Ian B. Robertson, Joanne McNaught-Davis, Paul Evans, David Stoddart, Penny A. Handford, Sacha A. Jensen, and Christina Redfield. 2013. “Structure of the Fibrillin-1 N-Terminal Domains Suggests That Heparan Sulfate Regulates the Early Stages of Microfibril Assembly.” *Structure* 21(10):1743–56.

Yamanouchi, Kaori, Eichi Tsuruga, Kyoko Oka, Yoshihiko Sawa, and Hiroyuki Ishikawa. 2012. “Fibrillin-1 and Fibrillin-2 Are Essential for Formation of Thick Oxytalan Fibers in Human Nonpigmented Ciliary Epithelial Cells in Vitro.” *Connective Tissue Research* 53(1):14–20.

Yanagisawa, Hiromi, Elaine C. Davis, Barry C. Starcher, Takashi Ouchi, Masashi Yanagisawa, James A. Richardson, and Eric N. Olson. 2002. “Fibulin-5 Is an Elastin-Binding Protein Essential for Elastic Fibre Development in Vivo.” *Nature* 415(6868):168.

Yen, Ten-Yang, Rajesh K. Joshi, Hui Yan, Nina O. L. Seto, Monica M. Palcic, and Bruce A. Macher. 2000. “Characterization of Cysteine Residues and Disulfide Bonds in Proteins by Liquid Chromatography/Electrospray Ionization Tandem Mass Spectrometry.” *Journal of Mass Spectrometry* 35(8):990–1002.

Young, Antony R. 2006. “Acute Effects of UVR on Human Eyes and Skin.” *Progress in Biophysics and Molecular Biology* 92(1):80–85.

Yuan, Xuemei, A. Kristina Downing, Vroni Knott, and Penny A. Handford. 1997. “Solution Structure of the Transforming Growth Factor Beta-Binding Protein-like Module, a Domain Associated with Matrix Fibrils.” *EMBO Journal* 16(22):6659–66.

Yurchenco, Peter D. 2011. “Basement Membranes: Cell Scaffoldings and Signaling Platforms.” *Cold Spring Harbor Perspectives in Biology* 3(2):1–27.

Yuspa, Stuart H., Henry Hennings, Robert W. Tucker, Susan Jaken, Anne E. Kilkenny, and Dennis R. Roop. 1988. “Signal Transduction for Proliferation and Differentiation in Keratinocytes.” *Annals of the New York Academy of Sciences* 548(1):191–96.

Zacchigna, Luca, Carmine Vecchione, Antonella Notte, Michelangelo Cordenonsi, Sirio Dupont, Silvia Maretto, Giuseppe Cifelli, Alessandra Ferrari, Angelo Maffei, and Carla Fabbro. 2006. “Emilin1 Links TGF-β Maturation to Blood Pressure Homeostasis.” *Cell* 124(5):929–42.

Zhang, Hui, Stephen D. Apfelroth, Wei Hu, Elaine C. Davis, Chiara Sanguineti, Jeffrey Bonadio, Robert P. Mecham, and Francesco Ramirez. 1994. “Structure and Expression of Fibrillin-2, a Novel Microfibrillar Component Preferentially Located in Elastic Matrices.” *Journal of Cell Biology* 124(5):855–63.

Zheng, Qian, Siming Chen, Ying Chen, John Lyga, Russell Wyborski, and Uma Santhanam. 2013. “Investigation of Age-Related Decline of Microfibril-Associated Glycoprotein-1 in Human Skin through Immunohistochemistry Study.” *Clinical, Cosmetic and Investigational Dermatology* 6:317.

Zilberberg, Lior, Vesna Todorovic, Branka Dabovic, Masahito Horiguchi, Thomas Couroussé, Lynn Y. Sakai, and Daniel B. Rifkin. 2012. “Specificity of Latent TGF-β Binding Protein (LTBP) Incorporation into Matrix: Role of Fibrillins and Fibronectin.” *Journal of Cellular Physiology* 227(12):3828–36.

Structural and compositional diversity of fibrillin microfibrils in human tissues

JBC ARTICLE

⌘ *Author's Choice*

Structural and compositional diversity of fibrillin microfibrils in human tissues

Received for publication, December 15, 2017, and in revised form, February 7, 2018 Published, Papers in Press, February 16, 2018, DOI 10.1074/jbc.RA117.001483

Alexander Eckersley[‡], Kieran T. Mellody[‡], Suzanne Pilkington[§], Christopher E. M. Griffiths[§¶], Rachel E. B. Watson[§¶], Ronan O'Cualain[‖], Clair Baldock[‡1], David Knight[‖], and Michael J. Sherratt[‖1,2]**

*From the [‡]Division of Cell Matrix Biology and Regenerative Medicine, the [§]Division of Musculoskeletal and Dermatological Sciences, the [‖]School of Biological Sciences, and the **Wellcome Trust Centre for Cell-Matrix Research, Faculty of Biology, Medicine and Health, University of Manchester, Manchester M13 9PT, United Kingdom and the [¶]NIHR Manchester Biomedical Research Centre, Central Manchester University Hospitals NHS Foundation Trust, Manchester Academic Health Science Centre, Manchester M13 9PT, United Kingdom*

Edited by Gerald W. Hart

Elastic fibers comprising fibrillin microfibrils and elastin are present in many tissues, including the skin, lungs, and arteries, where they confer elasticity and resilience. Although fibrillin microfibrils play distinct and tissue-specific functional roles, it is unclear whether their ultrastructure and composition differ between elastin-rich (skin) and elastin-poor (ciliary body and zonule) organs or after *in vitro* synthesis by cultured cells. Here, we used atomic force microscopy, which revealed that the bead morphology of fibrillin microfibrils isolated from the human eye differs from those isolated from the skin. Using newly developed pre-MS preparation methods and LC-MS/MS, we detected tissue-specific regions of the fibrillin-1 primary structure that were differentially susceptible to proteolytic extraction. Comparing tissue- and culture-derived microfibrils, we found that dermis- and dermal fibroblast–derived fibrillin microfibrils differ in both bead morphology and periodicity and also exhibit regional differences in fibrillin-1 proteolytic susceptibility. In contrast, collagen VI microfibrils from the same dermal or fibroblast samples were invariant in ultrastructure (periodicity) and protease susceptibility. Finally, we observed that skin- and eye-derived microfibril suspensions were enriched in elastic fiber– and basement membrane–associated proteins, respectively. LC-MS/MS also identified proteins (such as calreticulin and protein-disulfide isomerase) that are potentially fundamental to fibrillin microfibril biology, regardless of their tissue source. Fibrillin microfibrils synthesized in cell culture lacked some of these key proteins (MFAP2 and -4 and fibrillin-2). These results showcase the structural diversity of these key extracellular matrix assemblies, which may relate to their distinct roles in the tissues where they reside.

Extracellular matrices (ECM)[3] are commonly composed of a diverse array of assemblies, which make key contributions to tissue mechanics and cell-mediated homeostasis. Some of these assemblies, such as the fibrillar collagens and the elastic fibers, are large, insoluble, and supramacromolecular. Some are markedly long-lived, laid down early in development, where they persist and undergo a process of maturation (1) and subsequent age- and disease-related accumulation of damage (2, 3). During these processes, the ultrastructure of these assemblies can be tissue-specific (1). Therefore, although these ECM assemblies are present in multiple tissues, they may exhibit distinct development-mediated ultrastructures that have evolved to fulfill their unique functionality.

Elastic fibers (composed of fibrillin microfibrils and elastin (4)) are present in many tissues, including skin (5), lungs (6), arteries (7), and ligaments (8), where they play a major role in conferring elasticity and resilience (4). The fibrillin microfibril, along with elastin, is a key component of the elastic fiber and adopts a bead-on-a-string appearance (9) when extracted and viewed with atomic force microscopy (AFM) and EM. Additionally, these microfibrils exist also as stand-alone assemblies, forming candelabra-like structures (10) (for a review, see Ref. 11) in the papillary dermis. They also play a role in tissue homeostasis, sequestering and storing the latent forms of members of the TGF-β (12, 13) and BMP families (14). In eyes, fibrillin microfibrils play an architectural role very different from that in skin. They form the ciliary zonules, stand-alone suspensory ligaments that connect the lens capsule to the ciliary muscle (15). These zonules come under tensile stress as the ciliary muscle exerts a strain to deform the lens during accommodation. Although fibrillin microfibrils appear structurally and compositionally similar in mammalian tissues and cell culture systems

This work was supported by a program grant from Walgreens Boots Alliance (Nottingham, UK). The authors declare that they have no conflicts of interest with the contents of this article. Walgreens Boots Alliance has approved this manuscript's submission but exerted no editorial control over the content.

This article contains Table S1 and Fig. S1.

The mass spectrometric raw data and spectral libraries associated with this manuscript are available from ProteomeXchange with the accession number PXD008450.

[1] Supported by Biotechnology and Biological Sciences Research Council (BBSRC) Grant BB/N015398/1.

[2] To whom correspondence should be addressed: 1.529 Stopford Bldg., University of Manchester, Oxford Rd., Manchester M13 9PT, United Kingdom. Tel.: 44-161-275-1439; Fax: 44-161-275-5171; E-mail: michael.sherratt@manchester.ac.uk.

[3] The abbreviations used are: ECM, extracellular matrix; AFM, atomic force microscopy; TGF, transforming growth factor; BMP, bone morphogenetic protein; CB, ciliary body; MFAP, microfibril-associated protein; HDF, human dermal fibroblast; EMILIN, elastin microfibril interface-located protein; PDI, protein-disulfide isomerase; FDR, false discovery rate; PSM, peptide spectrum match; EGF, epidermal growth factor.

and retain a beadlike structure (and presence of the main component, fibrillin-1) throughout different tissues (9), little is known about whether they have evolved to be distinct in each. Only two studies have shown that fibrillin microfibril ultrastructure is tissue- and developmentally dependent. In 1997, we showed that intertissue differences in mass and periodicity (interbead distance) exist in microfibrils derived from bovine fetal aorta and skin (16). We also showed that fibrillin microfibrils undergo a process of post-translational maturation as their mass increases during fetus development. Lu *et al.* (17) also reported similar differences in bead morphology between bovine adult aorta- and ciliary zonule-derived fibrillin microfibrils.

Because fibrillin microfibrils are present in a variety of tissues, the different roles they play may be reflected in the ultrastructure they adopt. These intertissue comparisons have never been made in humans or between fibrillin microfibrils sourced from ciliary body (CB) and skin, where they play very different architectural and mechanical roles. Additionally, the fibrillin microfibril's biomolecular composition has never been compared between tissues. Although their ultrastructure has been extensively studied using AFM (18–20) and EM (9, 18, 21), characterization of the biomolecular composition through conventional biochemical approaches such as gel electrophoresis can be problematic due to their large size and insolubility. As a consequence, it is necessary to develop proteomic approaches to characterize fibrillin microfibril composition.

Recently, De Maria *et al.* (22) performed whole-tissue proteomics on dissected human and bovine ciliary zonules and effectively characterized the zonular proteome. However, to date, only a single published proteomic study, performed by Cain *et al.* (23), has attempted to characterize both the structure and composition of fibrillin microfibrils purified from human tissue. Through LC-MS/MS, Cain *et al.* (23) achieved a 30% primary coverage of fibrillin-1 and identified several microfibril-associated proteins, such as microfibril-associated protein 2 (MFAP2). They demonstrated that MS-based proteomic approaches have the potential to identify the proteins involved in these supramolecular ECM assemblies. However, they observed that peptide generation from the core fibrillin-1 proteins, and their interacting proteins, was challenging due to their large size and high number of cross-links (24). Since this study took place, over 10 years ago, advances have been made in mass spectrometer technology allowing greater resolving power with expanded functionalities (25). Coupled with improved sample preparation, we believe that these proteomic approaches can be enhanced further to allow effective intertissue comparisons of fibrillin microfibril composition and structure.

In this study, we optimized two effective methods of pre-MS sample preparation: elastase digestion and SMART^{TM} digestion, for the enhanced generation of fibrillin peptides and their microfibril-associated proteins. This led to an improved compositional analysis via LC-MS/MS, compared with Cain *et al.* (23). We go on to test differences between the ultrastructure (bead morphology and interbead periodicity) using AFM and biomolecular composition (fibrillin-1 structural and enzymatic susceptibly and associated protein presence) using MS of fibrillin microfibrils isolated from human eye (CB), human skin, and cultured human dermal fibroblasts (HDFs). Because collagen VI microfibrils co-purify with fibrillin microfibrils in skin- and HDF-derived samples, we use them as a comparative control. We perform these analyses to test the following hypotheses: 1) fibrillin microfibril ultrastructure and composition are tissue-dependent and 2) culture-derived, newly synthesized fibrillin microfibril ultrastructure and composition are distinct from those of native, mature, tissue-sourced microfibrils.

Results and discussion

Elastase digestion methods enhance fibrillin-1 peptide generation and, combined with SMART^{TM} digestion methods, enhance the detection of microfibril-associated proteins

To improve the generation of peptides from core microfibril components, porcine elastase, a highly active and nonspecific enzyme (which preferentially cleaves leucine, isoleucine, alanine, serine, valine, and glycine) (26, 27) was used instead of conventional trypsin-based methodologies (for a review, see Ref. 28). For human CB-derived fibrillin microfibrils, this method, along with the use of a latest-generation mass spectrometer, led to an improved primary coverage (33%) and domain coverage (76%) of fibrillin-1, compared with that achieved by Cain *et al.* (23) (30% primary, 64% domain) (Fig. 1*A*) and, for the first time, the identification of peptides from the C-terminal region of fibrillin-1 (*orange arrow*). A similar primary sequence and domain coverage were achieved when applied to human skin. Crucially, this improved coverage was achieved by the digestion and MS of single CB and skin samples, whereas Cain *et al.* (23) reported a total primary sequence coverage of 30% from peptides identified in 13 separately prepared human Gu-HCl– and/or trypsin-treated ciliary zonule samples.

To improve peptide generation from proteins that co-purify with the microfibril, SMART^{TM} digestion was used. Collectively, the elastase and SMART^{TM} digestion methods led to the successful identification of 13 known microfibril-associated proteins (Fig. 1*B*) from human CB. These include annexin V, annexin II, and MFAP2, identified by Cain *et al.* (23) in 2006.

Fibrillin microfibril bead morphology is tissue-dependent

The fibrillin microfibril is composed predominantly of fibrillin-1 (~8 monomers per single bead and interbead repeat) with a total mass of ~2.5 MDa per repeat (9). The average periodicity and bead width has been approximated to 56 and 19 nm, respectively (for a detailed breakdown of microfibril dimensions, see Ref. 9). Our data showed that fibrillin microfibrils derived from human eye (CB) had a significantly higher mean central bead height than those derived from human skin. (Fig 2*A*, *i*). Central bead height frequency distributions indicate that the majority of eye-derived fibrillin microfibrils had larger beads than skin-derived (Fig. 2*A*, *ii*). Additionally, average axial height profiles showed that although eye-derived fibrillin microfibrils beads are significantly higher within a ~10-nm radius of the center, they were significantly lower at the shoulder region, ~20 nm from the peak (Fig. 2*A*, *iii*, *orange arrow*) than skin-derived. These height differences in bead morphology are further exemplified in the contour heat map (Fig. 2*A*, *iv*), where eye-derived microfibrils appear to have a more pro-

A

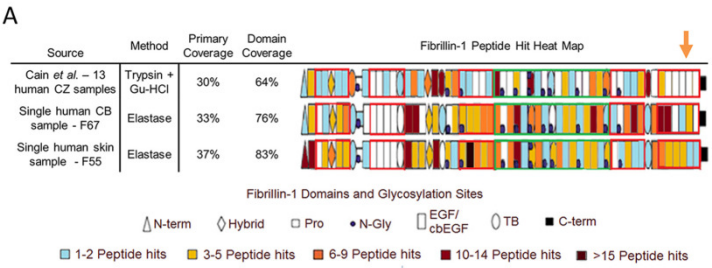

B

		Peptide Spectrum Matches	
Identified Associates	Cain *et al.* 2006 (3)	Elastase (10)	SMART™ (9)
Annexin V	✓	74	17
Annexin II	✓	52	17
MFAP2	✓	5	
Vimentin		11	18
Nidogen-1		2	5
Laminin β2		3	16
βig-H3		4	5
MFAP4		2	
MFAP5		7	
EMILIN-1		2	
Versican			3
Hyaluronan link-1			3
Prelamin-A/C			3

Figure 1. Elastase and SMART™ methods led to the improved detection of fibrillin-1 and improved identification of microfibril-associated proteins compared with previous published efforts. The ability of the elastase method to produce peptides of fibrillin-1 from a single human CB sample (female age 67; F67) and a single human skin sample (F55) is compared with the efforts of Cain *et al.* (23) (*A*). As performed by Cain *et al.* (23), PSMs (Peptide Prophet FDR ≤ 5%) were counted for each respective fibrillin-1 domain and heat-mapped. Our method led to a greater primary coverage and domain coverage from a single sample run than Cain *et al.* (23), whose coverages were achieved from 13 separate sample runs. Peptides from the C-terminal region of fibrillin-1 were also successfully detected (*orange arrow*), which Cain *et al.* (23) failed to identify. The known fibrillin microfibril-interacting proteins identified by Cain *et al.* (23) (*green*) are compared with those identified by elastase and SMART™ methods (Protein Prophet FDR ≤ 0.1%, Peptide Prophet FDR ≤ 5%) (*B*). The elastase method (*red*) and SMART™ method (*blue*) were both performed on the same human CB microfibril extract (F73). The elastase method appears to enhance the detection of microfibril-associated proteins thought to be tightly bonded to the structure (*i.e.* the MFAP family), whereas the SMART™ method appears to enhance the detection of weakly interacting proteins (*i.e.* versican and hyaluronan proteins). Collectively, these methods led to an enhanced detection of known microfibril-associated proteins compared with Cain *et al.* (23).

nounced bead with a lower shoulder region than skin. Between beads, however, there was no significant difference in the mean periodicity of fibrillin microfibrils derived from eye and skin (Fig. 2*B*, *i* and *ii*)

Many past studies exclusively used differences in periodicity to gauge ultrastructural differences in fibrillin microfibrils (19, 29–32) and other fibrillar components of the ECM (19, 33–35). However, not only does the majority of the fibrillin microfibril's mass rest within the bead, much of microfibril's functionality is thought to be mediated via the interaction between the bead and its associated proteins (36–38). Our data showed that eye-derived fibrillin microfibril beads differ in morphology in comparison with skin-derived, but periodicity did not. By omitting analysis of the microfibril bead, these studies may have missed some key ultrastructural changes linked to health and disease.

The ultrastructural variances seen between the beads of adult human eye- and skin-derived fibrillin microfibrils are similar to those we observed previously (16), where differences were detected in bead mass of microfibrils from bovine fetal skin and aorta. Lu *et al.* (17) also detected differences in bead morphology, including the shoulder regions, from bovine adult ciliary zonule and aorta.

Fibrillin-1 derived from human eye and skin exhibit intertissue, regional differences in elastase susceptibility

To further compare and substantiate the ultrastructural differences seen between CB and skin fibrillin microfibrils, it was necessary to characterize at their biomolecular composition (fibrillin-1 structure and known microfibril-associated protein presence). Previous studies have used differences in fibrillin-1's susceptibility to proteolysis to gauge abnormalities in fibrillin microfibril structure (39) and function (40, 41). It is possible that the fibrillin-1 structure may exhibit regional differences in proteolytic susceptibilities depending on its tissue of origin.

LC-MS/MS–detected peptide hit patterns (23) indicate several regions of human eye-derived fibrillin-1 (Fig. 3) with differing susceptibilities to elastase in comparison with skin-derived (*green brackets*). These regional differences indicate that, not only are fibrillin microfibrils ultrastructurally variable between tissues, but their fibrillin-1 structure may also be as

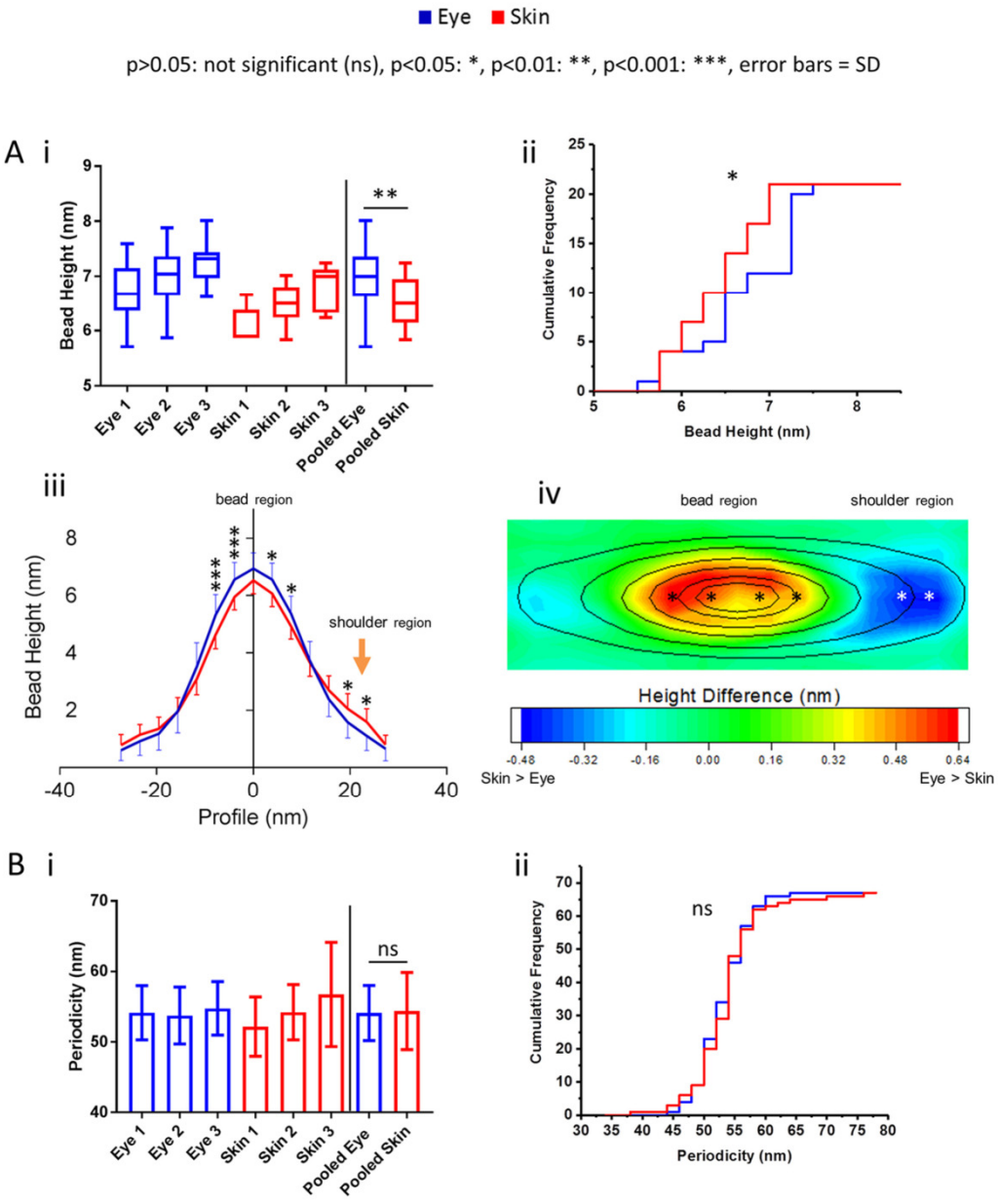

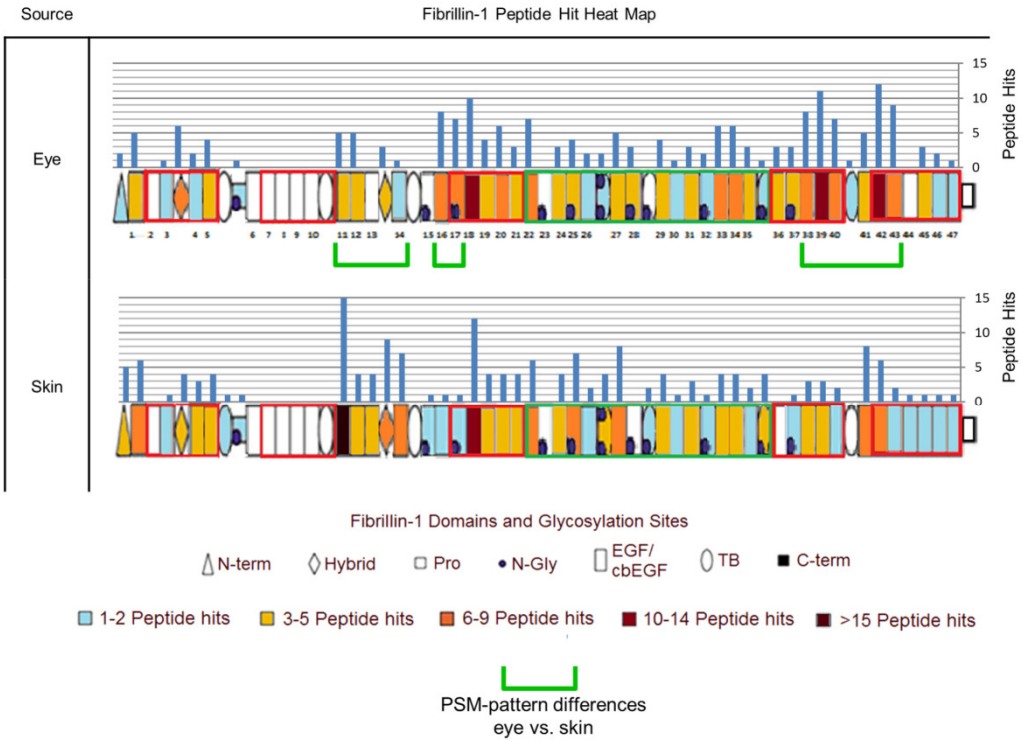

Figure 3. Eye-derived fibrillin-1 exhibits different regional patterns of elastase susceptibility compared with skin-derived. LC-MS/MS–detected fibrillin-1 PSMs (Peptide Prophet FDR ≤ 5%) were counted for each respective protein domain, per sample ($n = 3$), averaged (normalized based on total spectrum count), and subsequently heat-mapped to their corresponding domain. Eye-derived fibrillin-1 yielded more peptides between epidermal growth factor-like domains 38 (EGF38) and EGF43 than skin-derived (53 total from eye-derived *versus* 24 total from skin-derived) (*green brackets*). Eye-derived fibrillin-1 also yielded more peptides at EGF16 and EGF17 than skin-derived (15 *versus* 2); however, it yielded fewer peptides between EGF11 and EGF14 (14 *versus* 39).

well. Collectively, the differences in structure suggest that these supramolecular assemblies may have evolved distinct ultrastructures and compositions to cope with their different architectural, mechanical, and biochemical roles in their respective tissues of origin. It is possible that the presence of different cell types within each tissue may have contributed to these differences. Baldwin *et al.* showed that the epithelial-mesenchymal state of retinal pigment epithelial cells influenced their ability to assemble fibrillin microfibrils (42). Although fibroblasts (mesenchymal cells) are thought to be responsible for microfibril deposition in skin (43) and in eye (44), it remains unknown whether epithelial cells contribute to fibrillin microfibril synthesis *in vivo* (45). It is also unclear whether populations of fibroblasts from different tissues exhibit differences in epithelial-mesenchymal states, as shown in retinal pigment epithelial cells (42). It is possible, therefore, that different cell types (or cells in different states) may synthesize fibrillin microfibrils with localized differences in structure.

So far, we have demonstrated that fibrillin microfibril ultrastructure and fibrillin-1 regional susceptibility are tissue-depen-

Figure 2. Fibrillin microfibril ultrastructure is tissue source– dependent. Eye-derived fibrillin microfibril mean central bead height was significantly higher (6.94 nm; $n = 100$ repeats/sample, averaged per microfibril; $n = 300$ repeats in pooled data) than skin-derived (6.51 nm; $p = 0.0023$, Mann–Whitney *U* test) (*A*, *i*). Cumulative frequency distributions of central bead height (averaged per microfibril, $n = 21$ pooled) indicate a large population of eye-derived fibrillin microfibrils with significantly larger beads ($p = 0.0423$; Kolmogorov–Smirnov) than skin-derived (*A*, *ii*). Axial bead profiles show that, although skin-derived fibrillin microfibril beads are significantly smaller, within ~10 nm of the bead peak, than eye-derived (*A*, *iii*; Bonferroni corrected multiple comparison test), they also have significantly higher slopes at the shoulder regions than eye-derived (*orange arrow*). This may suggest that skin-derived fibrillin microfibril beads have a different volume distribution than that of eye-derived. To visualize these differences in bead morphology, the whole AFM height maps of skin-derived fibrillin microfibril beads were averaged and subtracted from that of eye-derived. The resulting height differences are represented as a heat map overlaid with the average height contour of the eye-derived beads (*A*, *iv*). The significant differences seen in the axial profile panel (*iii*) were also added to the heat map (*iv*, *stars*). The biggest differences in bead morphology were around the central peak, where eye-derived beads were higher than skin-derived, and at the shoulder region, where skin-derived beads were higher than eye-derived. There was no significant difference (*ns*) in the mean periodicity ($p = 0.9737$; Mann–Whitney *U* test, $n = 500$ repeats/sample, averaged per microfibril; $n = 1500$ repeats in pooled data) (*B*, *i*) and in the cumulative frequency distributions of periodicities ($p = 0.8580$; Kolmogorov–Smirnov, averaged per microfibril, $n = 67$ pooled) (*B*, *ii*) between eye- and skin-derived fibrillin microfibrils. *Error bars*, S.D.

dent. These differences may also relate to microfibril post-translational maturation in development. To study this, we applied the same analysis to newly synthesized fibrillin microfibrils derived from cultured HDFs and compared them with skin fibrillin microfibrils, derived *ex vivo*.

Newly synthesized, HDF-derived fibrillin microfibrils exhibit marked differences in ultrastructure compared with skin-derived

On average, cultured HDF-derived, newly synthesized, fibrillin microfibrils had a significantly lower central bead height than human skin-derived (Fig. 4*A*, *i*). Additionally, central bead height frequency distributions indicate a subpopulation of cultured HDF-derived fibrillin microfibrils with smaller beads than human skin-derived (Fig. 4*A*, *ii*, *orange arrow*). Average axial height profiles indicate that, although skin fibrillin microfibril beads have a significantly larger central peak height than cultured HDF-derived microfibrils, the reverse is true on the slopes of the beads (opposite to the shoulder region) (Fig. 4*A*, *iii*, *purple arrow*). This difference in bead morphology is further shown in the contour heat map (Fig. 4*A*, *iv*). Skin-derived beads have a higher peak with a more pronounced slope (except near the shoulder region) than HDF-derived beads. This indicates that beads of newly synthesized fibrillin microfibrils from cultured-HDFs have a morphology different from those derived from human skin.

On average, cultured HDF-derived fibrillin microfibrils also exhibited a significantly higher periodicity in comparison with skin-derived fibrillin microfibrils (Fig. 4*B*, *i*). In addition, periodicity frequency distributions show a large population of cultured HDF-derived fibrillin microfibrils with significantly higher periodicities than skin-derived (Fig. 4*B*, *ii*).

Similar differences in fibrillin microfibril bead morphology and periodicity have been reported previously in three cases. The first is between tissues where we showed that bovine fetal aorta fibrillin microfibrils had a higher bead mass and a lower periodicity than those derived from skin (16) and where Lu *et al.* (17) also reported that aorta-derived fibrillin microfibrils had differing bead morphologies and a higher periodicity compared with those from bovine zonules. The second is during developmental microfibril maturation, where we also showed that the gradual increase in fetal fibrillin microfibril bead mass and the gradual decrease in periodicity correlated with gestation time (16). The third is during photoaging, where two studies highlighted the structural susceptibility of fibrillin microfibrils to UV irradiation. We showed that a low-dose UVB irradiation of both HDF- and human skin-derived fibrillin microfibrils directly led to the marked loss and redistribution of their bead mass and a significant increase in their periodicity (20). Since then, our group has also showed that physiological doses of both solar-simulated radiation (~5% UVB and ~95% UVA) and pure UVA led to a significant decrease in the periodicity of HDF-derived fibrillin microfibrils (19).

Although these fibrillin microfibril ultrastructural differences have been reported between tissues, during maturation, and in photodamage, this study has identified them between microfibrils derived *in vitro*, from primary fibroblasts (natively found in human skin), and those derived *ex vivo*, directly from human skin. It is possible, therefore, that 1) the fibrillin microfibrils generated by HDFs are structurally immature in comparison with native microfibrils sourced from skin (either through lack of development or through the cell culture process) or that 2) the native skin-derived microfibrils have accumulated structural damage during aging in comparison with those newly synthesized from HDFs. The aging process would be more intrinsic than extrinsic (photoaging) because abdominal skin is relatively photoprotected compared with forearm skin used in previous photoaging studies (5). Because elastic fiber production is commonly thought to be fibroblast-driven (43), these changes may have profound implications for skin-regenerative therapies, especially if they are linked to developmental maturation or aging.

Fibrillin-1 derived from newly synthesized, HDF fibrillin microfibrils exhibited regional differences in elastase susceptibility compared with skin-derived

LC-MS/MS–detected peptide hit patterns (23) indicate several regions of human skin-derived fibrillin-1 (Fig. 5) with differing susceptibilities to elastase in comparison with HDF-derived (*purple brackets*). The observations that 1) these regions of cultured HDF-derived fibrillin-1 have a structural susceptibility to elastase different from skin-derived and 2) HDF-derived fibrillin microfibrils have different ultrastructures compared with skin (Fig. 4) both support the possibility that either newly synthesized fibrillin microfibrils, derived from HDFs, are structurally immature compared with the more developmental (46), long-lived (2) microfibrils from skin or that the skin-derived fibrillin microfibrils are exhibiting signs of aging in comparison with those newly synthesized from cells.

It is possible that these long-lived (2), skin-derived fibrillin microfibrils may have accumulated age-related damage through the formation of oxidative cross-links (47) (for a review, see Ref. 48) induced by the long-term exposure to reactive oxygen species in tissue and also via the accrual of advanced-glycation end products on fibrillin-1 (49) (for a review, see Ref. 50). This process may have led to a differential susceptibility to enzyme digestion and to an accrual of sugar on the surface of the bead, which would explain the variations in bead morphology.

HDF and skin-derived collagen VI microfibril structure is conserved compared with the fibrillin microfibril

Like the fibrillin microfibril, tissue collagen VI microfibrils are long-lived (3), supramolecular, beaded assemblies (52). Both microfibrillar species are highly abundant in connective tissue (53) and, as such, regularly co-purify (19, 53). This allowed us to a make a useful comparison between periodicity differences in collagen VI microfibrils and periodicity differences of fibrillin microfibrils in the same skin- and HDF-derived samples. However, because collagen VI microfibril beads are relatively small in comparison with fibrillin microfibril beads (19), unfortunately, AFM resolution was not good enough to assess differences in collagen VI bead morphology. Encouragingly, however, the optimized elastase method generated sufficient collagen VI α-3 (COL6A3) peptides (Fig. S1) to enable its regional susceptibility to elastase to also be compared

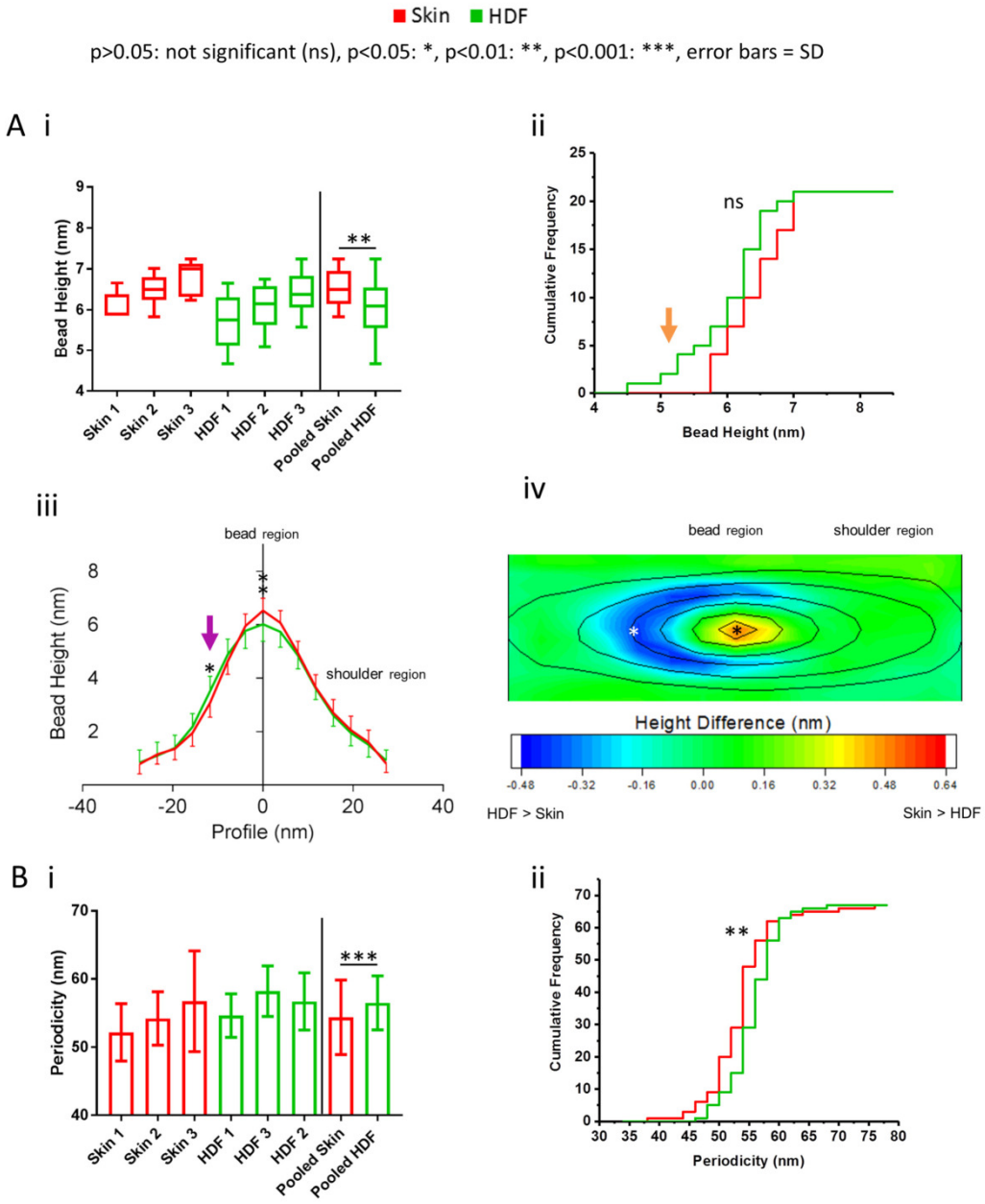

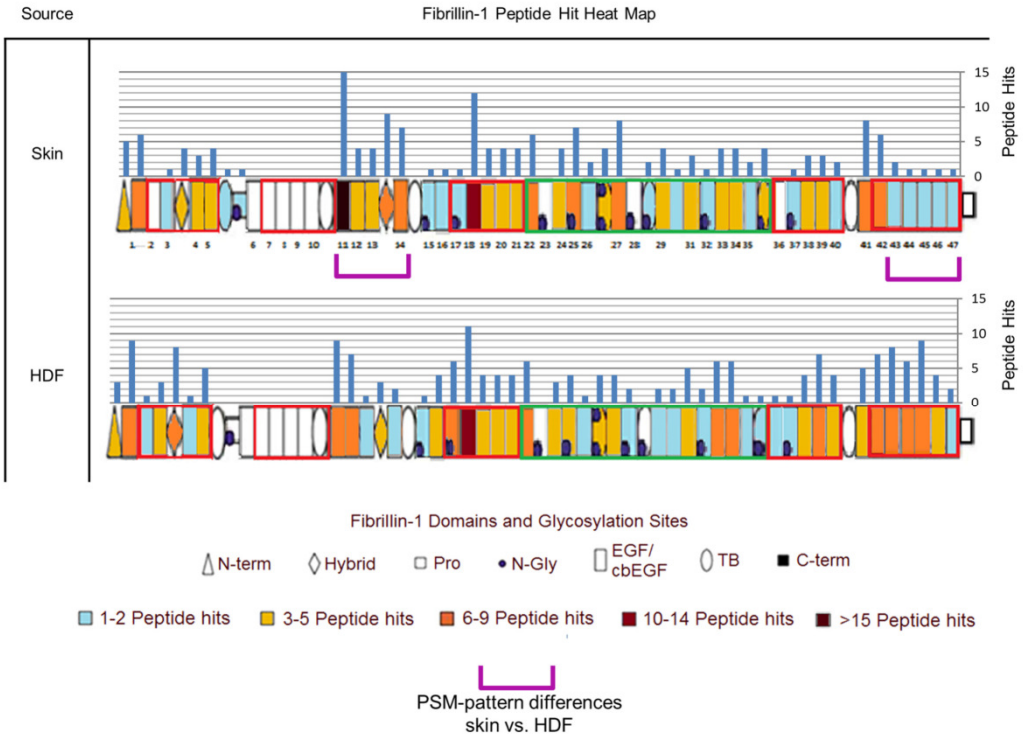

Figure 5. Fibrillin-1, derived from newly synthesized HDF fibrillin microfibrils, exhibits different regional patterns of elastase susceptibility compared with skin-derived. LC-MS/MS–detected fibrillin-1 PSMs (Peptide Prophet FDR ≤ 5%) were counted for each respective protein domain, per sample (n = 3), averaged (normalized based on total spectrum count), and subsequently heat-mapped to their corresponding domain. Skin-derived fibrillin-1 yielded fewer peptides from the last five domains at the C-terminal region, between EGF43 and EGF47 (6 *versus* 29), than HDF-derived; however, skin-derived yielded more peptides between EGF11 and EGF14 (39 *versus* 22) than HDF-derived (*purple brackets*).

with fibrillin-1. These comparisons allow us to differentiate whether the changes seen so far, between newly synthesized fibrillin microfibrils in culture and those derived in tissue, extrapolate to another predominating component of the ECM.

The periodicity and elastase susceptibility differences seen between HDF- and skin-derived fibrillin microfibrils (Fig. 4*B*) are in stark contrast to the lack of differences seen in collagen VI microfibrils within the same samples (Fig. 6*A*). Newly synthesized, cultured HDF-derived collagen VI microfibril periodicity was not significantly different from that of skin collagen VI microfibrils, derived *ex vivo* (Fig. 6*A*, *i*). In addition, no distinctly different subpopulations of collagen VI microfibrils were seen when looking at periodicity frequency distributions of cultured HDF- and skin-derived collagen VI microfibrils (Fig. 6*A*, *ii*). In fact, both distributions follow almost the same pattern, suggesting that there is very little difference in the periodicity of collagen VI microfibrils from these two sources, unlike the fibrillin microfibril (Fig. 4*B*).

LC-MS/MS–detected peptide hit patterns, in response to elastase digestion of COL6A3 (Fig. 6*B*), were similar at the tri-

Figure 4. Newly synthesized, HDF-derived fibrillin microfibril ultrastructure is significantly different from native skin-derived. HDF-derived fibrillin microfibrils had significantly lower central bead heights (6.02 nm; n = 100 repeats/sample, averaged per microfibril; n = 300 repeats in pooled data) than skin-derived (6.51 nm, p = 0.0038, Mann–Whitney U test) (*A*, *i*). Cumulative frequency distributions of central bead height were not significantly different (p = 0.1938, Kolmogorov–Smirnov; averaged per microfibril, n = 21 pooled); however, they indicate a subpopulation of HDF-derived fibrillin microfibrils with smaller beads than skin-derived (*A*, *ii*; *orange arrow*). Axial bead profiles (*A*, *iii*) show that skin-derived fibrillin microfibril beads are significantly higher than HDF-derived beads close to the central peak and significantly lower than HDF-derived beads at the slope opposite to the shoulder region (*purple arrow*) (Bonferroni corrected multiple-comparison test; n = 300 repeats pooled, averaged per microfibril). These changes in bead morphology are reflected in the height difference contoured heat map (*A*, *iv*) (AFM height maps of HDF-derived fibrillin microfibril beads were averaged and subtracted from that of skin-derived and subsequently heat-mapped; the contour height of the average skin bead was then overlaid). Skin beads were higher than HDF beads only near the central peaks, whereas HDF beads had higher slopes around the peaks (except near the shoulder region). HDF-derived fibrillin microfibrils exhibited a significantly higher periodicity (56.5 nm; n = 500 repeats/sample, averaged per microfibril; n = 1500 repeats in pooled data) compared with skin-derived (54.4 nm; p = 0.0004, Mann–Whitney U test) (*B*, *i*). Periodicity cumulative frequency distributions indicate a large population of HDF-derived fibrillin microfibril with significantly higher periodicities (*B*, *ii*) in comparison with skin-derived (p = 0.0051; Kolmogorov–Smirnov, averaged per microfibril, n = 67 pooled). *Error bars*, S.D.

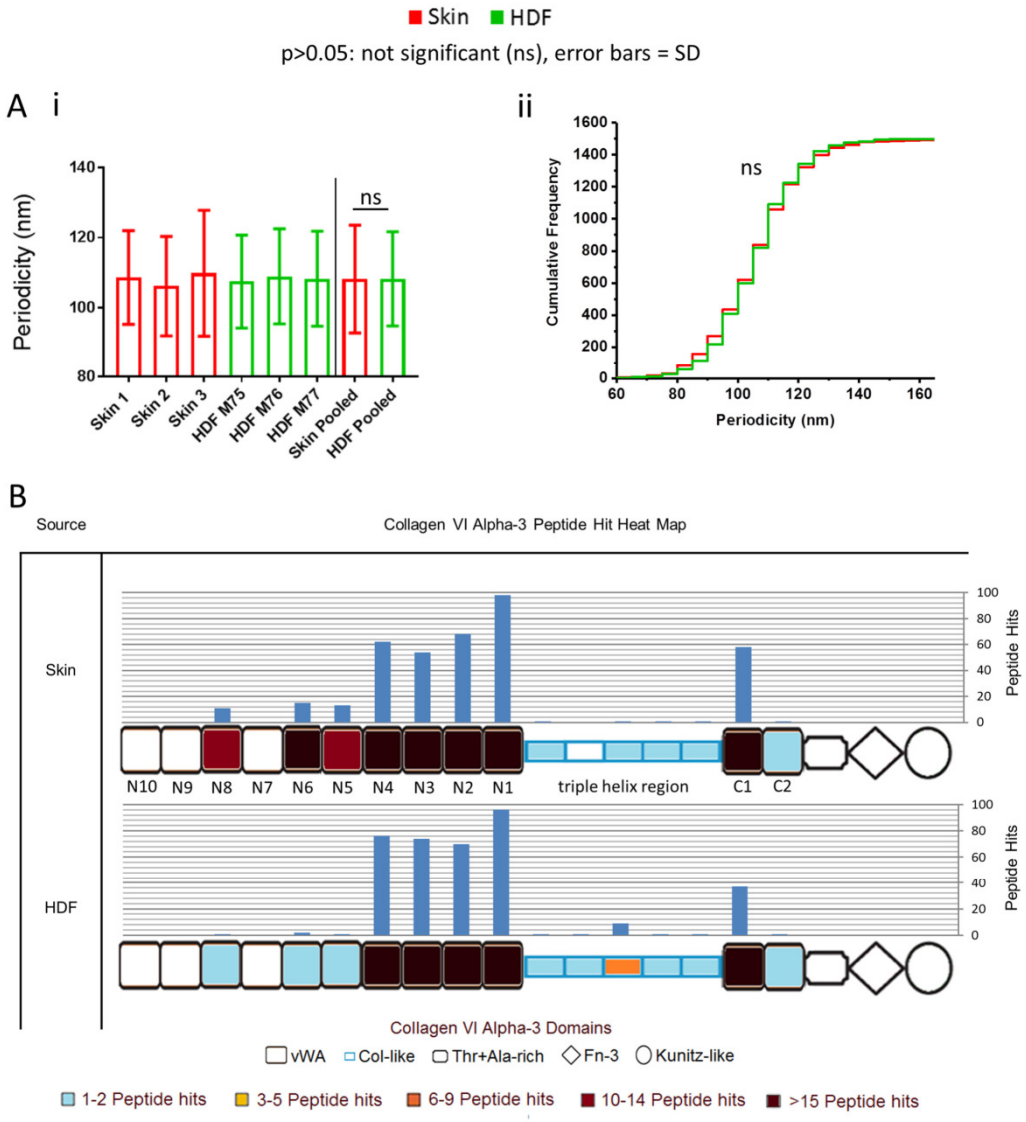

Figure 6. HDF- and skin-derived collagen VI microfibril ultrastructure and its susceptibility to elastase is predominantly invariant. There was no significant difference (*ns*) in periodicity between HDF-derived (108.2 nm; $n = 500$ repeats/sample, averaged per repeat; $n = 1500$ repeats in pooled data) and skin-derived (108.2 nm; $p = 0.6310$, Mann-Whitney *U* test) collagen VI microfibrils (*A*, *i*). Additionally, there was no significant difference between periodicity-cumulative frequency distributions of HDF- and skin-derived collagen VI microfibrils ($p = 0.2656$, Kolmogorov–Smirnov) (*A*, *ii*). LC-MS/MS–detected collagen VI α-3 (COL6A3) peptide sequences (Peptide Prophet FDR $\leq$ 5%) were counted for each respective protein domain, per sample ($n = 3$), averaged (normalized based on total spectrum count), and subsequently heat-mapped to their corresponding domain (*B*). There were similar PSM patterns between skin- and HDF-derived COL6A3 in all regions except at domains N5, N6, and N8, which yielded more peptides from skin-derived (39 total) than HDF-derived (four total). This analysis could not be effectively performed on eye-derived samples, due to low abundance of collagen VI microfibrils.

ple-helix region (52), at the N1–N4 region, and at the C1 domain of both skin- and HDF-derived samples. This is, again, in contrast to fibrillin-1, which did exhibit regional differences in response to elastase digestion (Fig. 5). However, domains N5, N6, and N8 yielded many more peptides from skin-derived COL6A3 than from cultured HDF-derived (Fig. 6*B*). Alternative splicing of COLA3 has been shown previously both in mice and in humans (54), and isoforms of this COL6A3 lacking domains N5 and N7–N10 have been identified previously in human cell lines (54, 55). It is possible, therefore, that cultured HDFs are also synthesizing collagen VI microfibrils that are lacking these domains, which would explain the reduction in peptide hits seen from these regions in the HDF-derived preparations compared with skin.

Previously, we have shown that collagen VI microfibril ultrastructure (periodicity) is resistant to both UVA and solar-simulated radiation, whereas fibrillin microfibril ultrastructure is susceptible (19). Additionally, Watson *et al.* (56) demonstrated that collagen VI microfibril distribution is unaffected in photoaged skin, also in contrast to fibrillin microfibrils in elastic fibers, which are markedly reduced in photoaged skin (5). Kielty *et al.* (57) also reported that skin-derived collagen VI microfibril ultrastructure was indistinguishable at each stage of bovine fetal development, unlike fibrillin microfibril ultrastructure, which is (16). The observations made in this study, that newly synthesized, HDF-derived collagen VI microfibrils are structurally similar to the long-lived microfibrils derived from tissue, corroborate evidence that they are resistant to age-related damage accumulation and that their ultrastructure may not undergo the developmental process of maturation seen in other components of the ECM. These findings are divergent in comparison with the degradation seen in fibrillin microfibrils in aging and to their maturation process (16) and accentuate the complexity of the fibrillin microfibril in tissue development and aging.

Differences in the presence of co-purifying microfibril-associated proteins may provide insight into tissue functions of fibrillin microfibrils

So far, differences have been observed in both the ultrastructure of fibrillin microfibrils and their fibrillin-1 regional susceptibility to elastase, derived, *ex vivo*, from eye and skin and *in vitro* from cultured HDFs. The fibrillin microfibril's function is tied to the network it forms with a wide variety of proteins within the ECM (see the references cited in Table 1). It is possible, therefore, that gauging the presence of these associated proteins may provide insight into the role they play within a specific tissue and into the underlying composition of the fibrillin microfibril.

Within the eye, skin, and HDF microfibril purifications, a large variety of known fibrillin microfibril-associated proteins (21, 30, 37, 46, 58–71) were identified using LC-MS/MS (Table 1). A large proportion of these associated proteins were uniquely detected in either tissue. Four proteins key to elastic fiber biology were identified in skin: the elastic fiber component elastin (21); elastin microfibril interface-located protein (EMILIN)-2, key to the microfibril's deposition onto elastic fibers (71); fibulin-1 (69), which exists as an interface between elastin and the fibrillin microfibril; and fibulin-2 (66), which co-localizes with elastic fibers *in vivo*. This indicates that fibrillin microfibrils play a dominant role as an elastic fiber component in skin. Conversely, four basement membrane proteins were identified in eye-microfibril samples: perlecan, which was shown to connect fibrillin microfibrils directly to basal laminas, along with two laminins and nidogen-1 which bind to perlecan itself (65). This indicates that fibrillin microfibrils play a major role in linking basement membranes within the CB epithelium of the eye.

Table 1
Published fibrillin microfibril-associated proteins identified in eye, skin, and HDF microfibril samples
Proteins, detected using LC-MS/MS (Protein Prophet FDR ≤0.1%), along with their peptide hit score (sum of $n = 3$) are shown. Peptide hit scores are as follows: *, 2–5; **, 6–14; ***, >15.

Protein	Published interaction	Microfibril-associated protein presence		
		Eye	Skin	HDF
Annexin A2	Cain *et al.* (58)	***	***	***
Annexin A5	Cain *et al.* (58)	***	***	***
Vimentin	Cain *et al.* (58)	***	***	***
Protein-disulfide isomerase	Meirelles *et al.* 2016 (59)	***	***	***
Calreticulin	Ashworth *et al.* (60)	***	***	***
MFAP5 (MAGP2)	Penner *et al.* (61)	**	***	***
βig-h3	Cain *et al.* (58)	*	***	***
Versican	Isogai *et al.* (37)	*	***	***
MMP14	Ashworth *et al.* (30)	*	**	***
Prelamin-A/C	Cain *et al.* (58)	*	*	**
Vitronectin	Dahlbäck *et al.* (62)	***	**	
MFAP2 (MAGP1)	Trask *et al.* (63)	**	**	
MFAP4	Pilecki *et al.* (64)	*	***	
Fibrillin-2	Zhang *et al.* (46)	*	**	
Laminin β2	Tiedemann *et al.* (65)	***		*
SERBP1	Cain *et al.* (58)	*		*
IGFBP7	Cain *et al.* (58)	*		*
Fibulin-2	Reinhardt *et al.* (66)		**	**
Laminin α5	Tiedemann *et al.* (65)	***		
Nidogen-1	Tiedemann *et al.* (65)	**		
Perlecan	Tiedemann *et al.* (65)	**		
Hyaluronan link protein 1	Ohno-Jinno *et al.* (67)	*		
LTBP2	Hirani *et al.* (68)	*		
Elastin	Sakai *et al.* (21)		*	
Fibulin-1	Roark *et al.* (69)		*	
EMILIN-2	Schiavinato *et al.* (71)		*	
Fibronectin 1	Sabatier *et al.* (70)			***
Thrombospondin 1	Cain *et al.* (58)			***
MMP2	Ashworth *et al.* (30)			**
MMP3	Ashworth *et al.* (30)			*
Decorin	Trask *et al.* (63)			*

The advantage of size-exclusion chromatography–purified microfibril proteomic analysis over whole tissue is that we can state with high confidence that the associated proteins identified must have been bound to the fibrillin microfibrils. Many of the proteins (fibrillin-2, MFAP2, MFAP5, and LTBP2) that directly co-purified with eye-derived microfibrils (Table 1) were the same as those found in the human zonule proteome published by De Maria *et al.* (22). Two of these proteins, metalloproteinase inhibitor 2 (TIMP3) and α-2 macroglobulin (A2M) were also identified in these suspensions (Table S1); however, they had no previously published interactions with fibrillin microfibrils. Because these proteins (TIMP3 in particular) were two of the most abundant protease inhibitors found in their whole-zonule proteome, they could be newly identified associated proteins of the fibrillin microfibrils. However, some of most abundant glycoproteins identified by De Maria *et al.*

(22) (emilin-1 and hemicentin-1) in their zonule proteome did not co-purify with our eye-derived fibrillin microfibrils. It could be that these proteins do not associate with the microfibrils directly or that the enzymatic extraction process and purification procedures stripped them from the microfibrils.

Many of the detected fibrillin microfibril-associated proteins were shared between tissues (Table 1). This may provide a key insight into identifying the integral components, fundamental to fibrillin microfibril assembly and function, regardless of the tissue of origin. Fibrillin microfibril assembly begins with the secretion of the fibrillin-1 monomer from the cell (60, 72), where it is N- and C-terminally processed by furin. It is proposed that the fibrillin-1 monomers then dimerize in the extracellular space (60) and that these dimers then form the basic intermediates for further microfibril assembly. This process is thought to occur at the cell surface through the homotypic interaction between the N and C termini of fibrillin-1 dimers (24). Microfibril assembly is thought to be cell-driven, as previous studies have shown that the deposition of fibrillin microfibrils by fibroblasts requires both fibronectin and the RGD-dependent $\alpha5\beta1$ integrins (70). The molecular chaperone calreticulin and the disulfide bond–forming protein-disulfide isomerase (PDI), (60) were identified in skin, eye, and HDF microfibril samples. Ashworth *et al.* (60) showed that both of these intracellular proteins bind to fibrillin-1, thereby inhibiting their dimerization and preventing their intracellular aggregation. They go on to propose that when the fibrillin-1 monomers are then secreted from the cell, the loss of these binding partners leads to their dimerization in the extracellular space. The microfibrils tested in this study were purified via size-exclusion chromatography, which separates structures of high molecular mass (MDa) from those of lower mass (kDa). This means the fractions used should be enriched with only mature fibrillin and collagen VI microfibrils of varying lengths. Theoretically, immature forms of fibrillin-1, already bound to calreticulin and PDI, could have associated with these mature microfibrils. However, the N terminus and C terminus of immature fibrillins are cleaved by furin (at positions 44 and 1732, respectively) (73, 74) only after secretion from the cell (72). In all samples tested, LC–MS/MS failed to detect any peptides corresponding to these cleaved propeptides. This suggests that immature fibrillin-1 was not detected in any of the samples tested. As such, it is possible that the intracellular proteins calreticulin and PDI were released from cells during the extraction process, where they then associated with the mature fibrillin microfibrils. Another explanation for the presence of PDI in the extracellular space is the recent evidence of its secretion from cells via an activation of $\alpha v\beta3$ integrin (75). In either case, the co-purification of calreticulin and PDI supports their proposed roles in microfibril assembly.

MFAP5, -2, and -4 were also identified in microfibril samples from both eye and skin tissues. Gibson *et al.* (76) previously showed in bovine that MFAP5 (also known as MAGP-2) is localized in CB but not in the zonule, in contrast to MFAP2 (also known as MAGP-1), which was found in both. This fits with our identification, because the microfibrils used in this study were extracted from human CB. However, De Maria *et al.* (22) did detect MFAP5 both in high abundance in the human zonule and in lesser abundance in the bovine zonule. It is possible that either the CB was a contaminant within the De Maria *et al.* (22) zonular samples (as in this study, they also detected the basement membrane proteins nidogen and laminin, which can be attributed to the CB epithelium) or that perhaps there exists a genuine disparity between the composition of human and bovine ciliary zonules.

MFAP4 and -5 are both instrumental to the proper formation and organization of elastic fibers (61, 64) by interacting and co-localizing with fibrillin-1, tropoelastin, and the cross-linking enzyme desmosine as well as promoting tropoelastin self-assembly on top of fibrillin microfibrils. MFAP2 (also known as MAGP-1) binds strongly to fibrillin microfibrils (63, 77) and was found to interact directly with both TGF-β and BMP-7 (78). Disrupting this interaction in mice leads to a marked increase in TGF-β signaling attributed to the loss of its sequestration into the fibrillin microfibril network (79). As such, MFAP2 plays a key role in modulating fibrillin-growth factor signaling. Fibrillin-2, a key component of maturing fibrillin microfibrils in developing elastic (80) and non-elastic (81) tissues, was also identified in microfibril preparations from both eye and skin. It is likely that these fibrillin microfibril-associated proteins were identified from both tissues because of the fundamental role they play in fibrillin microfibril assembly and function.

Fibrillin-2 and MFAP2 and -4, which were identified in both eye- and skin-derived microfibril samples, were not detected in cultured HDF-derived microfibril samples. The observation that all three HDF-derived fibrillin microfibril purifications lacked detection of fibrillin-2, MFAP2, and MFAP4 compared with tissue-derived indicates the possibility that these microfibrils may be immature and functionally impaired in 1) forming mature fibrillin microfibrils, 2) forming elastic fibers, and 3) modulating growth factor signaling. The differences seen in the ultrastructure and presence of key associated proteins, observed in cell-derived fibrillin microfibrils compared with tissue-derived, could be due to the limitations of the cell culture model itself. Removing HDFs from their native, homeostatic environments could have contributed directly to the formation of immature and possibly defective fibrillin microfibrils. Many studies have exclusively used cell culture-derived microfibrils to elucidate their functional role in the ECM (63, 82, 83). The differences seen in this study demonstrate a problem with this approach, as functional observations based on cell-derived fibrillin microfibrils may not necessarily reflect those in native tissue.

The differences in protein presence between HDF- and skin-derived fibrillin microfibril samples may have also contributed to the differences observed in bead morphology. MFAP2, for instance, binds to the fibrillin microfibril bead directly (38). As a consequence, it is possible that the redistribution of HDF-derived microfibril bead height compared with skin-derived (Fig. 4*A*, *iv*) may be due to the loss of these associated proteins from the surface.

Conclusion

Building upon previous evidence (16, 17), this study has found that not only is fibrillin microfibril bead morphology tis-

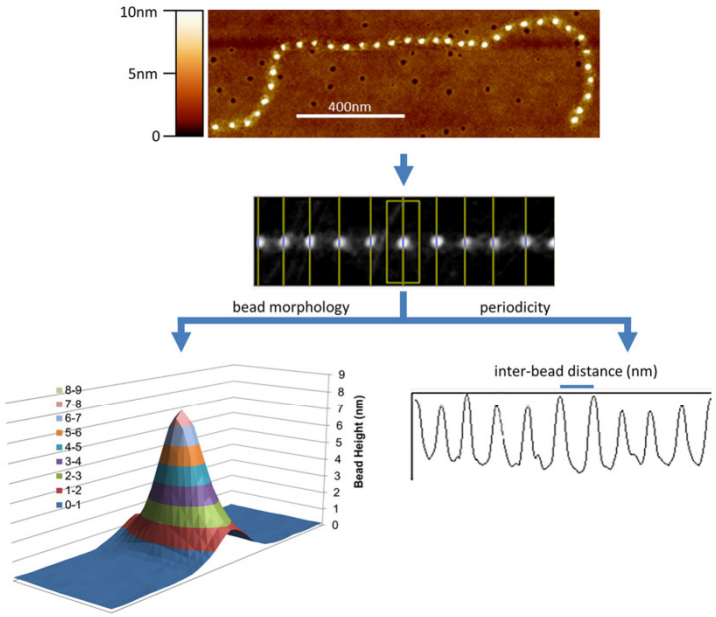

Figure 7. Ultrastructural measurements of the fibrillin microfibril, performed with AFM. Fibrillin microfibrils adopt a beads-on-a-string appearance when viewed with AFM. The height maps generated were used to measure and compare the bead morphology and the periodicity (interbead distance) of eye (CB)-, skin-, and HDF-derived fibrillin microfibrils.

sue source–dependent, but fibrillin-1 regional proteolytic susceptibility is too. This study is first to show ultrastructural and compositional changes between human fibrillin microfibrils from elastin-rich (skin) and elastin-poor (ciliary body) tissues, which have evolved to play very different architectural roles. Additionally, this study observed that newly synthesized fibrillin microfibrils derived from HDFs had a different bead morphology and periodicity compared with native skin-microfibrils. This indicated that these newly synthesized microfibrils may be structurally immature in comparison with those developmentally formed in tissue or that they may lack the structure-altering damage accumulation seen in microfibrils from aged tissue. Additionally, this study demonstrated that collagen VI microfibrils, derived from HDFs and skin, are relatively invariable in periodicity and in regional elastase susceptibility in comparison with the fibrillin microfibril. Finally, this study found that analyzing the presence of the fibrillin microfibril-associated proteins within skin, eye, and HDF-derived samples provides insight into the role they play in the elastic fiber and the basement membrane. Additionally, it allowed the potential identification of proteins that could be fundamental to fibrillin microfibril biology regardless of their tissue source and the observation that newly synthesized microfibrils from cell culture lacked some of these proteins.

Although the loss and deterioration of the fibrillin microfibril network in response to chronic photoaging has been observed immunohistochemically (5), the effects on fibrillin microfibril ultrastructure, fibrillin-1 protease susceptibility, and associated protein composition have yet to be studied. The techniques and methodology used in this tissue and culture comparison would be well-suited to this goal.

Experimental procedures

Study design

Microfibrils were extracted and purified from 1) adult human eye (CB) (n = 3; M74 (male aged 74 years), F79, F76), 2) adult human abdominal skin (n = 3; F49, F55, F56), and 3) cultured HDFs (n = 3; M75, M76, M77). The ultrastructure of these purified fibrillin microfibrils (bead morphology and bead-bead periodicity), from these three different sources, was measured and compared using AFM (Fig. 7). The regional susceptibility of the fibrillin-1 domain structure to elastase digestion was measured and compared by counting the average number of LC-MS/MS–detected peptide spectrum matches (PSMs) from each domain. Finally, the presence of known microfibril-associated proteins was detected and compared for each of these purifications using LC-MS/MS.

Collagen VI microfibrils, which are also present in these purifications, were treated as a control, and their periodicity and COL6A3 regional susceptibility to elastase were compared with those of the fibrillin microfibrils in the same samples.

Reagents and human tissue and cell acquisition

All chemicals were sourced from Sigma-Aldrich Co. Ltd. (Poole, UK) unless stated otherwise. This study was conducted in accordance with the European Medicines Agency Note for

Guidance on Good Clinical Practice and the Declaration of Helsinki (1964) (revised Seoul (2008)). The use of human donor eye tissue was approved by the University of Manchester ethics committee (ethics reference number 11305). Tissue was received within 24 h of corneal dissection (for corneal transplant services) from the Manchester Eye Bank, in accordance with the Human Tissue Act. The CB was carefully dissected from each tissue sample, followed by snap-freezing in liquid nitrogen and storage at −80 °C.

Human abdominal skin samples were acquired from the University of Manchester Skin Health Biobank. This biobank was approved by the North West Research Committee (reference number 09/H1010/10). Samples were snap-frozen in liquid nitrogen and stored at −80°C.

Primary human dermal fibroblasts were cultivated from skin biopsies taken from donor photoprotected buttock. The use of this skin was approved by the North West Research Ethics Committee (reference number 14415), where all donors gave written and informed consent. All incubations and cultures were performed at 37 °C (5% CO_2). Biopsies were incubated in Hanks' balanced salt solution (Fisher Scientific, Loughborough, UK) with 10% dispase overnight. The dermis was then dissected and minced before incubation in fibroblast medium: Dulbecco's modified Eagle's medium (Fisher Scientific) containing 10% fetal calf serum, 1% L-glutamine, 1% amphotericin, and 1% penicillin-streptomycin (Gibco, Paisley, UK). Tissue samples were then cultured with weekly fibroblast medium changes until HDFs could be observed on sample plates.

Microfibril isolation and purification

Human eye and skin tissue samples were minced and added to a 2-ml aliquot of salt buffer (50 mM Tris-HCl, 400 mM NaCl, and 1 mM $CaCl_2$, pH 7.4). 1 mg of bacterial collagenase IA, 0.01 mM phenylmethylsulfonyl fluoride, and 0.03 mM *N*-ethylmaleimide were then added to the tissue, which was digested for 4 h on a rotary mixer, at room temperature (8, 19).

Post-confluent (passage 2) HDFs were maintained for 5 weeks in Dulbecco's modified Eagle's medium + GlutaMAX (Fisher Scientific) containing 10% fetal calf serum and 50 μg/ml 1% penicillin–streptomycin. HDFs were then washed with PBS, and 2 ml of salt buffer was added directly to the culture flasks. 1 mg of bacterial collagenase IA, 0.01 mM phenylmethylsulfonyl fluoride, and 0.03 mM *N*-ethylmaleimide were then added and digested on an orbital shaker for 2 h at room temperature.

Microfibril purification was achieved using an ÄKTA Prime Plus Liquid Chromatography System (GE Healthcare, Little Chalfont, UK). Post-digestion, tissue- and HDF-derived samples were centrifuged at 5000 × *g* for 5 min, and supernatant was run within a column buffer (composed of 50 mM Tris-HCl and 400 mM NaCl at pH 7.4), through a GE HiScale 16/40 column containing Sepharose® Cl2B beads (Sigma-Aldrich), at 0.5 ml/min. Co-purifying fibrillin and collagen VI microfibrils were enriched in the void volume peak, where fractions were collected based on spectrophotometric absorbance at 280 nm (8, 19). Aliquots of the purification were kept for AFM, and the rest were desalted in 0.22-μm–filtered ultrapure water using Slide-A-Lyzer™ MINI dialysis devices (Thermo Fisher Scientific, Paisley, UK) for 4 h at 4 °C. Samples were subsequently frozen at −80°C and freeze-dried at −60°C for 48 h before storage at −80 °C until their use in MS experiments.

Microfibril peptide generation using elastase and SMART™ digestion before mass spectrometry

To enhance fibrillin-1 peptide generation, half of the freeze-dried samples were resuspended in 0.1 M Tris-HCl, pH 8.5. Proteins were denatured in 8 M urea, reduced in 10 mM DTT for 30 min at room temperature, and alkylated using 50 mM iodoacetamide for 30 min at room temperature in darkness. The solution was then diluted down to 2 M urea, and elastase (catalogue no. E1250) was added at a 2:1 enzyme/substrate ratio. This was incubated at 37 °C for 4 h. Elastase activity was then quenched with 5% formic acid in ultrapure water.

To enhance microfibril-associated protein peptide generation, the other half of the freeze-dried samples were resuspended in ultrapure water and directly digested for 75 min using a SMART Digest™ kit (Thermo Scientific), which allows the fast digestion of the sample through immobilized trypsin beads, at a high, denaturing temperature (70 °C) (84), as per the manufacturer's instructions. All samples were then desalted using POROS R3 (Life Technologies, Paisley, UK) beads and vacuum-dried before MS analysis.

Mass spectrometry

All MS was performed by the Biological Mass Spectrometry Core Facility in the Faculty of Biology, Medicine, and Health at the University of Manchester (Manchester, UK). As dictated by their protocols (85, 86), vacuum-dried samples were analyzed by LC-MS/MS using an UltiMate® 3000 Rapid Separation LC (Dionex Corp.; Sunnyvale, CA) and an Orbitrap Elite mass spectrometer (Thermo Fisher Scientific). Peptide mixtures were separated using a gradient from 92% A (0.1% formic acid in water) and 8% B (0.1% formic acid in acetonitrile) to 33% B in 30 min at 300 nl min^{-1}, using a 250 mm × 75-μm inner diameter 1.7-μm BEH C18, analytical column (Waters). Peptides were selected for fragmentation automatically by data-dependent analysis.

Mass spectrometry data analysis

Mass spectra were extracted using extract_msn (Thermo Fisher Scientific) correlated against the Uniprot human database (87) using Mascot version 2.5.1 (Matrix Science, London, UK).

Search parameters were as follows: species, *Homo sapiens*; enzyme, trypsin for SMART™-digested samples and nonspecific for elastase-digested samples; maximum missed cleavages, 1; fixed modifications, carbamidomethyl (mass, 57.02; AA, C); variable modification, oxidation (mass, 15.99; AA, M); peptide tolerance, 10 ppm (monoisotopic); fragment tolerance, 0.6 Da (monoisotopic); searched database, SwissProt_2016_04 (152,544 protein entries).

Data generated were validated using Scaffold (Proteome Software; Portland, OR). Only exclusive, unique peptide counts are reported. False discovery rate (FDR) was calculated by Scaffold using protein and peptide probabilities assigned by the Trans-Proteomic Pipeline and the Protein Prophet™ (88) and Peptide Prophet™ (89) algorithm (Sourceforge, Seattle, WA). Peptide Prophet FDR was thresholded to ≤5%, and Protein

Prophet FDR was thresholded to ≤0.1% (minimum of 2 peptides) for every data set.

The mass spectrometry proteomics data have been deposited to the ProteomeXchange Consortium via the PRIDE (90) partner repository with the data set identifier PXD008450 and 10.6019/PXD008450.

Microfibril atomic force microscopy

Glass coverslips were soaked in absolute ethanol overnight and then attached to metal stubs with clear nail varnish. Samples were pipetted directly onto the coverslips and left for 1 min, so microfibrils could adsorb to the surface. Liquid was removed, and the stubs were left to dry overnight. Stubs were washed three times with ultrapure water and left to dry before being scanned using AFM. Fibrillin and collagen VI microfibrils were imaged using peak force and Scan-Asyst® mode on a Multimode 8 atomic force microscope (Bruker, Billerica, MA), as described previously (18, 19). Using a single, new Scan-Asyst® air tip (Bruker), single fibrillin MFs were captured at 512 pixels/line in 2 × 2-μm scans. This gave a resolution of 3.9 nm/pixel, which was deemed high enough for fibrillin microfibril ultrastructural analysis (18, 19). Fibrillin MFs that were laterally associated with collagen VI microfibrils were omitted from the analysis.

Scans were digitally flattened using the WSxM version 5.0 AFM image processing package (91) and exported in text image format. Height was corrected by subtracting negative background (92). Using ImageJ, fibrillin microfibrils were straightened using the Straighten Curved Objects plugin (93), enabling the generation of 41-pixel-wide images of single straightened fibrillin microfibrils (Fig. 7). LFA image processing software, developed by our group using Microsoft Visual Basic version 6.0 as described previously (94), was then used to specify the location of the maximum height of each bead and create a 15 × 41-pixel snapshot of each individual bead with the height maxima at the central pixel of the image. Maximum bead height and morphology were taken from these snapshots. Fibrillin microfibril periodicity was measured using the Periodicity and Angles software package developed by our group using Microsoft Visual Basic version 6.0 as described previously (51).

Author contributions—A. E., C. E. G., R. E. B. W., and M. J. S. conceptualization; A. E., R. O., and D. K. data curation; A. E. formal analysis; A. E., C. B., and M. J. S. validation; A. E. investigation; A. E. visualization; A. E., K. T. M., S. M. P., R. O., and D. K. methodology; A. E. writing-original draft; A. E. and M. J. S. project administration; A. E., K. T. M., S. M. P., C. E. G., R. E. B. W., R. O., C. B., D. K., and M. J. S. writing-review and editing; C. E. G., R. E. B. W., and M. J. S. funding acquisition; R. E. B. W. and M. J. S. supervision; R. O. and D. K. resources; A. E. designed, performed all experiments, analyzed all of the data, prepared the figures, and wrote the paper; K. T. M. contributed to cell culture of primary fibroblasts; S. M. P. contributed to the isolation of primary fibroblasts from human skin; C. E. G. and R. E. B. W. contributed to the study design and to the editing of the paper; R. O. and D. K. provided design, technical assistance, and support for all LC-MS/MS; C. B. contributed to the editing of the paper and interpretation of the results; M. J. S. conceived and coordinated the study and contributed to the preparation of the figures and writing of the paper.

Acknowledgment—The Wellcome Trust Centre for Cell-Matrix Research, University of Manchester is supported by core funding from the Wellcome Trust (088785/Z/09/Z).

References

1. Parry, D. A. D., Barnes, G. R. G., and Craig, A. S. (1978) A comparison of the size distribution of collagen fibrils in connective tissues as a function of age and a possible relation between fibril size distribution and mechanical properties. *Proc. R. Soc. Lond. B Biol. Sci.* **203,** 305–321 CrossRef Medline
2. Shapiro, S. D., Endicott, S. K., Province, M. A., Pierce, J. A., Campbell, E. J. (1991) Marked longevity of human lung parenchymal elastic fibers deduced from prevalence of D-aspartate and nuclear weapons-related radiocarbon. *J. Clin. Invest.* **87,** 1828–1834 CrossRef Medline
3. Sell, D. R., and Monnier, V. M. (2010) Aging of long-lived proteins: extracellular matrix (collagens, elastins, proteoglycans) and lens crystallins. In *Comprehensive Physiology*, pp. 235–305, John Wiley & Sons, Inc., New York
4. Kielty, C. M., Sherratt, M. J., and Shuttleworth, C. A. (2002) Elastic fibres. *J. Cell Sci.* **115,** 2817–2828 Medline
5. Watson, R. E. B., Griffiths, C. E. M., Craven, N. M., Shuttleworth, C. A., and Kielty, C. M. (1999) Fibrillin-rich microfibrils are reduced in photoaged skin: distribution at the dermal-epidermal junction. *J. Invest. Dermatol.* **112,** 782–787 CrossRef Medline
6. Wright, R. R. (1961) Elastic tissue of normal and emphysematous lungs: a tridimensional histologic study. *Am. J. Pathol.* **39,** 355–367 Medline
7. Wagenseil, J. E., and Mecham, R. P. (2009) Vascular extracellular matrix and arterial mechanics. *Physiol. Rev.* **89,** 957–989 CrossRef Medline
8. Kielty, C. M., Cummings, C., Whittaker, S. P., Shuttleworth, C. A., and Grant, M. E. (1991) Isolation and ultrastructural analysis of microfibrillar structures from foetal bovine elastic tissues: relative abundance and supramolecular architecture of type VI collagen assemblies and fibrillin. *J. Cell Sci.* **99**, 797–807 Medline
9. Baldock, C., Koster, A. J., Ziese, U., Rock, M. J., Sherratt, M. J., Kadler, K. E., Shuttleworth, C. A., and Kielty, C. M. (2001) The supramolecular organization of fibrillin-rich microfibrils. *J. Cell Biol.* **152,** 1045–1056 CrossRef Medline
10. Cotta-Pereira, G., Guerra Rodrigo, F., and Bittencourt-Sampaio, S. (1976) Oxytalan, elaunin and elastic fibers in the human skin. *J. Investig. Dermatol.* **66,** 143–148 CrossRef Medline
11. Naylor, E. C., Watson, R. E., and Sherratt, M. J. (2011) Molecular aspects of skin ageing. *Maturitas* **69,** 249–256 CrossRef Medline
12. Neptune, E. R., Frischmeyer, P. A., Arking, D. E., Myers, L., Bunton, T. E., Gayraud, B., Ramirez, F., Sakai, L. Y., and Dietz, H. C. (2003) Dysregulation of TGF-β activation contributes to pathogenesis in Marfan syndrome. *Nat. Genet.* **33,** 407–411 CrossRef Medline
13. Kaartinen, V., and Warburton, D. (2003) Fibrillin controls TGF-β activation. *Nat. Genet.* **33,** 331–332 CrossRef Medline
14. Sengle, G., Charbonneau, N. L., Ono, R. N., Sasaki, T., Alvarez, J., Keene, D. R., Bächinger, H. P., and Sakai, L. Y. (2008) Targeting of bone morphogenetic protein growth factor complexes to fibrillin. *J. Biol. Chem.* **283,** 13874–13888 CrossRef Medline
15. Ashworth, J. L., Kielty, C. M., and McLeod, D. (2000) Fibrillin and the eye. *Br. J. Ophthalmol.* **84,** 1312–1317 CrossRef Medline
16. Sherratt, M. J., Holmes, D. F., Shuttleworth, C. A., and Kielty, C. M. (1997) Scanning transmission electron microscopy mass analysis of fibrillin-containing microfibrils from foetal elastic tissues. *Int. J. Biochem. Cell Biol.* **29,** 1063–1070 CrossRef Medline
17. Lu, Y., Sherratt, M. J., Wang, M. C., and Baldock, C. (2006) Tissue specific differences in fibrillin microfibrils analysed using single particle image analysis. *J. Struct. Biol.* **155,** 285–293 CrossRef Medline
18. Sherratt, M. J., Baldock, C., Morgan, A., and Kielty, C. M. (2007) The morphology of adsorbed extracellular matrix assemblies is critically dependent on solution calcium concentration. *Matrix Biol.* **26,** 156–166 CrossRef Medline
19. Hibbert, S. A., Watson, R. E. B., Gibbs, N. K., Costello, P., Baldock, C., Weiss, A. S., Griffiths, C. E. M., and Sherratt, M. J. (2015) A potential role

for endogenous proteins as sacrificial sunscreens and antioxidants in human tissues. *Redox Biol.* **5,** 101–113 CrossRef Medline
20. Sherratt, M. J., Bayley, C. P., Reilly, S. M., Gibbs, N. K., Griffiths, C. E., and Watson, R. E. (2010) Low-dose ultraviolet radiation selectively degrades chromophore-rich extracellular matrix components. *J. Pathol.* **222,** 32–40 Medline
21. Sakai, L. Y., Keene, D. R., and Engvall, E. (1986) Fibrillin, a new 350-kD glycoprotein, is a component of extracellular microfibrils. *J. Cell Biol.* **103,** 2499–2509 CrossRef Medline
22. De Maria, A., Wilmarth, P. A., David, L. L., and Bassnett, S. (2017) Proteomic analysis of the bovine and human ciliary zonule proteomic analysis of the ciliary zonule. *Invest. Ophthalmol. Vis. Sci.* **58,** 573–585 CrossRef Medline
23. Cain, S. A., Morgan, A., Sherratt, M. J., Ball, S. G., Shuttleworth, C. A., and Kielty, C. M. (2006) Proteomic analysis of fibrillin-rich microfibrils. *Proteomics* **6,** 111–122 CrossRef Medline
24. Marson, A., Rock, M. J., Cain, S. A., Freeman, L. J., Morgan, A., Mellody, K., Shuttleworth, C. A., Baldock, C., and Kielty, C. M. (2005) Homotypic fibrillin-1 interactions in microfibril assembly. *J. Biol. Chem.* **280,** 5013–5021 CrossRef Medline
25. Schilling, B., MacLean, B., Held, J. M., Sahu, A. K., Rardin, M. J., Sorensen, D. J., Peters, T., Wolfe, A. J., Hunter, C. L., MacCoss, M. J., and Gibson, B. W. (2015) Multiplexed, scheduled, high-resolution parallel reaction monitoring on a full scan QqTOF instrument with integrated data-dependent and targeted mass spectrometric workflows. *Anal. Chem.* **87,** 10222–10229 CrossRef Medline
26. Sziegoleit, A., Linder, D., Schlüter, M., Ogawa, M., Nishibe, S., and Fujimoto, K. (1985) Studies on the specificity of the cholesterol-binding pancreatic proteinase and identification as human pancreatic elastase 1. *Eur. J. Biochem.* **151,** 595–599 CrossRef Medline
27. Rietschel, B., Arrey, T. N., Meyer, B., Bornemann, S., Schuerken, M., Karas, M., and Poetsch, A. (2009) Elastase digests: new ammunition for shotgun membrane proteomics. *Mol. Cell. Proteomics* **8,** 1029–1043 CrossRef Medline
28. Hustoft, H. K., Malerod, H., Wilson, S. R., Reubsaet, L., Lundanes, E., and Greibrokk, T. (2012) A critical review of trypsin digestion for LC-MS based proteomics. In *Integrative Proteomics* (Leung, H.-C., ed) InTech, Rijeka, Croatia
29. Kielty, C. M., Davies, S. J., Phillips, J. E., Jones, C. J., Shuttleworth, C. A., and Charles, S. J. (1995) Marfan syndrome: fibrillin expression and microfibrillar abnormalities in a family with predominant ocular defects. *J. Med. Genet.* **32,** 1–6 CrossRef Medline
30. Ashworth, J. L., Murphy, G., Rock, M. J., Sherratt, M. J., Shapiro, S. D., Shuttleworth, C. A., and Kielty, C. M. (1999) Fibrillin degradation by matrix metalloproteinases: implications for connective tissue remodelling. *Biochem. J.* **340,** 171–181 Medline
31. Kielty, C. M., Raghunath, M., Siracusa, L. D., Sherratt, M. J., Peters, R., Shuttleworth, C. A., and Jimenez, S. A. (1998) The tight skin mouse: demonstration of mutant fibrillin-1 production and assembly into abnormal microfibrils. *J. Cell Biol.* **140,** 1159–1166 CrossRef Medline
32. Hibbert, S. A., Costello, P., O'Connor, C., Bell, M., Griffiths, C. E. M., Watson, R. E. B., and Sherratt, M. J. (2017) A new *in vitro* assay to test UVR protection of dermal extracellular matrix components by a flat spectrum sunscreen. *J. Photochem. Photobiol. B* **175,** 58–64 CrossRef Medline
33. Fang, M., Goldstein, E. L., Turner, A. S., Les, C. M., Orr, B. G., Fisher, G. J., Welch, K. B., Rothman, E. D., and Banaszak Holl, M. M. (2012) Type I collagen D-spacing in fibril bundles of dermis, tendon and bone: bridging between nano- and micro-level tissue hierarchy. *ACS Nano.* **6,** 9503–9514 CrossRef Medline
34. Fang, M., Liroff, K. G., Turner, A. S., Les, C. M., Orr, B. G., and Holl, M. M. B. (2012) Estrogen depletion results in nanoscale morphology changes in dermal collagen. *J. Invest. Dermatol.* **132,** 1791–1797 CrossRef Medline
35. Erickson, B., Fang, M., Wallace, J. M., Orr, B. G., Les, C. M., and Banaszak Holl, M. M. (2013) Nanoscale structure of type I collagen fibrils: quantitative measurement of D-spacing. *Biotechnol. J.* **8,** 117–126 CrossRef Medline
36. Isogai, Z., Ono, R. N., Ushiro, S., Keene, D. R., Chen, Y., Mazzieri, R., Charbonneau, N. L., Reinhardt, D. P., Rifkin, D. B., and Sakai, L. Y. (2003) Latent transforming growth factor β-binding protein 1 interacts with fibrillin and is a microfibril-associated protein. *J. Biol. Chem.* **278,** 2750–2757 CrossRef Medline
37. Isogai, Z., Aspberg, A., Keene, D. R., Ono, R. N., Reinhardt, D. P., and Sakai, L. Y. (2002) Versican interacts with fibrillin-1 and links extracellular microfibrils to other connective tissue networks. *J. Biol. Chem.* **277,** 4565–4572 CrossRef Medline
38. Henderson, M., Polewski, R., Fanning, J. C., and Gibson, M. A. (1996) Microfibril-associated glycoprotein-1 (MAGP-1) is specifically located on the beads of the beaded-filament structure for fibrillin-containing microfibrils as visualized by the rotary shadowing technique. *J. Histochem. Cytochem.* **44,** 1389–1397 CrossRef Medline
39. Gayraud, B., Keene, D. R., Sakai, L. Y., and Ramirez, F. (2000) New insights into the assembly of extracellular microfibrils from the analysis of the fibrillin 1 mutation in the tight skin mouse. *J. Cell Biol.* **150,** 667–680 CrossRef Medline
40. Reinhardt, D. P., Ono, R. N., and Sakai, L. Y. (1997) Calcium stabilizes fibrillin-1 against proteolytic degradation. *J. Biol. Chem.* **272,** 1231–1236 CrossRef Medline
41. Reinhardt, D. P., Ono, R. N., Notbohm, H., Müller, P. K., Bächinger, H. P., and Sakai, L. Y. (2000) Mutations in calcium-binding epidermal growth factor modules render fibrillin-1 susceptible to proteolysis. *J. Biol. Chem.* **275,** 12339–12345 CrossRef Medline
42. Baldwin, A. K., Cain, S. A., Lennon, R., Godwin, A., Merry, C. L. R., and Kielty, C. M. (2014) Epithelial-mesenchymal status influences how cells deposit fibrillin microfibrils. *J. Cell Sci.* **127,** 158–171 CrossRef Medline
43. Long, J. L., and Tranquillo, R. T. (2003) Elastic fiber production in cardiovascular tissue-equivalents. *Matrix Biol.* **22,** 339–350 CrossRef Medline
44. Stahnke, T., Löbler, M., Kastner, C., Stachs, O., Wree, A., Sternberg, K., Schmitz, K.-P., and Guthoff, R. (2012) Different fibroblast subpopulations of the eye: a therapeutic target to prevent postoperative fibrosis in glaucoma therapy. *Exp. Eye Res.* **100,** 88–97 CrossRef Medline
45. Haynes, S. L., Shuttleworth, C. A., and Kielty, C. M. (1997) Keratinocytes express fibrillin and assemble microfibrils: implications for dermal matrix organization. *Br. J. Dermatol.* **137,** 17–23 CrossRef Medline
46. Zhang, H., Apfelroth, S. D., Hu, W., Davis, E. C., Sanguineti, C., Bonadio, J., Mecham, R. P., and Ramirez, F. (1994) Structure and expression of fibrillin-2, a novel microfibrillar component preferentially located in elastic matrices. *J. Cell Biol.* **124,** 855–863 CrossRef Medline
47. Wang, Z., Lyons, B., Truscott, R. J. W., and Schey, K. L. (2014) Human protein aging: modification and crosslinking through dehydroalanine and dehydrobutyrine intermediates. *Aging Cell* **13,** 226–234 CrossRef Medline
48. Stadtman, E. R. (1992) Protein oxidation and aging. *Science* **257,** 1220–1224 CrossRef Medline
49. Atanasova, M., Konova, E., Betova, T., and Baydanoff, S. (2009) Non-enzymatic glycation of human fibrillin-1. *Gerontology* **55,** 73–81 CrossRef Medline
50. Goldin, A., Beckman, J. A., Schmidt, A. M., and Creager, M. A. (2006) Advanced glycation end products. *Circulation* **114,** 597–605 CrossRef Medline
51. Sherratt, M. J., Bax, D. V., Chaudhry, S. S., Hodson, N., Lu, J. R., Saravanapavan, P., and Kielty, C. M. (2005) Substrate chemistry influences the morphology and biological function of adsorbed extracellular matrix assemblies. *Biomaterials* **26,** 7192–7206 CrossRef Medline
52. Baldock, C., Sherratt, M. J., Shuttleworth, C. A., and Kielty, C. M. (2003) The supramolecular organization of collagen VI microfibrils. *J. Mol. Biol.* **330,** 297–307 CrossRef Medline
53. Kielty, C. M., Hanssen, E., and Shuttleworth, C. A. (1998) Purification of fibrillin-containing microfibrils and collagen VI microfibrils by density gradient centrifugation. *Anal. Biochem.* **255,** 108–112 CrossRef Medline
54. Dziadek, M., Kazenwadel, J. S., Hendrey, J. A., Pan, T.-C., Zhang, R.-Z., and Chu, M.-L. (2002) Alternative splicing of transcripts for the α3 chain of mouse collagen VI: identification of an abundant isoform lacking domains N7–N10 in mouse and human. *Matrix Biol.* **21,** 227–241 CrossRef Medline

55. Beecher, N., Roseman, A. M., Jowitt, T. A., Berry, R., Troilo, H., Kammerer, R. A., Shuttleworth, C. A., Kielty, C. M., and Baldock, C. (2011) Collagen VI, conformation of A-domain arrays and microfibril architecture. *J. Biol. Chem.* **286,** 40266–40275 CrossRef Medline
56. Watson, R. E. B., Ball, S. G., Craven, N. M., Boorsma, J., East, C. L., Shuttleworth, C. A., Kielty, C. M., and Griffiths, C. E. M. (2001) Distribution and expression of type VI collagen in photoaged skin. *Br. J. Dermatol.* **144,** 751–759 CrossRef Medline
57. Kielty, C. M., Berry, L., Whittaker, S. P., Grant, M. E., and Shuttleworth, C. A. (1993) Microfibrillar assemblies of foetal bovine skin: developmental expression and relative abundance of type VI collagen and fibrillin. *Matrix* **13,** 103–112 CrossRef Medline
58. Cain, S. A., McGovern, A., Small, E., Ward, L. J., Baldock, C., Shuttleworth, A., and Kielty, C. M. (2009) Defining elastic fiber interactions by molecular fishing: an affinity purification and mass spectrometry approach. *Mol. Cell. Proteomics* **8,** 2715–2732 CrossRef Medline
59. Meirelles, T., Araujo, T. L. S., Nolasco, P., Moretti, A. I. S., Guido, M. C., Debbas, V., Pereira, L. V., and Laurindo, F. R. (2016) Fibrillin-1 mgΔ lpn Marfan syndrome mutation associates with preserved proteostasis and bypass of a protein disulfide isomerase-dependent quality checkpoint. *Int. J. Biochem. Cell Biol.* **71,** 81–91 CrossRef Medline
60. Ashworth, J. L., Kelly, V., Wilson, R., Shuttleworth, C. A., and Kielty, C. M. (1999) Fibrillin assembly: dimer formation mediated by amino-terminal sequences. *J. Cell Sci.* **112,** 3549–3558 Medline
61. Penner, A. S., Rock, M. J., Kielty, C. M., and Shipley, J. M. (2002) Microfibril-associated glycoprotein-2 interacts with fibrillin-1 and fibrillin-2 suggesting a role for MAGP-2 in elastic fiber assembly. *J. Biol. Chem.* **277,** 35044–35049 CrossRef Medline
62. Dahlbäck, K., Ljungquist, A., Löfberg, H., Dahlbäck, B., Engvall, E., and Sakai, L. Y. (1990) Fibrillin immunoreactive fibers constitute a unique network in the human dermis: immunohistochemical comparison of the distributions of fibrillin, vitronectin, amyloid P component, and orcein stainable structures in normal skin and elastosis. *J. Invest. Dermatol.* **94,** 284–291 CrossRef Medline
63. Trask, B. C., Trask, T. M., Broekelmann, T., and Mecham, R. P. (2000) The microfibrillar proteins MAGP-1 and fibrillin-1 form a ternary complex with the chondroitin sulfate proteoglycan decorin. *Mol. Biol. Cell.* **11,** 1499–1507 CrossRef Medline
64. Pilecki, B., Holm, A. T., Schlosser, A., Moeller, J. B., Wohl, A. P., Zuk, A. V., Heumüller, S. E., Wallis, R., Moestrup, S. K., Sengle, G., Holmskov, U., and Sorensen, G. L. (2016) Characterization of microfibrillar-associated protein 4 (MFAP4) as a tropoelastin- and fibrillin-binding protein involved in elastic fiber formation. *J. Biol. Chem.* **291,** 1103–1114 CrossRef Medline
65. Tiedemann, K., Sasaki, T., Gustafsson, E., Göhring, W., Bätge, B., Notbohm, H., Timpl, R., Wedel, T., Schlötzer-Schrehardt, U., and Reinhardt, D. P. (2005) Microfibrils at basement membrane zones interact with perlecan via fibrillin-1. *J. Biol. Chem.* **280,** 11404–11412 CrossRef Medline
66. Reinhardt, D. P., Sasaki, T., Dzamba, B. J., Keene, D. R., Chu, M.-L., Göhring, W., Timpl, R., and Sakai, L. Y. (1996) Fibrillin-1 and fibulin-2 interact and are colocalized in some tissues. *J. Biol. Chem.* **271,** 19489–19496 CrossRef Medline
67. Ohno-Jinno, A., Isogai, Z., Yoneda, M., Kasai, K., Miyaishi, O., Inoue, Y., Kataoka, T., Zhao, J.-S., Li, H., and Takeyama, M., Keene, D. R., Sakai, L. Y., Kimata, K., Iwaki, M., and Zako, M. (2008) Versican and fibrillin-1 form a major hyaluronan-binding complex in the ciliary body. *Invest. Ophthalmol. Vis. Sci.* **49,** 2870–2877 CrossRef Medline
68. Hirani, R., Hanssen, E., and Gibson, M. A. (2007) LTBP-2 specifically interacts with the amino-terminal region of fibrillin-1 and competes with LTBP-1 for binding to this microfibrillar protein. *Matrix Biol.* **26,** 213–223 CrossRef Medline
69. Roark, E. F., Keene, D. R., Haudenschild, C. C., Godyna, S., Little, C. D., and Argraves, W. S. (1995) The association of human fibulin-1 with elastic fibers: an immunohistological, ultrastructural, and RNA study. *J. Histochem. Cytochem.* **43,** 401–411 CrossRef Medline
70. Sabatier, L., Chen, D., Fagotto-Kaufmann, C., Hubmacher, D., McKee, M. D., Annis, D. S., Mosher, D. F., and Reinhardt, D. P. (2009) Fibrillin assembly requires fibronectin. *Mol. Biol. Cell.* **20,** 846–858 Medline
71. Schiavinato, A., Keene, D. R., Wohl, A. P., Corallo, D., Colombatti, A., Wagener, R., Paulsson, M., Bonaldo, P., and Sengle, G. (2016) Targeting of EMILIN-1 and EMILIN-2 to fibrillin microfibrils facilitates their incorporation into the extracellular matrix. *J. Invest. Dermatol.* **136,** 1150–1160 CrossRef Medline
72. Jensen, S. A., Aspinall, G., and Handford, P. A. (2014) C-terminal propeptide is required for fibrillin-1 secretion and blocks premature assembly through linkage to domains cbEGF41–43. *Proc. Natl. Acad. Sci. U.S.A.* **111,** 10155–10160 CrossRef Medline
73. Reinhardt, D. P., Gambee, J. E., Ono, R. N., Bächinger, H. P., and Sakai, L. Y. (2000) Initial steps in assembly of microfibrils: formation of disulfide-cross-linked multimers containing fibrillin-1. *J. Biol. Chem.* **275,** 2205–2210 CrossRef Medline
74. Lönnqvist, L., Reinhardt, D., Sakai, L., and Peltonen, L. (1998) Evidence for furin-type activity-mediated C-terminal processing of profibrillin-1 and interference in the processing by certain mutations. *Hum. Mol. Genet.* **7,** 2039–2044 CrossRef Medline
75. Ponamarczuk, H., Popielarski, M., Stasiak, M., Bednarek, R., Studzian, M., Pulaski, L., Babinska, A., and Swiatkowska, M. (2018) Contribution of activated beta3 integrin in the PDI release from endothelial cells. *Front. Biosci.* **23,** 1612–1627 CrossRef Medline
76. Gibson, M. A., Finnis, M. L., Kumaratilake, J. S., and Cleary, E. G. (1998) Microfibril-associated glycoprotein-2 (MAGP-2) is specifically associated with fibrillin-containing microfibrils but exhibits more restricted patterns of tissue localization and developmental expression than its structural relative MAGP-1. *J. Histochem. Cytochem.* **46,** 871–886 CrossRef Medline
77. Gibson, M. A., Kumaratilake, J. S., and Cleary, E. G. (1989) The protein components of the 12-nanometer microfibrils of elastic and nonelastic tissues. *J. Biol. Chem.* **264,** 4590–4598 Medline
78. Weinbaum, J. S., Broekelmann, T. J., Pierce, R. A., Werneck, C. C., Segade, F., Craft, C. S., Knutsen, R. H., and Mecham, R. P. (2008) Deficiency in microfibril-associated glycoprotein-1 leads to complex phenotypes in multiple organ systems. *J. Biol. Chem.* **283,** 25533–25543 CrossRef Medline
79. Walji, T. A., Turecamo, S. E., DeMarsilis, A. J., Sakai, L. Y., Mecham, R. P., and Craft, C. S. (2016) Characterization of metabolic health in mouse models of fibrillin-1 perturbation. *Matrix Biol.* **55,** 63–76 CrossRef Medline
80. Mariencheck, M. C., Davis, E. C., Zhang, H., Ramirez, F., Rosenbloom, J., Gibson, M. A., Parks, W. C., and Mecham, R. P. (1995) Fibrillin-1 and fibrillin-2 show temporal and tissue-specific regulation of expression in developing elastic tissues. *Connect. Tissue Res.* **31,** 87–97 CrossRef Medline
81. Yamanouchi, K., Tsuruga, E., Oka, K., Sawa, Y., and Ishikawa, H. (2012) Fibrillin-1 and fibrillin-2 are essential for formation of thick oxytalan fibers in human nonpigmented ciliary epithelial cells *in vitro*. *Connect. Tissue Res.* **53,** 14–20 CrossRef Medline
82. Kielty, C. M., and Shuttleworth, C. A. (1993) The role of calcium in the organization of fibrillin microfibrils. *FEBS Lett.* **336,** 323–326 CrossRef Medline
83. Kinsey, R., Williamson, M. R., Chaudhry, S., Mellody, K. T., McGovern, A., Takahashi, S., Shuttleworth, C. A., and Kielty, C. M. (2008) Fibrillin-1 microfibril deposition is dependent on fibronectin assembly. *J. Cell Sci.* **121,** 2696–2704 CrossRef Medline
84. Moore, R., and Samonig, M. (2016) High-throughput, high-resolution peptide maps. *Genet. Eng. Biotechnol. News* **36,** 20–21
85. Buckley, M. (2015) Ancient collagen reveals evolutionary history of the endemic South American "ungulates". *Proc. Biol. Sci.* **282,** 20142671 CrossRef Medline
86. Lennon, R., Byron, A., Humphries, J. D., Randles, M. J., Carisey, A., Murphy, S., Knight, D., Brenchley, P. E., Zent, R., and Humphries, M. J. (2014) Global analysis reveals the complexity of the human glomerular extracellular matrix. *J. Am. Soc. Nephrol.* **25,** 939–951 CrossRef Medline
87. UniProt Consortium (2015) UniProt: a hub for protein information. *Nucleic Acids Res.* **43,** D204–D212 CrossRef Medline

88. Nesvizhskii, A. I., Keller, A., Kolker, E., and Aebersold, R. (2003) A statistical model for identifying proteins by tandem mass spectrometry. *Anal. Chem.* **75,** 4646–4658 CrossRef Medline
89. Keller, A., Nesvizhskii, A. I., Kolker, E., and Aebersold, R. (2002) Empirical statistical model to estimate the accuracy of peptide identifications made by MS/MS and database search. *Anal. Chem.* **74,** 5383–5392 CrossRef Medline
90. Vizcaíno, J. A., Csordas, A., del-Toro, N., Dianes, J. A., Griss, J., Lavidas, I., Mayer, G., Perez-Riverol, Y., Reisinger, F., and Ternent, T., Xu, Q. W., Wang, R., and Hermjakob, H. (2016) 2016 update of the PRIDE database and its related tools. *Nucleic Acids Res.* **44,** D447–D456 CrossRef Medline
91. Horcas, I., Fernández, R., Gómez-Rodríguez, J. M., Colchero, J., Gómez-Herrero, J., and Baro, A. M. (2007) WSXM: a software for scanning probe microscopy and a tool for nanotechnology. *Rev. Sci. Instrum.* **78,** 013705 CrossRef Medline
92. Ratcliff, G. C., and Erie, D. (2001) A novel single-molecule study to determine protein-protein association constants. *J. Am. Chem. Soc.* **123,** 5632–5635 CrossRef Medline
93. Kocsis, E., Trus, B. L., Steer, C. J., Bisher, M. E., and Steven, A. C. (1991) Image averaging of flexible fibrous macromolecules: the clathrin triskelion has an elastic proximal segment. *J. Struct. Biol.* **107,** 6–14 CrossRef Medline
94. Sherratt, M. J., Baldock, C., Louise Haston, J. L., Holmes, D. F., Jones, C. J. P., Shuttleworth, C. A., Wess, T. J., and Kielty, C. M. (2003) Fibrillin microfibrils are stiff reinforcing fibres in compliant tissues. *J. Mol. Biol.* **332,** 183–193 CrossRef Medline

Fibrillin microfibrils and elastic fibre proteins: Functional interactions and extracellular regulation of growth factors

G Model
YSCDB-2621; No. of Pages 9
ARTICLE IN PRESS

Seminars in Cell & Developmental Biology xxx (2018) xxx–xxx

Contents lists available at ScienceDirect

Seminars in Cell & Developmental Biology

journal homepage: www.elsevier.com/locate/semcdb

Review

Fibrillin microfibrils and elastic fibre proteins: Functional interactions and extracellular regulation of growth factors

Jennifer Thomson[a,b], Mukti Singh[a,b], Alexander Eckersley[b], Stuart A. Cain[a,b], Michael J. Sherratt[b], Clair Baldock[a,b,*]

[a] Wellcome Trust Centre for Cell-Matrix Research, School of Biological Sciences, Faculty of Biology, Medicine and Health, University of Manchester, Manchester Academic Health Science Centre, Manchester, M13 9PT, UK
[b] Division of Cell-Matrix Biology and Regenerative Medicine, School of Biological Sciences, Faculty of Biology, Medicine and Health, University of Manchester, Manchester Academic Health Science Centre, Manchester, M13 9PT, UK

ARTICLE INFO

Article history:
Received 15 April 2018
Received in revised form 4 July 2018
Accepted 13 July 2018
Available online xxx

Keywords:
Fibrillin
Elastin
Fibulin
LTBP
ADAMTS

ABSTRACT

Fibrillin microfibrils are extensible polymers that endow connective tissues with long-range elasticity and have widespread distributions in both elastic and non-elastic tissues. They act as a template for elastin deposition during elastic fibre formation and are essential for maintaining the integrity of tissues such as blood vessels, lung, skin and ocular ligaments. A reduction in fibrillin is seen in tissues in vascular ageing, chronic obstructive pulmonary disease, skin ageing and UV induced skin damage, and age-related vision deterioration. Most mutations in fibrillin cause Marfan syndrome, a genetic disease characterised by overgrowth of the long bones and other skeletal abnormalities with cardiovascular and eye defects. However, mutations in fibrillin and fibrillin-binding proteins can also cause short-stature pathologies. All of these diseases have been linked to dysregulated growth factor signalling which forms a major functional role for fibrillin.

Contents

* Corresponding author.
E-mail address: clair.baldock@manchester.ac.uk (C. Baldock).

https://doi.org/10.1016/j.semcdb.2018.07.016
1084-9521/

Please cite this article in press as: J. Thomson, et al., Fibrillin microfibrils and elastic fibre proteins: Functional interactions and extracellular regulation of growth factors, Semin Cell Dev Biol (2018), https://doi.org/10.1016/j.semcdb.2018.07.016

1. Introduction

Fibrillin, an extracellular matrix glycoprotein, assembles into microfibrils, a component of many connective tissues, where they form the template for elastic fibre formation. Fibrillin is also found in tissues devoid of elastin such as the ciliary zonules of the eye. In elastic fibre assembly, it is understood that elastin globules are deposited directly onto a microfibril template and the elastic fibre is comprised of an amorphous elastin central core surrounded by a fibrillin microfibril sheath [1]. A wide array of fibrillin binding proteins are known to facilitate the assembly of elastic fibres and contribute to their functionality, and these will be discussed herein.

2. Fibrillin microfibrils

Fibrillin microfibrils, which have a beads-on-a-string appearance, are a major component of elastic fibres, conferring long range extensibility and contributing to the elastic deformation of tissues. Microfibrils also play a key role in tissue homeostasis through their interaction with growth factors such as transforming growth factor-β (TGFβ) and bone morphogenetic proteins (BMPs) and through interaction with cell surface receptors such as the integrins [2,3] and syndecans [4]. The importance of fibrillin-1 in the function of tissues is further highlighted by fibrillin-1 mutations that cause a number of heritable connective tissue disorders termed fibrillinopathies, such as Marfan syndrome (MFS) [5], Weill Marchesani syndrome (WMS) [6] and geleophysic dysplasia (GD) [7].

Though three fibrillin isoforms have been identified in humans, fibrillin-1 (FBN1) is most abundant in adult tissues. Fibrillin-1 is a glycoprotein composed of 2871 amino acids with a molecular mass of ~320 kDa [1]. It consists of 59 domains including an N-terminal region, epidermal growth factor-like repeats (EGF), most of which are calcium binding (cb), TB (TGFβ-binding like) domains and hybrid domains which bear homology to both cbEGF domains and TB domains (Fig. 1). It has been suggested that arrays of domains have a linear, rod-like structure, modelled from high resolution structures of domain pairs and triplets [8,9]. However, X-ray scattering data show that, in solution, longer domain arrays from fibrillin and the homologous latent TGFβ binding protein (LTBP)-1 are flexible and adopt non-linear conformations [10,11]. Fibrillin assembles into microfibrils, but despite knowing the structures of some domains, how individual fibrillin monomers are arranged in the microfibril is still not understood. Fibrillin microfibrils imaged in tissues have a diameter of ~10-12 nm [12] with a 57 nm periodic beaded structure [13] and in cross-section they appear hollow with a ring of eight filaments [14,15]. They have a mass per repeat ranging from ~1400 kDa, in some early foetal tissues and cell culture, to ~2500 kDa in adult tissues [16]. This mass is consistent with up to eight fibrillin monomers per repeat [13].

3. Fibrillin-binding proteins

A large number of molecules have been shown to colocalise or interact with fibrillin. Here we have focussed on key binding proteins that have been shown to bind directly with fibrillin or tropoelastin, the soluble elastin precursor, and have roles in microfibril assembly or growth factor regulation. Table 1 shows the direct molecular interactions between fibrillin and tropoelastin that have been quantified and these are also presented in Fig. 2.

Table 1
Affinity between fibrillin-1 or tropoelastin and their binding proteins with the protein interaction analysis approach (SPR = surface plasmon resonance, IP = immunoprecipitation, Solid Phase = solid phase binding assay) and dissociation constant (Kd).

Protein A	Protein B	Reference	Approach	Kd (nM)
FBN1 N-ter	ADAMTS10	[17,18,19]	SPR	11-35; 245
FBN1 N-ter	ADAMTS6	[18]	SPR	1-7
FBN1 N-ter	ADAMTSL2	[19]	SPR	200
FBN1 N-ter	ADAMTSL3	[19]	SPR	6
FBN1 N-half	ADAMTSL5	[20]	IP	N/A
FBN1 N-half	ADAMTSL6β	[21]	SPR	80
FBN1 N-half	Aggrecan	[22]	SPR	49 and 42
FBN1 cbEGF22-TB4-cbEGF23	Integrin αVβ6	[3]	SPR	1
FBN1 N-ter	BMP-2, 4, 5, 7, 10, GDF5	[23,24]	SPR	6 - 34
FBN1 N-ter	Brevican, Neurocan, Versican	[22]	SPR	20, 2, 7.1
FBN1 N-ter	Calsyntenin-1	[25]	SPR	240
FBN1 N- and C-ter	FBN1	[26]	Solid Phase	5-11
FBN1 N-ter	FBN1 C-ter	[27]	SPR	3-25
FBN1 N-ter	FBN2 C-ter	[27]	SPR	10-74
FBN1 N-ter	Fibulin-2	[28]	SPR	160
FBN1 N-ter	Fibulin-4	[28,29]	SPR	74; 54
FBN1 N-ter	Fibulin-5	[28,29]	Solid Phase, SPR	63; 23
FBN1 C-half	Fibronectin	[30]	SPR	55
FBN1 N- and C-ter	Heparan Sulphate	[30,31]	SPR	27, 93; 16
FBN1 N-ter	LTBP1	[28]	SPR	21
FBN1 N-ter	LTBP2	[32]	Solid Phase	22
FBN1 N-ter	LTBP-4	[28]	SPR	24
FBN1 N-ter	Lysyl Oxidase	[29]	Solid Phase	26
FBN1 N-ter	MAGP1	[31,33]	SPR, Solid Phase	140-240; 36.5
FBN1 N-half	Perlecan	[34]	SPR	6-9
FBN1 N-ter	MFAP4	[35]	SPR	N.D.
Tropoelastin	Biglycan	[36]	Solid Phase	195
Tropoelastin	FBN1 N-ter, Mid, C-ter	[31,33]	SPR	280, 5; 27
Tropoelastin	Fibulin-1C	[37]	SPR	18
Tropoelastin	Fibulin-2	[38]	Solid Phase	1-2
Tropoelastin	Fibulin-2	[37]	SPR	18
Tropoelastin	Fibulin-4	[29,38]	Solid Phase	8, 131
Tropoelastin	Fibulin-5	[29,38]	Solid Phase; SPR	2; 64
Tropoelastin	Lysyl Oxidase	[29]	Solid Phase	49
Tropoelastin	MAGP1	[33]	SPR	22
Tropoelastin	Perlecan	[37]	SPR	21

Please cite this article in press as: J. Thomson, et al., Fibrillin microfibrils and elastic fibre proteins: Functional interactions and extracellular regulation of growth factors, Semin Cell Dev Biol (2018), https://doi.org/10.1016/j.semcdb.2018.07.016

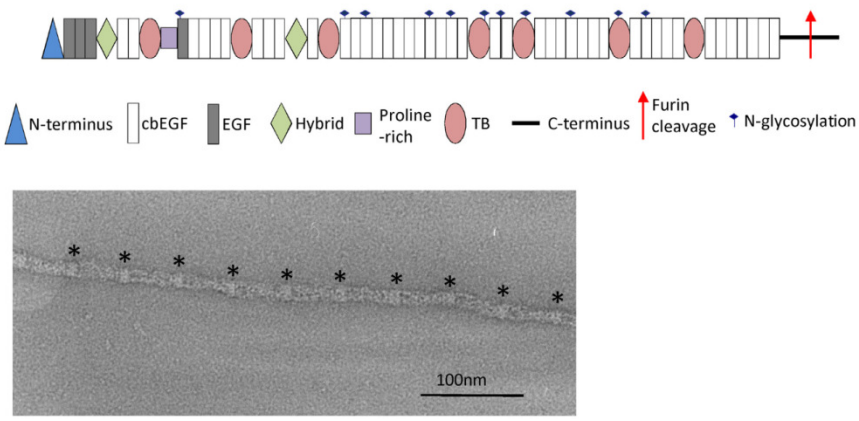

Fig. 1. The domain organisation of fibrillin-1 is shown. Fibrillin assembles into microfibrils with a beads on a string appearance. A microfibril is imaged by negative stain TEM and the beaded structure is highlighted by asterisks.

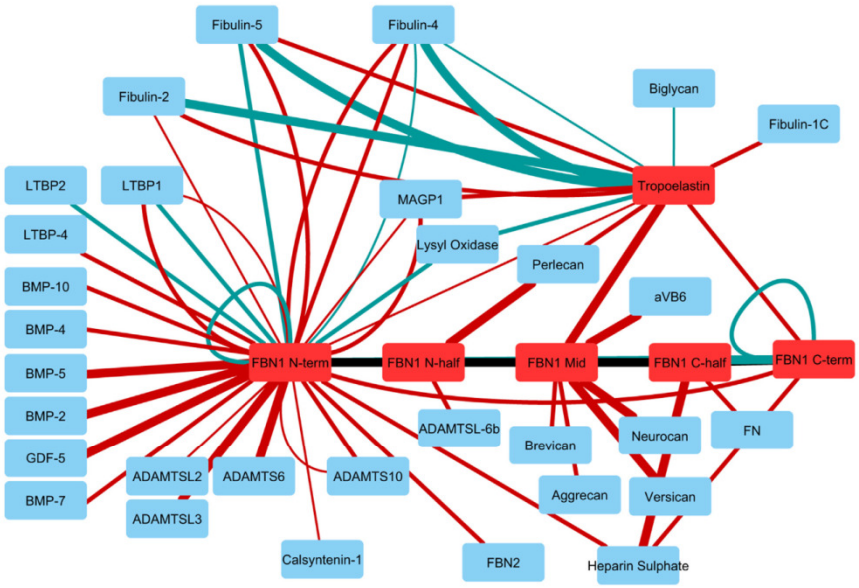

Fig. 2. An interaction network showing the fibrillin and tropoelastin interactions with their binding proteins listed in Table 1. The line width increases with increasing interaction strength (from >100, 10–100 to 1–10 nM Kd) and the line colour indicates either SPR (red) or solid phase binding (blue).

3.1. *Latent TGFβ binding proteins*

Latent TGFβ binding proteins (LTBPs) 1–4 are extracellular glycoproteins with structural similarities to fibrillins, with long or short splice forms (L and S). LTBPs -1, -3 and -4 can covalently bind to the latency-associated peptide of TGFβ, producing the large latent complex (LLC) [39,40]. The LLC becomes sequestered within the matrix, and can regulate TGFβ bioavailability [39–41]. Both LTBP-1 L knockout and complete null mice (i.e LTBP-1S and L) die at birth from severe aortopathy [42,43]; the phenotype produced is similar to that observed in TGFβ-knockout aortic smooth muscle cells [44], supporting the requirement of LTBP-1 L for TGFβ signalling. LTBP-2 binds to the matrix via fibrillin [45,46] and, through binding to fibulin-5, negatively regulates elastic fibre assembly [47,48]. Mutations cause ectopia lentis (EL) [49,50] (a manifestation of MFS) and WMS and WMS-like syndrome [51] and loss of LTBP-2 in patients leads to congenital glaucoma [52,53]. LTBP-2 has also been implicated in wound healing [54]. LTBP-3 deletion in humans

Please cite this article in press as: J. Thomson, et al., Fibrillin microfibrils and elastic fibre proteins: Functional interactions and extracellular regulation of growth factors, Semin Cell Dev Biol (2018), https://doi.org/10.1016/j.semcdb.2018.07.016

produces similar phenotypes to those of LTBP-3 null mice, including short stature, spinal curvature, craniofacial abnormalities and increased bone mass [55–57]. Aberrant LTBP-3-TGFβ complexes may be responsible for aortic dilation and dissection in MFS as MFS mice lacking LTBP-3 had fewer aneurysms and less fragmented elastic fibres [58]. LTBP-4 is required for proper elastogenesis, involving fibulin-4 and -5 incorporation into the matrix [59–62]. Humans with inactive LTBP-4 develop autosomal recessive cutis laxa type 1C (ARCL1C), characterised by severe craniofacial, developmental and potentially fatal pulmonary defects [63]. Knockout studies using both LTBP-4S-/- and/or LTBP-4L-/- mice have uncovered discrete roles for these isoforms. Whereas mice that express only LTBP-4 L normally survive to adulthood [64], complete null mice develop an ARCL1C-like phenotype where mice die perinatally with highly impaired elastogenesis [60], likely due to lack of fibulin-4 in the matrix [61]. LTBP-4 has also been identified as a modifier of muscular dystrophy (MD) [65–68]. MD mice with an LTBP-4 allele that contains an insertion in the hinge region had a less severe phenotype, including increased muscle mass and reduced fibrosis [65,68], coinciding with lower levels of extracellular TGFβ.

3.2. Fibulins

Fibulin-4 and -5 are extracellular glycoproteins that have roles in elastogenesis [38,69]. They bind to both tropoelastin and lysyl oxidase (LOX) or LOX-like 1 (LOXL1) [29,70,71] as well as to fibrillin-1 [29], thereby facilitating elastin cross-linking by LOX/LOXL1 and deposition onto microfibrils. Mutations in fibulin-4 (*EFEMP2*) cause ARCL1B, characterised by severe cardiovascular abnormalities, joint laxity and arachnodactyly [72]. LTBP-4S-/- mice with additional fibulin-4 deficiency have more perturbed elastogenesis [60,61], and fibulin-4 -/- mice develop significant lung and vascular defects and die perinatally [69], potentially due to altered LOX-mediated cross-linking and matrix interactions [73]. However, this dependency on fibulin-4 may vary with vessel type [74]. Mice with a human fibulin-4 mutation (E57 K) have disrupted elastic fibres and developed ascending aortic aneurysms [74,75], whereas muscular arteries and resistance vessels, such as those in the kidney and mesentery, have normal elastic fibres and cross-linking is unaffected [74]. Upregulation of fibulin-4 (and colocalisation with LOX1) has been observed in exfoliation syndrome, an elastic fibre disorder that leads to glaucoma [76] and bronchopulmonary dysplasia (BPD) [77]. Fibulin-5 depletion disrupts elastic fibre assembly to a lesser extent than fibulin-4 [78,79]. Patients with fibulin-5 (*DANCE*) mutations develop ARCL1A, characterised by loose skin, emphysema and arterial tortuosity. These mutations produce conformational changes that lower fibulin-5 secretion and affinity for tropoelastin [80–84].

3.3. Microfibril associated glycoproteins

Microfibril associated glycoproteins (MAGPs)-1 and -2 (also known as microfibrillar associated proteins (MFAPs)-2 and -5, respectively) copurify and colocalise with microfibrils [85–89]. Although neither is required for elastic fibre assembly [90–92], both may promote elastin deposition onto microfibrils [33,87,93]. However, MAGP-1 has been shown to influence wound healing, ciliary zonule formation, ageing, bone remodelling and thrombus formation [90,91,94–97]. Despite the apparent lack of cardiovascular effects observed in either MAGP-1 or MAGP-2 knockout mice, depletion of both genes resulted in aortic dilation in older mice, suggesting a possible compensation mechanism [92]. Additionally, Barbier et al discovered an association between MAGP-2 mutations and thoracic aortic aneurysms and dissection (TAAD) [98]. Although little is known about the role of MFAP-4 in elastogenesis, Pilecki et al identified tropoelastin, fibrillin-1 and -2 and desmosine as MFAP-4 interaction partners in vitro. MFAP-4 also enhanced elastin assembly and colocalised with fibrillin-1 microfibrils in vivo [35].

3.4. ADAMTS and ADAMTSL proteins

A Disintegrin And Metalloprotease with Thrombospondin type-1 repeats (ADAMTS) and ADAMTS-Like (ADAMTSL) are matrix glycoproteins with many biological functions including morphogenesis, development, angiogenesis, inflammation and coagulation, as well as maintaining the structural integrity of tissues [99]. Recently, a subset of ADAMTS and ADAMTSL proteins have been implicated in microfibril assembly, adhesion and matrix stability [100]. Mutations in ADAMTS6 and -10 give rise to WMS [101]; gene disruption of ADAMTS17 leads to WMS-like syndrome [102]; and mutations in ADAMTSL2 and –L4 result in GD [103] and EL, respectively [104]. The association of ADAMTSs and ADAMTSLs with fibrillin-1 related pathologies suggests that they modulate fibrillin-1 function. Indeed, perturbations in the expression of ADAMTSs and ADAMTSLs disrupt the deposition of fibrillin microfibrils and TGFβ regulation [17,102,103]. Mouse models either lacking ADAMTSL2 or bearing a nonsense mutation in ADAMTSL4 mimic phenotypic characteristics observed in patients with GD or EL, further corroborating the involvement of ADAMTSs and ADAMTSLs in these fibrillinopathies [105–107].

ADAMTS10 is involved in the biogenesis and maintenance of fibrillin-1 microfibrils, whereas ADAMTS6 inhibits microfibril deposition [17,18]. ADAMTS10 binds the N- and C-terminal regions of fibrillin-1 [17,19], while ADAMTS6 also interacts with the N-terminus of fibrillin-1 and the C-terminus of LTBP1 [18]. ADAMTS10 is required for and can enhance the formation of focal adhesion complexes through interactions with fibronectin and heparan sulphate (HS), whereas ADAMTS6 depletes HS and hence focal adhesions [18]. ADAMTS10 has a negative effect on ADAMTS6 expression, whereas ADAMTS6 shows synergistic effects on ADAMTS10 expression [18]. ADAMTS10 colocalises with fibrillin and addition of exogenous ADAMTS10 enhances microfibril deposition [17]. Mutations in ADAMTS17 also result in the dislocation of the ocular lens due to progressive degradation of the ciliary zonules in WMS-like patients [102], implying ADAMTS17 is also an accessory to fibrillin microfibril biogenesis and regulation.

ADAMTSL2 binds to the N- and C-terminus of fibrillin-1 [7,19], and the N-terminal binding site overlaps with a three domain fibrillin-1 deletion that causes WMS [19]. Increased levels of fibrillin-2 but not fibrillin-1 were observed in ADAMTSL2-deficient mouse lung [107]. This study also showed enhanced staining of LTBP-1 in bronchial tissues, increased levels of active TGFβ, as well as substantial epithelial dysplasia. ADAMTSL2 interacts with different regions of LTBP-1 suggesting that ADAMTSL2 may also play a role in regulating TGFβ availability in the matrix [19,103]. Found in ocular tissue, ADAMTSL4 is deposited in the matrix in a fibrillar arrangement co-localised with fibrillin microfibrils and addition of ADAMTSL4 to cultured fibroblasts enhances microfibril deposition [108,109]. Furthermore, analysis of ciliary zonules in mutant mice bearing a nonsense mutation in ADAMTSL4 revealed disorganised arrangements of fibrillin microfibrils [106] supporting a role for ADAMTSL4 in microfibril deposition.

3.5. Potential new associated proteins

Mass spectrometry has proven useful for identifying new fibrillin microfibril-associated proteins. MMP3 and annexins V and II co-purified with fibrillin microfibrils purified from human ciliary zonules [86]. Molecular fishing identified elastic fibre-associated proteins including fibronectin, perlecan, LOX, fibrillin-2, and TGFβ2 [25]. Again, the annexins were detected along with other candidate proteins, such as vimentin, βig-H3, thrombospondin-1, S100-A7,

Please cite this article in press as: J. Thomson, et al., Fibrillin microfibrils and elastic fibre proteins: Functional interactions and extracellular regulation of growth factors, Semin Cell Dev Biol (2018), https://doi.org/10.1016/j.semcdb.2018.07.016

Table 2
Fibrillin-associated candidate proteins co-identification by molecular fishing and native tissue co-purification [25,110].

New Associated Protein Candidates	Known extracellular matrix interactions
Annexins V, II	Ca^{2+} channels, major components of matrix vesicles with activity stimulated by matrix binding e.g. collagens II and X [112].
Vimentin	Intracellular intermediate filaments interact with matrix indirectly via vimentin-associated matrix adhesions (VAMs) [113].
βig-H3	Matrix molecule with versatile roles in tissue homeostasis; interacts with numerous matrix components [114].
IGFBP3, -7	Modulate IGF in tissue which can be affected by their direct interaction with fibronectin [115].
PAI-1	Protease inhibitor mediates the degradation of matrix [116].

plasminogen activator inhibitor 1 (PAI-1) and IGF-binding proteins (IGFBP)-3 and -7 [25]. More recent characterisation of potential associated proteins from purified human ciliary body and skin fibrillin microfibrils identified MFAP5, versican and fibrillin-2 in both eye and skin-derived samples, whereas perlecan was identified solely in eye-derived samples and elastin, EMILIN-2 and fibulin-2 and -1 were identified solely in skin-derived samples [110]. Concordant with the molecular fishing study, annexins V and II, vimentin and βig-H3 all co-purified with eye and skin fibrillin microfibrils, whereas IGFBP7 and PAI-1 co-purified with only those derived from eyes. Interestingly the chaperones, protein disulphide isomerase and calreticulin, which play a role in intracellular fibrillin assembly [111], were also identified in both tissues (Table 2).

4. Functional modifiers of elastic fibres

4.1. Transglutaminase

Transglutaminases regulate matrix remodelling and are associated with numerous pathologies including cancer, inflammation and fibrosis [117]. Tissue transglutaminase is known to have a significant role in elastic fibre assembly, both in the cross-linking of fibrillin microfibrils [118] and between fibrillin-1 and tropoelastin [33,119]. The LLC and LTBP-1 N-terminus are also transglutaminase substrates [120], and LTBP-1 forms multimers (both N-N and N-C) that may be cross-linked [11], enhancing its incorporation into the matrix [121] and consequently, regulation of TGFβ signalling. Since proper incorporation of the latent complex is required for normal TGFβ regulation, this finding has implications for fibrillinopathies such as MFS, where these processes may become dysregulated when aberrant complexes are formed. Abnormal transglutaminase activity is also associated with BPD in premature infants and impaired mitral valve development, both attributed to a dysregulated matrix [122,123].

4.2. Lysyl oxidases

Lysyl oxidases LOX and LOX-like1 promote the cross-linking of elastin and its subsequent deposition onto microfibril scaffolds to form elastic fibres [124]. Consequently, LOX is essential for cardiovascular development and function, indeed null mice have defective arterial wall structure with fragmented elastic fibres and die perinatally from aortic aneurysms [125]. Lysyl oxidases may protect against aortic aneurysm formation in MFS, as both LOX and LOXL1 were expressed more highly in a MFS mouse model and in aortic tissue from MFS patients. In the mouse model, LOX inhibition prevented collagen deposition and exacerbated elastic fibre defects, leading to aggressive aortic dilation and death [126]. Guo et al recently identified the LOX mutation that causes familial TAAD: the Ser280Arg mutation produced a less active variant that led to disorganised elastic fibres and increased collagen in patients' aortas [127]. Several reports have described an association between LOXL1 and glaucoma, specifically in the early stages of the elastic fibre disorder exfoliation syndrome (XFS) [76,128–131]. LOXL1 colocalised with elastin, fibrillin-1 and fibulin-4, which were also upregulated, and its expression was enhanced by TGFβ1 and other XFS-associated stimuli in Tenon's capsule fibroblasts [76].

5. Extracellular regulation of growth factor signalling

5.1. Transforming growth factor (TGF)β

As mentioned, dysregulated TGFβ signalling is a defining characteristic of MFS and other fibrillinopathies. Several studies have reported a direct association between elevated TGFβ signalling and MFS pathology in mouse models, where injection of a TGFβ-neutralising antibody restored alveolarisation and atrioventricular valve integrity and prevented aortic aneurysms, the most severe clinical feature of MFS [132–134]. However, there are a number of compelling reports that mitigate TGFβ's role in disease pathology [135,136], while some point to angiotensin II as the major factor [137–139]. Some also argue a protective role for TGFβ [140,141]. Whereas TGFβ neutralisation reduced the incidence of aortic aneurysms in the study by Habashi et al [134], recent data suggests otherwise and, in some cases, show enhanced aneurysm formation upon TGFβ antagonism [140,141]. Neutralising TGFβ in smooth muscle cells increased aortic aneurysms in an AngII-induced model, but not when the antibody was administered systemically [136]. In order to directly address whether excess TGFβ signalling is responsible for the aortopathy observed in MFS, the same group deleted the type II TGFβ receptor in the smooth muscle cells of fibrillin-1 deficient mice. Aortopathy was exacerbated upon loss of TGFβ signalling, and was still observed even without changes to signalling in young mice [135].

A number of clinical trials support this emerging hypothesis. A trial using Losartan to block or diminish the effect of excess TGFβ appeared successful in reducing aortic dilation in MFS patients [142]. However, the same group later reported that Losartan efficacy depended on the patients' fibrillin-1 status: patients with haploinsufficiency (i.e. a lower quantity of normal fibrillin-1) responded to Losartan better than those with dominant negative fibrillin-1 mutations (i.e. defective fibrillin-1) [137]. In a separate study, the authors determined that patient responsiveness to Losartan correlated with higher baseline levels of TGFβ and a higher aortic dilation rate; they concluded that TGFβ could be considered a biomarker for MFS status (as did Radonic et al [143]), but that angiotensin II triggers initial aortic dilation and increases TGFβ levels [138]. In support of these data, Losartan was no more effective in trials comparing it with other MFS therapies. For example, in the largest study of its kind, aortic dilation was not significantly different with Losartan than standard therapy with beta-blockers [139,144].

5.2. Bone morphogenetic proteins (BMP) and growth and differentiation factors (GDF)

MFS patients and fibrillin-1 insufficient mice have reduced bone mass, suggesting perturbed BMP signalling. Fibrillin-2 null mice have reduced bone formation and impaired osteoblast maturation, implicating a direct role for microfibrils in bone formation [145].

Please cite this article in press as: J. Thomson, et al., Fibrillin microfibrils and elastic fibre proteins: Functional interactions and extracellular regulation of growth factors, Semin Cell Dev Biol (2018), https://doi.org/10.1016/j.semcdb.2018.07.016

Moreover, abnormal activation of BMP signalling causes myopathy in fibrillin-2 null mice but deletion of a single allele of BMP7 rescues the muscle phenotype [146]. A direct interaction between BMP and the related GDF growth factors and fibrillin-1 was shown; BMP7 is secreted with its bound prodomain which binds fibrillin-1 [147]. Furthermore, GDF5, BMP2, BMP4 and BMP10 but not GDF8 prodomains bind fibrillin-1 via the N-terminal region showing widespread interaction of BMP/GDF family members with fibrillin-1 [23]. Indeed binding to fibrillin-1 was shown to induce latency for proBMP7 where a conformational change from the activatable open form to the closed latent form was observed upon fibrillin-1 binding [148]. A role for BMP antagonists in modulating extracellular regulation of BMPs via fibrillin was shown for gremlin-1. Fibrillin-2 is upregulated in mesothelioma and localises gremlin-1 to the tumour microenvironment where it binds fibrillin-1 and -2 and colocalises with microfibrils in cells and mesothelioma tumours [149].

6. Summary and future directions

Fibrillin microfibrils are periodic, multi-component assemblies with a widespread tissue distribution. In most organs they associate with elastin to form elastic fibres and hence make key contributions to tissue mechanics and structure function. Although there are three fibrillin isoforms, in adults fibrillin-1 is most abundant. In tissues it forms calcium-stabilised microfibrils which are thought to be composed of eight monomers per repeat. In addition to elastin, fibrillin microfibrils interact and/or co-localise with proteins from the ADAMTS/L, LTBP and fibulin families and with proteoglycans and enzymes. The LTBPs and fibulins both share considerable structural homology with the fibrillins as all three families are characterised by multiple cbEGF domains. These proteins play key roles in elastogenesis and mutations in LTBP and fibulin genes, in common with Marfan syndrome causing fibrillin-1 mutations, can manifest as pathologies in multiple organ systems. The pathological mechanisms conferred by LTBP mutations are driven by dysregulation of TGFβ signalling whilst fibulin mutations may induce aberrant tissue remodelling as a consequence of impaired LOX interactions. In contrast the role of MAGPs in elastogenesis is less well defined but knockout experiments and MAGP genetic mutations are clearly associated with pathologies in elastin-rich tissues such as the aorta. Recently the importance of the ADAMTS and ADAMTS-like glycoproteins in mediating pathological changes (which may be phenotypically indistinguishable from some mutations in the FBN1 gene) has been recognised. Members of this large family of proteins exhibit diverse and complex biological functions including both the inhibition and promotion of microfibril deposition and the mediation of focal adhesion formations. Finally it is clear that elastic fibre formation and function may be influenced enzymatically by the expression of transglutaminase, LOX and LOXL and that elastic fibres can exert considerable influence over tissue homeostasis via regulation of TGFβ and the BMP/GDF families of cytokines.

Fibrillin microfibril and elastic fibre biology is highly complex. This complexity presents the research community with a difficult technical challenge in unravelling the multiple molecular and cellular interactions. However, understanding the multiplicity of elastic fibre protein interactions also presents a clear future opportunity to intervene in, and to recognise, disease processes and mechanisms of ageing and to control tissue development for tissue engineering applications.

Acknowledgements

The Wellcome Trust Centre for Cell-Matrix Research is supported by funding from the Wellcome Trust (088785/Z/09/Z). C.B gratefully acknowledges BBSRC (Ref: BB/N015398/1 and BB/R008221/1) and MRC funding (Ref: MR/L016540/1) and A.E. and M.J.S. Walgreens Boots Alliance for programme grant funding.

References

[1] C.M. Kielty, M.J. Sherratt, A. Marson, C. Baldock, Fibrillin microfibrils, Adv. Protein Chem. 70 (2005) 405–436.
[2] D.V. Bax, S.E. Bernard, A. Lomas, A. Morgan, J. Humphries, C.A. Shuttleworth, M.J. Humphries, C.M. Kielty, Cell adhesion to fibrillin-1 molecules and microfibrils is mediated by alpha 5 beta 1 and alpha v beta 3 integrins, J. Biol. Chem. 278 (2003) 34605–34616.
[3] J. Jovanovic, J. Takagi, L. Choulier, N.G. Abrescia, D.I. Stuart, P.A. van der Merwe, H.J. Mardon, P.A. Handford, alphaVbeta6 is a novel receptor for human fibrillin-1. Comparative studies of molecular determinants underlying integrin-rgd affinity and specificity, J. Biol. Chem. 282 (2007) 6743–6751.
[4] D.V. Bax, Y. Mahalingam, S. Cain, K. Mellody, L. Freeman, K. Younger, C.A. Shuttleworth, M.J. Humphries, J.R. Couchman, C.M. Kielty, Cell adhesion to fibrillin-1: identification of an Arg-Gly-Asp-dependent synergy region and a heparin-binding site that regulates focal adhesion formation, J. Cell Sci. 120 (2007) 1383–1392.
[5] P.N. Robinson, E. Arteaga-Solis, C. Baldock, G. Collod-Beroud, P. Booms, A. De Paepe, H.C. Dietz, G. Guo, P.A. Handford, D.P. Judge, et al., The molecular genetics of Marfan syndrome and related disorders, J. Med. Genet. 43 (2006) 769–787.
[6] L. Faivre, R.J. Gorlin, M.K. Wirtz, M. Godfrey, N. Dagoneau, J.R. Samples, M. Le Merrer, G. Collod-Beroud, C. Boileau, A. Munnich, et al., In frame fibrillin-1 gene deletion in autosomal dominant Weill-Marchesani syndrome, J. Med. Genet. 40 (2003) 34–36.
[7] C. Le Goff, C. Mahaut, L.W. Wang, S. Allali, A. Abhyankar, S. Jensen, L. Zylberberg, G. Collod-Beroud, D. Bonnet, Y. Alanay, et al., Mutations in the TGFbeta binding-protein-like domain 5 of FBN1 are responsible for acromicric and geleophysic dysplasias, Am. J. Hum. Genet. 89 (2011) 7–14.
[8] A.K. Downing, V. Knott, J.M. Werner, C.M. Cardy, I.D. Campbell, P.A. Handford, Solution structure of a pair of calcium-binding epidermal growth factor-like domains: implications for the Marfan syndrome and other genetic disorders, Cell 85 (1996) 597–605.
[9] S.A. Jensen, S. Iqbal, E.D. Lowe, C. Redfield, P.A. Handford, Structure and interdomain interactions of a hybrid domain: a disulphide-rich module of the fibrillin/LTBP superfamily of matrix proteins, Structure 17 (2009) 759–768.
[10] C. Baldock, V. Siegler, D.V. Bax, S.A. Cain, K.T. Mellody, A. Marson, J.L. Haston, R. Berry, M.C. Wang, J.G. Grossmann, et al., Nanostructure of fibrillin-1 reveals compact conformation of EGF arrays and mechanism for extensibility, Proc. Natl. Acad. Sci. U. S. A. 103 (2006) 11922–11927.
[11] H. Troilo, R. Steer, R.F. Collins, C.M. Kielty, C. Baldock, Independent multimerization of latent TGFbeta binding Protein-1 stabilized by cross-linking and enhanced by heparan sulfate, Sci. Rep. 6 (2016) 34347.
[12] L.Y. Sakai, D.R. Keene, E. Engvall, Fibrillin, a new 350-kD glycoprotein, is a component of extracellular microfibrils, J. Cell Biol. 103 (1986) 2499–2509.
[13] C. Baldock, A.J. Koster, U. Ziese, M.J. Rock, M.J. Sherratt, K.E. Kadler, C.A. Shuttleworth, C.M. Kielty, The supramolecular organization of fibrillin-rich microfibrils, J. Cell Biol. 152 (2001) 1045–1056.
[14] E.C. Davis, R.A. Roth, J.E. Heuser, R.P. Mecham, Ultrastructural properties of ciliary zonule microfibrils, J. Struct. Biol. 139 (2002) 65–75.
[15] M.C. Wang, Y. Lu, C. Baldock, Fibrillin microfibrils: a key role for the interbead region in elasticity, J. Mol. Biol. 388 (2009) 168–179.
[16] M.J. Sherratt, C.P. Bayley, S.M. Reilly, N.K. Gibbs, C.E. Griffiths, R.E. Watson, Low-dose ultraviolet radiation selectively degrades chromophore-rich extracellular matrix components, J. Pathol. 222 (2010) 32–40.
[17] W.E. Kutz, L.W. Wang, H.L. Bader, A.K. Majors, K. Iwata, E.I. Traboulsi, L.Y. Sakai, D.R. Keene, S.S. Apte, ADAMTS10 protein interacts with fibrillin-1 and promotes its deposition in extracellular matrix of cultured fibroblasts, J. Biol. Chem. 286 (2011) 17156–17167.
[18] S.A. Cain, E.J. Mularczyk, M. Singh, T. Massam-Wu, C.M. Kielty, ADAMTS-10 and -6 differentially regulate cell-cell junctions and focal adhesions, Sci. Rep. 6 (2016) 35956.
[19] G. Sengle, K. Tsutsui, D.R. Keene, S.F. Tufa, E.J. Carlson, N.L. Charbonneau, R.N. Ono, T. Sasaki, M.K. Wirtz, J.R. Samples, et al., Microenvironmental regulation by fibrillin-1, PLos Genet. 8 (2012) e1002425.
[20] H.L. Bader, L.W. Wang, J.C. Ho, T. Tran, P. Holden, J. Fitzgerald, R.P. Atit, D.P. Reinhardt, S.S. Apte, A disintegrin-like and metalloprotease domain containing thrombospondin type 1 motif-like 5 (ADAMTSL5) is a novel fibrillin-1-, fibrillin-2-, and heparin-binding member of the ADAMTS superfamily containing a netrin-like module, Matrix Biol. 31 (2012) 398–411.
[21] K. Tsutsui, R. Manabe, T. Yamada, I. Nakano, Y. Oguri, D.R. Keene, G. Sengle, L.Y. Sakai, K. Sekiguchi, ADAMTSL-6 is a novel extracellular matrix protein

Please cite this article in press as: J. Thomson, et al., Fibrillin microfibrils and elastic fibre proteins: Functional interactions and extracellular regulation of growth factors, Semin Cell Dev Biol (2018), https://doi.org/10.1016/j.semcdb.2018.07.016

that binds to fibrillin-1 and promotes fibrillin-1 fibril formation, J. Biol. Chem. 285 (2010) 4870–4882.
[22] Z. Isogai, A. Aspberg, D.R. Keene, R.N. Ono, D.P. Reinhardt, L.Y. Sakai, Versican interacts with fibrillin-1 and links extracellular microfibrils to other connective tissue networks, J. Biol. Chem. 277 (2002) 4565–4572.
[23] G. Sengle, N.L. Charbonneau, R.N. Ono, T. Sasaki, J. Alvarez, D.R. Keene, H.P. Bachinger, L.Y. Sakai, Targeting of bone morphogenetic protein growth factor complexes to fibrillin, J. Biol. Chem. 283 (2008) 13874–13888.
[24] G. Sengle, R.N. Ono, T. Sasaki, L.Y. Sakai, Prodomains of transforming growth factor beta (TGFbeta) superfamily members specify different functions: extracellular matrix interactions and growth factor bioavailability, J. Biol. Chem. 286 (2011) 5087–5099.
[25] S.A. Cain, A. McGovern, E. Small, L.J. Ward, C. Baldock, A. Shuttleworth, C.M. Kielty, Defining elastic fiber interactions by molecular fishing: an affinity purification and mass spectrometry approach, Mol. Cell. Proteomics 8 (2009) 2715–2732.
[26] A. Marson, M.J. Rock, S.A. Cain, L.J. Freeman, A. Morgan, K. Mellody, C.A. Shuttleworth, C. Baldock, C.M. Kielty, Homotypic fibrillin-1 interactions in microfibril assembly, J. Biol. Chem. 280 (2005) 5013–5021.
[27] G. Lin, K. Tiedemann, T. Vollbrandt, H. Peters, B. Batge, J. Brinckmann, D.P. Reinhardt, Homo- and heterotypic fibrillin-1 and -2 interactions constitute the basis for the assembly of microfibrils, J. Biol. Chem. 277 (2002) 50795–50804.
[28] R.N. Ono, G. Sengle, N.L. Charbonneau, V. Carlberg, H.P. Bachinger, T. Sasaki, S. Lee-Arteaga, L. Zilberberg, D.B. Rifkin, F. Ramirez, et al., Latent transforming growth factor beta-binding proteins and fibulins compete for fibrillin-1 and exhibit exquisite specificities in binding sites, J. Biol. Chem. 284 (2009) 16872–16881.
[29] R. Choudhury, A. McGovern, C. Ridley, S.A. Cain, A. Baldwin, M.C. Wang, C. Guo, A. Mironov Jr, Z. Drymoussi, D. Trump, et al., Differential regulation of elastic fiber formation by fibulin-4 and -5, J. Biol. Chem. 284 (2009) 24553–24567.
[30] L. Sabatier, J. Djokic, D. Hubmacher, D. Dzafik, V. Nelea, D.P. Reinhardt, Heparin/heparan sulfate controls fibrillin-1, -2 and -3 self-interactions in microfibril assembly, FEBS Lett. (2014).
[31] S.A. Cain, A.K. Baldwin, Y. Mahalingam, B. Raynal, T.A. Jowitt, C.A. Shuttleworth, J.R. Couchman, C.M. Kielty, Heparan sulfate regulates fibrillin-1 N- and C-terminal interactions, J. Biol. Chem. 283 (2008) 27017–27027.
[32] R. Hirani, E. Hanssen, M.A. Gibson, LTBP-2 specifically interacts with the amino-terminal region of fibrillin-1 and competes with LTBP-1 for binding to this microfibrillar protein, Matrix Biol. 26 (2007) 213–223.
[33] M.J. Rock, S.A. Cain, L.J. Freeman, A. Morgan, K. Mellody, A. Marson, C.A. Shuttleworth, A.S. Weiss, C.M. Kielty, Molecular basis of elastic fiber formation. Critical interactions and a tropoelastin-fibrillin-1 cross-link, J. Biol. Chem. 279 (2004) 23748–23758.
[34] K. Tiedemann, T. Sasaki, E. Gustafsson, W. Gohring, B. Batge, H. Notbohm, R. Timpl, T. Wedel, U. Schlotzer-Schrehardt, D.P. Reinhardt, Microfibrils at basement membrane zones interact with perlecan via fibrillin-1, J. Biol. Chem. 280 (2005) 11404–11412.
[35] B. Pilecki, A.T. Holm, A. Schlosser, J.B. Moeller, A.P. Wohl, A.V. Zuk, S.E. Heumuller, R. Wallis, S.K. Moestrup, G. Sengle, et al., Characterization of Microfibrillar-associated Protein 4 (MFAP4) as a Tropoelastin- and fibrillin-binding protein involved in elastic fiber formation, J. Biol. Chem. 291 (2016) 1103–1114.
[36] B. Reinboth, E. Hanssen, E.G. Cleary, M.A. Gibson, Molecular interactions of biglycan and decorin with elastic fiber components: biglycan forms a ternary complex with tropoelastin and microfibril-associated glycoprotein 1, J. Biol. Chem. 277 (2002) 3950–3957.
[37] T. Sasaki, W. Gohring, N. Miosge, W.R. Abrams, J. Rosenbloom, R. Timpl, Tropoelastin binding to fibulins, nidogen-2 and other extracellular matrix proteins, FEBS Lett. 460 (1999) 280–284.
[38] N. Kobayashi, G. Kostka, J.H. Garbe, D.R. Keene, H.P. Bachinger, F.G. Hanisch, D. Markova, T. Tsuda, R. Timpl, M.L. Chu, et al., A comparative analysis of the fibulin protein family. Biochemical characterization, binding interactions, and tissue localization, J. Biol. Chem. 282 (2007) 11805–11816.
[39] P.E. Gleizes, R.C. Beavis, R. Mazzieri, B. Shen, D.B. Rifkin, Identification and characterization of an eight-cysteine repeat of the latent transforming growth factor-beta binding protein-1 that mediates bonding to the latent transforming growth factor-beta1, J. Biol. Chem. 271 (1996) 29891–29896.
[40] J. Saharinen, J. Taipale, J. Keski-Oja, Association of the small latent transforming growth factor-beta with an eight cysteine repeat of its binding protein LTBP-1, EMBO J. 15 (1996) 245–253.
[41] Y. Chen, T. Ali, V. Todorovic, J.M. O'Leary, A. Kristina Downing, D.B. Rifkin, Amino acid requirements for formation of the TGF-beta-latent TGF-beta binding protein complexes, J. Mol. Biol. 345 (2005) 175–186.
[42] V. Todorovic, D. Frendewey, D.E. Gutstein, Y. Chen, L. Freyer, E. Finnegan, F. Liu, A. Murphy, D. Valenzuela, G. Yancopoulos, et al., Long form of latent TGF-beta binding protein 1 (Ltbp1L) is essential for cardiac outflow tract septation and remodeling, Development 134 (2007) 3723–3732.
[43] M. Horiguchi, V. Todorovic, K. Hadjiolova, R. Weiskirchen, D.B. Rifkin, Abrogation of both short and long forms of latent transforming growth factor-beta binding protein-1 causes defective cardiovascular development and is perinatally lethal, Matrix Biol. 43 (2015) 61–70.
[44] B. Choudhary, Y. Ito, T. Makita, T. Sasaki, Y. Chai, H.M. Sucov, Cardiovascular malformations with normal smooth muscle differentiation in neural crest-specific type II TGFbeta receptor (Tgfbr2) mutant mice, Dev. Biol. 289 (2006) 420–429.
[45] M. Hyytiainen, J. Taipale, C.H. Heldin, J. Keski-Oja, Recombinant latent transforming growth factor beta-binding protein 2 assembles to fibroblast extracellular matrix and is susceptible to proteolytic processing and release, J. Biol. Chem. 273 (1998) 20669–20676.
[46] P. Vehvilainen, M. Hyytiainen, J. Keski-Oja, Matrix association of latent TGF-beta binding protein-2 (LTBP-2) is dependent on fibrillin-1, J. Cell. Physiol. 221 (2009) 586–593.
[47] M. Hirai, M. Horiguchi, T. Ohbayashi, T. Kita, K.R. Chien, T. Nakamura, Latent TGF-beta-binding protein 2 binds to DANCE/fibulin-5 and regulates elastic fiber assembly, EMBO J. 26 (2007) 3283–3295.
[48] M.A. Sideek, C. Menz, M.K. Parsi, M.A. Gibson, LTBP-2 competes with tropoelastin for binding to fibulin-5 and heparin, and is a negative modulator of elastinogenesis, Matrix Biol. 34 (2014) 114–123.
[49] J. Desir, Y. Sznajer, F. Depasse, F. Roulez, M. Schrooyen, F. Meire, M. Abramowicz, LTBP2 null mutations in an autosomal recessive ocular syndrome with megalocornea, spherophakia, and secondary glaucoma, Eur. J. Hum. Genet. 18 (2010) 761–767.
[50] A.O. Khan, M.A. Aldahmesh, F.S. Alkuraya, Congenital megalocornea with zonular weakness and childhood lens-related secondary glaucoma - a distinct phenotype caused by recessive LTBP2 mutations, Mol. Vis. 17 (2011) 2570–2579.
[51] R. Haji-Seyed-Javadi, S. Jelodari-Mamaghani, S.H. Paylakhi, S. Yazdani, N. Nilforushan, J.B. Fan, B. Klotzle, M.J. Mahmoudi, M.J. Ebrahimian, N. Chelich, et al., LTBP2 mutations cause Weill-Marchesani and Weill-Marchesani-like syndrome and affect disruptions in the extracellular matrix, Hum. Mutat. 33 (2012) 1182–1187.
[52] M. Narooie-Nejad, S.H. Paylakhi, S. Shojaee, Z. Fazlali, M. Rezaei Kanavi, N. Nilforushan, S. Yazdani, F. Babrzadeh, F. Suri, M. Ronaghi, et al., Loss of function mutations in the gene encoding latent transforming growth factor beta binding protein 2, LTBP2, cause primary congenital glaucoma, Hum Mol Genet 18 (2009) 3969–3977.
[53] M. Ali, M. McKibbin, A. Booth, D.A. Parry, P. Jain, S.A. Riazuddin, J.F. Hejtmancik, S.N. Khan, S. Firasat, M. Shires, et al., Null mutations in LTBP2 cause primary congenital glaucoma, Am. J. Hum. Genet. 84 (2009) 664–671.
[54] C. Menz, M.K. Parsi, J.R. Adams, M.A. Sideek, Z. Kopecki, A.J. Cowin, M.A. Gibson, LTBP-2 Has a single High-affinity binding site for FGF-2 and blocks FGF-2-induced cell proliferation, PLoS One 10 (2015).
[55] S. Morkmued, J. Hemmerle, E. Mathieu, V. Laugel-Haushalter, B. Dabovic, D.B. Rifkin, P. Dolle, K. Niederreither, A. Bloch-Zupan, Enamel and dental anomalies in latent-transforming growth factor beta-binding protein 3 mutant mice, Eur. J. Oral Sci. 125 (2017) 8–17.
[56] B. Dabovic, Y. Chen, C. Colarossi, L. Zambuto, H. Obata, D.B. Rifkin, Bone defects in latent TGF-beta binding protein (Ltbp)-3 null mice; A role for Ltbp in TGF-beta presentation, J. Endocrinol. 175 (2002) 129–141.
[57] B. Dabovic, R. Levasseur, L. Zambuto, Y. Chen, G. Karsenty, D.B. Rifkin, Osteopetrosis-like phenotype in latent TGF-beta binding protein 3 deficient mice, Bone 37 (2005) 25–31.
[58] L. Zilberberg, C.K. Phoon, I. Robertson, B. Dabovic, F. Ramirez, D.B. Rifkin, Genetic analysis of the contribution of LTBP-3 to thoracic aneurysm in Marfan syndrome, Proc. Natl. Acad. Sci. U. S. A. 112 (2015) 14012–14017.
[59] R. Aya, T. Ishiko, K. Noda, S. Yamawaki, Y. Sakamoto, K. Tomihata, Y. Katayama, K. Yoshikawa, H. Kubota, T. Nakamura, et al., Regeneration of elastic fibers by three-dimensional culture on a collagen scaffold and the addition of latent TGF-beta binding protein 4 to improve elastic matrix deposition, Biomaterials 72 (2015) 29–37.
[60] I. Bultmann-Mellin, A. Conradi, A.C. Maul, K. Dinger, F. Wempe, A.P. Wohl, T. Imhof, F.T. Wunderlich, A.C. Bunck, T. Nakamura, et al., Modeling autosomal recessive cutis laxa type 1C in mice reveals distinct functions for Ltbp-4 isoforms, Dis Model Mech 8 (2015) 403–415.
[61] I. Bultmann-Mellin, J. Essers, P.M. van Heijingen, H. von Melchner, G. Sengle, A. Sterner-Kock, Function of Ltbp-4L and fibulin-4 in survival and elastogenesis in mice, Dis Model Mech 9 (2016) 1367–1374.
[62] K. Noda, B. Dabovic, K. Takagi, T. Inoue, M. Horiguchi, M. Hirai, Y. Fujikawa, T.O. Akama, K. Kusumoto, L. Zilberberg, et al., Latent TGF-beta binding protein 4 promotes elastic fiber assembly by interacting with fibulin-5, Proc. Natl. Acad. Sci. U. S. A. 110 (2013) 2852–2857.
[63] Z. Urban, V. Hucthagowder, N. Schurmann, V. Todorovic, L. Zilberberg, J. Choi, C. Sens, C.W. Brown, R.D. Clark, K.E. Holland, et al., Mutations in LTBP4 cause a syndrome of impaired pulmonary, gastrointestinal, genitourinary, musculoskeletal, and dermal development, Am. J. Hum. Genet. 85 (2009) 593–605.
[64] A. Sterner-Kock, I.S. Thorey, K. Koli, F. Wempe, J. Otte, T. Bangsow, K. Kuhlmeier, T. Kirchner, S. Jin, J. Keski-Oja, et al., Disruption of the gene encoding the latent transforming growth factor-beta binding protein 4 (LTBP-4) causes abnormal lung development, cardiomyopathy, and colorectal cancer, Genes Dev. 16 (2002) 2264–2273.
[65] A. Heydemann, E. Ceco, J.E. Lim, M. Hadhazy, P. Ryder, J.L. Moran, D.R. Beier, A.A. Palmer, E.M. McNally, Latent TGF-beta-binding protein 4 modifies muscular dystrophy in mice, J. Clin. Invest. 119 (2009) 3703–3712.
[66] K.M. Flanigan, E. Ceco, K.M. Lamar, Y. Kaminoh, D.M. Dunn, J.R. Mendell, W.M. King, A. Pestronk, J.M. Florence, K.D. Mathews, et al., LTBP4 genotype predicts age of ambulatory loss in Duchenne muscular dystrophy, Ann. Neurol. 73 (2013) 481–488.

Please cite this article in press as: J. Thomson, et al., Fibrillin microfibrils and elastic fibre proteins: Functional interactions and extracellular regulation of growth factors, Semin Cell Dev Biol (2018), https://doi.org/10.1016/j.semcdb.2018.07.016

[67] E. Ceco, S. Bogdanovich, B. Gardner, T. Miller, A. DeJesus, J.U. Earley, M. Hadhazy, L.R. Smith, E.R. Barton, J.D. Molkentin, et al., Targeting latent TGFbeta release in muscular dystrophy, Sci. Transl. Med. 6 (2014).
[68] K.M. Lamar, S. Bogdanovich, B.B. Gardner, Q.Q. Gao, T. Miller, J.U. Earley, M. Hadhazy, A.H. Vo, L. Wren, J.D. Molkentin, et al., Overexpression of latent TGFbeta binding Protein 4 in muscle ameliorates muscular dystrophy through Myostatin and TGFbeta, PLos Genet. 12 (2016).
[69] P.J. McLaughlin, Q. Chen, M. Horiguchi, B.C. Starcher, J.B. Stanton, T.J. Broekelmann, A.D. Marmorstein, B. McKay, R. Mecham, T. Nakamura, et al., Targeted disruption of fibulin-4 abolishes elastogenesis and causes perinatal lethality in mice, Mol. Cell. Biol. 26 (2006) 1700–1709.
[70] M. Horiguchi, T. Inoue, T. Ohbayashi, M. Hirai, K. Noda, L.Y. Marmorstein, D. Yabe, K. Takagi, T.O. Akama, T. Kita, et al., Fibulin-4 conducts proper elastogenesis via interaction with cross-linking enzyme lysyl oxidase, Proc. Natl. Acad. Sci. U. S. A. 106 (2009) 19029–19034.
[71] M. Hirai, T. Ohbayashi, M. Horiguchi, K. Okawa, A. Hagiwara, K.R. Chien, T. Kita, T. Nakamura, Fibulin-5/DANCE has an elastogenic organizer activity that is abrogated by proteolytic cleavage in vivo, J. Cell Biol. 176 (2007) 1061–1071.
[72] C.L. Papke, H. Yanagisawa, Fibulin-4 and fibulin-5 in elastogenesis and beyond: insights from mouse and human studies, Matrix Biol. 37 (2014) 142–149.
[73] T. Sasaki, F.G. Hanisch, R. Deutzmann, L.Y. Sakai, T. Sakuma, T. Miyamoto, T. Yamamoto, E. Hannappel, M.L. Chu, H. Lanig, et al., Functional consequence of fibulin-4 missense mutations associated with vascular and skeletal abnormalities and cutis laxa, Matrix Biol. 56 (2016) 132–149.
[74] C.M. Halabi, T.J. Broekelmann, M. Lin, V.S. Lee, M.L. Chu, R.P. Mecham, Fibulin-4 is essential for maintaining arterial wall integrity in conduit but not muscular arteries, Sci. Adv. 3 (2017).
[75] O. Igoucheva, V. Alexeev, C.M. Halabi, S.M. Adams, I. Stoilov, T. Sasaki, M. Arita, A. Donahue, R.P. Mecham, D.E. Birk, et al., Fibulin-4 E57K knock-in mice recapitulate cutaneous, vascular and skeletal defects of recessive cutis Laxa 1B with both elastic fiber and collagen fibril abnormalities, J. Biol. Chem. 290 (2015) 21443–21459.
[76] M. Zenkel, U. Schlotzer-Schrehardt, Expression and regulation of LOXL1 and elastin-related genes in eyes with exfoliation syndrome, J. Glaucoma 23 (2014) S48–50.
[77] W. Han, C. Guo, Q. Liu, B. Yu, Z. Liu, J. Yang, C. Deng, Aberrant elastin remodeling in the lungs of O(2)-exposed newborn mice; Primarily results from perturbed interaction between integrins and elastin, Cell Tissue Res. 359 (2015) 589–603.
[78] H. Yanagisawa, E.C. Davis, B.C. Starcher, T. Ouchi, M. Yanagisawa, J.A. Richardson, E.N. Olson, Fibulin-5 is an elastin-binding protein essential for elastic fibre development in vivo, Nature 415 (2002) 168–171.
[79] T. Nakamura, P.R. Lozano, Y. Ikeda, Y. Iwanaga, A. Hinek, S. Minamisawa, C.F. Cheng, K. Kobuke, N. Dalton, Y. Takada, et al., Fibulin-5/DANCE is essential for elastogenesis in vivo, Nature 415 (2002) 171–175.
[80] B. Loeys, L. Van Maldergem, G. Mortier, P. Coucke, S. Gerniers, J.M. Naeyaert, A. De Paepe, Homozygosity for a missense mutation in fibulin-5 (FBLN5) results in a severe form of cutis laxa, Hum Mol Genet 11 (2002) 2113–2118.
[81] Q. Hu, B.L. Loeys, P.J. Coucke, A. De Paepe, R.P. Mecham, J. Choi, E.C. Davis, Z. Urban, Fibulin-5 mutations: mechanisms of impaired elastic fiber formation in recessive cutis laxa, Hum Mol Genet 15 (2006) 3379–3386.
[82] E. Elahi, R. Kalhor, S.S. Banihosseini, N. Torabi, H. Pour-Jafari, M. Houshmand, S.S. Amini, A. Ramezani, B. Loeys, Homozygous missense mutation in fibulin-5 in an Iranian autosomal recessive cutis laxa pedigree and associated haplotype, J. Invest. Dermatol. 126 (2006) 1506–1509.
[83] S. Claus, J. Fischer, H. Megarbane, A. Megarbane, F. Jobard, R. Debret, S. Peyrol, S. Saker, M. Devillers, P. Sommer, et al., A p.C217R mutation in fibulin-5 from cutis laxa patients is associated with incomplete extracellular matrix formation in a skin equivalent model, J. Invest. Dermatol. 128 (2008) 1442–1450.
[84] B. Callewaert, C.T. Su, T. Van Damme, P. Vlummens, F. Malfait, O. Vanakker, B. Schulz, M. Mac Neal, E.C. Davis, J.G. Lee, et al., Comprehensive clinical and molecular analysis of 12 families with type 1 recessive cutis laxa, Hum. Mutat. 34 (2013) 111–121.
[85] M.A. Gibson, J.S. Kumaratilake, E.G. Cleary, The protein components of the 12-nanometer microfibrils of elastic and nonelastic tissues, J. Biol. Chem. 264 (1989) 4590–4598.
[86] S.A. Cain, A. Morgan, M.J. Sherratt, S.G. Ball, C.A. Shuttleworth, C.M. Kielty, Proteomic analysis of fibrillin-rich microfibrils, Proteomics 6 (2006) 111–122.
[87] R. Lemaire, J. Bayle, R.P. Mecham, R. Lafyatis, Microfibril-associated MAGP-2 stimulates elastic fiber assembly, J. Biol. Chem. 282 (2007) 800–808.
[88] M.A. Gibson, M.L. Finnis, J.S. Kumaratilake, E.G. Cleary, Microfibril-associated glycoprotein-2 (MAGP-2) is specifically associated with fibrillin-containing microfibrils but exhibits more restricted patterns of tissue localization and developmental expression than its structural relative MAGP-1, J. Histochem. Cytochem. 46 (1998) 871–886.
[89] E. Hanssen, F.H. Hew, E. Moore, M.A. Gibson, MAGP-2 has multiple binding regions on fibrillins and has covalent periodic association with fibrillin-containing microfibrils, J. Biol. Chem. 279 (2004) 29185–29194.
[90] J.S. Weinbaum, T.J. Broekelmann, R.A. Pierce, C.C. Werneck, F. Segade, C.S. Craft, R.H. Knutsen, R.P. Mecham, Deficiency in microfibril-associated glycoprotein-1 leads to complex phenotypes in multiple organ systems, J. Biol. Chem. 283 (2008) 25533–25543.
[91] C.S. Craft, W. Zou, M. Watkins, S. Grimston, M.D. Brodt, T.J. Broekelmann, J.S. Weinbaum, S.L. Teitelbaum, R.A. Pierce, R. Civitelli, et al., Microfibril-associated glycoprotein-1, an extracellular matrix regulator of bone remodeling, J. Biol. Chem. 285 (2010) 23858–23867.
[92] M.D. Combs, R.H. Knutsen, T.J. Broekelmann, H.M. Toennies, T.J. Brett, C.A. Miller, D.L. Kober, C.S. Craft, J.J. Atkinson, J.M. Shipley, et al., Microfibril-associated glycoprotein 2 (MAGP2) loss of function has pleiotropic effects in vivo, J. Biol. Chem. 288 (2013) 28869–28880.
[93] S.A. Jensen, D.P. Reinhardt, M.A. Gibson, A.S. Weiss, Protein interaction studies of MAGP-1 with tropoelastin and fibrillin-1, J. Biol. Chem. 276 (2001) 39661–39666.
[94] T. Fujita, E. Tsuruga, K. Yamanouchi, Y. Sawa, H. Ishikawa, Microfibril-associated glycoprotein-1 controls human ciliary zonule development in vitro, Acta Histochem. Cytochem. 47 (2014) 11–17.
[95] Q. Zheng, S. Chen, Y. Chen, J. Lyga, R. Wyborski, U. Santhanam, Investigation of age-related decline of microfibril-associated glycoprotein-1 in human skin through immunohistochemistry study, Clin Cosmet Investig Dermatol 6 (2013) 317–323.
[96] C.C. Werneck, C.P. Vicente, J.S. Weinberg, A. Shifren, R.A. Pierce, T.J. Broekelmann, D.M. Tollefsen, R.P. Mecham, Mice lacking the extracellular matrix protein MAGP1 display delayed thrombotic occlusion following vessel injury, Blood 111 (2008) 4137–4144.
[97] T. Vassequi-Silva, D.S. Pereira, A.C.C. Nery Diez, G.G. Braga, J.A. Godoy, C.B. Mendes, L. Dos Santos, J.E. Krieger, E. Antunes, F.T.M. Costa, et al., Losartan and captopril treatment rescue normal thrombus formation in microfibril associated glycoprotein-1 (MAGP1) deficient mice, Thromb. Res. 138 (2016) 7–15.
[98] M. Barbier, M.S. Gross, M. Aubart, N. Hanna, K. Kessler, D.C. Guo, L. Tosolini, B. Ho-Tin-Noe, E. Regalado, M. Varret, et al., MFAP5 loss-of-function mutations underscore the involvement of matrix alteration in the pathogenesis of familial thoracic aortic aneurysms and dissections, Am. J. Hum. Genet. 95 (2014) 736–743.
[99] S.S. Apte, A disintegrin-like and metalloprotease (reprolysin-type) with thrombospondin type 1 motif (ADAMTS) superfamily: functions and mechanisms, J. Biol. Chem. 284 (2009) 31493–31497.
[100] D. Hubmacher, S.S. Apte, ADAMTS proteins as modulators of microfibril formation and function, Matrix Biol. 47 (2015) 34–43.
[101] N. Dagoneau, C. Benoist-Lasselin, C. Huber, L. Faivre, A. Megarbane, A. Alswaid, H. Dollfus, Y. Alembik, A. Munnich, L. Legeai-Mallet, et al., ADAMTS10 mutations in autosomal recessive Weill-Marchesani syndrome, Am. J. Hum. Genet. 75 (2004) 801–806.
[102] J. Morales, L. Al-Sharif, D.S. Khalil, J.M. Shinwari, P. Bavi, R.A. Al-Mahrouqi, A. Al-Rajhi, F.S. Alkuraya, B.F. Meyer, N. Al Tassan, Homozygous mutations in ADAMTS10 and ADAMTS17 cause lenticular myopia, ectopia lentis, glaucoma, spherophakia, and short stature, Am. J. Hum. Genet. 85 (2009) 558–568.
[103] C. Le Goff, F. Morice-Picard, N. Dagoneau, L.W. Wang, C. Perrot, Y.J. Crow, F. Bauer, E. Flori, C. Prost-Squarcioni, D. Krakow, et al., ADAMTSL2 mutations in geleophysic dysplasia demonstrate a role for ADAMTS-like proteins in TGF-beta bioavailability regulation, Nat. Genet. 40 (2008) 1119–1123.
[104] D. Ahram, T.S. Sato, A. Kohilan, M. Tayeh, S. Chen, S. Leal, M. Al-Salem, H. El-Shanti, A homozygous mutation in ADAMTSL4 causes autosomal-recessive isolated ectopia lentis, Am. J. Hum. Genet. 84 (2009) 274–278.
[105] A. Chandra, J.A. Aragon-Martin, K. Hughes, S. Gati, M.A. Reddy, C. Deshpande, G. Cormack, A.H. Child, D.G. Charteris, G. Arno, A genotype-phenotype comparison of ADAMTSL4 and FBN1 in isolated ectopia lentis, Invest. Ophthalmol. Vis. Sci. 53 (2012) 4889–4896.
[106] G.B. Collin, D. Hubmacher, J.R. Charette, W.L. Hicks, L. Stone, M. Yu, J.K. Naggert, M.P. Krebs, N.S. Peachey, S.S. Apte, et al., Disruption of murine Adamtsl4 results in zonular fiber detachment from the lens and in retinal pigment epithelium dedifferentiation, Hum. Mol. Genet. 24 (2015) 6958–6974.
[107] D. Hubmacher, L.W. Wang, R.P. Mecham, D.P. Reinhardt, S.S. Apte, Adamtsl2 deletion results in bronchial fibrillin microfibril accumulation and bronchial epithelial dysplasia – a novel mouse model providing insights into geleophysic dysplasia, Disease Models & Mechanisms 8 (2015) 487–499.
[108] L.A. Gabriel, L.W. Wang, H. Bader, J.C. Ho, A.K. Majors, J.G. Hollyfield, E.I. Traboulsi, S.S. Apte, ADAMTSL4, a secreted glycoprotein widely distributed in the eye, binds fibrillin-1 microfibrils and accelerates microfibril biogenesis, Invest. Ophthalmol. Vis. Sci. 53 (2012) 461–469.
[109] A. Chandra, M. Jones, P. Cottrill, K. Eastlake, G.A. Limb, D.G. Charteris, Gene expression and protein distribution of ADAMTSL-4 in human iris, choroid and retina, Br. J. Ophthalmol. 97 (2013) 1208–1212.
[110] A. Eckersley, K.T. Mellody, S.M. Pilkington, C.E. Griffiths, R.E.B. Watson, R. O'Cualain, C. Baldock, D. Knight, M.J. Sherratt, Structural and compositional diversity of fibrillin microfibrils in human tissues, J. Biol. Chem. (2018).
[111] J.L. Ashworth, V. Kelly, R. Wilson, C.A. Shuttleworth, C.M. Kielty, Fibrillin assembly: dimer formation mediated by amino-terminal sequences, J. Cell Sci. 112 (Pt 20) (1999) 3549–3558.
[112] T. Kirsch, G. Harrison, E.E. Golub, H.D. Nah, The roles of annexins and types II and X collagen in matrix vesicle-mediated mineralization of growth plate cartilage, J. Biol. Chem. 275 (2000) 35577–35583.
[113] J. Ivaska, H.M. Pallari, J. Nevo, J.E. Eriksson, Novel functions of vimentin in cell adhesion, migration, and signaling, Exp. Cell. Res. 313 (2007) 2050–2062.

Please cite this article in press as: J. Thomson, et al., Fibrillin microfibrils and elastic fibre proteins: Functional interactions and extracellular regulation of growth factors, Semin Cell Dev Biol (2018), https://doi.org/10.1016/j.semcdb.2018.07.016

[114] E. Hanssen, B. Reinboth, M.A. Gibson, Covalent and non-covalent interactions of betaig-h3 with collagen VI. Beta ig-h3 is covalently attached to the amino-terminal region of collagen VI in tissue microfibrils, J. Biol. Chem. 278 (2003) 24334–24341.
[115] J. McIntosh, G. Dennison, J.M. Holly, C. Jarrett, A. Frankow, E.J. Foulstone, Z.E. Winters, C.M. Perks, IGFBP-3 can either inhibit or enhance EGF-mediated growth of breast epithelial cells dependent upon the presence of fibronectin, J. Biol. Chem. 285 (2010) 38788–38800.
[116] J.F. Cajot, J. Bamat, G.E. Bergonzelli, E.K. Kruithof, R.L. Medcalf, J. Testuz, B. Sordat, Plasminogen-activator inhibitor type 1 is a potent natural inhibitor of extracellular matrix degradation by fibrosarcoma and colon carcinoma cells, Proc. Natl. Acad. Sci. U. S. A. 87 (1990) 6939–6943.
[117] R.J. Collighan, M. Griffin, Transglutaminase 2 cross-linking of matrix proteins: biological significance and medical applications, Amino Acids 36 (2009) 659–670.
[118] R.Q. Qian, R.W. Glanville, Alignment of fibrillin molecules in elastic microfibrils is defined by transglutaminase-derived cross-links, Biochemistry 36 (1997) 15841–15847.
[119] A.W. Clarke, S.G. Wise, S.A. Cain, C.M. Kielty, A.S. Weiss, Coacervation is promoted by molecular interactions between the PF2 segment of fibrillin-1 and the domain 4 region of tropoelastin, Biochemistry 44 (2005) 10271–10281.
[120] I. Nunes, P.E. Gleizes, C.N. Metz, D.B. Rifkin, Latent transforming growth factor-beta binding protein domains involved in activation and transglutaminase-dependent cross-linking of latent transforming growth factor-beta, J. Cell Biol. 136 (1997) 1151–1163.
[121] E. Verderio, C. Gaudry, S. Gross, C. Smith, S. Downes, M. Griffin, Regulation of cell surface tissue transglutaminase: effects on matrix storage of latent transforming growth factor-beta binding protein-1, J. Histochem. Cytochem. 47 (1999) 1417–1432.
[122] T.J. Witsch, G. Niess, E. Sakkas, T. Likhoshvay, S. Becker, S. Herold, K. Mayer, I. Vadasz, J.D. Roberts Jr, W. Seeger, et al., Transglutaminase 2: a new player in bronchopulmonary dysplasia? Eur. Respir. J. 44 (2014) 109–121.
[123] K.L. Pang, M. Parnall, S. Loughna, Effect of altered haemodynamics on the developing mitral valve in chick embryonic heart, J. Mol. Cell. Cardiol. 108 (2017) 114–126.
[124] J. Molnar, K.S. Fong, Q.P. He, K. Hayashi, Y. Kim, S.F. Fong, B. Fogelgren, K.M. Szauter, M. Mink, K. Csiszar, Structural and functional diversity of lysyl oxidase and the LOX-like proteins, Biochim. Biophys. Acta 1647 (2003) 220–224.
[125] J.M. Maki, J. Rasanen, H. Tikkanen, R. Sormunen, K. Makikallio, K.I. Kivirikko, R. Soininen, Inactivation of the lysyl oxidase gene Lox leads to aortic aneurysms, cardiovascular dysfunction, and perinatal death in mice, Circulation 106 (2002) 2503–2509.
[126] O. Busnadiego, D. Gorbenko Del Blanco, J. Gonzalez-Santamaria, J.P. Habashi, J.F. Calderon, P. Sandoval, D. Bedja, J. Guinea-Viniegra, M. Lopez-Cabrera, T. Rosell-Garcia, et al., Elevated expression levels of lysyl oxidases protect against aortic aneurysm progression in Marfan syndrome, J. Mol. Cell. Cardiol. 85 (2015) 48–57.
[127] D.C. Guo, E.S. Regalado, L. Gong, X. Duan, R.L. Santos-Cortez, P. Arnaud, Z. Ren, B. Cai, E.M. Hostetler, R. Moran, et al., LOX mutations predispose to thoracic aortic aneurysms and dissections, Circ. Res. 118 (2016) 928–934.
[128] J.A. Vranka, M.J. Kelley, T.S. Acott, K.E. Keller, Extracellular matrix in the trabecular meshwork: intraocular pressure regulation and dysregulation in glaucoma, Exp. Eye Res. 133 (2015) 112–125.
[129] R. Laczko, K.M. Szauter, K. Csiszar, LOXL1-associated candidate epithelial pathomechanisms in exfoliation glaucoma, J. Glaucoma 23 (2014) S43–7.
[130] L.E. Vazquez, R.K. Lee, Genomic and proteomic pathophysiology of pseudoexfoliation glaucoma, Int. Ophthalmol. Clin. 54 (2014) 1–13.
[131] U. Schlotzer-Schrehardt, F. Pasutto, P. Sommer, I. Hornstra, F.E. Kruse, G.O. Naumann, A. Reis, M. Zenkel, Genotype-correlated expression of lysyl oxidase-like 1 in ocular tissues of patients with pseudoexfoliation syndrome/glaucoma and normal patients, Am. J. Pathol. 173 (2008) 1724–1735.
[132] E.R. Neptune, P.A. Frischmeyer, D.E. Arking, L. Myers, T.E. Bunton, B. Gayraud, F. Ramirez, L.Y. Sakai, H.C. Dietz, Dysregulation of TGF-beta activation contributes to pathogenesis in Marfan syndrome, Nat. Genet. 33 (2003) 407–411.
[133] C.M. Ng, A. Cheng, L.A. Myers, F. Martinez-Murillo, C. Jie, D. Bedja, K.L. Gabrielson, J.M. Hausladen, R.P. Mecham, D.P. Judge, et al., TGF-beta-dependent pathogenesis of mitral valve prolapse in a mouse model of Marfan syndrome, J. Clin. Invest. 114 (2004) 1586–1592.
[134] J.P. Habashi, D.P. Judge, T.M. Holm, R.D. Cohn, B.L. Loeys, T.K. Cooper, L. Myers, E.C. Klein, G. Liu, C. Calvi, et al., Losartan, an AT1 antagonist, prevents aortic aneurysm in a mouse model of Marfan syndrome, Science 312 (2006) 117–121.
[135] H. Wei, J.H. Hu, S.N. Angelov, K. Fox, J. Yan, R. Enstrom, A. Smith, D.A. Dichek, Aortopathy in a mouse model of Marfan syndrome Is not mediated by altered transforming growth factor beta signaling, J Am Heart Assoc 6 (2017).
[136] S.N. Angelov, J.H. Hu, H. Wei, N. Airhart, M. Shi, D.A. Dichek, TGF-beta (transforming growth factor-beta) signaling protects the thoracic and abdominal aorta from angiotensin II-induced pathology by distinct mechanisms, Arterioscler. Thromb. Vasc. Biol. 37 (2017) 2102–2113.
[137] R. Franken, A.W. den Hartog, T. Radonic, D. Micha, A. Maugeri, F.S. van Dijk, H.E. Meijers-Heijboer, J. Timmermans, A.J. Scholte, M.P. van den Berg, et al., Beneficial outcome of losartan therapy depends on type of FBN1 mutation in Marfan syndrome, Circ Cardiovasc Genet 8 (2015) 383–388.
[138] R. Franken, T. Radonic, A.W. den Hartog, M. Groenink, G. Pals, M. van Eijk, R. Lutter, B.J. Mulder, A.H. Zwinderman, V. de Waard, The revised role of TGF-beta in aortic aneurysms in Marfan syndrome, Neth Heart J 23 (2015) 116–121.
[139] O. Milleron, F. Arnoult, J. Ropers, P. Aegerter, D. Detaint, G. Delorme, D. Attias, F. Tubach, S. Dupuis-Girod, H. Plauchu, et al., Marfan Sartan: a randomized, double-blind, placebo-controlled trial, Eur. Heart J. 36 (2015) 2160–2166.
[140] X. Chen, D.L. Rateri, D.A. Howatt, A. Balakrishnan, J.J. Moorleghen, L.A. Cassis, A. Daugherty, TGF-beta neutralization enhances AngII-induced aortic rupture and aneurysm in both thoracic and abdominal regions, PLoS One 11 (2016) e0153811.
[141] J.R. Cook, N.P. Clayton, L. Carta, J. Galatioto, E. Chiu, S. Smaldone, C.A. Nelson, S.H. Cheng, B.M. Wentworth, F. Ramirez, Dimorphic effects of transforming growth factor-beta signaling during aortic aneurysm progression in mice suggest a combinatorial therapy for Marfan syndrome, Arterioscler. Thromb. Vasc. Biol. 35 (2015) 911–917.
[142] M. Groenink, A.W. den Hartog, R. Franken, T. Radonic, V. de Waard, J. Timmermans, A.J. Scholte, M.P. van den Berg, A.M. Spijkerboer, H.A. Marquering, et al., Losartan reduces aortic dilatation rate in adults with Marfan syndrome: a randomized controlled trial, Eur. Heart J. 34 (2013) 3491–3500.
[143] T. Radonic, P. de Witte, M. Groenink, V. de Waard, R. Lutter, M. van Eijk, M. Jansen, J. Timmermans, M. Kempers, A.J. Scholte, et al., Inflammation aggravates disease severity in Marfan syndrome patients, PLoS One 7 (2012) e32963.
[144] R.V. Lacro, H.C. Dietz, L.A. Sleeper, A.T. Yetman, T.J. Bradley, S.D. Colan, G.D. Pearson, E.S. Selamet Tierney, J.C. Levine, A.M. Atz, et al., Atenolol versus losartan in children and young adults with Marfan's syndrome, N. Engl. J. Med. 371 (2014) 2061–2071.
[145] H. Nistala, S. Lee-Arteaga, S. Smaldone, G. Siciliano, L. Carta, R.N. Ono, G. Sengle, E. Arteaga-Solis, R. Levasseur, P. Ducy, et al., Fibrillin-1 and -2 differentially modulate endogenous TGF-beta and BMP bioavailability during bone formation, J. Cell Biol. 190 (2010) 1107–1121.
[146] G. Sengle, V. Carlberg, S.F. Tufa, N.L. Charbonneau, S. Smaldone, E.J. Carlson, F. Ramirez, D.R. Keene, L.Y. Sakai, Abnormal activation of BMP signaling causes myopathy in Fbn2 null mice, PLos Genet. 11 (2015) e1005340.
[147] K.E. Gregory, R.N. Ono, N.L. Charbonneau, C.L. Kuo, D.R. Keene, H.P. Bachinger, L.Y. Sakai, The prodomain of BMP-7 targets the BMP-7 complex to the extracellular matrix, J. Biol. Chem. 280 (2005) 27970–27980.
[148] A.P. Wohl, H. Troilo, R.F. Collins, C. Baldock, G. Sengle, Extracellular regulation of bone morphogenetic protein activity by the microfibril component fibrillin-1, J. Biol. Chem. 291 (2016) 12732–12746.
[149] J.A. Tamminen, V. Parviainen, M. Ronty, A.P. Wohl, L. Murray, S. Joenvaara, M. Varjosalo, O. Lepparanta, O. Ritvos, G. Sengle, et al., Gremlin-1 associates with fibrillin microfibrils in vivo and regulates mesothelioma cell survival through transcription factor slug, Oncogenesis 2 (2013) e66.

Please cite this article in press as: J. Thomson, et al., Fibrillin microfibrils and elastic fibre proteins: Functional interactions and extracellular regulation of growth factors, Semin Cell Dev Biol (2018), https://doi.org/10.1016/j.semcdb.2018.07.016